Tesis Doctoral
Doctorado en Ingeniería Automática, Electrónica y de Telecomunicación

Lead Pursuit Control of Multiphase Drives

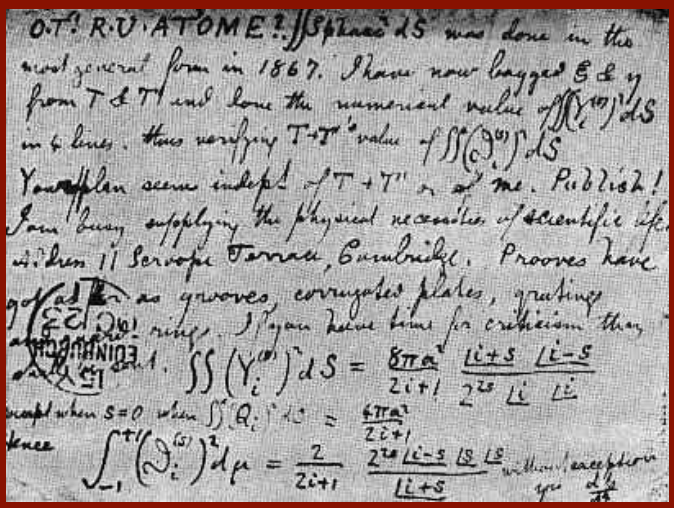

Autor: Cristina Martín Torres
Directores: Federico José Barrero García
Manuel Ruiz Arahal
Mario Javier Durán Martínez

Departamento de Ingeniería Electrónica
Escuela Técnica Superior de Ingeniería
Universidad de Sevilla

Sevilla, 2019

Tesis Doctoral
Doctorado en Ingeniería Automática, Electrónica y de Telecomunicación

Lead Pursuit Control of Multiphase Drives

Autor:

Cristina Martín Torres

Directores:

Federico José Barrero García
Manuel Ruiz Arahal
Mario Javier Durán Martínez

Departamento de Ingeniería Electrónica
Escuela Técnica Superior de Ingeniería
Universidad de Sevilla

2019

Tesis Doctoral: Lead Pursuit Control of Multiphase Drives

Autor: Cristina Martín Torres
Directores: Federico José Barrero García
Manuel Ruiz Arahal
Mario Javier Durán Martínez

El tribunal nombrado para juzgar la Tesis arriba indicada, compuesto por los siguientes doctores:

Presidente:

Vocales:

Secretario:

acuerdan otorgarle la calificación de:

El Secretario del Tribunal

Fecha:

Dedicado a:

Mis padres y hermanos,
sinónimos de apoyo
y amor incondicional.

Y a Mario,
mi pilar constante
en un mundo de variables.

Agradecimientos

Llegado este momento, me gustaría agradecer el apoyo recibido durante el desarrollo de esta Tesis. Han sido casi cinco años de evolución profesional y personal en los que diferentes personas han aportado su granito de arena.

En primer lugar, dar las gracias a mi tutor y directores de Tesis, quienes me han guiado a lo largo de este importante reto. Gracias Federico, por brindarme la oportunidad de iniciarme en la investigación, por la confianza que pusiste en mí desde el primer día, por presionarme y saber sacar lo mejor de mí, además de aceptarme dentro de tu familia como una más. Gracias Manolo, por todas tus excelentes ideas, tu ayuda y plena dedicación, por enseñarme a ser metódica y perfeccionista, lo cual ha sido clave para lograr el éxito en este trabajo. Y, por último, pero no por ello menos importante, gracias Mario, por tus sabios consejos, por apoyarme y guiarme durante todos estos años y por tu pasión por la investigación, que se contagia inevitablemente.

Gracias a mis compañeros del grupo ACETI, tanto de Sevilla como de Málaga, de los que me llevo muy buenas experiencias y un gran aprendizaje, profesional y personal.

Gracias a mis compañeros de "la sala" de la Universidad de Sevilla, los que se fueron y los que aún siguen, por los cafés matutinos, las charlas, las risas y, en general, los momentos de desconexión tan necesarios. También, gracias por toda la ayuda prestada, sin esperar nada a cambio. Echaré de menos pasar tiempo cada día con todos, pero espero mantener la amistad para siempre.

Por supuesto, gracias a mis padres Juan y María, y a mis hermanos Juan y María, por creer siempre en mis posibilidades, apoyarme en todas mis decisiones y darme la fuerza para luchar por mis metas, a pesar de estar separados por unos cuantos kilómetros y no poder compartir con ellos todo lo que me gustaría.

Finalmente, gracias Mario, mi compañero de andaduras en este largo y difícil camino. Gracias por ser mi soporte en los momentos difíciles y mi guía cuando no he sabido cómo continuar. Pero, sobre todo, gracias por toda la comprensión y paciencia que has tenido en estos años, y gracias por el cariño y el amor que me das cada día.

Cristina Martín Torres

Sevilla, 2019

Summary

Multiphase drives, constituted by an electric machine with more than three phases fed by a power converter, have recently attracted an important interest in the research community due to the advantages that they present over the conventional three-phase ones. This is the case of the better power distribution per phase, the lower harmonic production in the power converter, and the most important one, the fault-tolerant capability, which means that the multiphase machine can still be operated when one or several phases are missing, provided that the number of remaining phases is equal or greater than three. Due to this high reliability, multiphase drives are specially well suited for applications related to electric vehicles (terrestrial, maritime and aerial) and renewable energies for safety and/or economical reasons.

The use of advanced and high-performance controllers in multiphase drives is particularly relevant, since the control strategies conventionally applied to three-phase drives do not reach a standard in their extension to the multiphase case. The reason is the greater complexity and number of variables that must be controlled. In this context, predictive controllers have found an interesting niche of application in power converters and multiphase drives due to their intuitive and flexible formulation: a model of the system is used to compute predictions of the controlled variables, which are later compared with the imposed references in a cost function. This strategy permits incorporating several control objectives and constraints in the control process through the cost function. However, it is well known that this type of controller suffers from a high computational cost and current harmonic content that limit its application in multiphase drives.

The research developed in this Thesis work is focused on the mitigation of the cited limitations following two main goals:

- The incorporation of rotor current observers in the predictive controller in order to improve the accuracy of the predictive model and, consequently, the control system performance, principally in terms of harmonic content and commutation losses in the power converter. A Luenberger observer is constructed for that purpose using an innovative pole-placement strategy in its design.
- The introduction of an additional degree of freedom in the predictive controller based on variable sampling times and implemented using the lead-pursuit concept.

The result is a novel controller that leads to a finer resolution in the commuting times in comparison with more conventional predictive techniques, which provides an important reduction in the harmonic content.

The proposed control strategies are validated by simulation and experimentation using a five-phase induction machine drive as case example. The results and conclusions derived from this research have been presented in five main works published in high-impact international journals, which constitute the contributions of this article compendium Thesis. Nevertheless, other related works have also been published in journal and conference papers and a book chapter.

Resumen

Los accionamientos multifásicos, compuestos por una máquina eléctrica de más de tres fases alimentada por un convertidor de potencia, han atraído recientemente un importante interés en la comunidad investigadora debido a las ventajas que presentan frente a las máquinas trifásicas convencionales. Este es el caso de la mejor distribución de potencia por fase, la menor producción de armónicos en el convertidor de potencia y, la más importante, la tolerancia a fallos, lo cual significa que la máquina multifásica puede seguir funcionando cuando una o varias fases se pierden, siempre que el número restante de fases sea igual o mayor que tres. Debido a esta alta fiabilidad, los accionamientos multifásicos son especialmente adecuados para aplicaciones relacionadas con los vehículos eléctricos (terrestres, marítimos y aéreos) y las energías renovables por razones de seguridad y/o económicas.

El uso de controladores avanzados y de alto rendimiento en accionamientos multifásicos es particularmente relevante, ya que las estrategias de control convencionalmente aplicadas a los accionamientos trifásicos no terminan de alcanzar un estándar en su extensión al caso multifásico. La razón es la mayor complejidad y número de variables a controlar. En este contexto, los controladores predictivos han encontrado un interesante nicho de aplicación en convertidores de potencia y accionamientos multifásicos debido a su formulación intuitiva y flexible: un modelo del sistema es usado para calcular las predicciones de las variables controladas, que luego se comparan con las referencias impuestas dentro de una función de coste. Esta estrategia permite incorporar varios objetivos de control y restricciones en el proceso de control a través de la función de coste. Sin embargo, es bien sabido que este tipo de controlador sufre de un alto coste computacional y contenido armónico de corriente que limita su aplicación en los accionamientos multifásicos.

La investigación desarrollada en esta Tesis se centra en la mitigación de las limitaciones citadas siguiendo dos objetivos principales:

- La incorporación de observadores de corrientes rotóricas en el controlador predictivo para mejorar así la precisión del modelo predictivo y, consecuentemente, el rendimiento del sistema de control, principalmente en términos de contenido armónico y pérdidas por conmutación en el convertidor de potencia. Un observador

de Luenberger es construido para este propósito utilizando una estrategia innovadora de posicionamiento de polos en su diseño.

- La introducción de un grado de libertad adicional en el controlador predictivo basado en tiempos de muestreo variables e implementado usando el concepto de *lead pursuit*. El resultado es un controlador novedoso que conduce a una resolución en los tiempos de conmutación más fina en comparación con las técnicas predictivas más convencionales, lo que proporciona una reducción importante en el contenido armónico.

Las estrategias de control propuestas son validadas mediante simulación y experimentación utilizando un accionamiento compuesto por una máquina de inducción de cinco fases como caso de ejemplo. Los resultados y conclusiones derivadas de esta investigación han sido presentados en cinco trabajos principales publicados en revistas internacionales de alto impacto, los cuales constituyen las contribuciones de esta Tesis por compendio de artículos. Sin embargo, otros trabajos relacionados con la línea de investigación han sido también publicados en artículos de revista y conferencia y en un capítulo de libro.

Table of Contents

Agradecimientos III
Summary V
Resumen VII
List of Figures XI

1 Introduction **1**
1.1 Scientific context 1
1.2 Objectives 2
1.3 Document organization 3

2 Predictive Control in Multiphase Drives: State-of-the-Art **5**
2.1 A general outline of multiphase machines 5
2.2 Multiphase drives modeling: the five-phase case 7
2.2.1 Five-phase induction machine modeling 8
2.2.2 Power converter modeling 17
2.3 Multiphase drives control techniques 20
2.4 Model Predictive Control 23
2.4.1 General scheme of the FCS-MPC 25
2.4.2 Key design and implementation features in FCS-MPC 29
2.5 Contributions in the context 35

3 Rotor Observer for Harmonic Content Reduction **37**
3.1 Contribution 1 39
3.2 Contribution 2 51

4 Variable Sampling Time as a New Degree of Freedom **63**
4.1 Contribution 3 65
4.2 Contribution 4 75
4.3 Contribution 5 84

5 Conclusions and Future Works **97**
5.1 Conclusions 97
5.2 Summary of the research work 98
5.3 Future works 100
Bibliography 103

List of Figures

2.1	Scheme of the symmetrical and distributed-windings five-phase IM	9
2.2	Reference frames of stator (α–β) and rotor (α'–β') variables	13
2.3	Rotating reference frame (d–q)	15
2.4	Scheme of the five-phase two-level VSI with star-connected load	18
2.5	Space vector diagrams in the α–β and x–y subspaces	19
2.6	IRFOC technique for the distributed-windings five-phase IM drive	21
2.7	DTC technique for the distributed-windings five-phase IM drive	23
2.8	FCS-MPC technique for the distributed-windings five-phase IM drive	26
2.9	Flow diagram of the FCS-MPC technique	27
2.10	Real-time implementation and task distribution during a sampling period of the FCS-MPC current control applied to the five-phase IM drive	33
2.11	Schematic representation of the optimal switching vector selection in FCS-MPC with prediction horizon N_p	34

Chapter 1

Introduction

1.1 Scientific context

The industrial application of electric machines has grown in the last decades thanks to the development of microprocessors and power converters, which have permitted their use as variable-speed drives. It is expected that 80% of all the produced energy will be used by electric drives by 2030, playing Electric Vehicles (EVs) a major role in this situation, as they will account for at least 48% of the automotive market by that year [1]. Furthermore, electric drives are the basis of locomotive traction, electric ship propulsion, more-electric aircraft for various auxiliary functions (e.g., fuel pumps, starter/generator solutions, etc.) and renewable energy production.

Although three-phase machines are the common trend in the cited applications, the interest of the research community is recently focused on machines with more than three phases, known as multiphase machines. Their advantages in terms of reliability, i.e., post-fault working condition, is the principal reason [2]. In other words, multiphase drives can still be operated, without the need for heavy topological changes in the power converter, even if a phase is missing, provided that the number of remaining phases is equal or greater than three. Consequently, they are specially well suited for applications where reliability is essential for safety and/or economical reason, as it is the case of EVs. Additionally, multiphase machines provide better current distribution among phases and lower current harmonic production in the power converter than conventional three-phase ones, being them an ideal candidate for applications related to transport electrification and energy generation. This has been the main driving force behind the research developments in drives and power electronics during the last 20 years and in the multiphase machines' field.

However, multiphase drives' applications require the development of complex controllers to regulate the torque (or speed) and flux of the machine. In this regard, Model Predictive Control (MPC) has recently appeared as a viable alternative to conventional controllers, specially in its Finite-Control-Set version (FCS-MPC). The most used control structure is formed by an inner FCS-MPC stator current controller and an outer Field Oriented Control (FOC) for the torque/speed regulation. Although this technique presents an easy formulation and a high flexibility to incorporate different control objectives and to be

applied to multidimensional systems, it faces some limitations that require attention. The most notable ones are the high computational cost, which increases with the number of phases, and the high harmonic content in the electrical variables of the system, being the latter principally caused by the absence of a modulator and the fixed-time discretization nature of the control algorithm. This Doctoral Thesis is focused on the development of new control strategies based on predictive control techniques in order to overcome the aforementioned problems.

1.2 Objectives

The main objective of this Thesis work is the development of new model predictive current control techniques in order to mitigate the inherent problems that the application of FCS-MPC to multiphase machines presents. The focus will be, principally, the reduction of the high harmonic content in the controlled currents while maintaining a low computational cost. To this end, two research directions are followed. The first one is the improvement of the predictive model, since its accuracy highly affects the control performance. This is done by incorporating rotor current observers in order to estimate the non-measurable system components, which also form part of the predictive model. The second line of research, which must be highlighted here due to its novelty, is the addition of a new degree of freedom in the predictive controller in relation to the application of variable sampling times. It will be studied later that the fixed-time discretizacion nature of the conventional FCS-MPC algorithm leads to the appearance of not only high harmonic components but also inter-harmonics and electrical noise in the currents. A simple and natural way to reduce this problem can be the application of variable sampling times. This idea combined with the lead-pursuit concept leads to an innovative current control structure that is analyzed and implemented for the first time in this work.

The development of the new control techniques will be done using a particular multiphase drive based on a five-phase induction machine, currently used by the ACETI research team at the Electronic Engineering Department of the University of Seville, Spain. This will permit obtaining experimental results and perform the analysis, diffusion and international publication of the obtained results.

The general objective can be divided in the following particular tasks:

- State-of-the-art analysis of multiphase machines, their industrial applications and advantages over conventional three-phase ones. In this regard, the analysis and design of current controllers based on predictive control techniques, particularly the FCS-MPC, constitute the main focus.
- Study of the observer theory as a tool for the estimation of non-measurable quantities of the system, and its extension for the rotor current estimation in the FCS-MPC current control of a multiphase induction machine. For this purpose, different observer designs based on the Luenberger theory are analyzed and compared in order to obtain the best current performance improvement in comparison with conventional predictive controllers.
- Incorporation of the non-fixed discretization and the lead-pursuit concept in the FCS-MPC current controller in order to naturally reduce the harmonic content in the

stator currents. The feasibility of the proposal will be verified using the five-phase induction machine, and a comparison analysis over conventional predictive control techniques will be carried out in order to quantify the interest and utility of the proposal.

1.3 Document organization

The document has been divided in three main parts following the directives of the University of Seville in regard to an article compendium Thesis, which are published in the Real Decreto 99/2011 (BOE February 10th, 2011).

In the first part, the scientific context and objectives of this Doctoral Thesis are presented (Chapter 1), followed by a deep review of the most recent research works in relation to the application, modeling and control of multiphase machines (Chapter 2). In this review, the exploration and analysis of the latest and most significant implementations of MPC techniques, particularizing for the FCS-MPC current control approach, constitute the main focus in order to disclose their interest, applicability and limitations.

Afterwards, the original contributions of the Thesis are presented and discussed in a second part, which is composed of two chapters. In Chapter 3, the observer theory is applied in conjunction with the FCS-MPC current control for the estimation of non-measurable parts of the system with the aim of improving the current performance, specially in term of harmonic content. The obtained improvements comparing with conventional FCS-MPC techniques are quantified by simulations and experiments using the five-phase induction machine. In Contribution 1, a reduced-order version of the rotor current observer is used looking for a low increment in the total computational cost of the implemented controller. Then, the study is extended to a full-order version of the observer in Contribution 2. On the other hand, the development of a variable sampling time predictive controller based on the lead-pursuit concept is presented in Chapter 4, where three different contributions are shown. First, a proof-of-concept study of the proposed method is presented in Contribution 3. Then, a variation in the implementation of the lead-pursuit concept is proposed in Contribution 4, where an assessment in different operating conditions and a comparison with the most conventional FCS-MPC methods is also performed. Finally, the comparative analysis is extended in Contribution 5 by including the predictive controllers with rotor observers developed in Chapter 3. This last contribution aims to reveal the advantages and disadvantages of the innovative controllers, presented for the first time in this Doctoral Thesis, in their applications to multiphase machines. The five-phase induction machine is employed for the simulation and experimental validation in these contributions.

Finally, Chapter 5 highlights the conclusions derived from this study and raises future research lines to explore and continue the present work.

Chapter 2

Predictive Control in Multiphase Drives: State-of-the-Art

In this chapter, an up-to-date state-of-the-art in model predictive control of multiphase drives is presented in order to define the framework of the Thesis' contributions. For that purpose, a general overview of the applications, modeling, and control of multiphase drives is presented at first, including the most recent research works in the field (from Section 2.1 to Section 2.3). Afterwards, a deep insight in the model predictive control of multiphase drives is done in Section 2.4, particularizing for the FCS-MPC case. After an introduction to the predictive control techniques and their classification, the general FCS-MPC control scheme is presented together with the most concerning implementation and design aspects that can compromise the control performance. Hence, the main disadvantages of the FCS-MPC are brought to light, which constitute the basis of the problematic addressed in the Thesis' contributions (Section 2.5).

2.1 A general outline of multiphase machines

Any energy conversion system formed by a multiphase electric machine that is fed from a multiphase converter and regulated by a certain control technique is called multiphase drive. The first application of such a system, particularized for a five-phase drive, was done in the late 60s and described in [3], where the advantages of using these multiphase systems over the conventional three-phase standard were brought to light. The main interest of the proposal was that the higher number of phases yields a torque ripple three-times lower with respect to the equivalent three-phase case due to a better power distribution per phase, this being one of the most reported problems in conventional drives by that time. However, it was not until the beginning of the 21st century that the interest of researchers in multiphase machines was renewed due to two principal reasons. Firstly, the development of high-power and high-frequency semiconductors and, consequently, the appearance of Pulse Wide Modulation (PWM) methods to control the ON and OFF states of these electronic devices, as well as the energy conversion process. And secondly, the development of the microelectronic technology and the appearance of powerful electronic

devices with the ability of implementing control algorithms in real time, such as Digital Signal Processors (DSP) and Field-Programmable Gate Arrays (FPGA).

Notwithstanding the foregoing, the crucial reason for the renewed interest in multiphase drives can be found in the intrinsic benefits that they provide versus the conventional three-phase ones. These benefits are based on the extra degrees of freedom introduced by the higher number of phases, and are principally the followings:

- The fault-tolerant capability against a fault situation in the machine and/or the power converter, firstly presented in [4]. A n-phase machine can operate after one or several fault occurrences without any external equipment, as long as the number of healthy phases remains greater than or equal to three. Consequently, the system reliability is enhanced at the expense of a reduction in the generated electrical torque.

- The capability of increasing the power density in healthy operation by injecting specific current harmonics, firstly exposed in [5]. This is possible in certain multiphase machine's configurations based on concentrated windings, where the lower current harmonic components can be used to increase the torque production.

These advances and advantages underlie the adoption of multiphase drives in specific industry applications as variable-speed drives [6, 7]. Electric propulsion of ships, traction of electric vehicles (hybrid/electric vehicles and locomotives), wind energy generation and low-power electric systems for more-electric aircraft are fields where the investigation in the last 20 years has been focused on [8, 9]. The interest of multiphase machines in the cited applications, instead of the conventional three-phase counterparts, arises from the high toque/current production and/or more robust and cheaper fault-tolerant capability that are usually required. Benchmark solutions adopted by important companies are the ultrahigh-speed elevator of Hyundai, based on a 1.1 MW nine-phase electric drive [10]; the 5 MW twelve-phase electric drives in the wind turbines of Gamesa, for onshore and offshore plants; and the 20 MW fifteen-phase electric drive for ship propulsion introduced by the GE Power Conversion company in the Royal Navy [2].

In order to create a body of knowledge, recent research works review the advances in the field of multiphase drives including their industrial applications, machine design and modeling, types of converters, modulation techniques, and control strategies; and explore innovative uses of their degrees of freedom (i.e., multimotor, battery chargers, post-fault control or dynamic breaking) [2, 11–13]. In general, they show that symmetrical five-phase and asymmetrical six-phase machines with isolated neutrals are the most popular multiphase machine types in the research community, and that an evolution in the control techniques has been necessary in order to optimally exploit their inherent advantages. In this regard, MPC techniques have recently appeared as a promising alternative to conventional FOC and Direct Torque Control (DTC) methods, as it will be shown in following sections. However, further research on the topic is necessary in order to meet industry and safety standards while exploiting their benefits at reasonable costs.

2.2 Multiphase drives modeling: the five-phase case

A common feature in most control techniques applied to multiphase drives, particularly MPC methods, is the necessity of a precise and complete knowledge of the system's dynamic, or part of it, through a mathematical model. To obtain that model, different construction aspects of the multiphase machine and the power converter must be taken into account, beginning with the type of machine and converter used.

Depending on the rotor construction, multiphase machines can be divided into two main types, multiphase Induction Machines (IM) and multiphase Synchronous Machines (SM), usually of the Permanent Magnet type (PMSM). Although both types present similar modeling approaches, IMs benefit from a rugged construction with cheaper materials, low maintenance requirements, and well-proven technology, making them an usual election in industrial applications. Diversely, PMSMs provide better power density and efficiency, do not need reactive power, and have better fault tolerance against open-phase faults. Concerning the winding arrangement, the division is done between symmetrical or asymmetrical multiphase machines. First ones are constituted by consecutive phase windings equally displaced $2\pi/n$, while second ones are formed by independent sets of windings displaced π/n. Another classification considers the number of phases, thus, machines with an odd or an even number of phases, and machines with a multiple of three phases are distinguished. The higher the number of phases, the more complex the model. Finally, multiphase machines are differentiated between machines with concentrated or distributed windings. The most relevant interest in the concentrated-windings type is the existence of higher order spatial harmonics in the Magneto-Motive Force (MMF) that contribute to the electrical toque enhancement. Conversely, these harmonics can be neglected in distributed-windings machines (with an appropriate stator winding design), resulting in near sinusoidal MMF. Among these topologies, six-phase and five-phase IMs are the most studied ones in the research literature [11,12], where the symmetrical winding arrangement is preferable for an odd number of phases and the asymmetrical one for the even case [14]. Also, the five-phase case seems to be more attractive in medium power applications due to the lower complexity of the controller in terms of the computational cost.

Regarding the power converter, the most widespread configuration is the one named back-to-back, usually formed by a grid-connected three-phase rectifier electrically coupled to a n-phase inverter through a DC-link. This configuration permits the independent regulation of the inverter stage, which is decoupled from the distribution grid. In addition, it presents the capacity to generate an output with a wide range of frequencies and a small content of low-order harmonics by means of a suitable control algorithm (principally PWM-based techniques). The most used inverter type is the IGBT-based two-level Voltage Source Inverter (VSI) that single-sided supplies the electric machine. However, depending on the application requirements, other types and topologies of converters can be found in the literature. Thus, multilevel VSIs and multiphase matrix converters have been recently proposed in multiphase applications, as well as the open-end winding topology with dual inverter supply [15–17].

In the following sections, the model of the multiphase drive used as case example in this Doctoral Thesis is described. It is composed by a five-phase two-level VSI, which supplies a symmetrical five-phase IM with distributed windings. First, the physical model

of the induction machine is presented covering the phase variables model (or original model), and the additional transformations conventionally applied to this model in order to reduce the complexity of the mathematical equations. These are the decoupled (Clarke's) transformation and the rotational (Park's) transformation. Finally, the model of the power converter is presented, completing the system's model.

2.2.1 Five-phase induction machine modeling

Any multiphase machine can be described as a set of differential equations in the phase variables domain (currents, voltages and fluxes) using the general theory of electric machines [18]. However, the generalization of Fortescue and Clarke [19, 20] laid the foundations for different mathematical transformations. Their principal objective is the replacement of the original phase-variable model by equivalent equations using a reduced set of new (fictitious) variables, thus permitting the simplification of the machine's model. These transformations are collected in what it is usually named Vector Space Decomposition (VSD) approach [21, 22], where matrix representation is conventionally adopted. This approach is slightly different depending on the winding arrangement of the machine (symmetrical or asymmetrical, and distributed or concentrated) and if the number of phases is multiple of three or not. Thus, multiple works have been developed in the field of multiphase machines modeling, considering different topologies of both induction and synchronous machines [5, 11, 23–25].

The focus of this Thesis is the symmetrical five-phase induction machine with distributed windings, hence exclusively its model is presented in this section. This machine is based on a 30-slots three-phase IM with two pairs of poles whose stator has been rewound in order to obtain a five-phase IM with three pairs of poles. It is assumed that the new stator windings are equally distributed along the stator with an electrical displacement of $\vartheta = 2\pi/5$. Since the rotor is of squirrel-cage type, it can be treated as five windings equally displaced $\vartheta = 2\pi/5$ around the rotor circumference. A schematic representation of the machine is presented in Figure 2.1, where s_a to s_e and r_a to r_e denote each phase of the stator and rotor windings, respectively. These windings are star-connected with isolated neutral point. Additional simplifying assumptions are considered in the modeling:

- All phase windings in the stator/rotor are considered identical.
- The distribution of the MMF and, consequently, the flux around the air-gap can be regarded as sinusoidal, assuming symmetrical distributed windings. This means that all spatial harmonics can be discarded, except for the fundamental one.
- The magnetization characteristic of the ferromagnetic material is assumed linear. Therefore, the effects of magnetic field saturation are negligible and mutual inductances are constant.
- The air-gap is regarded as uniform by neglecting the impact of slotting.
- Stator and rotor resistances and leakage inductances are considered constant. Variations due to temperature and frequency factors are neglected.
- Losses in the ferromagnetic material due to hysteresis and eddy currents are not considered.

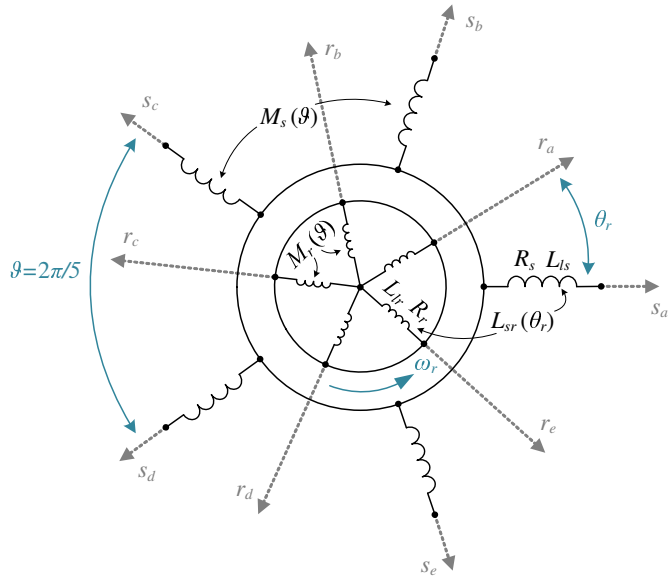

Figure 2.1 Scheme of the symmetrical and distributed-windings five-phase IM.

Regarding the power flow, it is assumed henceforth that the positive direction for the currents is from the supply source to the machine phases, i.e., motoring convention.

Phase variables model

Taking into account the previous hypotheses and due to the resistive-inductive nature of the machine windings, the voltage equilibrium equations that describe each phase of the machine, both of the stator and rotor, can be expressed in the following matrix form:

$$\begin{aligned} \mathbf{v_s} &= R_s\,\mathbf{i_s} + \frac{d\boldsymbol{\lambda}_\mathbf{s}}{dt} \\ \mathbf{v_r} &= R_r\,\mathbf{i_r} + \frac{d\boldsymbol{\lambda}_\mathbf{r}}{dt} \end{aligned} \tag{2.1}$$

where R_s and R_r are the stator and rotor resistances, and stator and rotor currents ($\mathbf{i}$), voltages ($\mathbf{v}$), and fluxes ($\boldsymbol{\lambda}$) are defined as

$$\begin{aligned} \mathbf{v_s} &= \begin{bmatrix} v_{sa} & v_{sb} & v_{sc} & v_{sd} & v_{se} \end{bmatrix}^T & \mathbf{v_r} &= \begin{bmatrix} v_{ra} & v_{rb} & v_{rc} & v_{rd} & v_{re} \end{bmatrix}^T \\ \mathbf{i_s} &= \begin{bmatrix} i_{sa} & i_{sb} & i_{sc} & i_{sd} & i_{se} \end{bmatrix}^T & \mathbf{i_r} &= \begin{bmatrix} i_{ra} & i_{rb} & i_{rc} & i_{rd} & i_{re} \end{bmatrix}^T \\ \boldsymbol{\lambda}_\mathbf{s} &= \begin{bmatrix} \lambda_{sa} & \lambda_{sb} & \lambda_{sc} & \lambda_{sd} & \lambda_{se} \end{bmatrix}^T & \boldsymbol{\lambda}_\mathbf{r} &= \begin{bmatrix} \lambda_{ra} & \lambda_{rb} & \lambda_{rc} & \lambda_{rd} & \lambda_{re} \end{bmatrix}^T. \end{aligned} \tag{2.2}$$

Since the studied induction machine has a squirrel-cage topology, rotor voltages are equal to zero. Also, it is important to remark that rotor variables and parameters in (2.1) and (2.2) are referred to the stator, this being a common procedure in three-phase machines

modeling. Previous equations are completed with the definition of the stator and rotor fluxes in terms of the stator and rotor currents (2.3), which represent the coupling between the stator and the rotor.

$$\begin{aligned} \boldsymbol{\lambda}_{\mathbf{s}} &= \mathbf{L}_{\mathbf{s}}\,\mathbf{i}_{\mathbf{s}} + \mathbf{L}_{\mathbf{sr}}(\theta_r)\,\mathbf{i}_{\mathbf{r}} \\ \boldsymbol{\lambda}_{\mathbf{r}} &= \mathbf{L}_{\mathbf{r}}\,\mathbf{i}_{\mathbf{r}} + \mathbf{L}_{\mathbf{rs}}(\theta_r)\,\mathbf{i}_{\mathbf{s}} \end{aligned} \tag{2.3}$$

Under the previously cited considerations of identical windings with uniform distribution and constant parameters, stator and rotor inductance matrices, $\mathbf{L_s}$ and $\mathbf{L_r}$, are constituted by constant coefficients that only depend on the stator and rotor leakage inductances L_{ls} and L_{lr}, the mutual inductance M, and the winding electrical displacement ϑ as follows:

$$\begin{aligned} \mathbf{L}_{\mathbf{s}} &= L_{ls}\,\mathbf{I_5} + \mathbf{M}_{\mathbf{s}}(\vartheta) \\ \mathbf{L}_{\mathbf{r}} &= L_{lr}\,\mathbf{I_5} + \mathbf{M}_{\mathbf{r}}(\vartheta) \end{aligned}$$

$$\mathbf{M_s}(\vartheta) = \mathbf{M_r}(\vartheta) = M \begin{bmatrix} 1 & \cos(\vartheta) & \cos(2\vartheta) & \cos(3\vartheta) & \cos(4\vartheta) \\ \cos(4\vartheta) & 1 & \cos(\vartheta) & \cos(2\vartheta) & \cos(3\vartheta) \\ \cos(3\vartheta) & \cos(4\vartheta) & 1 & \cos(\vartheta) & \cos(2\vartheta) \\ \cos(2\vartheta) & \cos(3\vartheta) & \cos(4\vartheta) & 1 & \cos(\vartheta) \\ \cos(\vartheta) & \cos(2\vartheta) & \cos(3\vartheta) & \cos(4\vartheta) & 1 \end{bmatrix}. \tag{2.4}$$

On the other hand, mutual stator-to-rotor and rotor-to-stator inductance matrices in (2.3), which verify that $\mathbf{L_{sr}}(\theta_r) = \mathbf{L_{rs}}(\theta_r)^T$, are not constant but they depend on the instantaneous value of the rotor position with respect to the stator, i.e., the rotor angle θ_r, through

$$\mathbf{L_{sr}}(\theta_r) = M \begin{bmatrix} \cos(\Delta_0) & \cos(\Delta_1) & \cos(\Delta_2) & \cos(\Delta_3) & \cos(\Delta_4) \\ \cos(\Delta_4) & \cos(\Delta_0) & \cos(\Delta_1) & \cos(\Delta_2) & \cos(\Delta_3) \\ \cos(\Delta_3) & \cos(\Delta_4) & \cos(\Delta_0) & \cos(\Delta_1) & \cos(\Delta_2) \\ \cos(\Delta_2) & \cos(\Delta_3) & \cos(\Delta_4) & \cos(\Delta_0) & \cos(\Delta_1) \\ \cos(\Delta_1) & \cos(\Delta_2) & \cos(\Delta_3) & \cos(\Delta_4) & \cos(\Delta_0) \end{bmatrix} \tag{2.5}$$

where $\Delta_k = \theta_r + k\,\vartheta$, with $k = 1,2,\ldots,5$; and the rotor angle is obtained through the electrical rotor speed

$$\theta_r = \int_0^t \omega_r\,dt. \tag{2.6}$$

Equations (2.1)–(2.6) describe the electrical part of the five-phase induction machine that is complemented with the mechanical equation:

$$J_m \frac{d\omega_m}{dt} + B_m\,\omega_m = T_e - T_L \tag{2.7}$$

being ω_m the mechanical speed of the rotor shaft ($\omega_r = P\,\omega_m$, with P the number of pole pairs), T_L is the load torque applied to the machine, T_e is the electromagnetic torque, J_m is the inertia of the rotating masses, and B_m is the friction coefficient. The electromagnetic torque is responsible for the electromechanical energy conversion, linking the electrical

and mechanical subsystems. This torque is obtained with the following equation:

$$T_e = \frac{P}{2}\begin{bmatrix}\mathbf{i_s}\\ \mathbf{i_r}\end{bmatrix}^T \frac{d}{d\theta_r}\begin{bmatrix}\mathbf{L_s} & \mathbf{L_{sr}}(\theta_r)\\ \mathbf{L_{rs}}(\theta_r) & \mathbf{L_r}\end{bmatrix}\begin{bmatrix}\mathbf{i_s}\\ \mathbf{i_r}\end{bmatrix}. \tag{2.8}$$

Taking into account that stator and rotor inductance matrices do not depend on the rotor position, previous equation can be reduced to the one in (2.9), where it can be stated that the electromagnetic torque is entirely created from the interaction between the stator and the rotor.

$$T_e = \frac{P}{2}\mathbf{i_s}^T \frac{d\mathbf{L_{sr}}(\theta_r)}{d\theta_r}\mathbf{i_r} \tag{2.9}$$

To summarize, the five-phase induction machine can be represented in the phase-variable domain through $2n+1=11$ first-order differential equations, after the substitution of the flux expressions (2.3) into the voltage equilibrium equations (2.1), and the electromagnetic torque value (2.9) into the mechanical equation (2.7); plus 1 integral equation (2.6). Due to the time-dependence through the rotor position angle, these equations constitute a non-linear time-variant system. Similar equations can be derived for higher number of phases, only changing the number of obtained equations.

Decoupled machine's model (Clarke's transformation)

Even if the resolution of the phase-variable equations is possible with the advanced computational devices, important simplifications can be done through the VSD approach. Thus, using the Clarke's transformation, it is possible to represent the five-phase induction machine's model in a stationary reference frame formed by a new set of five fictitious variables. They are grouped into two two-dimensional orthogonal planes, named α–β and x–y, whose components are also orthogonal between them; plus and additional axis that contains the homopolar component, named z. The principal characteristic of this new reference frame is that the orthogonality of the planes ensures that they are totally decoupled, which leads to important simplifications in the resultant model and, consequently, makes it more suitable for control purposes. In addition, the transformation of the phase variables into the new stationary reference frame permits having a better insight into the physical phenomena of the energy conversion, since the α–β plane will be the one responsible for the electromechanical energy conversion while the x–y plane and the z–axis are only related to harmonic components and losses in the machine, as it will be demonstrated later.

The relationship between the original phase variables and the new fictitious ones is obtained by applying the decoupled (Clarke's) transformation matrix $\mathbf{T_c}$, defined in (2.11), to both the stator and the rotor variables in the following way:

$$\begin{aligned}
&\begin{bmatrix}v_{s\alpha} & v_{s\beta} & v_{sx} & v_{sy} & v_{sz}\end{bmatrix}^T = \mathbf{T_c}\,\mathbf{v_s} \qquad \begin{bmatrix}v_{r\alpha} & v_{r\beta} & v_{rx} & v_{ry} & v_{rz}\end{bmatrix}^T = \mathbf{T_c}\,\mathbf{v_r}\\
&\begin{bmatrix}i_{s\alpha} & i_{s\beta} & i_{sx} & i_{sy} & i_{sz}\end{bmatrix}^T = \mathbf{T_c}\,\mathbf{i_s} \qquad \begin{bmatrix}i_{r\alpha} & i_{r\beta} & i_{rx} & i_{ry} & i_{rz}\end{bmatrix}^T = \mathbf{T_c}\,\mathbf{i_r}\\
&\begin{bmatrix}\lambda_{s\alpha} & \lambda_{s\beta} & \lambda_{sx} & \lambda_{sy} & \lambda_{sz}\end{bmatrix}^T = \mathbf{T_c}\,\boldsymbol{\lambda_s} \qquad \begin{bmatrix}\lambda_{r\alpha} & \lambda_{r\beta} & \lambda_{rx} & \lambda_{ry} & \lambda_{rz}\end{bmatrix}^T = \mathbf{T_c}\,\boldsymbol{\lambda_r}
\end{aligned} \tag{2.10}$$

$$\mathbf{T_c} = \frac{2}{5}\begin{bmatrix} 1 & \cos(\vartheta) & \cos(2\vartheta) & \cos(3\vartheta) & \cos(4\vartheta) \\ 0 & \sin(\vartheta) & \sin(2\vartheta) & \sin(3\vartheta) & \sin(4\vartheta) \\ 1 & \cos(2\vartheta) & \cos(4\vartheta) & \cos(6\vartheta) & \cos(8\vartheta) \\ 0 & \sin(2\vartheta) & \sin(4\vartheta) & \sin(6\vartheta) & \sin(8\vartheta) \\ \frac{1}{2} & \frac{1}{2} & \frac{1}{2} & \frac{1}{2} & \frac{1}{2} \end{bmatrix}. \tag{2.11}$$

The coefficient $2/5$ in front of the transformation matrix is associated with the powers of the machine after the transformation. The selected value keeps the original values of the electrical variables invariant after the transformation, but not the total powers, thus being commonly known as power-variant transformation. However, another common practice uses the coefficient $\sqrt{2/5}$ instead, which keeps the total powers of the machine invariant [6, 26], being named power-invariant transformation in that case.

Substituting (2.3) in (2.1) and applying the decoupled transformation, the resultant stator and rotor equilibrium equations can be written as shown in (2.12) and (2.13), after some mathematical operations, where $L_m = (5/2)M$ is the equivalent mutual inductance, and the stator and rotor inductances in the new reference frame are defined as $L_s = L_{ls} + L_m$ and $L_r = L_{lr} + L_m$, respectively. The parameters that appear in these equations are, in essence, the same ones as in the well-known equivalent steady-state circuit of an induction machine, which can be obtained from standard no-load and locked rotor tests [27, 28].

$$\begin{aligned} v_{s\alpha} &= R_s\, i_{s\alpha} + L_s \frac{di_{s\alpha}}{dt} + L_m \frac{d}{dt}(i'_{r\alpha}\cos\theta_r - i'_{r\beta}\sin\theta_r) \\ v_{s\beta} &= R_s\, i_{s\beta} + L_s \frac{di_{s\beta}}{dt} + L_m \frac{d}{dt}(i'_{r\alpha}\sin\theta_r + i'_{r\beta}\cos\theta_r) \\ v_{sx} &= R_s\, i_{sx} + L_{ls} \frac{di_{sx}}{dt} \\ v_{sy} &= R_s\, i_{sy} + L_{ls} \frac{di_{sy}}{dt} \\ v_{sz} &= R_s\, i_{sz} + L_{ls} \frac{di_{sz}}{dt} \end{aligned} \tag{2.12}$$

$$\begin{aligned} v'_{r\alpha} = 0 &= R_r\, i'_{r\alpha} + L_r \frac{di'_{r\alpha}}{dt} + L_m \frac{d}{dt}(i_{s\alpha}\cos\theta_r + i_{s\beta}\sin\theta_r) \\ v'_{r\beta} = 0 &= R_r\, i'_{r\beta} + L_r \frac{di'_{r\beta}}{dt} + L_m \frac{d}{dt}(-i_{s\alpha}\sin\theta_r + i_{s\beta}\cos\theta_r) \\ v_{rx} = 0 &= R_r\, i_{rx} + L_{lr} \frac{di_{rx}}{dt} \\ v_{ry} = 0 &= R_r\, i_{ry} + L_{lr} \frac{di_{ry}}{dt} \\ v_{rz} = 0 &= R_r\, i_{rz} + L_{lr} \frac{di_{rz}}{dt} \end{aligned} \tag{2.13}$$

Again, rotor voltages are considered zero due to the squirrel-cage rotor. It can be seen that stator variables are referred to the stationary reference frame α–β, while the rotor

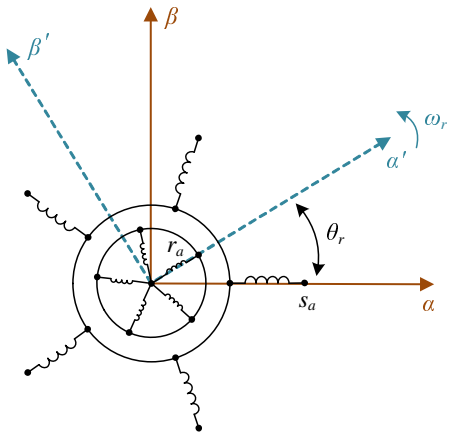

Figure 2.2 Reference frames of stator (α–β) and rotor (α'–β') variables.

ones are referred to a different reference frame α'–β' that rotates at the rotor speed ω_r (see Figure 2.2). This issue has been represented by the apostrophe in the rotor variables (v'_r and i'_r) only in the α–β equations, since it is exclusively in this plane where the stator and rotor coupling takes place. As a consequence of all this, the dependence on the rotor angle in some inductance terms still remains. In order to eliminate this dependence, it is necessary to apply an additional change of variables, which is a rotational transformation of the rotor α'–β' variables into the stationary α–β plane. This is done using the following rotational matrix:

$$\mathbf{T_r}(\theta_r) = \begin{bmatrix} \cos\theta_r & -\sin\theta_r \\ \sin\theta_r & \cos\theta_r \end{bmatrix}. \tag{2.14}$$

After the application of the rotational transformation to equations (2.12) and (2.13), the final electrical model of the machine in the stationary reference frame can be cast in the form

$$\begin{aligned}
v_{s\alpha} &= R_s i_{s\alpha} + L_s \frac{di_{s\alpha}}{dt} + L_m \frac{di_{r\alpha}}{dt} = R_s i_{s\alpha} + \frac{d\lambda_{s\alpha}}{dt} \\
v_{s\beta} &= R_s i_{s\beta} + L_s \frac{di_{s\beta}}{dt} + L_m \frac{di_{r\beta}}{dt} = R_s i_{s\beta} + \frac{d\lambda_{s\beta}}{dt} \\
v_{sx} &= R_s i_{sx} + L_{ls} \frac{di_{sx}}{dt} = R_s i_{sx} + \frac{d\lambda_{sx}}{dt} \\
v_{sy} &= R_s i_{sy} + L_{ls} \frac{di_{sy}}{dt} = R_s i_{sy} + \frac{d\lambda_{sy}}{dt} \\
v_{sz} &= R_s i_{sz} + L_{ls} \frac{di_{sz}}{dt} = R_s i_{sz} + \frac{d\lambda_{sz}}{dt}
\end{aligned} \tag{2.15}$$

$$
\begin{aligned}
v_{r\alpha} = 0 &= R_r\, i_{r\alpha} + L_r \frac{di_{r\alpha}}{dt} + L_m \frac{di_{s\alpha}}{dt} + \omega_r \left(L_r\, i_{r\beta} + L_m\, i_{s\beta}\right) = R_r\, i_{r\alpha} + \frac{d\lambda_{r\alpha}}{dt} + \omega_r\, \lambda_{r\beta} \\
v_{r\beta} = 0 &= R_r\, i_{r\beta} + L_r \frac{di_{r\beta}}{dt} + L_m \frac{di_{s\beta}}{dt} - \omega_r \left(L_r\, i_{r\alpha} + L_m\, i_{s\alpha}\right) = R_r\, i_{r\beta} + \frac{d\lambda_{r\beta}}{dt} - \omega_r\, \lambda_{r\alpha} \\
v_{rx} = 0 &= R_r\, i_{rx} + L_{lr} \frac{di_{rx}}{dt} = R_r\, i_{rx} + \frac{d\lambda_{rx}}{dt} \\
v_{ry} = 0 &= R_r\, i_{ry} + L_{lr} \frac{di_{ry}}{dt} = R_r\, i_{ry} + \frac{d\lambda_{ry}}{dt} \\
v_{rz} = 0 &= R_r\, i_{rz} + L_{lr} \frac{di_{rz}}{dt} = R_r\, i_{rz} + \frac{d\lambda_{rz}}{dt}.
\end{aligned} \tag{2.16}
$$

Notice that new expressions for the rotor and stator fluxes have been deduced:

$$
\begin{aligned}
\lambda_{s\alpha} &= L_s\, i_{s\alpha} + L_m\, i_{r\alpha} & \lambda_{r\alpha} &= L_r\, i_{r\alpha} + L_m\, i_{s\alpha} \\
\lambda_{s\beta} &= L_s\, i_{s\beta} + L_m\, i_{r\beta} & \lambda_{r\beta} &= L_r\, i_{r\beta} + L_m\, i_{s\beta} \\
\lambda_{sx} &= L_{ls}\, i_{sx} & \lambda_{rx} &= L_{lr}\, i_{rx} \\
\lambda_{sy} &= L_{ls}\, i_{sy} & \lambda_{ry} &= L_{lr}\, i_{ry} \\
\lambda_{sz} &= L_{ls}\, i_{sz} & \lambda_{rz} &= L_{lr}\, i_{rz}.
\end{aligned} \tag{2.17}
$$

The electromagnetic torque (2.9) can be expressed in the new stationary reference frame applying (2.11) and (2.14), and performing some calculations, giving rise to the following expression:

$$
T_e = P \frac{5}{2} L_m \left(i_{r\alpha}\, i_{s\beta} - i_{r\beta}\, i_{s\alpha}\right). \tag{2.18}
$$

It must be noted that the factor $5/2$ in this expression will not appear in the case of applying a power-invariant transformation. As expected, only variables in the α–β plane are involved in the electromechanical energy conversion process (remember that a distributed-winding machine is considered) or, in other words, in the fundamental torque and flux production.

Some analyses must be done regarding the electrical model in (2.15) and (2.16). Since the coupling between the rotor and stator windings exclusively takes place in the α–β plane, from the rotor voltage equations it can de deduced that x–y and z rotor voltages can be discarded. Furthermore, the star connection of the stator windings with isolated neutral avoids the flow of the homopolar current, so the z component of the stator voltage can be also considered equal to zero. After all these simplifications, the final machine model in the stationary reference frame can be totally described by 6 differential equations plus the mechanical equation with the new torque expression, which implies a significant reduction of the model complexity in comparison with the original phase-variable model. However, the non-linear and time-variant properties of the differential equations still remain.

Finally, the decoupled transformation permits a detailed analysis of the voltage and current harmonic components, since some of them are mapped into certain planes. Thus, in normal conditions, the fundamental frequency and harmonic components of the order $10k \pm 1$, with $k = 1,2,3,\ldots,\infty$, map into the α–β plane contributing to the electromechanical energy conversion. Conversely, harmonics of the order $10k \pm 3$ map into the x–y plane,

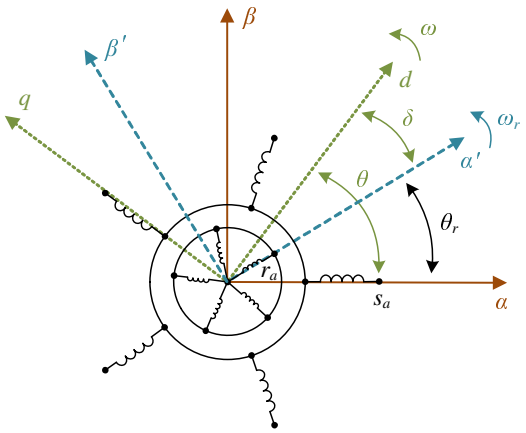

Figure 2.3 Rotating reference frame (d–q).

only contributing to the losses in the machine. And the DC component plus harmonics of the order $5k$ map into the homopolar component, which cannot flow in the case study.

Machine's model in the rotating reference frame (Park's transformation)

It has been demonstrated that the decoupled transformation permits the representation of the phase variables in a stationary reference frame, which leads to a significant simplification of the machine's model. The α–β components are the responsible for the torque/flux generation and, consequently, constitute the priority in the control process. However, these components present an oscillating nature, so they are usually expressed in a rotating reference frame, called d–q, to better regulate them. Thus, after the rotational transformation, called Park's transformation, the d–q components of the electrical variables are constant during steady state and variable during transients [29]. Regarding x–y components, assuming ideal symmetrical and balanced sinusoidal five-phase voltage supply, they are zero and it is not necessary to rotate them. Nonetheless, they are also rotated in situations where the aforementioned assumption of ideal supply is no longer applicable (as it is the case of fault conditions in the VSI legs [30]) and they present an oscillating nature too.

In this Park's transformation, the new d–q reference frame is considered to rotate at an arbitrary speed ω and its instantaneous position with respect to the stator α–β reference frame is defined by the electrical angle θ (see Figure 2.3), being both quantities mutually related through

$$\theta = \int_0^t \omega \, dt. \tag{2.19}$$

Consequently, α–β stator variables can be referred to the new rotating reference frame with the following expressions and rotational matrix:

$$\begin{aligned}
\begin{bmatrix} v_{sd} & v_{sq} \end{bmatrix}^T &= \mathbf{D_s}(\theta) \begin{bmatrix} v_{s\alpha} & v_{s\beta} \end{bmatrix}^T \\
\begin{bmatrix} i_{sd} & i_{sq} \end{bmatrix}^T &= \mathbf{D_s}(\theta) \begin{bmatrix} i_{s\alpha} & i_{s\beta} \end{bmatrix}^T \\
\begin{bmatrix} \lambda_{sd} & \lambda_{sq} \end{bmatrix}^T &= \mathbf{D_s}(\theta) \begin{bmatrix} \lambda_{s\alpha} & \lambda_{s\beta} \end{bmatrix}^T
\end{aligned} \tag{2.20}$$

$$\mathbf{D_s}(\theta) = \begin{bmatrix} \cos\theta & \sin\theta \\ -\sin\theta & \cos\theta \end{bmatrix}. \tag{2.21}$$

In the case of the rotor variables, expressed in the α'–β' plane after the Clarke's transformation, a different rotational matrix must be defined in order to refer both stator and rotor variables to the same reference frame d–q, eliminating the relative motion between stator and rotor windings. Following the representation in Figure 2.3, the instantaneous position of the rotor reference frame α'–β', which rotates at the rotor speed ω_r, with respect to the d–q reference frame is given by the electrical angle δ. This angle can be obtained with the following equation:

$$\delta = \theta - \theta_r = \int_0^t (\omega - \omega_r)\, dt = \int_0^t \omega_{sl}\, dt \tag{2.22}$$

where ω_{sl} is the relative speed between the rotating and the rotor reference frames, called slip speed. Hence, the rotor variables in the new rotating reference frame are obtained using the following equations and rotational matrix:

$$\begin{aligned}
\begin{bmatrix} v_{rd} & v_{rq} \end{bmatrix}^T &= \mathbf{D_r}(\delta) \begin{bmatrix} v'_{r\alpha} & v'_{r\beta} \end{bmatrix}^T \\
\begin{bmatrix} i_{rd} & i_{rq} \end{bmatrix}^T &= \mathbf{D_r}(\delta) \begin{bmatrix} i'_{r\alpha} & i'_{r\beta} \end{bmatrix}^T \\
\begin{bmatrix} \lambda_{rd} & \lambda_{rq} \end{bmatrix}^T &= \mathbf{D_r}(\delta) \begin{bmatrix} \lambda'_{r\alpha} & \lambda'_{r\beta} \end{bmatrix}^T
\end{aligned} \tag{2.23}$$

$$\mathbf{D_r}(\delta) = \begin{bmatrix} \cos\delta & \sin\delta \\ -\sin\delta & \cos\delta \end{bmatrix}. \tag{2.24}$$

Applying the rotational matrices (2.21) and (2.24) to the stator and rotor voltage equilibrium equations (2.12) and (2.13), the complete machine's model in the rotating reference frame can be expressed as

$$\begin{aligned}
v_{sd} &= R_s\, i_{sd} + L_s \frac{di_{sd}}{dt} + L_m \frac{di_{rd}}{dt} - \omega\,(L_s\, i_{sq} + L_m\, i_{rq}) = R_s\, i_{sd} + \frac{d\lambda_{sd}}{dt} - \omega\,\lambda_{sq} \\
v_{sq} &= R_s\, i_{sq} + L_s \frac{di_{sq}}{dt} + L_m \frac{di_{rq}}{dt} + \omega\,(L_s\, i_{sd} + L_m\, i_{rd}) = R_s\, i_{sq} + \frac{d\lambda_{sq}}{dt} + \omega\,\lambda_{sd} \\
v_{sx} &= R_s\, i_{sx} + L_{ls} \frac{di_{sx}}{dt} = R_s\, i_{sx} + \frac{d\lambda_{sx}}{dt} \\
v_{sy} &= R_s\, i_{sy} + L_{ls} \frac{di_{sy}}{dt} = R_s\, i_{sy} + \frac{d\lambda_{sy}}{dt}
\end{aligned} \tag{2.25}$$

$$
\begin{aligned}
v_{rd} = 0 &= R_r\, i_{rd} + L_r \frac{di_{rd}}{dt} + L_m \frac{di_{sd}}{dt} - \omega_{sl}\,(L_r\, i_{rq} + L_m\, i_{sq}) = R_r\, i_{rd} + \frac{d\lambda_{rd}}{dt} - \omega_{sl}\,\lambda_{rq} \\
v_{rq} = 0 &= R_r\, i_{rq} + L_r \frac{di_{rq}}{dt} + L_m \frac{di_{sq}}{dt} + \omega_{sl}\,(L_r\, i_{rd} + L_m\, i_{sd}) = R_r\, i_{rq} + \frac{d\lambda_{rq}}{dt} + \omega_{sl}\,\lambda_{rd}
\end{aligned}
\tag{2.26}
$$

where the relationship between stator and rotor fluxes, and the stator and rotor currents in the rotating frame is the following:

$$
\begin{aligned}
\lambda_{sd} &= L_s\, i_{sd} + L_m\, i_{rd} & \lambda_{rd} &= L_r\, i_{rd} + L_m\, i_{sq} \\
\lambda_{sq} &= L_s\, i_{sq} + L_m\, i_{rq} & \lambda_{rq} &= L_r\, i_{rq} + L_m\, i_{sq}. \\
\lambda_{sx} &= L_{ls}\, i_{sx} & & \\
\lambda_{sy} &= L_{ls}\, i_{sy} & &
\end{aligned}
\tag{2.27}
$$

Notice that equations in the x–y plane stay unaltered since the rotation is only performed in the α–β plane, as it was previously commented. For simplification purposes, the stator and rotor z–axis components and the rotor x–y components are omitted following the previous reasoning. Proceeding in an analogous way, a new expression of the electromagnetic torque can be derived:

$$
T_e = P\,\frac{5}{2}\,L_m\,(i_{rd}\, i_{sq} - i_{rq}\, i_{sd}). \tag{2.28}
$$

However, it is usual to find alternative expressions of this torque, as the ones shown in (2.29), where the correlation between stator and rotor fluxes and currents are applied to derive them. These alternative formulations are useful in some control strategies in order to reduce the number of calculations when the model is expressed in certain reference frames. Notice, again, that the $5/2$ coefficient will not appear if the power-invariant decoupling transformation is used instead of (2.11).

$$
T_e = P\,\frac{5}{2}\,(\lambda_{sd}\, i_{sq} - \lambda_{sq}\, i_{sd}) = P\,\frac{5}{2}\,\frac{L_m}{L_r}\,(\lambda_{rd}\, i_{sq} - \lambda_{rq}\, i_{sd}) \tag{2.29}
$$

As a final remark, the speed of the rotating reference frame (ω) can be arbitrarily selected in an induction machine. However, depending on the control strategy, some selections are more favourable than others in terms of the reduction of the machine's model complexity. This is the case of the Rotor Field Oriented Control (RFOC), where ω is selected in such a way that the d–axis is fixed to the rotor flux and, consequently, the projection of this flux in the q–axis disappears [7, 31]. Another option consists in the alignment of the reference frame to the stator flux, which is typically used in the DTC technique [32, 33].

2.2.2 Power converter modeling

In this section, the model of the power converter that supplies the five-phase IM is presented in order to complete the modeling of the multiphase drive used in this Doctoral Thesis. The selected configuration corresponds to the two-level five-phase VSI, which is formed by two IGBT per leg with their corresponding anti-parallel free-wheeling diodes. A

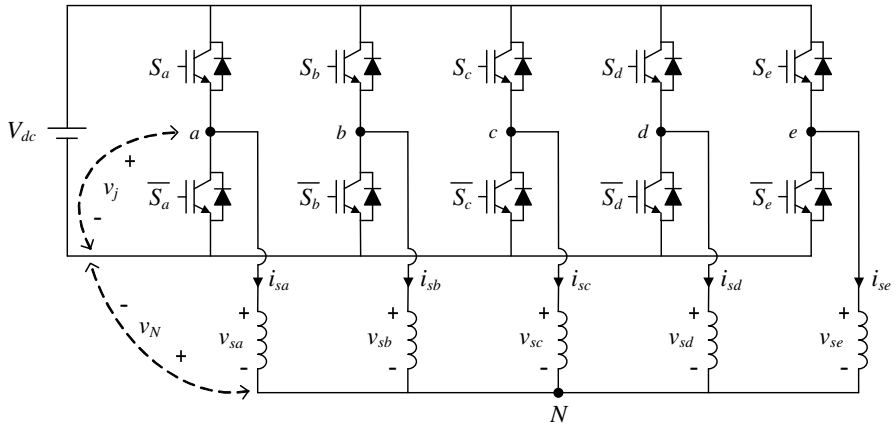

Figure 2.4 Scheme of the five-phase two-level VSI with star-connected load.

schematic representation of this VSI is depicted in Figure 2.4, where a balanced inductive load has been included to represent the machine' stator windings when they are star-connected, being N the common point. It is considered that a DC-link value equal to V_{dc} is provided by an external low-impedance DC source. For this scheme, the state of each converter's leg can be defined as $S_j = \{0,1\}$, with $j = \{a,b,c,d,e\}$; being $S_j = 1$ when the upper IGBT is ON and the lower one is OFF, while the opposite occurs when $S_j = 0$. In this way, short circuits when both IGBTs of the same leg are ON are avoided, as well as the impossibility to control the load when both IGBTs of the same leg are OFF. In practice, a small dead time is introduced between the commutations of the IGBTs with the aim of avoiding transient short circuits. However, it is not reflected in the final model of the VSI for simplicity purposes.

Under these considerations, the voltage v_j in the midpoint of the corresponding leg with respect to the negative bus of the DC-link can be defined in terms of the switching state of that leg using the following expression:

$$v_j = V_{dc} S_j. \tag{2.30}$$

This voltage is related to the stator phase voltage, v_{sj}, through the voltage between the common point of the star connection and the negative bus of the DC-link, v_N, in the following way:

$$v_j = v_{sj} + v_N. \tag{2.31}$$

Assuming balanced load, the sum of the five stator phase voltages must be equal to zero. Thus, adding all stator phase voltages derived form (2.31) and combining the result with (2.30), the voltage v_N can be defined as

$$v_N = \frac{1}{5}\sum_{i=a}^{e} v_i = \frac{V_{dc}}{5}\sum_{i=a}^{e} S_i. \tag{2.32}$$

Introducing this value in (2.31), an expression for the stator phase voltages in terms of the switching states of the VSI's legs can be derived

$$v_{sj} = v_j - v_N = V_{dc} S_j - \frac{V_{dc}}{5} \sum_{i=a}^{e} S_i = V_{dc} \left[S_j - \frac{1}{5} \sum_{i=a}^{e} S_i \right]. \tag{2.33}$$

Consequently, if the switching state of the VSI is defined as the vector $\mathbf{S} = [S_a\ S_b\ S_c\ S_d\ S_e]^T$, the above equation can be expressed in matrix form

$$\begin{bmatrix} v_{sa} \\ v_{sb} \\ v_{sc} \\ v_{sd} \\ v_{se} \end{bmatrix} = \frac{V_{dc}}{5} \begin{bmatrix} 4 & -1 & -1 & -1 & -1 \\ -1 & 4 & -1 & -1 & -1 \\ -1 & -1 & 4 & -1 & -1 \\ -1 & -1 & -1 & 4 & -1 \\ -1 & -1 & -1 & -1 & 4 \end{bmatrix} \begin{bmatrix} S_a \\ S_b \\ S_c \\ S_d \\ S_e \end{bmatrix}. \tag{2.34}$$

For the case of the five-phase configuration, there are $2^5 = 32$ possible switching states that lead to the phase voltage values of 0, $\pm 1/5 V_{dc}$, $\pm 2/5 V_{dc}$, $\pm 3/5 V_{dc}$ and $\pm 4/5 V_{dc}$ through (2.34). These states constitute different load conditions from the point of view of the VSI, characterized by the number of load windings connected to the positive and negative rails of the DC-link. The higher the number of phases of the VSI, the higher the number of voltage levels that the converter is capable of generating. This leads to a decrease in the harmonic content and a better reconstruction of the sine wave that is processed by the power converter, as well as the reduction of the common mode voltage [34].

Finally, the 32 possible phase voltages can be mapped into the VSD variables by applying the Clarke's transformation matrix (2.11), producing 32 voltage vectors represented in the α–β and x–y planes (z–axis component can be neglected in the star connection with isolated neutral). Figure 2.5 shows the projections of these vectors in each plane, where they have been numbered by the equivalent decimal number obtained from its corresponding switching state $\mathbf{S} = [S_a\ S_b\ S_c\ S_d\ S_e]^T$, being S_a and S_e the most and the least significant

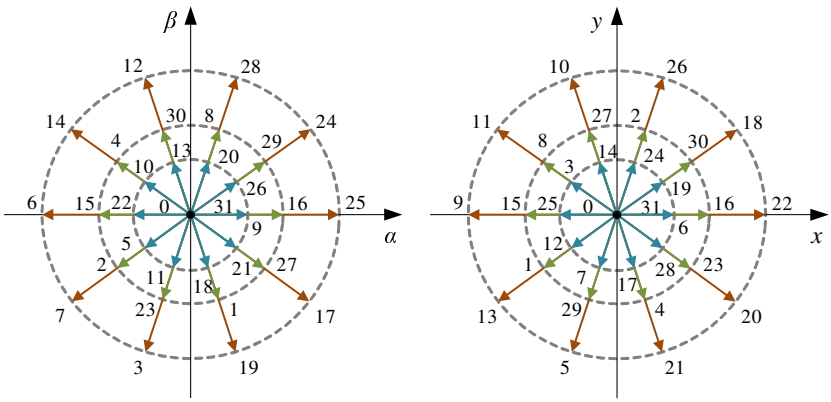

Figure 2.5 Space vector diagrams in the α–β and x–y subspaces.

bits, respectively. It can be seen that there exist 2 null vectors and 30 active vectors, the last ones being classified in large ($0.647V_{dc}$), medium ($0.4V_{dc}$) and short ($0.247V_{dc}$) vectors. Thus, the space is divided in ten sectors of the same size with a separation of $\pi/5$ between them.

2.3 Multiphase drives control techniques

With the increasing interest in multiphase drives for high-power and high-reliability variable-speed applications, the need for high-performance controllers has led the research activity in the last years. Conventionally, they are a complex extension of the ones applied to the three-phase case, and their principal objective is the accurate and fast regulation of the speed and the torque while fully exploiting their advantages. The most widespread control technique applied to multiphase drives in the research literature and in industrial applications is the Vector Control (VC) or FOC. It is based on the use of Proportional-Integral (PI) regulators followed by a PWM stage that linearly provides the VSI switching combination to be applied, and so it can be named as 'linear' controller. On the other hand, novel control strategies are appearing to simplify the multiphase control. These new techniques are based on 'non-linear' controllers, mostly known as 'direct' controllers, which do not include the PWM stage or other form of modulation, but directly commands the VSI forcing the controlled variables to rapidly follow their references. This is the case of the DTC method, which is the leading competitor of the FOC technique in three-phase drives; and the MPC technique, which has recently appeared as a promising alternative due to its flexibility and simple formulation.

In view of the above, it seems necessary to present a brief state-of-the-art in FOC and DTC control techniques, in order to lay the foundation for the definition of the emerging MPC technique. Consequently, this section will be focused on the description of both methodologies and their most recent applications to multiphase drives, particularly to IM drives. After that, a review of MPC controllers, which is the focal point of this Thesis, will be disclosed in Section 2.4.

Field Oriented Control

The basis of the FOC technique, founded at the beginning of the 70s [35, 36], is the independent control of the flux and the torque of the AC machine in a similar way that it is done in a DC machine. For that purpose, a proper transformation of the controlled variables to the d–q plane is mandatory, where the d–axis is aligned with one of the flux components (air-gap, stator or rotor flux) in order to achieve the decoupling. Nowadays, the level of maturity of the FOC for three-phase drives has permitted the total displacement of the DC machines by AC ones in most industrial applications based on variable-speed drives.

This is not the case in multiphase drives, due to the higher number of freedom degrees that increases the complexity of the controller extension, as it is shown in numerous research works mainly based on the Indirect Rotor FOC (IRFOC) [11, 37, 38]. In this particular version of the control technique, the d–current is aligned with the rotor flux through the proper selection of the rotating reference frame angle in the Park's transformation (θ in Figure 2.3). In this way, the machine is solely fluxed by the d–current component while

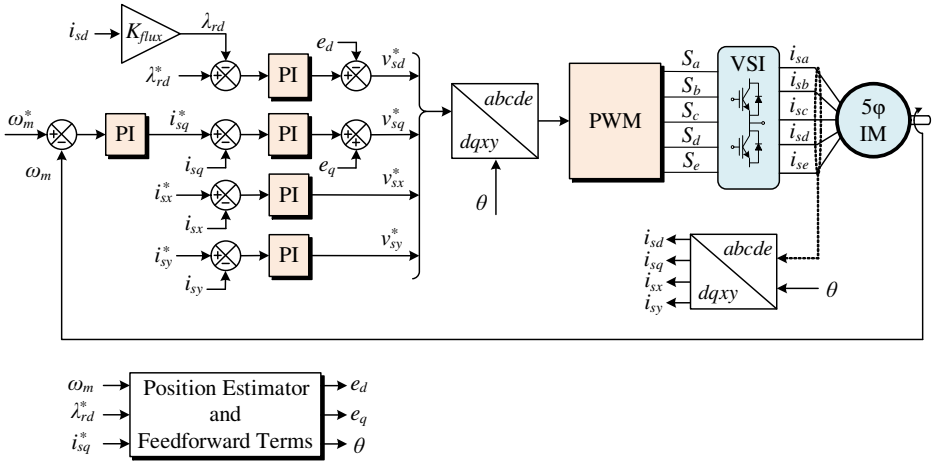

Figure 2.6 IRFOC technique for the distributed-windings five-phase IM drive.

the electromagnetic torque is regulated by the q–component of the stator current. When applying the IRFOC to an IM, the orientation of the rotor flux in the required direction is done through the imposition of the slip speed in the following way:

$$\theta = \int_0^t (\omega_r + \omega_{sl})\, dt = \int_0^t \left(\omega_r + \frac{R_r\, i^*_{sq}}{L_r\, i^*_{sd}}\right) dt \tag{2.35}$$

where reference values of the flux- and torque-producing stator currents (i^*_{sd} and i^*_{sq}) are normally used in the calculation process. However, a good knowledge of some machine's parameters in the previous equation is necessary for a good orientation. Other versions of the FOC technique can be encountered in the literature, the main difference being which flux component is aligned with the d–axis, as well as the estimation method applied in the calculation of the flux angle [25, 36, 39].

The general IRFOC control scheme for a five-phase IM with distributed windings is shown in Figure 2.6. It has the same cascade structure used for three-phase drives, with an outer speed controller and an inner current controller per current component. Both current and speed controllers are typically PI regulators. With this configuration, the speed regulator establishes the q–current reference while the d–current reference is set as constant. Conventionally, its nominal value is selected if the reference speed is below the synchronization speed of the machine, or regulated to deflux the machine if the speed goes beyond the synchronization point. The outputs of the current controllers are the reference voltages that must be applied to the machine in order to follow the current references. In this process, compensations terms, e_d and e_q, are summed to take into account the coupling of the d–q stator voltages equations and compensate in some manner the cross-coupling effect [40]. These terms are highly dependent on the machine's parameters.

The difference of the control scheme with respect to the three-phase case is the incorporation of additional PI regulators for the x–y currents. It should be emphasized

that, although these currents can be theoretically zeroed in distributed winding machines impressing stator voltages with zero x–y components, this is not the case in the reality since stator windings present some level of asymmetry, and the VSI has a dead time that also induces x–y voltages [30, 38]. Consequently, it is necessary to regulate x–y currents to zero. For the case of IMs without isolated neutral point, it is also necessary to include an additional controller for the homopolar current. From this, it is stated that the complexity of the control scheme increases with the number of phases, being necessary to add a higher number of PI regulators that should be independently tuned.

Once the voltage references are given by the PI regulators in the d–q and x–y planes, they are transformed using the inverse of the Park's and Clake's transformations to be expressed in phase variables. After that, these phase voltages are modulated with some type of PWM strategy, conventionally Carrier-Based or Space Vector PWM (CBPWM and SVPWM, respectively) techniques, providing the switching pattern to be released to the VSI. Although these PWM techniques are well established in the three-phase case and the extension of the CBPWM to multiphase drives does not imply further complexity, the same cannot be said for the SVPWM method, whose extension to the multiphase case has been recently investigated [2, 41].

As a final remark, more recent research works in the field of FOC are centered on the fully exploitation of the additional degrees of freedom in multiphase machines. For example, the extension of FOC techniques for the post-fault operation [30, 42, 43], or the torque enhancement through harmonic injection in concentrated-windings induction machines and in permanent magnet machines of different number of phases [44–48].

Direct Torque Control

Another well-established control technique in three-phase drives is the DTC, whose origin took place in mid 80s [49, 50]. Since then, numerous studies have been developed in the three-phase drives' case [51], being initiated the industrial implementation by ABB [52]. The extension of DTC to different multiphase drives topologies has also been proposed [6, 11], being nowadays a competitor to FOC due to its advantageous characteristics of robustness against machine's parameters variation and fast flux and torque responses [53]. In its standard form, the controller maintains the outer PI speed regulator as in FOC, but the inner current controllers are replaced by hysteresis blocks that directly regulate the fluctuations in the flux and the torque with respect to their references. In this case, the PI speed controller provides the torque reference (T_e^*) while the flux reference (λ_s^*) is again set constant or regulated to deflux the machine depending on the speed. Based on the output of these hysteresis blocks and an estimation of the flux position, the appropriate switching vector to be applied is selected through a predefined look-up table that takes into account all possible VSI states. The selected switching vector is directly released to the VSI without the intervention of a PWM stage. Continuing with the distributed windings five-phase drive case example, the described scheme of the DTC is shown in Figure 2.7.

As can be seen, the control structure is simpler than in FOC, since Park's transformation is no longer necessary, and the number of controlled variables is reduced to two, theoretically decreasing the computational cost. However, it presents important disadvantages, such as higher torque ripple and variable switching frequency, which depends

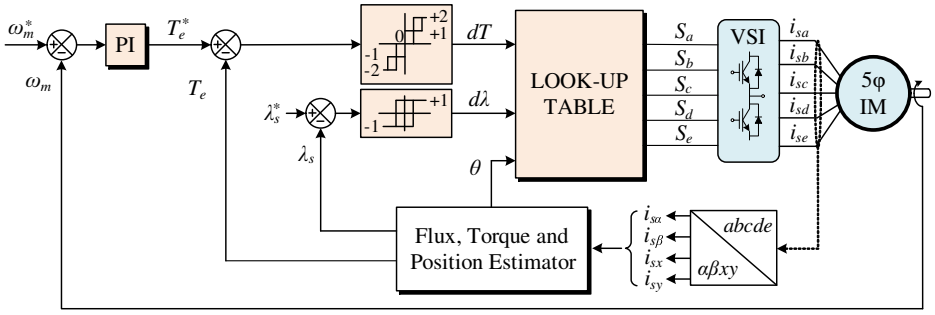

Figure 2.7 DTC technique for the distributed-windings five-phase IM drive.

on the operating point and the bandwidth of the hysteresis controllers. In addition, the control performance is highly dependent on the drive's topology [54]. In order to reduce these disadvantages, some modifications in the DTC structure have been proposed in the literature, such as the inclusion of PWM strategies [55, 56] that leads to constant switching frequency and reduces the harmonic content, particularly on the *x*–*y* plane.

Most importantly, the extension of DTC to multiphase drives cannot completely regulate the *x*–*y* (and homopolar) currents with the basic control structure presented before, since only two variables (flux and torque) are controlled. As it occurs in FOC, these currents must be regulated to zero since they are only related to harmonic components and losses, except for the case of concentrated windings machines. A recursive solution encountered in the literature is the definition of more elaborated look-up tables, or even the introduction of a second look-up table, in order to reduce the low-order harmonics and increase the efficiency [57–59]. Another solution just recently adopted is the use of virtual voltage vectors to nullify the voltages and mitigate the currents in the *x*–*y* plane, while maintaining the original control scheme [32, 60].

Most of the research works in the field of DTC are referred to five- and six-phase induction and permanent magnet machines, however, a recent research work aims to the extension of the DTC technique to a higher number of phases [61]. Also, the fault-tolerance capability of the DTC has been recently addressed for a five-phase IM, being compared with the conventional FOC [62].

2.4 Model Predictive Control

A promising alternative to classical FOC and DTC methods, particularly in the multiphase drives' field, is the model predictive control. This naming identifies a wide range of control techniques, whose functioning principle is based on prediction of the future behaviour of the system's variables employing a mathematical model. These predictions are used to select the optimal control action to be applied according to a predefined cost function, which represents the control objectives [63]. The simplicity and intuitive formulation of the control problem has boosted the interest of the research community in the MPC strategy applied to electric drives [2, 11]. Another reason has been the possibility to perform multi-objective and multi-variable control, or even to include non-linearities

or constraints to the control process, just defining a proper cost function. This permits eliminating the classical cascade structure in FOC, reduces the complexity of the controller and provides a fast dynamic response. Likewise, the high control flexibility of the MPC makes it a real alternative to DTC in the multiphase drive control area, since the main disadvantage of DTC is that it can manage the control of only two variables in its most conventional form.

However, MPC faces the important limitation of the high computational cost required to solve the optimization problem for all considered control actions, which increases when the number of phases grows. For that reason, although the concept of MPC was developed in the 70s, its use has been traditionally restricted to systems with a slow dynamic that permits performing the required calculations. This is the case of the petrochemical industry, which has constituted one of its main application fields during a long time [63, 64].

Only with the recent development of fast and powerful microprocessors, the use of MPC in power converters and electric drives has become affordable [65]. Since then, the research activity in the field has given rise to numerous control approaches, being quite difficult to develop a general classification for all MPC techniques. Conventionally, they are divided in two wide categories: Finite-Control-Set MPC (FCS-MPC) and Continuous-Control-Set MPC (CCS-MPC) [66–68]. In both cases, the control principle is the same, i.e., a predictive model is used to calculate the optimal control action according to the control objective. The main differences between them relate to the type of mathematical model used for the predictions and how the control actions are applied to the system. In the FCS-MPC method, a discrete model of the system is used to compute the predictions and a predefined cost function determines the control objectives, usually composed by the errors between the predictions of the controlled variables and their references. Considering that the power converter that supplies the machine presents a finite nature, with a limited number of possible switching states, the FCS-MPC takes advantage of this situation and the optimal switching state that minimizes the cost function is selected after an iterative process (optimization problem). The selected switching state of the power converter is then directly applied without any kind of modulator. On the other hand, a linearized or average model of the system is used in the CCS-MPC approach in order to provide continuous voltage references according to the control objective. Afterwards, the continuous voltages are modulated, conventionally by a PWM stage, providing the switching pattern to be applied to the power converter.

The differences between FCS-MPC and CCS-MPC schemes expose important advantages and disadvantages of both approaches. The inclusion of a modulator in the CCS-MPC eliminates the online optimization and fixes the switching frequency to a constant value, in contrast to the FCS-MPC where the switching frequency is variable. However, CCS-MPC offers a less flexible and more complex control scheme than FCS-MPC does, as a result of not taking into account the discrete nature of the power converter. For that reason, most of the research activity in relation with the MPC control of multiphase drives is focused on the FCS-MPC technique. In this regard, the five-phase and six-phase machine topologies constitute the center of attention, both of induction or permanent magnet types [11, 65, 69]. The extension of the FCS-MPC to a higher number of phases is still difficult due to the exponential increase of the computational cost that it implies.

Independently of the predictive control structure, the most common application of MPC

for multiphase drives is the result of its combination with a FOC technique. In this way, the outer speed control loop is maintained while the inner current regulators are substituted by a MPC current control. This control scheme is usually named Predictive Current Control (PCC) [70–74]. A comparative analysis between FOC and PCC techniques can be encountered in [73] and [74], where it is concluded that a better transient performance is obtained using predictive controllers. However, steady-state performance is superior with FOC, especially in terms of harmonic content in the controlled currents. Furthermore, the tuning of PCC requires less effort in contrast to FOC. As an alternative to the current regulation, the MPC scheme can be changed in order to control the flux and the torque while maintaining the outer speed control loop. This scheme is named Predictive Torque Control (PTC) [75–79] and appears as a big competitor of DTC. This is demonstrated in [79], where the comparison between both techniques is performed and analyzed. Although DTC is less computationally demanding than PTC, the later provides an extra flexibility for the regulation of non-torque/flux producing currents. As a result, the torque ripple is reduced in comparison with DTC, and faster torque and speed responses are observed. Further on, few proposals present a MPC approach in which both currents and speed are totally regulated with a MPC technique, and they are mostly referred to the three-phase case [80, 81].

Apart from the high computational cost, the application of the MPC technique to multiphase drives presents some important drawbacks, on which the research activity is currently focused. For the case of the FCS-MPC current controller, which constitutes the nucleus of this Thesis work and the major concern of the research community, these additional disadvantages are:

- The high harmonic distortion that appears in the controlled currents. This is a direct consequence of the absent of a modulator and the fixed-time discretization nature of the control implementation, where only one control action is applied within a sampling period.
- The high interdependence of the control performance with the predictive model. As a consequence, aspects not reflected in the predictive model act as disturbances that can damage the system performance. This is the case of non-modeled effects, variations in the machine's parameters, and non-measurable system variables such as rotor quantities in the IM case.

In the following sections, the general scheme of the FCS-MPC current control for the five-phase IM is presented. Afterwards, some implementation and design issues directly related with previous drawbacks are analyzed and disclosed, reviewing the recent proposals in the literature that try to alleviate them.

2.4.1 General scheme of the FCS-MPC

The basic scheme of FCS-MPC is shown in Figure 2.8, where the symmetrical five-phase IM fed by a two-level five-phase VSI is used as case example. This will be the basic scheme for the research work performed in this Thesis, so an in-depth description of its structure is presented hereafter. As it was previously described, the FCS-MPC scheme is conventionally constituted by an outer speed control loop based on a FOC strategy, and an

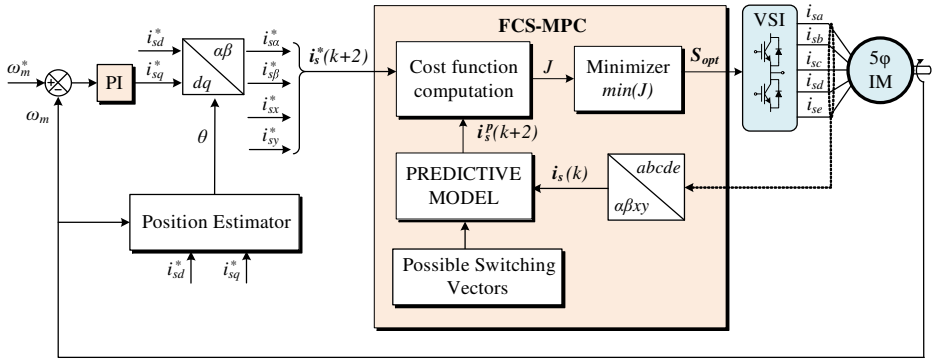

Figure 2.8 FCS-MPC technique for the distributed-windings five-phase IM drive.

inner stator current control loop based on the FCS-MPC. Notice that the described control scheme is formed by a fast inner current controller and an outer slower speed regulator that leads to a higher control bandwidth compared with the conventional cascade structure of FOC [82].

The main objective of the FCS-MPC stator current controller is to determine, at every sampling time, the most adequate switching vector of the VSI ($\mathbf{S}_{opt}$) that must be applied in order to track the stator current references ($\mathbf{i}_{\mathbf{s}}^{*}$) previously defined. To this end, a discrete model of the system, commonly named predictive model, is used to predict the future behaviour of the currents ($\mathbf{i}_{\mathbf{s}}^{p}$) for a certain prediction horizon. These predictions are computed for all possible switching vectors (32 for the case of the five-phase IM drive) using the real values of the stator currents and the mechanical rotor speed ($\mathbf{i}_{\mathbf{s}}$ and ω_m), which are measured through appropriate attached sensors. Then, the predictions are compared with their references in a cost function (J) that represents the control objectives. The minimization of the cost function gives as a result the switching state that must be applied to the VSI during the entire sampling period. After that, a receding horizon strategy is applied and the whole process is repeated in the next sampling instant. The flow diagram of the described process is presented in Figure 2.9.

The predictive model is obtained from the combination of the electrical equations of the IM expressed in terms of the VSD variables (2.15)–(2.16), and the VSI equation (2.34). The result is represented in the state-space form, as it is shown in (2.36). The state vector is composed by the stator and rotor currents in the α–β–x–y reference frame $\mathbf{x} = [i_{s\alpha}\, i_{s\beta}\, i_{sx}\, i_{sy}\, i_{r\alpha}\, i_{r\beta}]^T$, the control action is the switching vector $\mathbf{S}$, the controlled variables are the stator currents $\mathbf{x_s} = [i_{s\alpha}\, i_{s\beta}\, i_{sx}\, i_{sy}]^T$, and matrices $\mathbf{A}$ and $\mathbf{B}$ depend on the electrical machine's parameters and the present value of the rotor speed [71]. Notice that a similar formulation is obtained for any multiphase machine with a higher number of phase, with the difference of additional equations for the extra planes.

$$\begin{aligned} \frac{d\mathbf{x}}{dt}(t) &= \mathbf{A}\,\mathbf{x}(t) + \mathbf{B}\,\mathbf{S}(t) \\ \mathbf{x_s}(t) &= \mathbf{C}\,\mathbf{x}(t) \end{aligned} \tag{2.36}$$

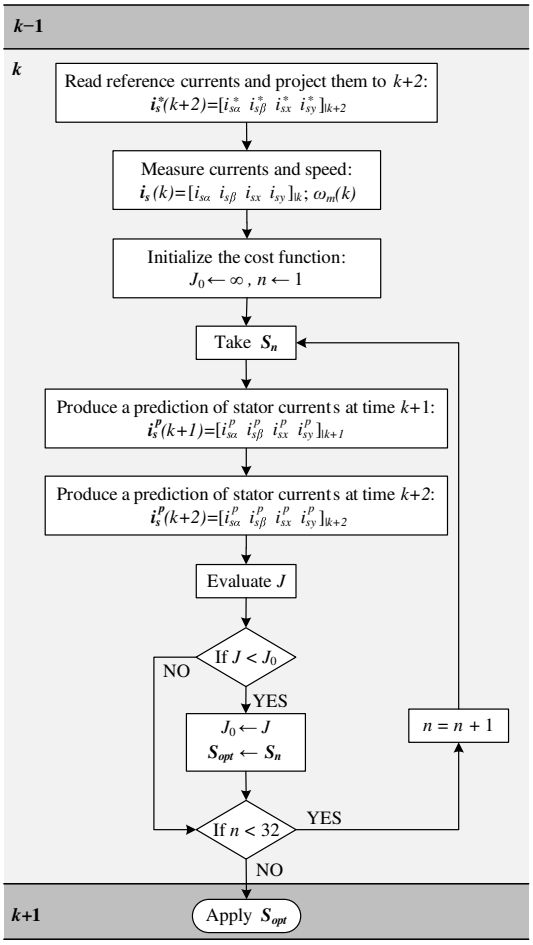

Figure 2.9 Flow diagram of the FCS-MPC technique.

Afterwards, this time-varying model is discretized in order to fit the discrete nature of the controller. For that purpose, an appropriate discretization technique is used. The forward Euler method is the choice of most FCS-MPC practitioners due to its simplicity, although different techniques can be used, as it will be detailed in the next section. As a result, the general expression of the predictive model is the following:

$$\begin{aligned}\mathbf{x}^{\boldsymbol{p}}(k+1) &= \mathbf{x}(k) + T_s(\mathbf{A}\,\mathbf{x}(k) + \mathbf{B}\,\mathbf{S}(k)) \\ \mathbf{x}_{\mathbf{s}}^{\boldsymbol{p}}(k+1) &= \mathbf{C}\,\mathbf{x}^{\boldsymbol{p}}(k+1)\end{aligned} \tag{2.37}$$

where T_s is the sampling time used in the discretization process and superscript p indicates predicted values. Some FCS-MPC approaches replace the rotor currents by the rotor fluxes $\lambda_{r\alpha}$ and $\lambda_{r\beta}$ [83], or represent the system's model in the rotating reference frame d–q [73]. In the latter case, the measured currents must be also rotated into the d–q

plane after the application of the Clarke's transformation. It is important to highlight the necessity to know the value of the rotor variables in order to compute the prediction of the stator currents. These variables cannot be usually measured in IMs, but they are estimated through the same predictive model and using past values of the stator and rotor currents [73]. Other conventional solution consists in gathering all unknown quantities of the system's model and other uncertainties into one single term, thus constituting a new state variable. This new variable is tracked and updated at every sampling instant using, again, the system's model and past measured values of the variables [71]. Considering the case under study, this technique leads to the new predictive model in (2.38), where $\mathbf{G^e}(k)$ is an estimation of the rotor currents' contribution to the stator currents. This estimation is done holding the previous value $\mathbf{G^e}(k-1)$, which is computed at instant k applying (2.39). In these equations, $\bar{\mathbf{A}}$ and $\bar{\mathbf{B}}$ are sub-matrices derived from the original ones through simple mathematical calculations.

$$\mathbf{x_s^p}(k+1) = \mathbf{x_s}(k) + T_s(\bar{\mathbf{A}}\,\mathbf{x_s}(k) + \bar{\mathbf{B}}\,\mathbf{S}(k)) + \mathbf{G^e}(k) \tag{2.38}$$

$$\mathbf{G^e}(k) = \mathbf{G^e}(k-1) = \mathbf{x_s}(k) - \mathbf{x_s}(k-1) - T_s(\bar{\mathbf{A}}\,\mathbf{x_s}(k-1) + \bar{\mathbf{B}}\,\mathbf{S}(k-1)) \tag{2.39}$$

Using either (2.37) or (2.38), the future values of the stator currents at instant $k+1$ are computed using the measured values at instant k for each possible switching vector. The one that minimizes the control objective is selected and applied, ideally at instant k. However, the time required for the measurement, predictions' calculation and selection of the optimal control action can be significant. Furthermore, this time is usually similar to the sampling time T_s, leading to an important delay between the instant when the measurements are done and used for predictions, and the instant when the next control action is released. As a result, the selected control action is not applied at the correct moment producing a bad tracking of the references. This effect, which has been studied in the research literature [71, 84], can be corrected using different methods. The most common and simple one is the second-step ahead prediction that consists in computing predictions for $k+2$ and applying the selected switching vector at $k+1$ (see Figure 2.9). Taking this into account, the predictive model is iterated two times and the cost function is defined for instant $k+2$ as follows:

$$\begin{aligned} J =& (i^p_{s\alpha}(k+2) - i^*_{s\alpha}(k+2))^2 + (i^p_{s\beta}(k+2) - i^*_{s\beta}(k+2))^2 + \\ &+ K_{xy}\,(i^p_{sx}(k+2) - i^*_{sx}(k+2))^2 + K_{xy}\,(i^p_{sy}(k+2) - i^*_{sy}(k+2))^2. \end{aligned} \tag{2.40}$$

As commented before, the cost function is conventionally constituted by the squared error between the stator current predictions and their references, and a common formulation in FCS-MPC current control of multiphase drives is the one presented in (2.40). Parameter K_{xy} is a weighting factor that permits to put more or less emphasis in the tracking of the x–y currents. However, different alternatives can be defined in order to include several control constraints and, thus, optimize the system performance. In that case, the definition of proper weighting factors for each control constraint is also possible. This flexibility is one of the main advantages of the FCS-MPC technique in comparison with classical

control methods.

Stator current references are provided by the external FOC-based speed controller, being the IRFOC approach used in this case, as shown in Figure 2.8. Thus, a PI regulator provides the reference for the torque-producing current (i^*_{sq}), based on the difference between the measured speed and its reference. Conversely, the machine is fluxed by imposing a constant value of i^*_{sd} equal to the nominal one and the losses are minimized by setting null references for the x–y currents (note that it is assumed that the machine is working below the nominal speed and a defluxing regulation is not considered). Afterwards, the d–q stator current references are rotated into the α–β plane using the inverse of the Park's transformation (2.21) and the estimation of the electrical angle θ (2.35). In order to be implemented in a microprocessor, equation (2.35) is discretized, usually applying a trapezoidal rule that uses past measured and estimated values at time instant k:

$$\theta(k+1) = \theta(k) + T_s(\omega_{sl}(k) + P\omega_m(k)). \tag{2.41}$$

It is finally interesting to highlight that the prediction horizon after the delay compensation is 2, so proper formulation of the rotating angle must be derived in order to estimate the future stator current references for instant $k+2$. This is possible assuming constant d–q current references for a sufficiently small sampling time [85].

2.4.2 Key design and implementation features in FCS-MPC

Currently, the control system technology finds itself in a paradigm-changing tipping point in which more demanding control goals, system flexibility and functionalities required by emerging applications are driving the control system development. In this context, FCS-MPC has proven to be a promising alternative in the control of multiphase drives, however it is far from being mature yet, showing important limitations that require attention. This is the case of the high computational cost, the harmonic content in the controlled variables, and the sensitivity to inaccuracies/uncertainties in the model, such as system's parameter mismatch and non-measurable rotor variables among the most concerning ones.

In this section, some implementation and design issues directly related to the quality of the control performance, as well as to the mentioned disadvantages, are commented. Recent proposals in the research literature that try to improve the control system operation and alleviate its limitations are also exposed.

Cost function design

In conventional FCS-MPC, the control goal is the tracking of the controlled variables according to their references. Thus, the cost function is formed by the difference between the predicted values of the controlled variables and their references, using an absolute or a quadratic norm for the error evaluation [65]. Both norms provide similar results in terms of tracking when only one error term is considered in the cost function, but the quadratic error is preferable when several error terms are evaluated [85], so it constitutes the usual selection in multiphase drives. For instance, in FCS-MPC current control the cost function only depends on the squared current error, as it was shown in (2.40) for the case of the five-phase IM drive. Conversely, when a FCS-MPC torque control is implemented, the

cost function is constituted by the error in the flux and torque tracking:

$$J = (T_e^p(k+2) - T_e^*(k+2))^2 + K_\lambda \left(|\boldsymbol{\lambda}_\mathbf{s}^\mathbf{p}(k+2)| - |\boldsymbol{\lambda}_\mathbf{s}^*(k+2)|\right)^2. \tag{2.42}$$

Regardless of the controlled variables, it is a common practice to include weighting factors (K_{xy}, K_λ) when several terms are considered in the control objective, specially when they are of different nature. This permits adjusting the importance of each controlled variable. Additionally, the cost function provides high flexibility to include additional terms that represent supplementary control objectives, as it was previously commented. Consequently, it is possible to improve several control aspects just modifying the cost function [68]. Concerning multiphase drives, several examples can be encountered in the literature. In [83], the cost function is designed in order to additionally reduce the common mode voltage in the FCS-MPC current control of a five-phase IM drive. The reduction or limitation of the switching frequency in the power converter (VSI losses) has also been studied in [77] for the torque control of a PMSM, and in [86] for the current control of a five-phase IM. This is achieved by restricting the number of commutations of the power switches at each sampling period. Another non-conventional control objective, barely applied to multiphase drives, is the reduction of the harmonic content in the controlled variables through the imposition of specific pulse patterns in the VSI or by the selective harmonic elimination. These techniques, particularly the last one, can require complex formulations/calculations and its application is principally restricted to particular topologies of power converters [67, 87–89].

Further on, the flexibility of the FCS-MPC permits the inclusion of non-linearities or constraints in the cost function, something that is more complicated to achieve using linear controllers. This is usually done by adding non-linear terms in the cost function, e.g. logic functions, which are multiplied by larger weighting factors. Thus, the control actions that do not comply with the restrictions are discarded during the optimization problem. Some examples can be found in [75, 79, 90] for the FCS-MPC torque control of multiphase drives, where the stator currents are limited to a maximum value in order to avoid over-current situations during transients.

In all previously described cases, the use of weighting factors is common. However, the performance of the controller can drastically change depending on the selected value of these weighting factors. Consequently, it is necessary to properly tune these parameters for the considered application and control requirements. This is usually done through trial and error experiments [91], or using more complex optimization algorithms [68, 86, 92]. In any case, the optimal selection is based on some established figures of merits, such as current tracking error, harmonic content or switching losses. For example, the weighting factors can be configured in order to provide a good current tracking performance while maintaining a reduced commutation losses [86]. However, the tuning of the weighting factors is not an easy task in some cases, since the optimal value can vary depending on the considered operating point, among other causes. As an example, in [73] the FCS-MPC current control of a five-phase IM is studied using the cost function in (2.40), where different sets of possible switching vectors are considered in the optimization process. This study concludes that the value of K_{xy} that provides a good trade-off between the current control in the primary plane and in the secondary plane can be slightly different

depending on the considered set of switching states and the operating point. A deeper analysis of the situation is performed in a recent research work [93], where it is stated that some of the figures of merit conventionally used in the tuning process are not independent (e.g. the harmonic content is directly related with the switching frequency). Consequently, there exist fundamental trade-offs that cannot be overcome just by the cost function design.

Predictive model design

The predictive model constitutes another key element in the performance of any MPC controller, since the selected control actions during the optimization problem depend on it. This implies that the more accurate the designed predictive model is, the more precise the predictions are and, consequently, the performance of the control system improves. Direct consequences of inaccurate predictions can be the increment in the steady-state tracking error or in the harmonic content of the controlled variables. However, the degree of complexity of the predictive model must guarantee a compromise between accuracy and computational burden.

In this regard, important aspects must be discussed, being the first one the discretization technique used in the design process of the predictive model. Although there exist several alternatives, the first-order forward Euler approximation is usually enough to obtain an accurate discrete model of a system, thus constituting the most widespread election for multiphase drives. It was previously seen that the application of the forward Euler discretization provides the predictive model in (2.37) for the five-phase IM case. This is a simple formulation that requires easy calculations, only being necessary to update the matrices' coefficients related to the rotor speed every sampling period. However, there are special situations where an alternative strategy is required, as it is the case of systems with an order greater than one, when the sampling frequency is too low or when there exist high pass filters in the plant. In these cases, a bilinear discretization or the so-called 'exact discretization' is more convenient. In the last years, the use of the exact discretization has appeared in some research works in relation with the FCS-MPC control of multiphase drives [63, 83, 94]. The triggering factor was the work in [75], where it was stated that the discretization technique based on the Cayley-Hamilton theorem provides better tracking and prediction performances than conventional Euler methods. Continuing with the five-phase IM drive example, the discretization of the system's equations using this method leads to the following predictive model:

$$\begin{aligned} \mathbf{x}^{\boldsymbol{p}}(k+1) &= \Phi\,\mathbf{x}(k) + \Gamma\,\mathbf{S}(k) \\ \mathbf{x}_{\mathbf{s}}^{\boldsymbol{p}}(k+1) &= \mathbf{C}\,\mathbf{x}^{\boldsymbol{p}}(k+1) \end{aligned} \tag{2.43}$$

where the new matrices are defined as $\Phi = e^{\mathbf{A}\,T_s}$ and $\Gamma = \int_0^{T_s} e^{\mathbf{A}\,t}\,\mathbf{B}\,dt$. Since matrix $\mathbf{A}$ depends on the instantaneous value of the rotor speed, the computation of these matrices is not straightforward and requires complex calculations. This constitutes the principal disadvantage of this discretization technique comparing with Euler approaches. Nonetheless, it is possible to simplify the calculations to some extend using the Cayley-Hamilton theorem and supposing that the mechanical dynamic is slow enough during a sampling period to consider constant rotor speed, as it is described in [75] and [95].

Table 2.1 Qualitative results of the sensitivity analysis to parameter variation performed in [94] for the FCS-MPC current control of a five-phase IM drive.

Impact on the system performance	L_m	R_r	L_{ls}	R_s	L_{lr}
Speed performance	–	–	–	–	–
Phase current RMS error	↑↑↑	↑↑↑	↑	–	–
d–q current performance	↑↑↑	↑↑↑	↑↑	↑	–
x–y current performance	↑↑↑	↑↑↑	↑	–	–

Another important aspect related to the predictive model is its high dependence on the system's parameters. For the case of electric drives, the electrical parameters of the machine are commonly estimated using offline methods, as the ones described in [27, 28, 96], and it is assumed a good agreement with the reality during the whole system operation. However, this is far from being a real assumption, since these parameters may not be precisely estimated and usually their values vary during operation due to thermal, saturation or deep-bar effects, which are not considered during the offline parameter estimation process. As a consequence, the parameter uncertainty can lead to inaccurate predictions, deteriorating the performance and stability of the predictive algorithm. This issue has been recently investigated in the literature, being the conventional three-phase power converters and permanent magnet drives the main focus [97–101]. In general, it is seen that errors in the inductances of the system are usually related to current ripple, while variation in resistances or flux linkages (in the case of permanent magnet machines) mostly affect steady-state errors and dynamic response.

Conversely, the sensitivity to parameters in the field of multiphase drives, where more electrical variables must be taken into account due to the higher degrees of freedom, has been barely investigated and only two significant sensitivity analyses can be encountered for a five-phase IM drive [94, 102]. Particularly, experimental results are conducted in [94] for a wide range of operating conditions and machine's parameters detuning. The obtained conclusions reveals that the FCS-MPC performance in terms of phase-current tracking is principally altered by the detuning of the mutual inductance (L_m) and the rotor resistance (R_r). Furthermore, this effect is boosted by changes in the operating point. On the contrary, stator leakage inductance (L_{ls}) hardly affects, and the impact of the stator resistance (R_s) and the rotor leakage inductance (L_{lr}) is negligible. A deeper analysis reports that the current control performance in the *d–q* and *x–y* planes is also principally influenced by the variations in L_m and R_r. Thus, inferior flux and torque regulation with higher harmonic content and cooper losses are reported when large variations are introduced in these parameters. In this concern, the *d–q* current tracking performance is slightly altered by the detuning of L_{ls} and R_s, while the electrical noise content in the *x–y* currents is not much influenced by changes on L_{ls}. It is important to highlight that disturbances in the speed response are not reported in any experimental test for the considered ranges of parameter detuning. A summary of the described conclusions are presented in Table 2.1, where symbol '–' indicates negligible impact.

Several online techniques have been proposed in the literature to cope with the parameter mismatch, as well as with other uncertainties and non-modeled effects that can compromise

the performance of the predictive controller. The main objective is to provide robustness and stability to the predictive controller against these disturbances. Some proposals are based on online parameter identification algorithms [100, 103], but the major interest is given to the use of adaptive and disturbance observers [90, 98, 104–107]. The observer theory permits the estimation of not only the parameter deviations, but also other unknown system variables, such as rotor fluxes, rotor position or speed (in the case of sensorless control). With these methods, an online estimation of these uncertainties is performed inside the control algorithm, where the same mathematical system's models and measured information that are employed for the prediction calculations are conventionally used. However, these models are slightly modified in the case of the observer technique, where some correction terms are added. This suppose that the observer will require a tuning process in most cases. As a consequence of the computation of the uncertainties' estimations, the system performance in terms of harmonic content, torque ripple and commutation losses is generally improved. It must be highlighted that these conclusions were obtained for conventional three-phase machines, particularly the PMSM topology, so special attention must be paid in the total computational burden in their extension to the multiphase case.

Implementation of the control algorithm

It is well-known that the FCS-MPC suffers from a considerable computational cost, particularly when it is applied to multiphase drives. To illustrate this issue, a particular real-time implementation of the FCS-MPC technique in a TMS320F28335 microprocessor is shown in Figure 2.10. The relative time-consuming load of every implemented task in a sampling period is represented using the FCS-MPC current control of the five-phase IM drive as a case example. It can be seen that the predictive current control algorithm constitutes the most time-demanding task, while the IRFOC-based speed controller is not heavy from the computational cost perspective.

In order to alleviate this problem, it is possible to consider a reduced set of switching vectors in the optimization algorithm of the FCS-MPC. This approach has been tested in [70, 71] for a six-phase IM drive, reducing the number of switching vectors from 64 to 49 and 13. However, suboptimal solutions are obtained since not all possible

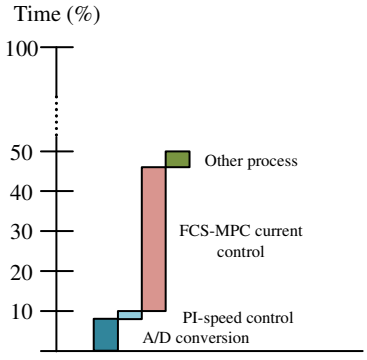

Figure 2.10 Real-time implementation and task distribution during a sampling period of the FCS-MPC current control applied to the five-phase IM drive.

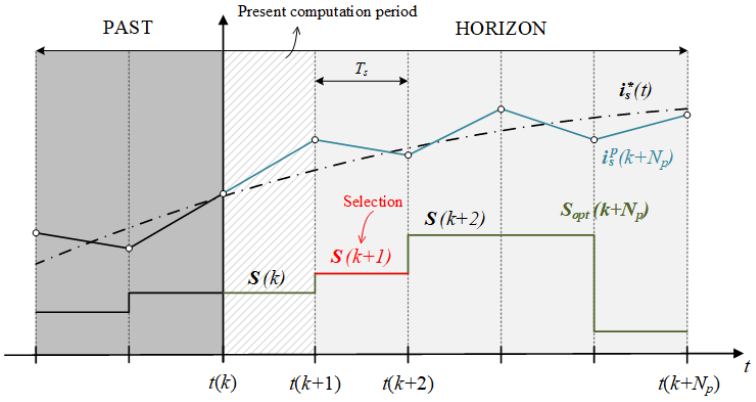

Figure 2.11 Schematic representation of the optimal switching vector selection in FCS-MPC with prediction horizon N_p.

control actions are considered, and this can be detrimental to other control performance aspects. Another proposal based on the previous ones is presented in [108]. Its basic functioning is the application of an algorithm, at every sampling time and before the optimization problem computation, in order to find a subgroup of possible switching vectors that comply with some conditions. These conditions look for the limitation of the power switching commutations, so this technique also provides lower average switching frequencies comparing with conventional FCS-MPC approaches. A more recent alternative in [109] proposes the selection of a subgroup of voltage vectors based on the instantaneous flux position and the torque deviation in the α–β–x–y axes for the PTC control of a PMSM. The imposed conditions principally try to reduce the harmonic and flux content in the x–y subspace. It is however remarkable that, in all cited techniques, a group of possible control actions are discarded, and the potential of using all available control actions is not fully exploited in the compliance of the main control objectives.

Concerning the FCS-MPC steady-state response, interesting alternatives to the conventional control algorithm can be encountered in the literature with the aim of improving the system performance. One of them is the use of an extended prediction horizon [110], defined as the number of future time instants that the controlled variables will be predicted in order to select the optimal control action. There exist different variations of this technique in its application to power converter and electric drives [111]. As an example, consider the case in which the switching horizon is equal to 1 ($N_s = 1$) and the prediction horizon is equal or superior to 2 ($N_p \geq 2$). The optimization algorithm has to find the optimal sequence of switching vectors $\mathbf{S_{opt}} = [\mathbf{S}(k+1)\,\mathbf{S}(k+2)\ldots\mathbf{S}(k+N_p)]$ that must be applied to the power converter in order to follow the imposed reference in the whole considered prediction horizon. Thus, predictions must be computed for all possible switching vectors and all time instants covered by the prediction horizon. In other words, the number of computed predictions reaches $(N_p - 1)\,2^n$, being n the number of phases in the converter. Afterwards, only the first switching vector in the selected sequence is applied at the next sampling instant (the process is illustrated in Figure 2.11). Although it has been demons-

trated that long prediction horizons can improve the FCS-MPC performance, particularly in relation with the harmonic content and steady-state error, the computational burden can be enormous. For this reason, advanced optimization algorithms are usually applied, such as move-blocking and extrapolation strategies, and combined with a compromise between performance improvement and computational burden [111]. However, there are still cases where the high calculation time introduced by long prediction horizons is hardly affordable at a reasonable cost with the computing capability of modern microprocessors and electronic devices. This is the case of multiphase drives.

Different approaches can be found with the more specific objective of reducing the harmonic content in the controlled variables. As it was previously stated, the main origin of this problem is the fixed-sampling nature of the FCS-MPC algorithm combined with the absence of a modulator. As a result, only one switching vector is applied in a sampling period but it can be maintained during several periods, hence its total application time depends on the imposed sampling time. This has a high impact on the harmonic content of the currents, as it has been recently studied in [112], leading to a spread spectrum with a significant amount of harmonics and electrical noise. Some recent research works mitigate this problem applying two or more switching vectors during the same sampling period, which can be seen as a kind of modulation process. For example, in [113] a combination of a zero and an active vector is applied every sampling instant, being the active vector selected following the same optimization problem than the one employed in the conventional FCS-MPC scheme. Then, the application time of the active vector is computed using a linearized and reduced order model that depends on predicted, measured and reference values of the controlled variables. Similar approaches can be found in [114, 115], where proper PWM methods are applied and fixed switching frequency is guaranteed. Finally, another strategy consists in the use of virtual voltage vectors instead of the conventional VSI's switching vectors, in a similar way that it is done in the DTC technique [116, 117]. The obtained results have demonstrated the improvement in the controller efficiency by reducing the harmonic content, mainly in the x–y plane. However, this technique tends to provide higher switching frequencies than the conventional approach in some cases and reduces the available voltage limits.

2.5 Contributions in the context

Main advantages and limitations of the predictive controller have been detailed in previous sections, being the high computational cost and the current harmonic content the most concerning ones. A proper predictive model design can be crucial in the FCS-MPC performance, contributing to alleviate these limitations. In this regard, the estimation of non-measurable variables that form part of the predictive model can be essential. Although the observer theory has been proven to be promising in the disturbance estimation field, their applications are mainly related to three-phase converters and drives and for the estimation of unknown variables in the PTC, FOC and sensorless control. One objective of this Thesis work is the extension of the observer theory to the multiphase case in order to effectively reduce the harmonic content and give robustness against parameter mismatch, while maintaining an affordable computational cost. Chapter 3 summarizes this research

line, where different Luenberger-based observers are introduced in the FCS-MPC control of a five-phase IM drive for the rotor current estimation.

The research work concludes with the introduction of an innovative predictive control technique detailed in Chapter 4 that reduces the current harmonic content in electric drives. Its basic principle consists in giving freedom to the sampling time value, i.e., applying variable sampling times. The proposal deviates from recent techniques that include a kind of modulation stage in the FCS-MPC, and from the technique proposed in [118] where the idea of variable sampling time is presented for the FCS-MPC current control of a three-phase converter. In the proposal, the sampling time is selected from a limited number of possibilities together with the switching vector through a time-consuming optimization algorithm. This basic idea is presented and extended to the multiphase case, using the five-phase IM drive with distributed and symmetrical windings as a case example.

Chapter 3

Rotor Observer for Harmonic Content Reduction

One of the main concerns in model predictive control is the accuracy of the predictive model. The selection of the switching state to be applied in the power converter is based on the predictions made by this model, and inaccurate predictions can lead to the application of non-optimal or even wrong control actions. As a consequence, the control system performance can be deteriorated and higher harmonic content in the controlled variables can appear, which is one of the main disadvantages of the application of predictive controllers to multiphase drives. As it was reviewed in the previous chapter, several techniques have been proposed in the literature in order to improve the system's model. An example is the application of observers for the estimation of non-measurable magnitudes and disturbances of the system.

Although the observer theory has been satisfactorily applied to electric drives for the estimation of unknown system's variables and disturbances, observers have been principally used in FOC and sensorless controllers and for fault detection. In this Thesis work, the observer theory is extended to the rotor current estimation for the FCS-MPC current control of multiphase IM drives, replacing the traditional backtracking procedure where non-measurable parts of the system model are gathered into one simple term that is actualized at each sampling period. The observer design is conducted based on the Luenberger theory that requires the solution of a sometimes complex pole placement problem. As an innovation, a Butterworth polynomial is used to place the poles of the observer, providing a good trade-off between stability and fast convergence to zero of the estimation error, and simplifying the pole placement problem. Also, two observer configurations are studied, a full-order and a reduced-order observer, which differ in the number of currents that are estimated. Simulation and experimental tests have been developed in a five-phase induction machine with symmetrical and distributed windings, as well as a mathematical analysis of the designed observers. The proposal have been also compared with traditional FCS-MPC approaches where the aforementioned backtracking procedure is used for the rotor estimation.

The main results derived from this research work are presented in the two contributions

listed below, which have been published in high-quality peer-reviewed international journals. In Contribution 1, a reduced-order version of the rotor current observer is used and optimized, and simulations and experiments are carried out for different operating points of the five-phase IM drive. In all considered operating conditions, the most conventional FCS-MPC techniques are compared with the proposal in order to present a complete comparative assessment. This comparative study has brought out the effectiveness of the observer in the improvement of the current predictions and, consequently, the current tracking performance. Furthermore, the harmonic content in the controlled currents is effectively reduced, as well as the switching frequency. The additional computational requirement derived from the inclusion of the rotor observer in the FCS-MPC technique is insignificant, what supports the viability of the proposal.

The previous study is extended in Contribution 2 with the definition of a full-order observer where both the rotor and stator currents are estimated. A mathematical analysis of this second approach reveals a high robustness of the observer to model uncertainties, in opposition to the conventional estimation method. Experimental results corroborate previous analysis and conclude that the full-order observer further improves the system performance in comparison with the reduced-order version.

- **Contribution 1:** C. Martin, M. R. Arahal, F. Barrero, and M. J. Duran, "Five-Phase Induction Motor Rotor Current Observer for Finite Control Set Model Predictive Control of Stator Current", *IEEE Transactions on Industrial Electronics*, vol. 63, no. 7, pp. 4527-4538, July 2016.

  DOI: 10.1109/TIE.2016.2536578.

  Times cited: 33 (Google Scholar, 8 June 2019).

- **Contribution 2:** C. Martin, M. R. Arahal, F. Barrero, and M. J. Duran, "Multiphase rotor current observers for current predictive control: A five-phase case study", *Control Engineering Practice*, vol. 49, pp. 101-111, April 2016.

  DOI: 10.1016/j.conengprac.2016.01.011.

  Times cited: 13 (Google Scholar, 8 June 2019).

IEEE TRANSACTIONS ON INDUSTRIAL ELECTRONICS

Five-Phase Induction Motor Rotor Current Observer for Finite Control Set Model Predictive Control of Stator Current

Cristina Martín, Manuel R. Arahal, *Member, IEEE,* Federico Barrero, *Senior Member, IEEE,* and Mario J. Durán

***Abstract*—Model predictive control (MPC) has recently been applied to induction motor (IM) drives in a configuration known as finite control set MPC (FCS-MPC). Its implementation must solve the problem of estimating rotor quantities, a task that is usually done using a simple backtracking procedure. On the other hand, observers have been used with field-oriented control (FOC), sensorless drives and for fault detection but they have not been used yet for finite control set predictive current control of drives. This paper shows the benefits of incorporating a rotor current observer in a finite control set model predictive controller for the stator current of a five-phase drive. The observer design methodology employed in this work uses pole placement based on Butterworth filter design. The new estimation scheme is compared with the standard one in which nonmeasurable state components and other variables are lumped into one term that is updated. The differences between both approaches are experimentally analyzed and verified.**

***Index Terms*—Finite control set, observers, pole placement, predictive control.**

I. Introduction

MODEL predictive control (MPC) is a well-established technique for process control that has been applied to electrical systems [1], later referred to as finite state MPC (FSMPC) in [2] and also finite control set MPC (FCS-MPC) in [3]. An up-to-date review of MPC applied to power electronics can be found in [4].

One implementation aspect, common to most MPC applications, is the estimation of nonmeasurable state components. These are typically rotor variables for which sensors are usually not attached. Controllers often need a good knowledge of such quantities in order to provide the best performance, being FCS-MPC a clear example. In this regard, observer theory [5] is a well-established discipline that provides a framework for understanding and designing estimation schemes for induction motor (IM) drives and other electrical systems. Its use in IM control takes either a full-order or reduced-order form. While the full-order observer makes it possible to estimate stator current and rotor components from measurements of stator voltages, stator currents, and speed [6], the reduced-order observer allows the rotor components estimation using only measurements of stator currents and speed.

Most proposals of observers for IM use the field-oriented control (FOC) scheme and related ones. However, FOC has been found in practice to be satisfactorily robust and effective without complex flux estimation methods. Otherwise, FCS-MPC is highly sensitive to prediction errors that can arise from parameter mismatch among other causes. In [7], sliding mode full-order and reduced-order observers are applied for flux and speed estimation for predictive torque control of IM. A robust model predictive current controller with a disturbance observer is also presented in [8], where a Luenberger observer is constructed for parameter mismatch and model uncertainty which affect the performance of the MPC. The gains of the disturbance observer are also determined using a root-locus analysis, and the stability of the disturbance observer is analyzed when there are errors in the inductor filter parameter. In [9], a nonlinear predictive control law with a disturbance observer is applied to track speed and flux profiles in an IM, considering the robustness to parameters' variations and the disturbance rejection. This is in contrast to most applications of FCS-MPC to electrical systems, where observers are not used as such. Instead nonmeasurable quantities, disturbances and parametric and nonparametric uncertainties are lumped into one single term of the predictive model. This term is then updated using a simple procedure and the update is hold until the next sampling period [2].

In this paper the benefits of incorporating a rotor current observer in a stator current FCS-MPC-based controller of a five-phase drive are analyzed. Research on multiphase and in five-phase IM has exploded in recent times [10]–[12], where fast control FCS-MPC-based techniques have been combined with the inherent robustness and fault tolerant characteristics of multiphase drives [13], [14].

This contribution analyzes the advantages of the proposed control scheme first using the state-space equations of the IM and later illustrating them by experimental tests. The observer design methodology employed in this paper uses pole placement based on Butterworth filter design. The new rotor quantities' estimation scheme is compared with the standard one used in FCS-MPC. The differences between both approaches are analyzed and verified with simulations and

Manuscript received May 29, 2015; revised October 28, 2015 and January 4, 2016; accepted February 3, 2016. Date of publication March 1, 2016. This work was supported in part by the Spanish Ministry of Science and Innovation under Project DPI2013-44278-R and Project ENE2014-52536-C2-1-R, in part by the Junta de Andalucía under Project P11-TEP-7555, and in part by the University of Seville, Spain (V Research Plan, action II.2).

C. Martín and F. Barrero are with the Department of Electronic Engineering, University of Seville, 41004 Seville, Spain (e-mail: cmartin15@us.es; fbarrero@us.es).

M. R. Arahal is with the Department of Systems Engineering and Automatic Control, University of Seville, 41004 Seville, Spain (e-mail: arahal@us.es).

M. J. Durán is with the Department of Electrical Engineering, University of Málaga, 29071 Málaga, Spain (e-mail: mjduran@uma.es).

Digital Object Identifier 10.1109/TIE.2016.2536578

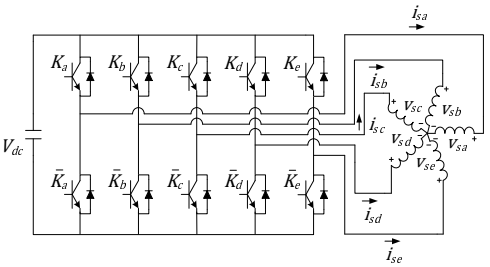

Fig. 1. Schematic diagram of the five-phase IM drive.

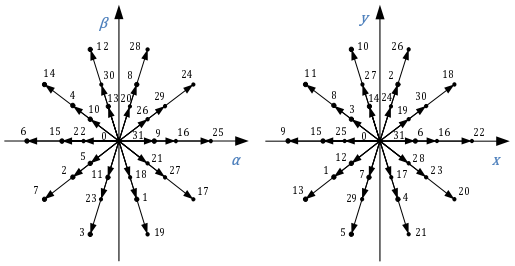

Fig. 2. Space vector diagrams in the α–β and x–y subspaces.

experiments.

This paper is organized as follows. The symmetrical five-phase IM with voltage source inverter (VSI) supply used in this work is analyzed in Section II. The general principles of the FCS-MPC technique and its application to the considered system are presented in Section III. The rotor current observer is introduced in Section IV, where its design is explained and simulation results are also included to illustrate the benefits of the observer. Later, experimental results are shown and discussed in Section V, where the conventional FCS-MPC using an update and hold technique and the FCS-MPC using the Cayley-Hamilton theorem are compared with the proposed FCS-MPC methods with rotor current observer. The paper ends with conclusion section.

II. Five-phase IM Drive Modeling

The IM drive used for testing is mainly composed of a symmetrical five-phase IM with distributed windings equally displaced $\vartheta = 2\pi/5$ and a five-phase two-level VSI. The components of the drive are schematically shown in Fig. 1 where the gating signals of the VSI are represented by $(K_a, \ldots, K_e)$.

The five-phase IM is modeled considering the standard assumptions: uniform air gap, symmetrical distributed windings, sinusoidal magnetomotive force (MMF) distribution and negligible core losses, and magnetic saturation. Then, following the vector space decomposition approach [15], the IM modeling is represented in two orthogonal subspaces. One of them is involved in the fundamental flux and the torque production (α–β subspace, representing the fundamental supply component plus supply harmonics of the order $10n \pm 1$ with $n = 0, 1, 2, 3, ...$). The other is related with the losses (x–y subspace, representing supply harmonics of the order $10n \pm 3$ with $n = 0, 1, 2, 3, ...$). A zero sequence harmonic component ($5n$ with $n = 1, 2, 3, ...$) is projected in the z–axis, but it is not considered because the neutral point is isolated. Selecting the α–β and x–y stator currents and the α–β rotor currents as state variables $x_1 = i_{s\alpha}$, $x_2 = i_{s\beta}$, $x_3 = i_{sx}$, $x_4 = i_{sy}$, $x_5 = i_{r\alpha}$ and $x_6 = i_{r\beta}$, the drive equations can be cast in the form

$$\dot{x}_1 = -R_s c_2 x_1 + c_4(M\omega_r x_2 + R_r x_5 + L_r \omega_r x_6) + c_2 v_1 \quad (1)$$

$$\dot{x}_2 = -R_s c_2 x_2 + c_4(-M\omega_r x_1 - L_r \omega_r x_5 + R_r x_6) + c_2 v_2 \quad (2)$$

$$\dot{x}_3 = -R_s c_3 x_3 + c_3 v_3 \quad (3)$$

$$\dot{x}_4 = -R_s c_3 x_4 + c_3 v_4 \quad (4)$$

$$\dot{x}_5 = R_s c_4 x_1 + c_5(-M\omega_r x_2 - R_r x_5 - L_r \omega_r x_6) - c_4 v_1 \quad (5)$$

$$\dot{x}_6 = R_s c_4 x_2 + c_5(M\omega_r x_1 + L_r \omega_r x_5 - R_r x_6) - c_4 v_2 \quad (6)$$

with coefficients given by

$$c_1 = L_s L_r - M^2, \quad c_2 = \frac{L_r}{c_1}, \quad c_3 = \frac{1}{L_{ls}} \quad (7)$$

$$c_4 = \frac{M}{c_1}, \quad c_5 = \frac{L_s}{c_1} \quad (8)$$

and being the input signals the applied stator voltages $v_1 = v_{s\alpha}$, $v_2 = v_{s\beta}$, $v_3 = v_{sx}$ and $v_4 = v_{sy}$. The equations also include the rotor electrical speed ω_r and the following machine parameters, stator and rotor resistances R_s and R_r, stator and rotor inductances L_s and L_r, stator leakage inductance L_{ls}, and mutual inductance M.

The drive includes not only the electrical machine but also the power electronics of the VSI. And ideal inverter converts gating signals into stator voltages that can be projected to α–β–x–y axes and gathered in a row vector computed as $v = (v_{s\alpha}, v_{s\beta}, v_{sx}, v_{sy}) = V_{dc} u T M$, where V_{dc} is the dc-link voltage, u is a row vector containing the gating signals, T is the connectivity matrix that takes into account how the VSI gating signals are distributed, and M is a coordinate transformation matrix accounting for the spatial distribution of the machine windings. In the case of a five-leg inverter, the gating signals vector is defined by $u = (K_a, K_b, ..., K_e)$ were K_j is the jth gating signal. Each gating signal can be either active $K_j = 1$ or inactive $K_j = 0$, yielding 2^5 possible control choices and voltage vectors (see Fig. 2) at each sampling period.

Combining the above mathematical expressions a nonlinear set of equations arises, that can be written in the state-space

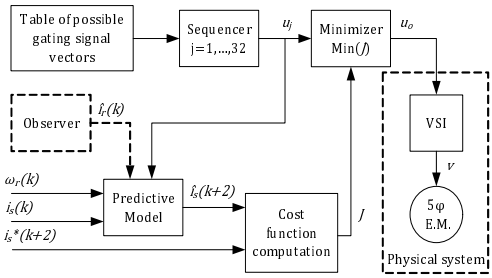

Fig. 3. FCS-MPC technique applied to a symmetrical five-phase IM drive.

form and constitutes the final drive model

$$\dot{X}(t) = AX(t) + Bv(t) \tag{9}$$

$$A = \begin{pmatrix} -a_{s2} & a_{m4} & 0 & 0 & a_{r4} & a_{l4} \\ -a_{m4} & -a_{s2} & 0 & 0 & -a_{l4} & a_{r4} \\ 0 & 0 & -a_{s3} & 0 & 0 & 0 \\ 0 & 0 & 0 & -a_{s3} & 0 & 0 \\ a_{s4} & -a_{m5} & 0 & 0 & -a_{r5} & -a_{l5} \\ a_{m5} & a_{s4} & 0 & 0 & a_{l5} & -a_{r5} \end{pmatrix} \tag{10}$$

$$B = \begin{pmatrix} c_2 & 0 & 0 & 0 \\ 0 & c_2 & 0 & 0 \\ 0 & 0 & c_3 & 0 \\ 0 & 0 & 0 & c_3 \\ -c_4 & 0 & 0 & 0 \\ 0 & -c_4 & 0 & 0 \end{pmatrix} \tag{11}$$

with state vector $X(t) = (x_1, ..., x_6)^T$ and input vector $v(t) = (v_1, ..., v_4)^T$. The coefficients of matrix A are defined as $a_{s2} = R_s c_2$, $a_{s3} = R_s c_3$, $a_{s4} = R_s c_4$, $a_{r4} = R_r c_4$, $a_{r5} = R_r c_5$, $a_{l4} = L_r c_4 \omega_r$, $a_{l5} = L_r c_5 \omega_r$, $a_{m4} = M c_4 \omega_r$, and $a_{m5} = M c_5 \omega_r$.

III. Finite Control Set Model Predictive Current Control for Drives

The FCS-MPC technique has been proposed in the literature for current control in VSI drives. The technique is illustrated by the diagram shown in Fig. 3. The objective of the controller is to track reference stator currents given by i_s^*. For this purpose, it uses a discrete model of the drive to predict the future behavior of the output variables $\hat{i}_s$. Then, an optimizer selects the most adequate gating signal u_o to minimize a cost function J. The optimization is done by exhaustive search over all possible control signal values. For each one, the predictive model is computed using the measured rotor speed ω_r and stator phase currents i_s to obtain the predicted values of the currents $\hat{i}_s$. Then, the cost function value is calculated and the voltage vector that minimizes the cost function is selected and applied to the VSI during the next sampling period.

The proposed FCS-MPC controller is based on [16], where a discretization technique derived from the Cayley-Hamilton equation is employed to obtain the predictive model. For simplicity, and to provide a comparison with more standard techniques, a forward Euler discretization method is also presented. It is well known that this can affect the prediction and control errors [17]. Taking this into account, the obtained predictive model from (9)–(11) yields

$$\hat{X}(k+1|k) = X(k) + T_s\left(AX(k) + Bv(k)\right) \tag{12}$$

Notice that matrix A depends on the instantaneous value of the rotor electrical speed, being the predictive model a time-variant linear system. However, the mechanical dynamic is slower than the electrical one, so constant speed within a sampling period can be assumed. Consequently, matrix A must be updated every sampling time using the measured ω_r and its value is held throughout the current sampling period.

The actual implementation of the FCS-MPC requires the second-step ahead prediction to be computed. This necessity arises from the fact that the computation of the control signal does take a significant amount of time which is comparable with the sampling time. In this situation, it is best to wait until the next sampling time to release the computed control signals (see [2] for details).

The final element in the FCS-MPC scheme is the cost function to be optimized. In current control, the most important figure of merit is the tracking error in predicted stator currents. For that reason, the usual cost function uses the predicted deviations from current references in the α–β and x–y subspaces as

$$J = \|\hat{e}_{\alpha\beta}\|^2 + \lambda_{xy}\|\hat{e}_{xy}\|^2 \tag{13}$$

where $\hat{e}$ is the second-step ahead predicted error computed as $\hat{e} = i_s^*(k+2) - \hat{i}_s(k+2|k)$ and λ_{xy} is a tuning parameter between 0 and 1 that allows to put more emphasis on α–β or x–y subspaces. Note that a future reference value is needed, which is typically obtained from outer speed/torque loops in variable speed drives applications. However, this paper deals with current control and, for this reason, the reference is set as an input. Also, this reference is assumed to be constant in the d–q reference frame and for sufficiently small sampling times, as it is indicated in [18], i.e. $i_{sdq}^*(k+2) \approx i_{sdq}^*(k+1) \approx i_{sdq}^*(k)$.

During the optimization process, both the cost function and the predictive model must be computed 32 times at each sampling period to guarantee optimality, since there are 32 possible voltage vectors for the five-phase half-bridge VSI used to drive the IM. A reduced set of voltage vectors can be, however, selected to speed up the optimization process and reduce the computational cost. In [10], a good analysis on this issue is realized, concluding that the selection of λ_{xy} mainly depends on the number of voltage vectors to be considered.

A. Rotor Quantities

The predictive model of (12) cannot be used in the normal operation case where rotor currents are not measured. This difficulty is usually overcome lumping all nonmeasurable terms in one factor that is later tracked and updated. As a consequence, the rotor current-related term constitutes a new variable that can be estimated using past values of the measured variables. The estimated term is projected into the future and used in the predictive model. For the case

of study, this is achieved splitting the state vector into a measurable part $X^1 = (x_1, x_2, x_3, x_4)^T$ and an unmeasurable part $X^2 = (x_5, x_6)^T$. The prediction is then obtained by simulating for a sample period the evolution of the measurable part as

$$\hat{X}^1(k+1|k) = RX^1(k) + Sv(k) + \hat{G}(k|k) \qquad (14)$$

where

$$\begin{aligned} R &= (I + A_{11}T_s) \\ S &= B_1 T_s \end{aligned} \qquad (15)$$

and term $\hat{G}(k|k)$ is an estimation of the contribution of $X^2(k)$ to $X^1(k+1)$. The usual estimation is obtained by holding the previous value $\hat{G}(k-1)$ computed at time k as

$$\hat{G}(k-1|k) = X^1(k) - RX^1(k-1) - Sv(k-1). \qquad (16)$$

To the best of our knowledge, this backtracking procedure has not been analyzed in the literature yet, and thus, the following study is novel and relevant as most proposed FCS-MPC applications rely on said procedure.

B. Analysis of the Simple Update Method

The usual way to cope with unmeasurable (i.e., rotor) quantities in FCS-MPC is to lump them into one term that is estimated in a simple manner. The term is designated as G and used in the first-step ahead prediction as

$$\hat{X}^1(k+1|k) = RX^1_m(k) + Sv(k) + \hat{G}(k). \qquad (17)$$

Ideally, the term $G(k-1)$ could be computed at time k by means of

$$G(k-1) = X^1(k) - RX^1(k-1) - Sv(k-1) \qquad (18)$$

but, due to measurement errors ε, the actual estimation is

$$\hat{G}(k-1|k) = X^1_m(k) - RX^1_m(k-1) - Sv(k-1) \qquad (19)$$

where $X^1_m(k)$ is the measured vector of stator quantities, linked to the real values through

$$X^1_m(k) = X^1(k) + \varepsilon(k). \qquad (20)$$

Making use of the state-space equations, the estimation can be written as

$$\hat{G}(k-1|k) = \varepsilon(k) - R\varepsilon(k)(k-1) + A_{12}T_s X^2(k-1). \qquad (21)$$

From this equality, it is inferred that the estimation of rotor quantities done in this way is corrupted by the measurement error. The error of the first-step ahead prediction is defined as

$$e_{1p}(k+1) \doteq X^1(k+1) - \hat{X}^1(k+1|k) \qquad (22)$$

and can be computed from previous expressions as

$$\begin{aligned} e_{1p}(k+1) = RX^1(k) + Sv(k) + G(k) - \\ - \left(RX^1_m(k) + Sv(k) + \hat{G}(k-1|k)\right). \end{aligned} \qquad (23)$$

It is easy to show that the above equation yields the following expression for the one-step ahead prediction error:

$$\begin{aligned} e_{1p}(k+1) = -(I+R)\varepsilon(k) + R\varepsilon(k)(k-1) + \\ + A_{12}T_s\left(X^2(k) - X^2(k-1)\right). \end{aligned} \qquad (24)$$

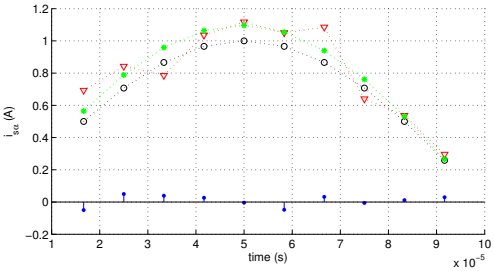

Fig. 4. Numerical example illustrating the simple method to estimate term G. The curve marked with circles is $i_{s\alpha}$, the real (simulated) α current without measurement noise. The curve marked with asterisks corresponds to an estimation using $\hat{X}^1(k+1|k) = RX^1_m(k) + Sv(k)$, i.e., without any correction for rotor quantities. The curve marked with triangles is the same estimation adding the simple update correction for G given by (18), considering noise. This corresponds to the usual estimation used in FCS-MPC. The noise values are shown as filled circles and gather around their zero mean. The negative effect over the prediction is quite apparent.

From (24) one can derive that the prediction error arising from this scheme does not filter measurement errors. On average the prediction error due to this factor will exhibit the same statistical properties as ε. Assuming uncorrelated error measurement with a distribution with zero mean and σ^2 variance, the contribution to e_{1p} variance is precisely σ^2. The instantaneous contribution can be large; for instance, if $\varepsilon(k) = -\varepsilon(k-1) = n$, then $-(I+R)\varepsilon(k) + R\varepsilon(k)(k-1) = (I+2R)n = (3I + 2A_{11}T_s)n \approx 3n$. A particular case has been simulated and illustrated in Fig. 4, where some noise in the stator current measurement has been included in the prediction process (shown as filled circles). It can be seen that a small amount of noise can produce larger deviations in the estimation of the stator current if the classical update and hold method is used.

Regarding rotor quantities, it is important to highlight that the contribution to the prediction error is filtered through the system dynamic via the term $A_{12}T_s$. For larger sampling frequencies, the effect is smaller, which is part of the reasons why most applications uses a high value of f_s. Also from the above expression, one can see that it is the change in rotor quantities what induces prediction error. In sinusoidal steady state, the rotor quantities are expected to evolve for the most part at the fundamental frequency f_e. Again, if a large f_s/f_e is used, then the changes from one sampling period to the next would be small (ceteris paribus), allowing this simple estimation scheme to work. A problem might arise during transients where changes can be more pronounced.

IV. Rotor Current Observer Design, Implementation, and Validation by Simulation

The FCS-MPC method can be modified to include an observer that estimates the nonmeasurable state components of the system. As depicted in Fig. 3, the rotor current estimation $\hat{i}_r$ is calculated by the observer using the measured rotor speed ω_r and stator phase currents i_s every sampling time. This

estimation allows to use the complete state-space model (9) for predictive purposes.

It is well know from observer theory that the closed-loop poles of the observer

$$\dot{\hat{x}}(t) = A\hat{x}(t) + Bv(t) - L\left(C\hat{x}(t) - y(t)\right) \tag{25}$$

are determined by the observer gain L also called Luenberger gain matrix. The error dynamic equation is simplified to

$$\dot{e}(t) = (A - LC)\, e(t) - (G - LH)\, d(t) \tag{26}$$

and the convergence toward zero is determined by the choice of the observer gain. The separation principle allows the choice of such matrix to be decoupled from the controller design.

In order to reduce the computational load required to provide estimates of all state variables of the system, a reduced-order observed can be built considering only a part of the state vector.

A. Reduced Order Rotor Current Observer

A reduced-order observer for i_r can be derived using Gopinath's method. The state is divided in two parts, the measurable one (x^1) and the unmeasurable part (x^2). In the present case, $x^1 = (x_1, x_2)^T$ and $x^2 = (x_5, x_6)^T$. Matrices A and B are accordingly divided so that

$$\begin{aligned} \dot{x}^1(t) &= A_{11}x^1(t) + A_{12}x^2(t) + B_1 v(t) \\ \dot{x}^2(t) &= A_{21}x^1(t) + A_{22}x^2(t) + B_2 v(t). \end{aligned} \tag{27}$$

The estimation for the unmeasurable part is

$$\hat{x}^2(t) = z(t) + Lx^1(t) \tag{28}$$

whose dynamic is dictated by

$$\begin{aligned} \dot{z}(t) = (A_{22} - LA_{12})\, z(t) + (A_{22} - LA_{12})\, Lx^1(t) + \\ + (A_{21} - LA_{11})\, x^1(t) + (B_2 - LB_1)\, v(t). \end{aligned} \tag{29}$$

B. Observer Design with Butterworth Pole Placement

A correct observer design should take into account the effect of the observer gain in all terms of the error dynamic to provide a trade-off between fast convergence and disturbance sensitivity. Ad hoc modifications of estimators suggested by observer theory often yield faster convergence without endangering stability [19]. In [20], it is noted that, "In classical observer for IM drives, the poles of observer are designed to be proportional to the poles of IM which produces high imaginary part at high speed and is harmful to the system stability. To address this issue, it is suggested to shift the real part of observer poles to the left in the complex plane compared to the poles of IM, and the imaginary part of observer poles are not changed". However, this leads to complicated expressions of observer gains. The authors propose a very simple constant gain matrix to improve the observer's stability.

For above reduced-order observer, the design implies the selection of the most adequate eigenvalues of $(A_{22} - LA_{12})$. As they determine the speed at which the estimation error decays, it is logical to make the real parts of those eigenvalues as negative as possible. That will force the error to decay very rapidly. However, there is a problem with this logic when there are modeling errors to be considered. In actual applications, the values in the model matrices may not be known exactly. Research has shown that in order for the observer to be robust against modeling errors, as well as causing the estimation error to decay rapidly, a different approach is required.

It is of importance that the observer has well-damped dynamic. Good damping of a system implies that the poles are located in some distance away from the origin to speed up the convergence and with imaginary parts no larger than the real parts. The latter is desirable to avoid oscillatory behavior. With poor damping, there is also a risk for instability if the observer is implemented using forward Euler discretization [19].

If the original system has z_1 stable zeros, then z_1 of the observer's eigenvalues should be placed at the values of those stable zeros. The remaining eigenvalues of the observer may be placed well into the left-half plane, but at locations that are equidistant from the origin in what is known as the Butterworth configuration. The characteristic equation from which the eigenvalues are calculated is then a Butterworth polynomial. They are a common way to specify the denominator of a low-pass filter in the area of signal processing. The step response of such filters has a slight overshoot, with good damping. The parameter T_B is used to define the speed of the response, being such speed inversely proportional to T_B.

A second-order Butterworth filter has the characteristic polynomial

$$B(s) = T_B^2 s^2 + \sqrt{2} T_B s + 1. \tag{30}$$

By placing the poles of the observer in the location given by the roots of $B(s)$, the error dynamic has some desired characteristics with respect to damping and rise times. It is easy to see that the poles of the filter are located at

$$p = -\frac{1}{T_B\sqrt{2}} \pm j\,\frac{1}{T_B\sqrt{2}} \tag{31}$$

providing an adequate damping factor of $\zeta = \frac{1}{\sqrt{2}}$. The Luenberger gain matrix has the usual form

$$L = \begin{pmatrix} g_1 & -g_2 \\ g_2 & g_1 \end{pmatrix} \tag{32}$$

where coefficients g_i are derived using the Kautsky-Nichols algorithm [21] to match the desired closed-loop observer poles. Now, as the coefficients of A_{22} are dependent of ω_r, it is necessary to solve the pole placement problem for the current value of ω_r. In order to avoid the computing load imposed by computing the coefficients online, it is convenient to derive expressions for the elements of the gain matrix L as a function of ω_r or to use a precomputed set of coefficients and interpolate. In the latter case, the resulting observer is equivalent to a gain-scheduled system and its performance depends on the schedule resolution as well as the accuracy of the measured values of ω_r.

Fig. 5 shows the variation of the L coefficients with f_e for $T_{B1} = 0.0025$ (s), $T_{B2} = 0.0014$ (s), and $T_{B3} = 0.001$ (s). It can be seen that the variation in the coefficients' values is smooth, allowing one to rely on interpolation if a sufficiently high number of discrete samples are given.

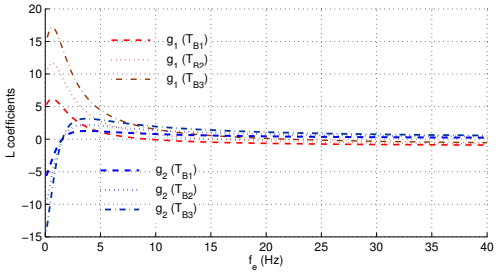

Fig. 5. Variation of L coefficients versus f_e for $T_{B1} = 0.0025$ (s), $T_{B2} = 0.0014$ (s) and $T_{B3} = 0.001$ (s).

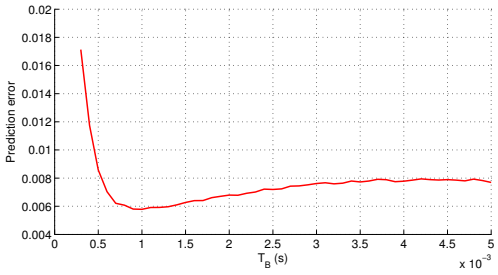

Fig. 6. Prediction error dependence on parameter T_B used to tune the observer.

Fig. 6 shows the variation of the prediction error with parameter T_B. The errors have been obtained via extensive simulation using a model of the IM with a FCS-MPC that makes use of the observer. It can be seen that there is a global minimum at $T_B = 0.001$ (s).

C. Simulation Results

Before showing the experimental results, the effectiveness of the proposed rotor current observer has been tested with simulations. A MATLAB simulation environment has been created for the VSI-fed symmetrical five-phase IM with distributed windings and the electrical parameters shown in Table II. Then, the conventional FCS-MPC controller and the proposed FCS-MPC controller with rotor current observer have been compared. All simulations have been carried out using a sampling time of $T_s = 67\mu$s and a stator current reference i_s^* defined by the electrical frequency $f_e = 30$ Hz and the amplitude $A_{ref} = 1.20$ A. The observer has been designed using the Butterworth pole placement method commented before, with an optimum T_B value of 0.001 (s). Both predictive controllers use the 32 available voltage vectors in the optimization process. Finally, different weighting factors for the x–y plane are introduced in the cost function (13) to investigate the impact of this parameter on the system performance.

Table I summarizes the obtained results, where the controllers are compared for each λ_{xy} value on the basis of the root-mean-squared (RMS) error in the current tracking for the α component (e_α^{RMS}) and for the x–y plane (e_{xy}^{RMS}), the RMS error in the two-step ahead prediction for the α current component ($\hat{e}_\alpha^{RMS}$), and the total harmonic distortion in the phase currents (THD$_p$). These figures of merit are computed as follows:

TABLE I
SIMULATION RESULTS FOR $f_e = 30$ HZ AND $A_{ref} = 1.20$ A USING DIFFERENT λ_{xy} VALUES

λ_{xy}	Controller	e_α^{RMS} (x10^{-2})	$\hat{e}_\alpha^{\text{RMS}}$ (x10^{-2})	e_{xy}^{RMS} (x10^{-2})	THD$_p$ (%)
0.1	FCS-MPC	1.91	1.39	8.09	9.52
	FCS-MPC + OBS	1.33	1.38	7.55	9.06
0.5	FCS-MPC	2.52	1.38	4.82	6.05
	FCS-MPC + OBS	1.82	1.37	3.74	4.98
1	FCS-MPC	5.02	1.37	3.45	5.08
	FCS-MPC + OBS	2.90	1.36	2.83	4.49

$$e_\alpha^{\text{RMS}} = \sqrt{\frac{\sum_{j=1}^{N}(i_{s\alpha}(j) - i_{s\alpha}^*(j))^2}{N}} \tag{33}$$

$$e_{xy}^{\text{RMS}} = \frac{1}{2}\left(\sqrt{\frac{\sum_{j=1}^{N} i_{sx}^2(j)}{N}} + \sqrt{\frac{\sum_{j=1}^{N} i_{sy}^2(j)}{N}}\right) \tag{34}$$

$$\hat{e}_\alpha^{\text{RMS}} = \sqrt{\frac{\sum_{j=1}^{N}(\hat{i}_{s\alpha}(j+2) - i_{s\alpha}(j+2))^2}{N}} \tag{35}$$

$$\text{THD}_p = \frac{1}{5}\sum_{j=a}^{e}\sqrt{\frac{\int_0^\infty (i_{sj}(t) - i_{sj1}(t))^2 dt}{\int_0^\infty (i_{sj1}(t))^2 dt}} \tag{36}$$

where i_{sj1} is the fundamental component of the considered current. THD$_p$ is obtained as the average value of the THD of all stator phase currents.

The use of the rotor current observer clearly improves the system performance in both α–β and x–y subspaces for all considered λ_{xy} values. This is confirmed by the reduction in the current tracking errors e_α^{RMS} and e_{xy}^{RMS} (see Table I) when the observer is included in the conventional FCS-MPC controller. The achieved reduction reaches 42% for e_α^{RMS} and 22% for e_{xy}^{RMS}. Since α–β components are in relation with the electromechanical energy conversion, the improved current tracking in this plane reduces the torque ripple and enhances the dynamic performance. Additionally, the lower RMS error value in the x–y plane improves the efficiency of the machine, diminishing copper losses. The harmonic content is also reduced using the rotor current observer, as evidences the lower THD$_p$ values and, consequently, stator phase current ripples. Regarding prediction errors, the FCS-MPC with rotor current observer generates lower $\hat{e}_\alpha^{\text{RMS}}$ values, as it is shown in Table I. These preliminary results are expected from observer theory [19] and must be confirmed through experimentation, where effects like measurement errors, electrical and mechanical noises or detuning of the IM modeling, among others, appear.

Notice that the use of different λ_{xy} factors generates different control criteria and can restrict the use of voltage

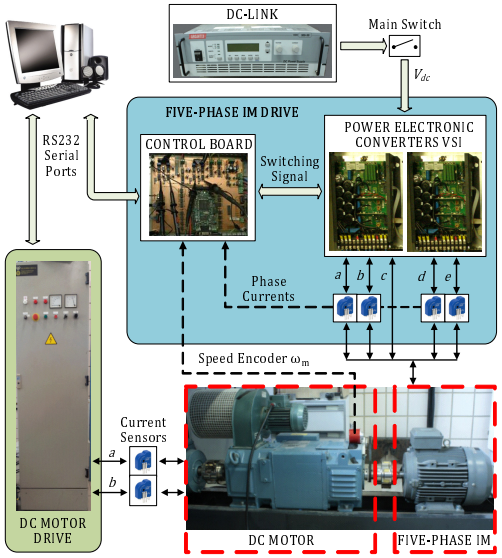

Fig. 7. Experimental apparatus diagram showing two conventional three-phase VSIs (upper right), the electronic control board (center middle), the dc motor drive (left side), the IM machine, and the dc motor (bottom right).

vectors, as it is stated in [10]. In this regard, Table I shows that the larger λ_{xy} is, the lower e_{xy}^{RMS} error is obtained for both controllers, although the RMS error in the α–β plane increases. In what follows, a low λ_{xy} value will be mainly used to improve the torque production in the multiphase drive.

V. Experimental Results

A laboratory experimental setup has been used for testing the proposed FCS-MPC with rotor current observer. A graphic diagram of the test rig is shown in Fig. 7. The principal element is a 30-slot symmetrical five-phase induction machine with distributed windings and three pairs of poles. The IM parameters are summarized in Table II and have been experimentally obtained using the methods described in [22] and [23]. Two SKS21F three-phase inverters from Semikron have been connected to a dc-link voltage of 300 V using an independent dc power supply. The control algorithm is deployed in a TM320F28335 digital signal processor (DSP) placed on a MSK28335 Technosoft board. A dc motor is used to introduce a variable load in the system. Finally, the rotor mechanical speed is measured using a GHM510296R/2500 digital encoder and the enhanced quadrature encoder pulse (eQEP) peripheral of the DSP.

Different tests have been carried out using four current control methods for comparison purposes: FCS-MPC technique without observer and employing the simple update and hold method for estimating the term G, where the effect of varying rotor quantities and perturbations are lumped (C1a in what follows), or using the Cayley-Hamilton theorem (C1b from now on); FCS-MPC with a rotor current observer used in the calculation of prediction at $(k+1)$ time (C2); and FCS-MPC with a rotor current observer used in the calculation of predictions at $(k+1)$ and $(k+2)$ times (C3). Notice that C1a controller is the one described in Section III and C1b controller is based on the predictive current control presented in [16] but using the cost function defined in (13). Also notice that both C2 and C3 controllers are introduced in the context of stator current control of IM drives and can be extended to any n–phase induction machine (including the three-phase one) provided that the machine has distributed windings and the torque/flux production is purely related to the α–β subspace.

TABLE II
Electrical and Nominal Parameters of the Five-Phase IM

Parameter		Value
Stator resistance	R_s (Ω)	19.45
Rotor resistance	R_r (Ω)	6.77
Stator leakage inductance	L_{ls} (mH)	100.7
Rotor leakage inductance	L_{lr} (mH)	38.6
Mutual inductance	M (mH)	656.5
Stator rated current	$I_n(A)$	2.5
Nominal speed	ω_n (rpm)	1000
Power	P (kW)	1
Pairs of poles	p	3

TABLE III
Experimental Results for Different Stator Current References

f_e, A_{ref} (Hz, A)	Ctrl	e_α^{RMS} (x10^{-2})	$\hat{e}_\alpha^{\text{RMS}}$ (x10^{-2})	e_{xy}^{RMS} (x10^{-2})	THD$_{\alpha\beta}$ (%)	THD$_p$ (%)	N_c (SCPC)
29, 1.62	C1a	10.9	15.1	13.0	7.09	13.4	68.1
	C1b	8.59	11.1	11.7	7.05	12.4	53.1
	C2	10.1	12.8	9.95	6.73	10.9	59.2
	C3	7.84	10.3	10.1	6.96	11.1	56.9
34, 1.56	C1a	11.2	15.4	13.3	7.24	13.6	50.6
	C1b	8.97	11.4	11.3	6.95	12.3	38.2
	C2	9.17	13.2	9.83	6.22	10.8	41.9
	C3	7.82	10.4	10.9	6.63	11.7	39.2
39, 1.60	C1a	12.1	16.0	15.4	6.39	14.4	35.3
	C1b	8.62	11.0	12.9	6.30	12.9	24.3
	C2	9.58	14.8	11.8	5.74	11.7	27.9
	C3	7.82	10.7	12.8	5.70	12.8	25.8

TABLE IV
Obtained Improvement Using C3 Over C1a and C1b Controllers

f_e, A_{ref}	Ctrl	e_α^{RMS}	$\hat{e}_\alpha^{\text{RMS}}$	e_{xy}^{RMS}	THD$_{\alpha\beta}$	THD$_p$	N_c
(Hz, A)		Improvement percentage (%)					
29, 1.62	C1a	28.1	31.6	22.4	1.92	16.7	16.5
	C1b	8.70	7.00	13.6	1.34	10.2	−7.14
34, 1.56	C1a	30.4	32.4	18.2	8.36	14.5	22.5
	C1b	12.9	8.44	4.15	4.53	4.92	−2.70
39, 1.60	C1a	35.5	33.3	16.5	10.9	11.4	26.8
	C1b	9.32	2.73	0.30	9.63	1.17	−6.50

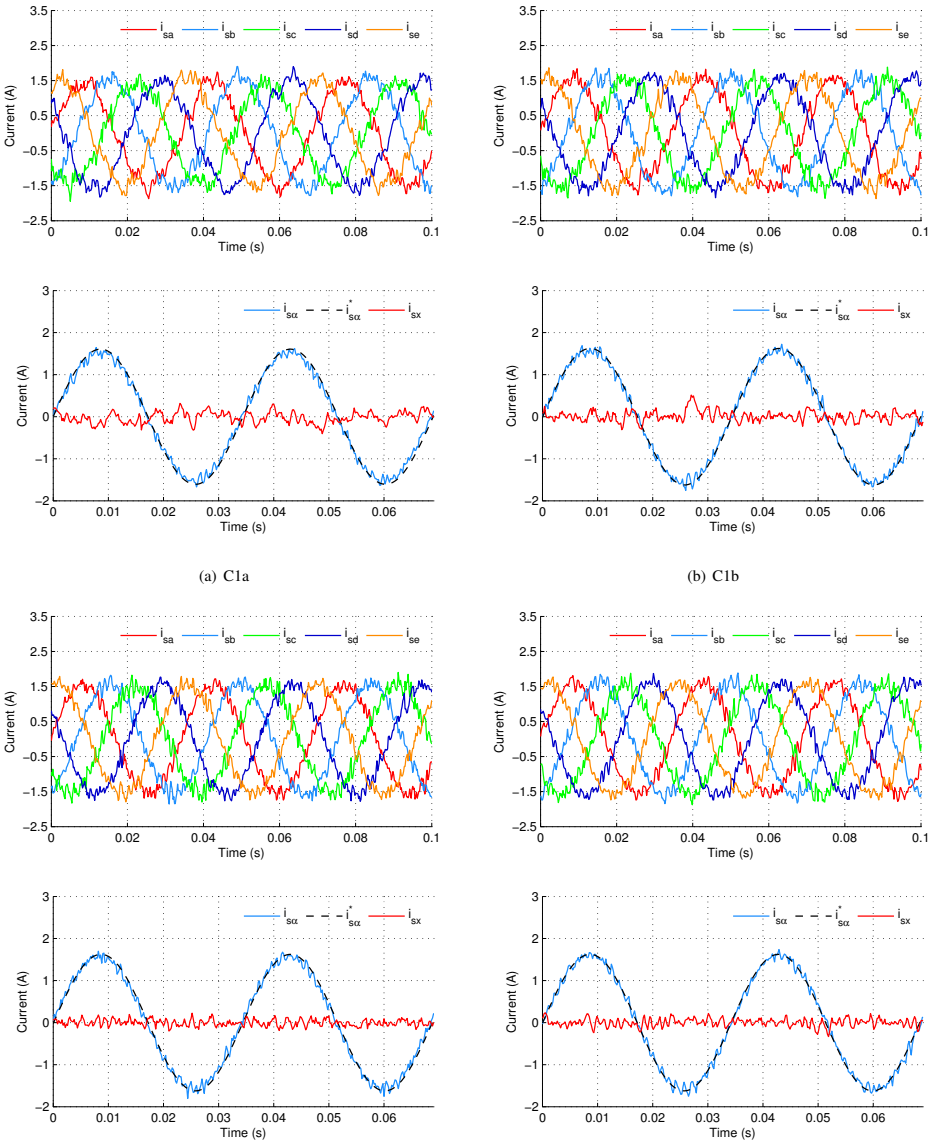

(a) C1a

(b) C1b

(c) C2

(d) C3

Fig. 8. Experimental results obtained for $A_{ref} = 1.62$ A and $f_e = 29$ Hz when it is applied the (a) C1a, (b) C1b, (c) C2, and (d) C3 controller. Upper plots show the stator phase currents i_{sa}, i_{sb}, i_{sc}, i_{sd}, and i_{se}, while α and x stator currents ($i_{s\alpha}$ and i_{sx}) are depicted in the lower drawings.

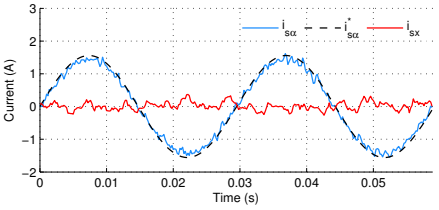

(a) C1a

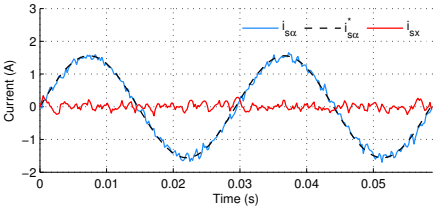

(b) C3

Fig. 9. Experimental results obtained for $A_{ref} = 1.56$ A and $f_e = 34$ Hz when it is applied the (a) C1a and (b) C3 controller. The α and x stator currents ($i_{s\alpha}$ and i_{sx}) are shown.

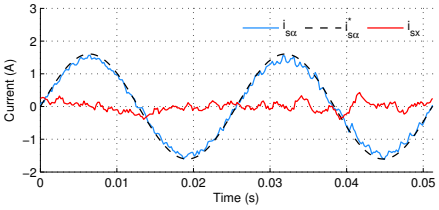

(a) C1a

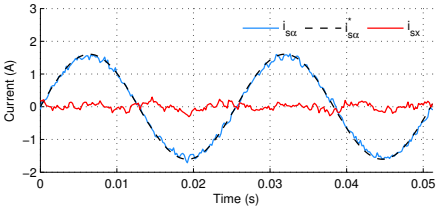

(b) C3

Fig. 10. Experimental results obtained for $A_{ref} = 1.60$ A and $f_e = 39$ Hz when it is applied the (a) C1a and (b) C3 controller. The α and x stator currents ($i_{s\alpha}$ and i_{sx}) are shown.

All experiments are realized using a sampling time of $T_s = 66.67\mu$s and considering the 32 available voltage vectors, while the observer is designed using the Butterworth pole placement method (31) with $T_B = 1/1300$ (s), which is an optimum value obtained from the theoretical one (see Fig. 6) and through experimentation. The steady-state response of the system has been tested for different stator current references, where a 58% of the nominal load torque is applied and a $\lambda_{xy} = 0.1$ weighting factor is used to favor the control of the α–β plane. Table III summarizes the conditions for each test and the obtained results. The first two columns indicate the electrical frequency f_e and amplitude A_{ref} of the stator current reference i_s^*, and the applied controller (C1a, C1b, C2 and C3). The next three columns detail: the RMS error in the current tracking for the α component (e_α^{RMS}) and for the x–y components (e_{xy}^{RMS}), as well as the RMS error of the two-step ahead prediction in the α current component ($\hat{e}_\alpha^{\text{RMS}}$). These quantities are computed using (33)–(35), respectively. The last three columns in Table III present the THD in the α–β plane ($\text{THD}_{\alpha\beta}$), THD_p and the number of switching changes per cycle (N_c). The N_c value is obtained as the average value (over the VSI phases) of the number of switch changes per cycle (SCPC), while the $\text{THD}_{\alpha\beta}$ value is calculated similarly to (36) as follows:

$$\text{THD}_{\alpha\beta} = \frac{1}{2} \sum_{j=\alpha,\,\beta} \sqrt{\frac{\int_0^\infty (i_{sj}(t) - i_{sj1}(t))^2 dt}{\int_0^\infty (i_{sj1}(t))^2 dt}}. \qquad (37)$$

Additionally, Table IV presents the benefits of using a rotor current observer in all figures of merit. Some of these experimental tests are graphically included to illustrate the obtained results. Fig. 8 shows the evolution of stator phase currents, and α and x stator currents using C1a, C1b, C2 and C3 controllers in an operation point defined by $f_e = 29$ Hz and $A_{ref} = 1.62$ A. For clarity reasons, β and y stator currents have been omitted since they show similar curves. Similarly, Figs. 9 and 10 present the α and x stator currents for C1a and C3 controllers, when the electrical frequency is set to 34 and 39 Hz, respectively. In this case, C1b and C2 controllers have not been included for simplicity reasons.

It can be stated from the obtained results that the α current tracking error e_α^{RMS} is reduced when a rotor current observer is included in the conventional FCS-MPC instead of the standard backtracking procedure (C1a). Additionally, this reduction is higher when the observer is applied not only to the first prediction but also to the first and second predictions (C3), obtaining an α-tracking improvement of up to 35.5% for the considered operation points. This is stated in Fig. 8, where

TABLE V
EXPERIMENTAL RESULTS USING DIFFERENT λ_{xy} VALUES FOR $f_e = 29$ HZ AND $A_{ref} = 2.03$ A

λ_{xy}	Ctrl	e_α^{RMS} (x10^{-2})	$\hat{e}_\alpha^{\text{RMS}}$ (x10^{-2})	e_{xy}^{RMS} (x10^{-2})	$\text{THD}_{\alpha\beta}$ (%)	THD_p (%)	N_c (SCPC)
0.1	C1a	11.8	16.3	12.4	5.28	9.83	54.3
	C1b	8.90	12.1	11.7	5.25	9.33	40.0
	C2	9.89	15.0	9.99	4.86	8.35	46.8
	C3	8.49	11.9	10.5	5.24	8.85	44.7
0.5	C1a	12.3	16.3	8.23	5.28	7.89	57.7
	C1b	9.18	12.1	8.49	5.34	7.92	42.2
	C2	10.1	15.0	7.58	4.92	7.18	49.9
	C3	8.91	11.2	7.27	5.14	7.10	47.9
1	C1a	15.3	16.5	7.82	5.64	8.15	61.1
	C1b	9.83	11.6	8.11	5.08	7.70	42.6
	C2	10.6	15.1	6.85	5.13	7.02	52.5
	C3	9.30	11.6	7.05	5.30	7.16	50.1

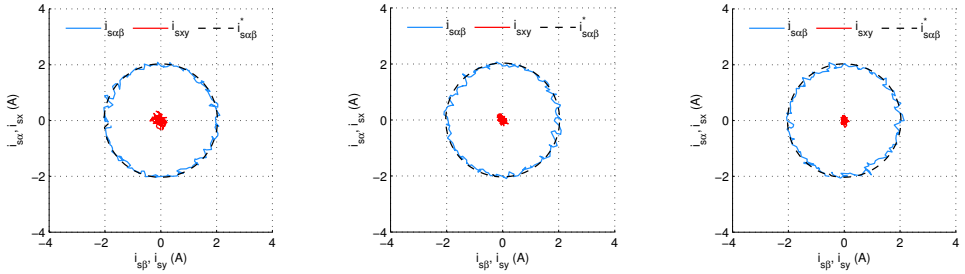

(a) $\lambda_{xy} = 0.1$ (b) $\lambda_{xy} = 0.5$ (c) $\lambda_{xy} = 1$

Fig. 11. Current trajectories in the α–β and x–y subspaces with a current reference defined by $f_e = 29$ Hz and $A_{ref} = 2.03$ A. The C3 controller is used with (a) $\lambda_{xy} = 0.1$, (b) $\lambda_{xy} = 0.5$, and (c) $\lambda_{xy} = 1$.

the measured α current ($i_{s\alpha}$) fits better to the reference when C2 and C3 controllers are used, being C3 the best case. Note that the current tracking reduction in the α–β plane results in a lower torque ripple and, consequently, a reduction of harmonic content and losses. Also note that this α-tracking improvement is larger with increasing frequency (see [24]), and that the use of an exact discretization technique (Cayley-Hamilton theorem C1b) can reduce the benefits of applying a rotor current observer if the estimated parameters agree with the real ones.

Moreover, the use of the rotor current observer allows to reduce considerably the RMS current tracking error in the x–y subspace compared with the standard C1a controller, as it is seen in Figs. 8–10. In this issue, C2 controller has the best performance with a maximum improvement percentage in the particular figure of merit of 26%. This is an interesting benefit in multiphase machines with distributed windings, where x–y components are not involved in the generation of electrical torque.

The main reason to use the rotor current observer in the conventional FCS-MPC is to produce more accurate predictions of the stator currents. Tables III and IV demonstrate this issue, where the prediction error $\hat{e}_{\alpha}^{\mathrm{RMS}}$ is reduced when C2 and C3 controllers are applied to the system. Again, C3 controller offers the best result with an improvement percentage of up to 33.3%. Similar conclusions can be obtained for the SCPC N_c. The use of the observer reduces up to 26.8% this figure of merit when the C3 controller is applied. It is remarkable the obtained improvement in the stator current tracking comparing with C1a when the rotor current observer is used, and this with lower VSI switching frequency. Regarding the harmonic content, its value is lower if the rotor current observer is used, being C2 the best controller in this particular figure of merit, reducing the $\mathrm{THD}_{\alpha\beta}$ and THD_p values 10.2% and 20.6%, respectively.

As mentioned before, the use of an exact discretization technique in the predictive model, C1b controller, improves the control performance compared with more extended C1a controllers (as it is claimed in [17]). Nevertheless, the obtained improvement using C3 remains the best, as it is shown in Table III and IV, and all considered figures of merit are reduced, except the SCPC.

TABLE VI
EXPERIMENTAL RESULTS USING DIFFERENT T_L VALUES FOR $f_e = 29$ HZ

T_L (%)	Ctrl	$e_{\alpha}^{\mathrm{RMS}}$ (x10^{-2})	$\hat{e}_{\alpha}^{\mathrm{RMS}}$ (x10^{-2})	e_{xy}^{RMS} (x10^{-2})	$\mathrm{THD}_{\alpha\beta}$ (%)	THD_p (%)	N_c (SCPC)
39	C1a	10.4	14.6	13.2	11.3	20.4	86.4
	C1b	8.70	10.9	11.5	10.7	18.3	68.1
	C2	9.01	11.2	9.29	10.4	15.8	75.5
	C3	8.29	9.83	9.05	10.7	15.7	69.5
58	C1a	10.9	15.1	13.0	7.09	13.4	68.1
	C1b	8.59	11.1	11.7	7.05	12.4	53.1
	C2	10.1	12.8	9.95	6.73	10.9	59.2
	C3	7.84	10.3	10.1	6.96	11.1	56.9
78	C1a	11.8	16.3	12.4	5.28	9.83	54.3
	C1b	8.90	12.1	11.7	5.25	9.33	40.0
	C2	9.89	15.0	9.99	4.86	8.35	46.8
	C3	8.49	11.9	10.5	5.24	8.85	44.7

Different experimental tests were also carried out, using the weighting factor λ_{xy} values of 0.1, 0.5 and 1, and using a load torque equivalent to the 78% of the nominal one. The frequency and amplitude of stator current reference were configured to be $f_e = 29$ Hz and $A_{ref} = 2.03$ A, while the rest of the applied experiment's conditions were the same that those used to obtain Table III. The obtained results confirm previous ones and are summarized in Table V for each controller and figure of merit. It can be concluded that C3 method offers the best performance in terms of α–β current tracking and prediction, although C2 technique shows better performance in the x–y current tracking and harmonic distortion.

Results in Table V also conclude that α current tracking error ($e_{\alpha}^{\mathrm{RMS}}$) increases with the weighting factor (λ_{xy}) in all the analyzed controllers, being lower this figure of merit for the C3 control technique. Furthermore, the x–y current tracking error (e_{xy}^{RMS}) is reduced when λ_{xy} increases, while the prediction error ($\hat{e}_{\alpha}^{\mathrm{RMS}}$) remains practically constant for all values of λ_{xy}. Fig. 11 depicts the polar trajectories of the stator currents in the α–β and x–y planes for the considered

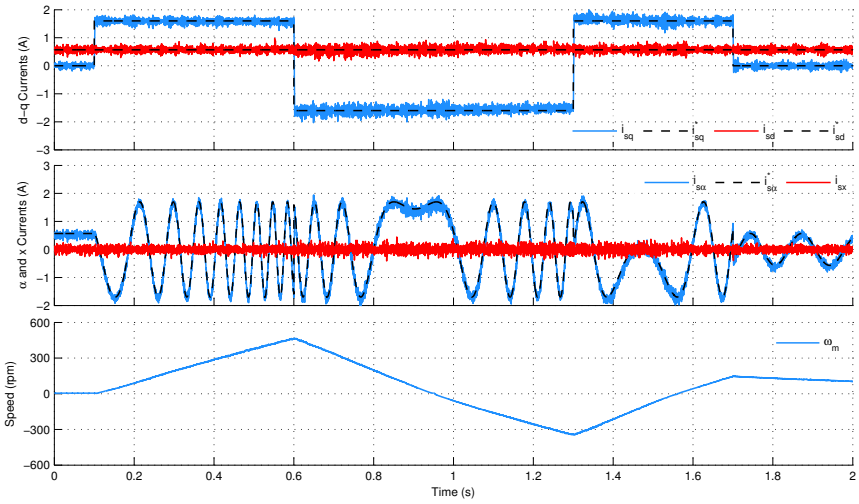

Fig. 12. Transient response using the C3 controller with stator current references $i^*_{sd} = 0.57$ A and $i^*_{sq} = 0(0,\ 0.1s),\ 1.6(0.1,\ 0.6s),\ -1.6(0.6,\ 1.3s),\ 1.6(1.3,\ 1.7s)$ and $0(1.7,\ 2s)$. From top to bottom: d–q stator currents i_{sd} and i_{sq}, and their references i^*_{sd} and i^*_{sq}; α and x stator currents $i_{s\alpha}$ and i_{sx}, with the imposed reference $i^*_{s\alpha}$; and mechanical speed ω_m.

values of λ_{xy}. Only the obtained results using C3 controller are plotted because similar curves are found using C1a, C1b and C2. It can be appreciated that x–y currents decrease when λ_{xy} value increases. On the contrary, α–β current trajectories perform worse when the weighting factor is increased.

Afterwards, some tests have been carried out varying the load torque in the multiphase drive. The experiments have been realized using a weighting factor $\lambda_{xy} = 0.1$ and an electrical frequency $f_e = 29$ Hz. Table VI resumes the obtained results for three different load toque values (T_L of 39%, 58%, and 78% of the nominal one), and all considered controllers. With respect to the current tracking and prediction errors, the obtained results and conclusions remain practically the same for all load torque values. However, a reduction in the switching frequency and THD values is observed when the stator current and the load torque also increase.

Finally, a dynamic test is carried out using the C3 controller to validate the transient performance of the proposed FCS-MPC technique with a rotor current observer (similar results are obtained with C2). The dc machine does not produce load torque during the proposed test. A λ_{xy} value of 0.1 is used, the observer is designed with the same poles than during steady-state tests, and a total of six observer matrices are evaluated offline to take into account different rotor speeds. The d stator current reference (i^*_{sd}) is set to 0.57 A and the q stator current reference (i^*_{sq}) varies in the following way: 0 A from 0 to 0.1 s, 1.6 A from 0.1 to 0.6 s, -1.6 A from 0.6 to 1.3 s, 1.6 A from 1.3 to 1.7 s, and 0 A from 1.7 to 2 s. Fig. 12 summarizes the obtained results. The measured d–q stator currents (i_{sd} and i_{sq}) fit their references well, and the step response of the q current is fast. The trajectories of the α and x currents ($i_{s\alpha}$ and i_{sx}) are also shown. It can be stated that the tracking performance is good even if a sudden reference change appears, displaying a rise time of about 0.002 s. The lower plot draws the mechanical speed ω_m of the drive during the test, showing a quasi-linear response with the applied reference torque (the outer speed control loop is not used in this experiment).

Notice that from the computational cost perspective, one of the main drawbacks for the implementation of FCS-MPC in industry applications, the addition of the rotor current observer produces a negligible increment in the computational load. The total computational cost of the control algorithm with rotor current observers (C2 and C3 controllers) is estimated in 35μs while it is of 32μs for C1a, being 67μs the sampling time.

VI. Conclusion

Observers have been normally used in relation to several controllers: FOC, sensorless drives, and for fault detection but not, to the best of our knowledge, to estimate rotor currents in FCS-MPC techniques. In this paper, it has been shown that it is possible to incorporate a rotor current observer to the FCS-MPC to enhance the predictions, without a considerable penalty in the computational burden of the implemented controller. The obtained simulation and experimental results show that, although the simple estimate and hold scheme used by most MPC practitioners in electrical applications or the more complex MPC technique that uses the Cayley-Hamilton theorem produce acceptable results, the observer outperforms the classic approach presenting some advantages such as better current tracking performance, less harmonic content, and less VSI gating commutations. These advantages result in lower torque ripple and in higher efficiency (lower copper losses and commutations of power switches), encouraging future research

in the field where the proposed observer-based FCS-MPC can be extended to conventional and n-phase induction machines, just adjusting the predictive model and the observer equations to the new system.

REFERENCES

[1] M. Lopez, J. Rodriguez, C. Silva, and M. Rivera, "Predictive torque control of a multidrive system fed by a dual indirect matrix converter," *IEEE Trans. Ind. Electron.*, vol. 62, no. 5, pp. 2731–2741, May 2015.

[2] M. Arahal, F. Barrero, S. Toral, M. Duran, and R. Gregor, "Multi-phase current control using finite-state model-predictive control," *Control Eng. Pract.*, vol. 17, no. 5, pp. 579–587, 2009.

[3] W. Xie, X. Wang, F. Wang, W. Xu, R. Kennel, D. Gerling, and R. Lorenz, "Finite control set-model predictive torque control with a deadbeat solution for PMSM drives," *IEEE Trans. Ind. Electron.*, vol. 62, no. 9, pp. 5402–5410, Sep. 2015.

[4] S. Kouro, M. A. Perez, J. Rodriguez, A. M. Llor, and H. A. Young, "Model predictive control: MPC's role in the evolution of power electronics," *IEEE Ind. Electron. Mag.*, vol. 9, no. 4, pp. 8–21, Dec. 2015.

[5] D. G. Luenberger, "An introduction to observers," *IEEE Trans. Autom. Control*, vol. AC-16, no. 6, pp. 596–602, Dec. 1971.

[6] P. L. Jansen and R. D. Lorenz, "A physically insightful approach to the design and accuracy assessment of flux observers for field oriented induction machine drives," *IEEE Trans. Ind. Appl.*, vol. 30, no. 1, pp. 101–110, Jan./Feb. 1994.

[7] S. A. Davari, D. A. Khaburi, F. Wang, and R. M. Kennel, "Using full order and reduced order observers for robust sensorless predictive torque control of induction motors," *IEEE Trans. Power Electron.*, vol. 27, no. 7, pp. 3424–3433, Jul. 2012.

[8] C. Xia, M. Wang, Z. Song, and T. Liu, "Robust model predictive current control of three-phase voltage source PWM rectifier with online disturbance observation," *IEEE Trans. Ind. Informat.*, vol. 8, no. 3, pp. 459–471, Aug. 2012.

[9] A. Merabet, M. Ouhrouche, and R.-T. Bui, "Nonlinear predictive control with disturbance observer for induction motor drive," in *Proc. IEEE Int. Symp. Ind. Electron. (ISIE)*, 2006, pp. 86–91.

[10] C. S. Lim, E. Levi, M. Jones, N. A. Rahim, and W. P. Hew, "FCS-MPC-based current control of a five-phase induction motor and its comparison with PI-PWM control," *IEEE Trans. Ind. Electron.*, vol. 61, no. 1, pp. 149–163, Jan. 2014.

[11] F. Barrero and M. J. Duran, "Recent advances in the design, modeling and control of multiphase machines-Part 1," *IEEE Trans. Ind. Electron.*, vol. 63, no. 1, pp. 449–458, Jan. 2016.

[12] M. J. Duran and F. Barrero, "Recent advances in the design, modeling and control of multiphase machines-Part 2," *IEEE Trans. Ind. Electron.*, vol. 63, no. 1, pp. 459–468, Jan. 2016.

[13] R. S. Arashloo, M. Salehifar, L. Romeral, and V. Sala, "A robust predictive current controller for healthy and open-circuit faulty conditions of five-phase BLDC drives applicable for wind generators and electric vehicles," *Energy Convers. Manage.*, vol. 92, pp. 437–447, 2015.

[14] C. Martín, M. R. Arahal, F. Barrero, and M. J. Duran, "Multiphase rotor current observers for current predictive control: A five-phase case study," *Control Eng. Pract.*, vol. 49, pp. 101–111, 2016.

[15] E. Levi, R. Bojoi, F. Profumo, H. Toliyat, and S. Williamson, "Multiphase induction motor drives-A technology status review," *IET Elect. Power Appl.*, vol. 1, no. 4, pp. 489–516, 2007.

[16] M. J. Duran, J. A. Riveros, F. Barrero, H. Guzman, and J. Prieto, "Reduction of common-mode voltage in five-phase induction motor drives using predictive control techniques," *IEEE Trans. Ind. Appl.*, vol. 48, no. 6, pp. 2059–2067, Nov./Dec. 2012.

[17] H. Miranda, P. Cortes, J. I. Yuz, and J. Rodriguez, "Predictive torque control of induction machines based on state-space models," *IEEE Trans. Ind. Electron.*, vol. 56, no. 6, pp. 1916–1924, Jun. 2009.

[18] S. Kouro, P. Cortes, R. Vargas, U. Ammann, and J. Rodriguez, "Model predictive control-A simple and powerful method to control power converters," *IEEE Trans. Ind. Electron.*, vol. 56, no. 6, pp. 1826–1838, Jun. 2009.

[19] G. C. Verghese and S. R. Sanders, "Observers for flux estimation in induction machines," *IEEE Trans. Ind. Electron.*, vol. IE-35, no. 1, pp. 85–94, Feb. 1988.

[20] Y. Zhang and H. Yang, "Model predictive torque control of induction motor drives with optimal duty cycle control," *IEEE Trans. Power Electron.*, vol. 29, no. 12, pp. 6593–6603, Dec. 2014.

[21] J. Kautsky, N. K. Nichols, and P. Van Dooren, "Robust pole assignment in linear state feedback," *Int. J. Control*, vol. 41, no. 5, pp. 1129–1155, 1985.

[22] A. G. Yepes, J. A. Riveros, J. Doval-Gandoy, F. Barrero, O. Lopez, B. Bogado, M. Jones, and E. Levi, "Parameter identification of multiphase induction machines with distributed windings-Part 1: Sinusoidal excitation methods," *IEEE Trans. Energy Convers.*, vol. 27, no. 4, pp. 1056–1066, Dec. 2012.

[23] J. A. Riveros, A. G. Yepes, F. Barrero, J. Doval-Gandoy, B. Bogado, O. Lopez, M. Jones, and E. Levi, "Parameter identification of multiphase induction machines with distributed windings-Part 2: Time-domain techniques," *IEEE Trans. Energy Convers.*, vol. 27, no. 4, pp. 1067–1077, Dec. 2012.

[24] W. S. Levine, *The control handbook*. Boca Raton, FL, USA: CRC Press, 1996.

Cristina Martín was born in Seville, Spain, in 1989. She received the Industrial Engineer degree from the University of Málaga, Málaga, Spain, in 2014. She has been working toward the Ph.D. degree in electronic engineering in the Department of Electronic Engineering, University of Seville, Seville, Spain, since 2015.

Her research interests include modeling and control of multiphase drives, microprocessor and DSP device systems, and electrical vehicles.

Manuel R. Arahal (M'06) was born in Seville, Spain, in 1966. He received the M.Sc. and Ph.D. degrees in industrial engineering from the University of Seville, Seville, Spain, in 1991 and 1996, respectively.

He is currently a Professor with the Department of Systems Engineering and Automation, University of Seville.

Dr. Arahal was the recipient of Best Paper Awards from the IEEE Transactions on Industrial Electronics for 2009, and from the IET Electric Power Applications for 2010-2011.

Federico Barrero (M'04–SM'05) received the M.Sc. and Ph.D. degrees in electrical and electronic engineering from the University of Seville, Seville, Spain, in 1992 and 1998, respectively.

In 1992, he joined the Department of Electronic Engineering, University of Seville, where he is currently an Associate Professor.

Dr. Barrero was the recipient of Best Paper Awards from the IEEE Transactions on Industrial Electronics for 2009 and from the IET Electric Power Applications for 2010-2011.

Mario J. Durán was born in Málaga, Spain, in 1975. He received the M.Sc. and Ph.D. degrees in electrical engineering from the University of Málaga, Málaga, Spain, in 1999 and 2003, respectively.

He is currently an Associate Professor with the Department of Electrical Engineering, University of Málaga. His research interests include modeling and control of multiphase drives and renewable energies conversion systems.

CONTROL ENGINEERING PRACTICE

Multiphase rotor current observers for current predictive control: A five-phase case study

Cristina Martín[a,*], Manuel R. Arahal[b], Federico Barrero[a], Mario J. Durán[c]

[a] *Dpto. Ing. Electrónica, Universidad de Sevilla, Spain*
[b] *Dpto. Ing. de Sistemas y Automática, Universidad de Sevilla, Spain*
[c] *Dpto. Ing. Eléctrica, Universidad de Málaga, Spain*

Abstract

The use of multiphase drives has gained importance in recent times due to some advantages that they provide over conventional three-phase ones. High performance stator current control can be achieved by means of direct command of voltage source inverter. In this context finite-state model predictive control is a very flexible strategy that has been recently proposed and analyzed. Nevertheless, its implementation must solve the problem of estimating rotor quantities, being the conventional solution a simple backtracking procedure. In this respect, observers appear as an attractive alternative. However, while they have been used with FOC, sensorless drives and for fault detection, they have not been used yet for predictive control of drives as a way to provide rotor values estimates. In this paper the authors propose to incorporate a full-order rotor current observer in a finite-state model predictive controller of a five-phase induction machine. Pole placement design based on Butterworth filters is used. The new estimation scheme and the standard procedure are compared. By means of experimental tests, the differences between both approaches and the benefits of including a rotor observer are illustrated and verified.

Keywords: Multiphase drives, predictive control, finite-state controller, observer, pole placement.

1. Introduction

In the last decade, research on multiphase electrical machines area has increased due to some specific advantages that they present over the conventional three-phase machines: less current harmonic content, higher overall system reliability, better power distribution per phase and better fault tolerance (Levi, 2008; Levi et al., 2007). Among these machines, asymmetrical six-phase and five-phase induction machines (IM) with sinusoidally distributed stator windings are the most analyzed and proposed in recent works.

Current control strategies in multiphase drives are usually based on a multidimensional extension of common three-phase current controllers, dealing with the difficulties of large harmonic current, unbalanced currents and machine asymmetries (Che et al., 2014; Jones et al., 2009; Yepes et al., 2015). However, these difficulties can be easily overcome eliminating the PWM and commanding the voltage source inverter (VSI) directly by means of model-based predictive control (MPC). Although MPC is a well-established control technique for electrical systems (Chai et al., 2013; Holtz and Stadtfeld, 1983; Lopez et al., 2015; Wang et al., 2014), its application to multiphase IM has increased well after the publication of Levi (2008). Particularly, a new MPC configuration was proposed in Holmes and Martin (1996) in order to eliminate the classical PWM method, giving birth to a control structure that was later named as finite-state MPC (FSMPC) used in multi-phase IM for the first time in Arahal et al. (2009). Since the number of available converter switching states is a finite set, this control structure is also known as finite control set MPC (Choi and Lee, 2015; Rodriguez et al., 2013; Xie et al., 2015). Whatever the denomination, the fast control derived from direct command of the VSI combined with robustness and fault tolerant features that characterize multiphase drives have been analyzed in a number of recent papers (Arashloo et al., 2015; Guzman et al., 2016; Lim et al., 2014; Martinez et al., 2015; Riveros et al., 2013).

A problem encountered in the implementation of FSMPC is the estimation of non-measurable state components; for instance rotor quantities for which sensors are not available. A good knowledge of such quantities is often required in order to provide high performance control. Concerning this, observer theory (Luenberger, 1971) is a well known discipline that provides a framework for understanding and designing estimation schemes and it has been used in electrical systems such as IM drives. Basically, observers used in IM machines can take two forms, a full-order one that permits estimation of stator and rotor components from measurements of stator voltages, sta-

*Corresponding author
Email addresses: cmartin15@us.es (Cristina Martín), arahal@us.es (Manuel R. Arahal), fbarrero@us.es (Federico Barrero), mjduran@uma.es (Mario J. Durán)

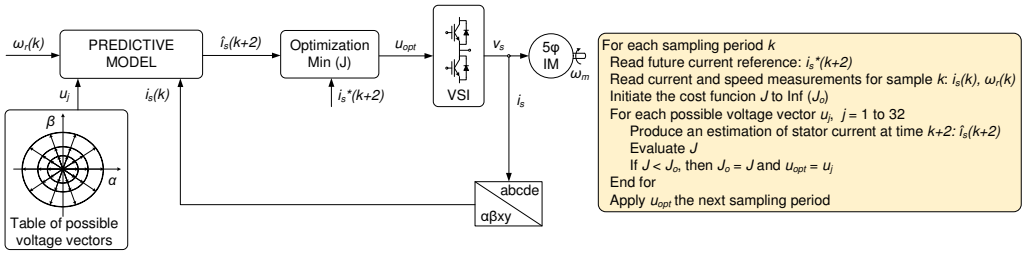

Figure 1: General scheme of the FSMPC method applied to a symmetrical five-phase IM drive (left), and control algorithm (right).

tor currents and speed (Jansen and Lorenz, 1994), and a reduced-order form which provides just the rotor components estimation using only measurements of stator currents and speed.

Most proposals of observers for IM have been made with field oriented control (FOC) method and related ones (El Fadili et al., 2014), even though FOC has been found in practice to be satisfactorily robust and effective without complex flux estimation structures. By contrast, FSMPC is highly sensitive to prediction errors (Arahal et al., 2013) that are caused by parameter mismatch among other reasons (Bogado et al., 2013). In Alireza Davari et al. (2012) sliding mode full-order and reduced-order observers are applied for flux and speed estimation for predictive torque control of IM. A robust model predictive current controller with a disturbance observer is also presented in Xia et al. (2012), where a Luenberger observer is constructed for parameter mismatch and model uncertainty which affects the performance of the MPC. The gains of the disturbance observer are also determined using a root-locus analysis, and the stability of the disturbance observer is analyzed when there are errors in the inductor filter parameter. In Merabet et al. (2006), a nonlinear predictive control law with a disturbance observer is applied to track speed and flux profiles in an IM, considering the robustness to parameters variations and the disturbance rejection. This is in contrast to most applications of FSMPC to electrical systems, where observers are not used as such. Instead nonmeasurable quantities, disturbances and parametric and non-parametric uncertainties are lumped into one single term of the predictive model. This term is then updated using a simple procedure and the update is held until the next sampling period (Arahal et al., 2009).

In this paper a rotor current observer is included in the conventional FSMPC structure. The advantages of this new estimation scheme over the original one are analyzed and experimentally illustrated. For this purpose, a five-phase IM drive is used as a case study. However, the control method can be extended to any n-phase IM drive. Two observers, full-order and reduced-order, are studied. The observer design is tackled using pole placement methodology based on Butterworth filters. The rest of the paper is organized as follows. The general principles of the FSMPC technique and its application to the considered case study system are presented in the next section, where the standard rotor quantities estimation is reviewed and analyzed. The rotor current observers, full-order and reduced-order, are presented in Section 3 together with the design procedure. Experimental results comparing the different estimation methods are shown and discussed in Section 4. The paper ends with the conclusion section.

2. Finite-state model predictive control in five-phase IM drives

The FSMPC application to stator current control in a five-phase drive is schematically illustrated in Fig. 1. The objective of the controller is to track the reference stator currents represented by i_s^*. For this purpose, a discrete model of the physical system is used to predict the future behavior of the output variables $\hat{i}_s$. The prediction is computed making use of measured values of the rotor speed ω_r and the stator phase currents i_s and tentative value of the control vector u_j (the VSI gating signal). The most adequate control action u_{opt} is selected by minimizing a cost function J by means of exhaustive search over all possible control signal values. The optimum gating signal is applied to the VSI during the next sampling period. Finally, this process is repeated every sampling period. More details can be found in Arahal et al. (2009).

2.1. IM drive model

A symmetrical five-phase induction machine with distributed windings equally displaced $\vartheta = 2\pi/5$ and fed by a five-phase two-level VSI is used for testing the proposed method. An approximate scheme of the five-phase IM is shown in Fig. 2, where the gating signals of the VSI are represented by $(K_a, \ldots, K_e)$ and their complementary values $(\bar{K}_a, \ldots, \bar{K}_e)$.

The drive modeling process is made using some standard assumptions: uniform air gap, symmetrical distributed windings, sinusoidal MMF distribution, and negligible core losses and magnetic saturation. The sinusoidal MMF distribution is a well-known assumption in conventional and multiphase induction machines' modelling, provided that

a distributed-winding induction machine is used, as it is discussed in Barrero and Duran (2016); Duran and Barrero (2016); Levi et al. (2007). Then, from the five-phase machine equations in phase variables and following the vector space decomposition (VSD) approach the machine modeling can be represented in two orthogonal subspaces (Levi et al., 2007). One of them, the α–β subspace, is involved in the fundamental flux and the torque production, representing the fundamental supply component plus supply harmonics of the order $10n \pm 1$ with $n = 0, 1, 2, 3, ...$ The other, the x–y subspace, is related to the losses and represents supply harmonics of the order $10n \pm 3$. Additionally, a zero sequence harmonic component of the order $5n$ with $n = 1, 2, 3, ...$ is projected in the z–axis, but it is not considered because the neutral point is isolated and consequently zero sequence currents cannot flow. Selecting the α–β and x–y stator currents and the α–β rotor currents as state variables $x = (i_{s\alpha}, i_{s\beta}, i_{sx}, i_{sy}, i_{r\alpha}, i_{r\beta})^T$, the drive equations can be cast in the form

$$\dot{x}(t) = A(\omega_r(t))x(t) + Bv(t)$$
$$y(t) = Cx(t) \tag{1}$$

The input signals are the applied stator voltages $v = (v_{s\alpha}, v_{s\beta}, v_{sx}, v_{sy})^T$, the output signals are the stator currents $y = (i_{s\alpha}, i_{s\beta}, i_{sx}, i_{sy})^T$ and the matrices A and B depend on the rotor electric speed ω_r and the following machine parameters, stator and rotor resistances R_s and R_r, stator and rotor inductances L_s and L_r, stator leakage inductance L_{ls} and mutual inductance M.

$$A(\omega_r) = \begin{pmatrix} -a_{s2} & a_{m4}(\omega_r) & 0 & 0 & a_{r4} & a_{l4}(\omega_r) \\ -a_{m4}(\omega_r) & -a_{s2} & 0 & 0 & -a_{l4}(\omega_r) & a_{r4} \\ 0 & 0 & -a_{s3} & 0 & 0 & 0 \\ 0 & 0 & 0 & -a_{s3} & 0 & 0 \\ a_{s4} & -a_{m5}(\omega_r) & 0 & 0 & -a_{r5} & -a_{l5}(\omega_r) \\ a_{m5}(\omega_r) & a_{s4} & 0 & 0 & a_{l5}(\omega_r) & -a_{r5} \end{pmatrix} \tag{2}$$

$$B = \begin{pmatrix} c_2 & 0 & 0 & 0 \\ 0 & c_2 & 0 & 0 \\ 0 & 0 & c_3 & 0 \\ 0 & 0 & 0 & c_3 \\ -c_4 & 0 & 0 & 0 \\ 0 & -c_4 & 0 & 0 \end{pmatrix} \tag{3}$$

The above matrix coefficients are given by $c_1 = L_s L_r - M^2$, $c_2 = L_r/c_1$, $c_3 = 1/L_{ls}$, $c_4 = M/c_1$, $c_5 = L_s c_1$, $a_{s2} = R_s c_2$, $a_{s3} = R_s c_3$, $a_{s4} = R_s c_4$, $a_{r4} = R_r c_4$, $a_{r5} = R_r c_5$, $a_{l4}(\omega_r) = L_r c_4 \omega_r$, $a_{l5}(\omega_r) = L_r c_5 \omega_r$, $a_{m4}(\omega_r) = M c_4 \omega_r$ and $a_{m5}(\omega_r) = M c_5 \omega_r$.

The predictive model must also include the VSI dynamic, since it forms part of the IM drive. An ideal inverter converts gating signals into stator voltages that can be projected to α–β–x–y axes and gathered in a row vector computed as $v = (v_{s\alpha}, v_{s\beta}, v_{sx}, v_{sy}) = V_{dc} u T M$, where

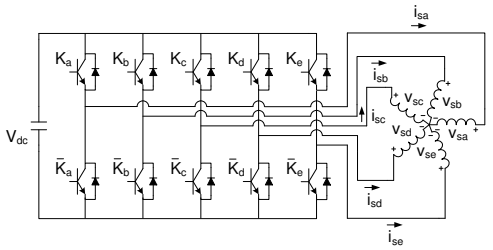

Figure 2: Five-phase IM drive schematic diagram.

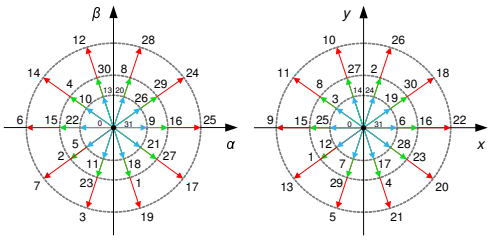

Figure 3: Space vector diagrams in the α–β and x–y subspaces.

V_{dc} is the DC-link voltage, u is a row vector containing the gating signals, T is the connectivity matrix that takes into account how the VSI gating signals are distributed and M is a coordinate transformation matrix accounting for the spatial distribution of the machine windings:

$$T = \frac{1}{5}\begin{pmatrix} 4 & -1 & -1 & -1 & -1 \\ -1 & 4 & -1 & -1 & -1 \\ -1 & -1 & 4 & -1 & -1 \\ -1 & -1 & -1 & 4 & -1 \\ -1 & -1 & -1 & -1 & 4 \end{pmatrix} \tag{4}$$

$$M = \frac{2}{5}\begin{pmatrix} 1 & \cos\vartheta & \cos 2\vartheta & \cos 3\vartheta & \cos 4\vartheta \\ 0 & \sin\vartheta & \sin 2\vartheta & \sin 3\vartheta & \sin 4\vartheta \\ 1 & \cos 2\vartheta & \cos 4\vartheta & \cos\vartheta & \cos 3\vartheta \\ 0 & \sin 2\vartheta & \sin 4\vartheta & \sin\vartheta & \sin 3\vartheta \\ 1/2 & 1/2 & 1/2 & 1/2 & 1/2 \end{pmatrix} \tag{5}$$

In the case of a 5-legged inverter, the gating signals vector is defined as $u = (K_a, K_b, ..., K_e)$ where K_j is the j-th gating signal. Since each gating signal can be either active $K_j = 1$ or inactive $K_j = 0$, there exist 2^5 possible control choices and voltage vectors. Fig. 3 shows all possible voltage vectors where each one is identified using the decimal number corresponding to the binary code of the switching state.

Eqs. (1)–(3) together with the inverter model define the final drive model as a nonlinear set of equations. These equations must be discretized in order to be used for the predictive controller. A forward Euler method is usually used, leading to the following expression that constitutes

the predictive model:

$$\hat{x}(k+1|k) = x(k) + T_s\left(A(\omega_r(k))x(k) + Bv(k)\right) \quad (6)$$

denoted by T_s the sampling time, k the current sample time and $\hat{x}(k+1|k)$ the one-step ahead prediction of the system state computed at current time k. Notice that matrix A depends on the instantaneous value of the rotor electric speed, thus the predictive model is a time-variant linear system. However, the mechanical speed dynamics are slower than the electrical dynamics, so constant speed within a sampling period can usually be assumed.

2.2. State estimation

The predictive model (6) presented in the previous section cannot be used as such in a typical configuration in which rotor currents are not measured. This difficulty is conventionally overcome lumping all non-measurable terms into one factor, constituting a new variable that is estimated using past values of the measured variables. The estimated term is then projected into the future and used in the predictive model, being updated every sampling period. In the present case, it is necessary to split the state vector into a measurable part $x^1 = (i_{s\alpha}, i_{s\beta}, i_{sx}, i_{sy})^T$ and an unmeasurable part $x^2 = (i_{r\alpha}, i_{r\beta})^T$. Thus, the prediction is obtained by simulating for a sampling period the evolution of the measurable part as

$$\hat{x}^1(k+1|k) = Rx^1(k) + Sv(k) + \hat{G}(k|k) \quad (7)$$

where

$$R = (I + A_{11}T_s) \quad (8)$$

$$S = B_1 T_s \quad (9)$$

and term $\hat{G}(k|k)$ is an estimation of the contribution of $x^2(k)$ to $x^1(k+1)$. It is usually obtained by holding its previous value $\hat{G}(k-1)$ computed at time k as

$$\hat{G}(k-1|k) = x^1(k) - Rx^1(k-1) - Sv(k-1) \quad (10)$$

The computation of the control signal takes a significant amount of time, being comparable with the sampling time. Consequently, it is desirable to wait until the next sampling time to release the computed control signal (more details in Arahal et al. (2009)). Taking this into account, a second-step ahead prediction has to be computed, being the current prediction at time $k+2$ obtained at time k as

$$\hat{x}^1(k+2|k) = Rx^1(k+1|k) + Sv(k) + \hat{G}(k|k) \quad (11)$$

In stator current control in multiphase IM, the cost function should incorporate the predicted deviations from current references in the α–β and x–y subspaces in the following way:

$$J = \|\hat{e}_{\alpha\beta}\|^2 + \lambda_{xy}\|\hat{e}_{xy}\|^2 \quad (12)$$

where $\hat{e}$ is the second-step ahead predicted error $\hat{e} = i_s^*(k+2) - \hat{i}_s(k+2|k)$ and λ_{xy} is a tuning parameter that allows more emphasis on α–β or x–y subspaces. More complicated cost functions can be devised in order to include other aspects to be optimized, such as harmonic content and VSI losses.

2.3. Analysis of the simple update and hold method

To the best of our knowledge, the backtracking procedure introduced in the previous section has not been analyzed in the literature yet, and thus the following study is novel and relevant as most proposed FSMPC applications rely on said procedure.

As already stated, the usual way to cope with unmeasurable quantities in FSMPC is to lump them into one term that is estimated in a simple manner. The term is designated as G and used in the first-step ahead prediction as

$$\hat{x}^1(k+1|k) = Rx^1_m(k) + Sv(k) + \hat{G}(k|k) \quad (13)$$

Ideally the term $G(k-1)$ could be computed at time k by means of

$$G(k-1) = x^1(k) - Rx^1(k-1) - Sv(k-1) \quad (14)$$

but, due to measurement errors ε, the actual estimation is

$$\hat{G}(k-1|k) = x^1_m(k) - Rx^1_m(k-1) - Sv(k-1) \quad (15)$$

where $x^1_m(k)$ is the measured vector of stator quantities, linked to the real values through

$$x^1_m(k) = x^1(k) + \varepsilon(k) \quad (16)$$

Making use of the state-space equations the estimation can be written as

$$\hat{G}(k-1|k) = \varepsilon(k) - R\varepsilon(k)(k-1) + A_{12}T_s x^2(k-1) \quad (17)$$

From this equality it is inferred that the estimation of rotor quantities done in this way is corrupted by the measurement error. The error of the first step ahead prediction is defined as

$$e_{1p}(k+1) \doteq x^1(k+1) - \hat{x}^1(k+1|k) \quad (18)$$

and can be computed from previous expressions as

$$e_{1p}(k+1) = Rx^1(k) + Sv(k) + G(k) - \\ - \left(Rx^1_m(k) + Sv(k) + \hat{G}(k-1|k)\right) \quad (19)$$

It is easy to show that the above equation yields the following expression for the one-step ahead prediction error

$$e_{1p}(k+1) = -(I+R)\varepsilon(k) + R\varepsilon(k)(k-1) + \\ + A_{12}T_s\left(x^2(k) - x^2(k-1)\right) \quad (20)$$

From (20) one can derive that the prediction error arising from this scheme does not filter measurement errors. On average, the prediction error due to this factor will exhibit the same statistical properties as ε. Assuming uncorrelated error measurement with a distribution with zero mean and σ^2 variance, the contribution to e_{1p} variance is precisely σ^2. However the instantaneous contribution can be large, for instance if $\varepsilon(k) = -\varepsilon(k-1) = n$ then $-(I+R)\varepsilon(k) + R\varepsilon(k)(k-1) = (I+2R)n = (3I + 2A_{11}T_s)n \approx 3n$.

Consequently, a small amount of noise can produce large deviations in the estimation of the state. This has a profound impact on the performance of the current control because a wrong voltage vector would be selected producing a disturbance that should be canceled at later sampling times. In Arahal et al. (2013) it is shown that current total harmonic distortion (THD) is greatly influenced by this phenomenon.

Regarding rotor quantities, it is interesting to see that the contribution to the prediction error is filtered through the system dynamic via the term $A_{12}T_s$. For larger sampling frequencies the effect is smaller, which is part of the reason why most applications uses a high value of f_s. Also from the above expression one can see that it is the change in rotor quantities that induces prediction error. In sinusoidal steady state the rotor quantities are expected to evolve, for the most part, at the fundamental frequency f_e. Again, if a large f_s/f_e is used then the changes from one sampling period to the next would be small (ceteris paribus), allowing the standard simple estimation scheme to provide acceptable results. A problem might arise during transients where changes can be more pronounced, or in situations where harmonics are noticeable and fast variations in rotor quantities appear. This is potentially dangerous as harmonics can be triggered by erroneous predictions as indicated in the previous paragraph.

Fig. 4 illustrates the effect of using the simple estimation procedure for rotor quantities. The graph is a state-space or phase-portrait diagram, where the q_1 and q_2 axis symbolize the state components. The state at time k (shown as a dot in the middle) can evolve with time, providing different values at $k+1$ depending on the choice of the control action $u(k)$. The standard simple estimation method provides predictions (blue lines) with an error given by (20). It will be shown later that observers can provide more adequate predictions (green lines).

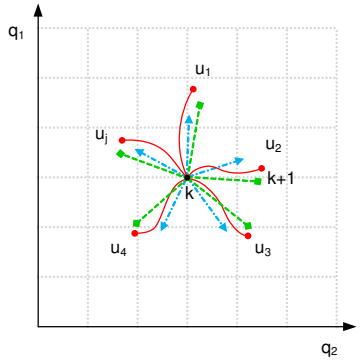

Figure 4: Illustration of conventional and observer-based predictions. Red lines with circle marks (solid) represent the real trajectory after applying a certain voltage vector. Blue lines with triangle marks are predicted trajectories using the simple rotor quantities estimation and green lines with square marks are predicted trajectories using an observer.

The correctness of the predictions plays a crucial role in FSMPC because control actions are based on them. Note that the large number of available voltage vectors in multiphase VSI and the particularity of the cost function provides a scenario in which mildly incorrect predictions result in the choice of different optimal voltages. This will be illustrated in the experimental results section.

3. Rotor current observer design and implementation

In Fig. 5 the conventional FSMPC technique is presented including an optional observer to estimate the rotor quantities. The rotor current estimation $\hat{i}_r$ is calculated by the observer using the measured rotor speed ω_r and stator phase currents i_s for every sampling time, allowing the complete state-space model (1) to be employed for predictive purposes.

The observer order is defined by the number of system state variables employed in its construction. In the following sections, the design and implementation of two observer configurations with different orders are presented: full-order observer and reduced-order observer.

3.1. Full-order rotor current observer

The basic observer configuration permits an estimation of all system states $\hat{x}(t)$ from the system model, plus a correction term which is proportional to the estimate error

$$\dot{\hat{x}}(t) = A\hat{x}(t) + Bv(t) - L\left(C\hat{x}(t) - y(t)\right) \tag{21}$$

From observer theory, it is known that the closed loop poles of the observer defined in (21) are determined by the observer gain L, also called Luenberger gain matrix. The observer error dynamic equation can be simplified to

$$\dot{e}(t) = \dot{\hat{x}} - \dot{x} = (A - LC)\, e(t) \tag{22}$$

and the convergence towards zero is determined by the choice of the observer gain. The separation principle allows the choice of such matrix to be decoupled from the controller design.

3.2. Reduced-order rotor current observer

The stator current's estimation obtained from the full-order observer leads to a redundancy, since they are already available by direct measurement. This redundancy can be eliminated by constructing an observer of lower dimension that might be useful for reducing the computation time.

A reduced-order observer for i_r can be derived using Gopinath's method (Gopinath, 1971). For the case of study, the system's state is divided in two parts, the measurable one $x^1 = (i_{s\alpha}, i_{s\beta})^T$ and the unmeasurable one

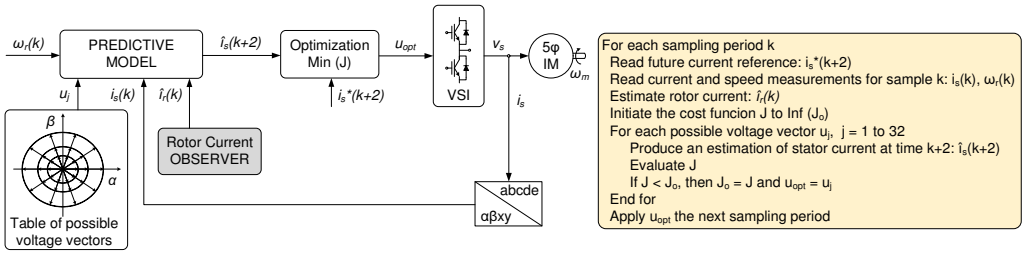

Figure 5: General scheme of the FSMPC with rotor current observer method applied to a symmetrical five-phase IM drive (left), and control algorithm (right).

$x^2 = (i_{r\alpha}, i_{r\beta})^T$. Matrices A and B are accordingly divided so that

$$\dot{x}^1(t) = A_{11}x^1(t) + A_{12}x^2(t) + B_1 v(t)$$
$$\dot{x}^2(t) = A_{21}x^1(t) + A_{22}x^2(t) + B_2 v(t) \quad (23)$$

The estimation for the unmeasurable part is computed in the following way

$$\hat{x}^2(t) = z(t) + Lx^1(t) \quad (24)$$

where the $z(t)$ dynamic is dictated by

$$\dot{z}(t) = (A_{22} - LA_{12})\, z(t) + (A_{22} - LA_{12})\, Lx^1(t) + (A_{21} - LA_{11})\, x^1(t) + (B_2 - LB_1)\, v(t) \quad (25)$$

Finally, the reduced-order estimator error is now

$$\dot{e}(t) = \hat{\dot{x}}^2 - \dot{x}^2 = (A_{22} - LA_{12})\, e(t) \quad (26)$$

This observer configuration reduces the computational load required to estimate all state variables when the full-order observer is employed.

3.3. Observer design with Butterworth pole placement

A correct observer design should consider the effect of gain matrix L in all terms of the error dynamic to provide a trade-off between fast convergence and disturbance sensitivity. Observer theory suggests ad hoc modifications of the estimator that often yield faster convergence without endangering stability (Verghese and Sanders, 1988). Additionally, the poles of classical observers for IM are placed proportionally to the IM poles, which produce high imaginary parts at high speed and deteriorate the system stability. In Zhang and Yang (2014) it is suggested the imaginary part be equal to that of the IM poles and the real part be shifted to the left in the complex plane compared to the original poles. However, this leads to complicated expressions of observer gains. The authors propose a very simple constant gain matrix to improve the stability of the observer.

The design of both full-order and reduced-order observers implies the selection of the most adequate eigenvalues of $(A - LC)$ and $(A_{22} - LA_{12})$, respectively. As they determine the speed at which the estimation error decays, it is logical to make the real parts of those eigenvalues as negative as possible. But this logic does not work well when modeling errors need to be considered. In this regard, research has shown that in order for the observer to be robust against modeling errors, as well as causing the estimation error to decay rapidly, a different approach is required.

It is also of importance that the observer has well-damped dynamics. Good damping of a system implies that the poles are located some distance away from the origin in order to speed-up the convergence and with imaginary parts no larger than the real parts. The latter is desirable in order to avoid oscillatory behavior. With poor damping, there is also a risk for instability if the observer is implemented using forward Euler discretization (Verghese and Sanders, 1988).

Finally, if the original system has z_1 stable zeros, then z_1 of the observer's eigenvalues should keep those positions. The remaining eigenvalues of the observer may be placed into the left-half plane, but at locations that are equidistant from the origin in what is known as the Butterworth configuration. Therefore, a Butterworth polynomial is the equation employed to calculate the eigenvalues. This polynomial represents the denominator of a low-pass filter in the area of signal processing. The step response of such filters has a slight overshoot, with good damping. Consequently, it is desirable to place the poles of the observer in the locations given by the roots of a proper Butterworth polynomial in order to obtain good damping and rising times with respect to the error dynamic.

The full-order observer needs a sixth order Butterworth filter to evaluate its poles. However, the model of the system presents two real poles for the case of study. A more proper solution consists of placing four of the observer poles using a fourth order filter and shifting the original two real poles to the left in order to speed up the observer error dynamic. The characteristic polynomial of a fourth order Butterworth filter is

$$B_4(s) = T_B^4 s^4 + 2.6131 T_B^3 s^3 + 3.4142 T_B^2 s^2 + 2.6131 T_B s + 1 \quad (27)$$

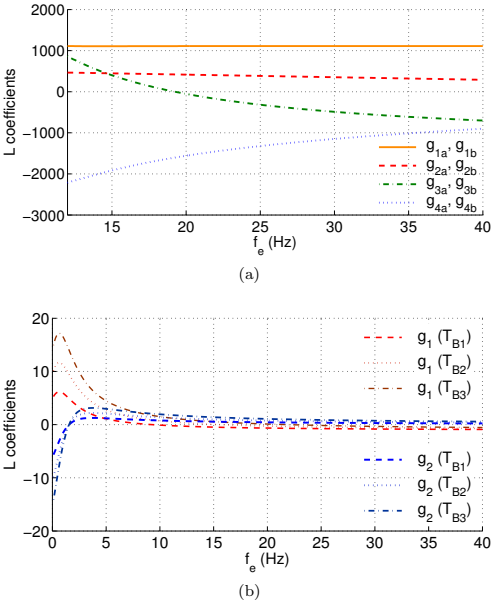

Figure 6: (a) Variation of L_{FO} coefficients vs f_e. (b) Variation of L_{RO} coefficients vs f_e for some values of T_B.

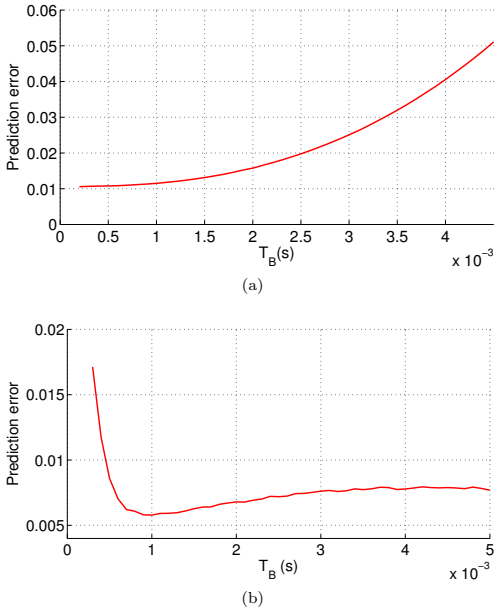

Figure 7: Prediction error dependence on parameter T_B used to tune (a) the full-order observer and (b) the reduced-order observer.

where parameter T_B is used to define the speed of the response, with such speed inversely proportional to T_B.

On the other hand, a second order Butterworth filter is necessary to determine the poles of the proposed reduced-order observer. The filter characteristic polynomial is now

$$B_2(s) = T_B^2 s^2 + \sqrt{2} T_B s + 1 \tag{28}$$

Once the desired closed loop observer poles are computed using (27) and (28), Luenberger matrix coefficients are derived using the Kautsky-Nichols algorithm (Kautsky et al., 1985), resulting in the following Luenberger matrices L_{FO} and L_{RO} for the full-order and reduced-order observers, respectively:

$$L_{FO} = \begin{pmatrix} g_{1a} & g_{2a} & 0 & 0 \\ -g_{2b} & g_{1b} & 0 & 0 \\ 0 & 0 & g_5 & 0 \\ 0 & 0 & 0 & g_5 \\ g_{3a} & -g_{4a} & 0 & 0 \\ g_{4b} & g_{3b} & 0 & 0 \end{pmatrix} \tag{29}$$

$$L_{RO} = \begin{pmatrix} g_1 & -g_2 \\ g_2 & g_1 \end{pmatrix} \tag{30}$$

Now, as the coefficients of A and A_{22} are dependent on ω_r, it is necessary to solve the pole placement problem for the current value of ω_r on-line. In order to avoid the required computing load, it is convenient to derive expressions for the elements of the gain matrices as a function of ω_r; or to use a pre-computed set of coefficients and interpolate. In the latter case, the resulting observer is equivalent to a gain scheduled system and its performance depends on the schedule resolution as well as on the accuracy of the measured values of ω_r.

Fig. 6a shows the variation of L_{FO} coefficients with the electrical frequency f_e. Coefficient g_5 has not been represented because its value is constant for all frequencies and T_B. Coefficients' values are almost equal in pairs throughout the frequency range. For that reason, they have been depicted as equal for clarity of representation. Also, the evolution of these parameters can be approximated by simple equations that permit the computation of a new gain matrix on-line, avoiding the Kautsky-Nichols algorithm. However, these coefficients vary with T_B, so different equations have to be defined.

On the other hand, the L_{RO} gain matrix coefficients are shown in Fig. 6b for different frequencies and for $T_{B1} = 0.0025$ s, $T_{B2} = 0.0014$ s, and $T_{B3} = 0.001$ s. It can be seen that the variation in the coefficients' values is smooth, allowing one to rely on interpolation if a sufficiently high number of discrete samples is given, validating this interpolation for all T_B.

To complete the observer design, an adequate value of T_B must to be chosen. Fig. 7 shows the variation of the

prediction error with T_B for both full-order and reduced-order observers. It can be seen in both cases that there is an optimum value of T_B that minimizes the error. The errors have been obtained via extensive simulation using a model of the IM with a FSMPC that makes use of the observer. In the real machine the minimum is obtained for a slightly different value that will be used in the experiments shown in the next section.

3.4. Analysis of the robustness of the observer

Changes in real parameters might cause the observer to use an inaccurate model. In the following a new derivation of the state estimation error is made taking into account this possibility. In the general case, the complete system model has the form

$$\dot{x} = Ax + Bu + Dd$$
$$y = Cx + Hd \tag{31}$$

If perfect knowledge of the parameters cannot be achieved then the observer model uses a different set of matrices

$$\dot{\hat{x}} = A_o\hat{x} + B_o u + K\left(C_o\hat{x} - y\right) \tag{32}$$

where x is the state vector of the system; u is the measurable, or otherwise known, inputs to the systems; d is the unmeasurable term representing external disturbances acting on the system (in most cases structural and parametric uncertainty are lumped into this term); y is the measurable output vector; A, B, C, D, H are matrices containing the coefficients of the state space representation; A_o, B_o, C_o are matrices containing the coefficients of the state space representation used by the observer; and K is the observer gain or Luenberger gain matrix. In this particular case $C_o = C$ as there is no uncertainty about which state variable is considered the output.

The state estimation error, defined as $\xi = \hat{x} - x$, is a dynamical variable that evolves from an initial condition given by the choice of $x(0)$. In most cases found in the literature, a good agreement is supposed between observer and system models and thus the error dynamics equation is simplified to (22). However, if the effect of parameter uncertainty is considered then the estimation error dynamics are given by

$$\dot{\xi} = \left(A_o + KC_o\right)\hat{x} - \left(A + KC\right)x + \left(B_o - B\right)u - \left(D + KH\right)d \tag{33}$$

By algebraic manipulation and after some renaming of terms, the above equation can be written as

$$\dot{\xi} = P_o\xi - \left(A - A_o\right)x + Qu - Zd \tag{34}$$

where $P_o = A_o + KC_o$, $Q = B_o - B$ and $Z = D + KH$. Lumping the last three terms into one variable $W = -\left(A - A_o\right)x + Qu - Zd$ one gets

$$\dot{\xi} = P_o\xi + W \tag{35}$$

Note that the state estimation error converges to zero thanks to the appropriate choice of K because the term W is bounded (as follows from the fact that x, u and d are bounded signals). This convergence of the estimated state to the real value ensures that the effect of parameter uncertainty appears only in the prediction phase, where matrices A_o and B_o are used again. This is in contrast with standard FSMPC where both the state estimation and the resulting predictions are subject to inaccuracies arising from parametric uncertainty.

4. Experimental results for the case of study

A laboratory experimental setup (depicted in Fig. 8) has been designed to compare the performance of FSMPC with different rotor quantities estimation procedures. The main component is a 30-slot five-phase induction machine with three pairs of poles, whose parameters have been obtained experimentally using assumptions and methods described in Yepes et al. (2012) and Riveros et al. (2012) and are summarized in Table 1. Notice that the leakage inductance in x–y plane is considered equal to the leakage inductance in α–β plane, since the five-phase induction machine is single-layer (Hadiouche et al., 2004). The IM is fed by means of two SKS21F three-phase inverters from Semikron, which are connected to a DC-link voltage of 300V using an independent DC power supply. The control algorithm is deployed in a TM320F28335 DSP placed on a MSK28335 Technosoft board. A variable load can be introduced in the system thanks to a DC motor attached directly to the shaft of the induction machine. Finally, for the purpose of measuring the mechanical rotor speed a GHM510296R/2500 digital encoder is used together with the enhanced quadrature encoder pulse (eQEP) peripheral of the DSP.

Several experiments have been carried out to provide data for comparison of three controllers: FSMPC employing the conventional backtracking procedure, FSMPC with a reduced-order rotor current observer or RLO from now on, and FSMPC with full-order rotor current observer or FLO. The steady-state response of the machine, which operates in torque mode, has been analyzed in each experiment for different stator current references i_s^* defined by a frequency f_e and an amplitude A_{ref}. This allows

Table 1: Electrical and mechanical parameters of the five-phase IM

Parameter		**Value**
Stator resistance	$R_s(\Omega)$	19.45
Rotor resistance	$R_r(\Omega)$	6.77
Stator leakage inductance	L_{ls}(mH)	100.7
Rotor leakage inductance	L_{lr}(mH)	38.6
Mutual inductance	M(mH)	656.5
Mechanical nominal speed	ω_n(rpm)	1000
Power	P(kW)	1
Pairs of poles	p	3

the characterization of the stator current control under different operation points and the comparison of the three controllers in a high range of operating conditions.

All tests are realized using a sampling frequency of $f_s = 15$ kHz (sampling time $T_s = 66.67\mu$s), a cost function tuning parameter of $\lambda_{xy} = 0.1$ and a load torque of 58% of the nominal one. The observers are implemented using the Butterworth pole placement method previously introduced with $T_B = 1/1000$ s for the full-order observer and $T_B = 1/1300$ s for the reduced-order observer. These are experimental values close to the theoretical ones found in Fig. 7, but they produce better results.

The experimental results and conditions are depicted in Table 2. The type of controller used in each experiment can be seen in the first column. The two following columns indicate the electrical frequency and amplitude of the stator current reference. The next three columns detail the root-mean-squared (RMS) error in the current tracking for the α component e_α^{RMS} and for the x–y components e_{xy}^{RMS}, and the RMS error of the two-step ahead prediction in the α current component $\hat{e}_\alpha^{RMS}$. These quantities are computed as follows:

$$e_\alpha^{RMS} = \sqrt{\frac{\sum_{j=1}^{N}(i_{s\alpha}(j) - i_{s\alpha}^*(j))^2}{N}} \tag{36}$$

$$e_{xy}^{RMS} = \sqrt{\frac{\sum_{j=1}^{N}(i_{sx}(j)^2 + i_{sy}(j)^2)}{N}} \tag{37}$$

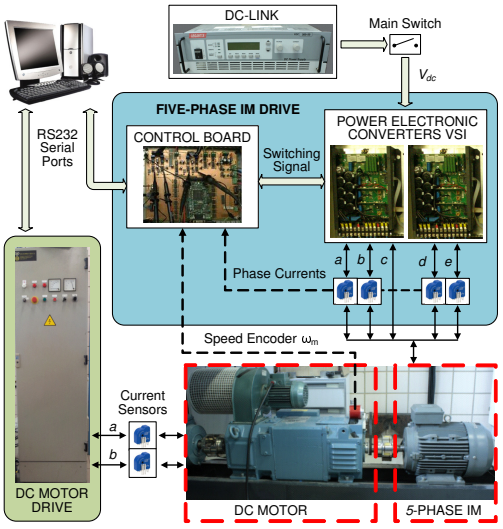

Figure 8: Experimental test rig diagram showing two conventional three-phase VSIs (upper right), the electronic control board (center middle), the DC motor drive (left side), and the IM machine and the DC motor (bottom right).

$$\hat{e}_\alpha^{RMS} = \sqrt{\frac{\sum_{j=1}^{N}(\hat{i}_{s\alpha}(j+2) - i_{s\alpha}(j+2))^2}{N}} \tag{38}$$

The last two columns in Table 2 present the total harmonic distortion THD and the number of switching changes per cycle N_c for each test. The first one is calculated as the average value of the total harmonic distortion in the α and β components of the stator current

$$THD_{\alpha\beta} = \sqrt{\frac{\int_0^\infty (i_{s\alpha\beta}(t) - i_{s\alpha\beta 1}(t))^2 dt}{\int_0^\infty (i_{s\alpha\beta 1}(t))^2 dt}} \tag{39}$$

where $i_{s\alpha\beta 1}$ is the fundamental component in the α and β axes of the measured current. The N_c parameter is obtained as the average value of the number of switch changes per cycle (SCPC).

It can be easily stated from the results that the use of a rotor observer improves the performance of the current controlled system, considerably reducing the tracking errors and the others considered figures of merit. What is more, this improvement is higher when the full-order observer is employed. To support the results shown in Table 2, the experimental results for one of the operation points are also presented in Fig. 9. The α–β–x–y current response of the system when $A_{ref} = 1.62$ A and $f_e = 29$ Hz is presented for the three considered controllers. It can be noted that using an observer produces a current response that better fits the reference than the conventional FSMPC method. Moreover, the current tracking is smoother for the full-order observer, as the ripple of the current signals is lower than in the reduced-order case. This is confirmed by the obtained RMS current tracking

Table 2: Experimental results for different controllers and references

Ctrl.	e_α^{RMS} (x10^{-2})	e_{xy}^{RMS} (x10^{-2})	$\hat{e}_\alpha^{RMS}$ (x10^{-2})	THD (%)	N_c (SCPC)
$f_e = 19$ Hz, $A_{ref} = 1.47$ A					
FSMPC	10.71	17.74	14.38	10.15	141.03
RLO	8.93	13.36	10.30	10.36	115.11
FLO	7.32	8.85	7.80	8.56	112.45
$f_e = 24$ Hz, $A_{ref} = 1.50$ A					
FSMPC	10.96	17.75	14.25	8.69	96.97
RLO	8.36	13.09	10.17	7.95	83.23
FLO	7.12	8.41	8.34	6.46	72.06
$f_e = 29$ Hz, $A_{ref} = 1.62$ A					
FSMPC	10.91	18.44	15.07	7.09	68.10
RLO	7.84	14.34	10.31	6.96	56.87
FLO	6.61	8.28	8.93	5.22	51.25
$f_e = 34$ Hz, $A_{ref} = 1.56$ A					
FSMPC	11.23	18.89	15.41	7.24	50.56
RLO	7.82	15.38	10.42	6.63	39.20
FLO	6.12	8.27	9.27	5.10	39.03
$f_e = 39$ Hz, $A_{ref} = 1.60$ A					
FSMPC	12.12	21.76	16.02	6.39	35.30
RLO	7.82	18.17	10.68	5.70	25.83
FLO	6.10	12.74	10.40	4.46	23.24

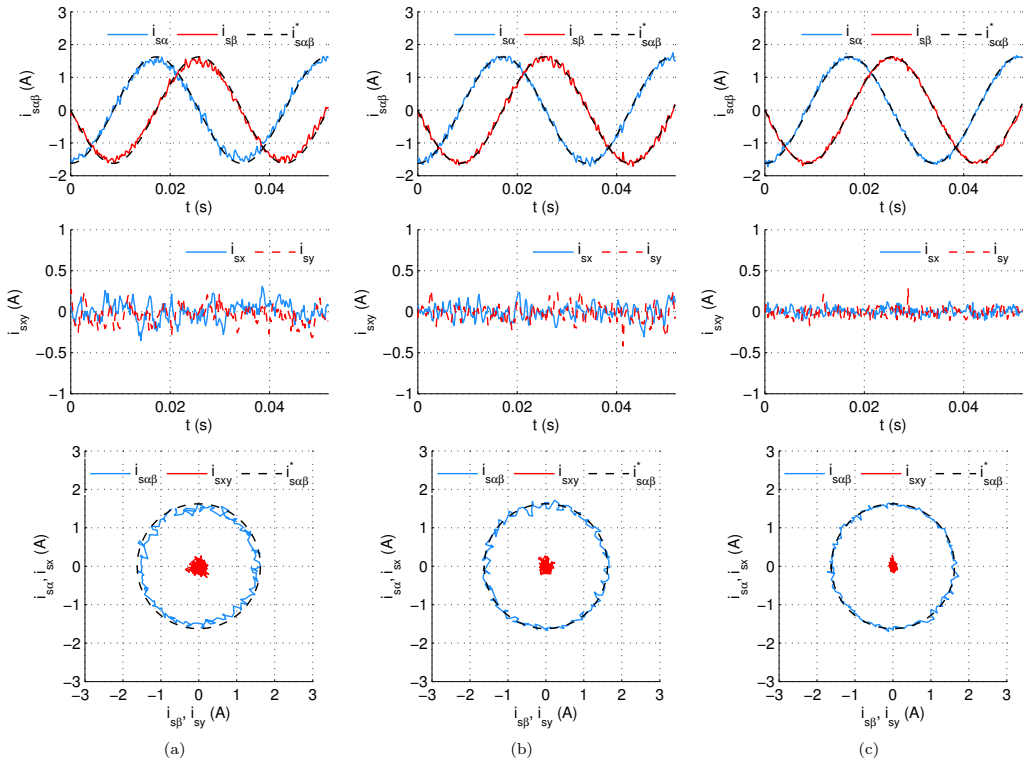

Figure 9: Experimental results obtained from the test rig for $A_{ref} = 1.62$ A and $f_e = 29$ Hz when it is applied the controller (a) FSMPC, (b) RLO and (c) FLO. Some graphics show the α–β stator currents (upper ones), x–y stator currents (middle plots) and the same currents represented in circular trajectories (bottom draws).

error values detailed in Table 2. For instance, the RMS error in the α current component is reduced by 28.12% and 39.36% for $f_e = 29$ Hz using RLO and FLO respectively. Similarly, the results for other operating points show that the reduction in e_α^{RMS} is higher for the full-order observer, with improvements of 31.60%, 35.04%, 45.46% and 49.63% for 19 Hz, 24 Hz, 34 Hz and 39 Hz respectively. Since α–β currents are directly related to the electromechanical energy conversion, the improved current tracking in the α–β plane reduces the torque ripple and enhances the dynamic performance. Also notice that the RMS current tracking error in the $x-y$ subspace is significantly reduced. The full-order observer achieves better e_{xy}^{RMS} values for all frequencies than the reduced-order one, obtaining an improvement in this figure of merit up to 56%. This is an interesting benefit of using observers because the lower RMS values of the x–y currents do not affect the torque production (in distributed-winding machines), but it favours efficiency by reducing the IM copper losses.

The significant difference between both observers is principally due to the more accurate estimation of rotor currents that the full-order one produces, as evidenced by the prediction RMS error in the α current component values shown in Table 2. Although both observers improve this error with respect to the FSMPC, the FLO achieves a reduction that ranges from 35.04% to 45.72% with decreasing frequency, while the reduction with RLO ranges from 28.36% to 33.32% with increasing frequency.

Similarly, it can be stated from the results that the switching changes per cycle N_c and the harmonic content THD are reduced when FSMPC is applied together with an observer, with the FLO control being the best option. Notice that the maximum improvement in N_c and THD is 26.81% and 10.85% for the reduced-order observer, and 34.15% and 30.27% for the full-order one. It is remarkable that the current tracking improvement obtained with the inclusion of observers is achieved with lower VSI switching frequency (i.e. lower values of N_c), which in turn implies

that the VSI losses are also reduced.

From the computational cost perspective, one of the main drawbacks for the implementation of FSMPC in industry applications, the required computational load for implementing the rotor observer is negligible. The total computational cost of the control algorithm without rotor observer is estimated as about 32.4μs, while the incorporation of the reduced-order observer or the full-order one implies a total computational cost of 35.3μs and 35.7μs, respectively, with a sampling time of 67μs. It is important to indicate that both observers have similar computational costs, though the full-order one produces remarkable results in all aspects.

5. Conclusion

The area of model predictive control for multiphase electrical drives has experienced a substantial growth in the last years. Particularly, FSMPC strategy has been presented in the literature applied to the dual three-phase and five-phase drives. On the other hand, observers have been principally used in relation to IFOC, sensorless drives and for fault detection but, to the best of our knowledge, they have not been yet used together with FSMPC techniques. In this work, authors have proposed a current control scheme based on the FSMPC method incorporating a rotor current observer. The new estimation scheme has been assessed for a five-phase IM and has been demonstrated that it is possible to enhance the predictions including an observer without a considerable penalty in the computational burden of the controller. The experimental results show that, although the simple update and hold scheme used by most MPC practitioners in electrical applications produces acceptable results, the observer clearly outperforms the classic approach, presenting some advantages such as better current tracking performance, less harmonic content and less VSI gating commutations. Consequently, the use of observers together with MPC strategies generates torque with lower ripple and improves the overall efficiency by reducing both the copper and VSI losses. Moreover, two different observer structures have been designed and experimentally tested, a full-order observer and a reduced-order observer. It has been stated that the full-order one constitutes the best solution reducing the ripple in the currents trajectories, specially in the x–y subspace, with a similar computational cost.

The proposed current control method can be applied to any n-phase induction machine, or even to conventional three-phase ones, just adjusting the predictive model and the observer equations to the new system. Consequently, these results encourage future research towards establishing the observer as a tool of choice for FSMPC to improve the behaviour in high-performance electrical drives.

Acknowledgments

The authors would like to thank the Junta de Andalucía and the Ministerio de Economía y Competitividad of the Spanish Government for their funding of this research under references P11-TEP-7555, DPI2013-44278-R, ENE2014-52536-C2-1-R.

References

Alireza Davari, S., Khaburi, D.A., Wang, F., Kennel, R.M., 2012. Using full order and reduced order observers for robust sensorless predictive torque control of induction motors. IEEE Transactions on Power Electronics 27, 3424–3433. doi:10.1109/TPEL.2011.2179812.

Arahal, M.R., Barrero, F., Toral, S., Duran, M.J., Gregor, R., 2009. Multi-phase current control using finite-state model-predictive control. Control Engineering Practice 17, 579–587. doi:10.1016/j.conengprac.2008.10.005.

Arahal, M.R., Castilla, M., Alvarez, J.D., Sánchez, J.A., 2013. Subharmonic content in finite-state model predictive current control of IM, in: IECON 2013-39th Annual Conference on IEEE Industrial Electronics Society, pp. 5866–5872.

Arashloo, R.S., Salehifar, M., Romeral, L., Sala, V., 2015. A robust predictive current controller for healthy and open-circuit faulty conditions of five-phase BLDC drives applicable for wind generators and electric vehicles. Energy Conversion and Management 92, 437–447. doi:10.1016/j.enconman.2014.12.075.

Barrero, F., Duran, M.J., 2016. Recent advances in the design, modeling, and control of multiphase machines-Part I. IEEE Transactions on Industrial Electronics 63, 449–458. doi:10.1109/TIE.2015.2447733.

Bogado, B., Barrero, F., Arahal, M.R., Toral, S., Levi, E., 2013. Sensitivity to electrical parameter variations of predictive current control in multiphase drives, in: IECON 2013-39th Annual Conference on IEEE Industrial Electronics Society, pp. 5215–5220.

Chai, S., Wang, L., Rogers, E., 2013. Model predictive control of a permanent magnet synchronous motor with experimental validation. Control Engineering Practice 21, 1584–1593. doi:10.1016/j.conengprac.2013.07.008.

Che, H.S., Levi, E., Jones, M., Hew, W.P., Rahim, N.A., 2014. Current control methods for an asymmetrical six-phase induction motor drive. IEEE Transactions on Power Electronics 29, 407–417. doi:10.1109/TPEL.2013.2248170.

Choi, D.K., Lee, K.B., 2015. Dynamic performance improvement of AC/DC converter using model predictive direct power control with finite control set. IEEE Transactions on Industrial Electronics 62, 757–767. doi:10.1109/TIE.2014.2352214.

Duran, M.J., Barrero, F., 2016. Recent advances in the design, modeling, and control of multiphase machines-Part II. IEEE Transactions on Industrial Electronics 63, 459–468. doi:10.1109/TIE.2015.2448211.

El Fadili, A., Giri, F., El Magri, A., Lajouad, R., Chaoui, F.Z., 2014. Adaptive control strategy with flux reference optimization for sensorless induction motors. Control Engineering Practice 26, 91–106. doi:10.1016/j.conengprac.2013.12.005.

Gopinath, B., 1971. On the control of linear multiple input-output systems. Bell System Technical Journal 50, 1063–1081.

Guzman, H., Duran, M.J., Barrero, F., Zarri, L., Bogado, B., Gonzalez Prieto, I., Arahal, M.R., 2016. Comparative study of predictive and resonant controllers in fault-tolerant five-phase induction motor drives. IEEE Transactions on Industrial Electronics 63, 606–617.

Hadiouche, D., Razik, H., Rezzoug, A., 2004. On the modeling and design of dual-stator windings to minimize circulating harmonic currents for VSI fed AC machines. IEEE Transactions on Industry Applications 40, 506–515.

Holmes, D.G., Martin, D.A., 1996. Implementation of a direct digital predictive current controller for single and three phase voltage source inverters, in: Industry Applications Conference, 1996.

Thirty-First IAS Annual Meeting, IAS '96., Conference Record of the 1996 IEEE, pp. 906–913 vol.2. doi:10.1109/IAS.1996.560191.

Holtz, J., Stadtfeld, S., 1983. A predictive controller for the stator current vector of AC machines fed from a switched voltage source, in: JIEE IPEC-Tokyo Conference, pp. 1665–1675.

Jansen, P.L., Lorenz, R.D., 1994. A physically insightful approach to the design and accuracy assessment of flux observers for field oriented induction machine drives. IEEE Transactions on Industry Applications 30, 101–110. doi:10.1109/28.273627.

Jones, M., Vukosavic, S.N., Dujic, D., Levi, E., 2009. A synchronous current control scheme for multiphase induction motor drives. IEEE Transactions on Energy Conversion 24, 860–868. doi:10.1109/TEC.2009.2025419.

Kautsky, J., Nichols, N.K., Van Dooren, P., 1985. Robust pole assignment in linear state feedback. International Journal of Control 41, 1129–1155. doi:10.1080.0020718508961188.

Levi, E., 2008. Multiphase electric machines for variable-speed applications. IEEE Transactions on Industrial Electronics 55, 1893–1909. doi:10.1109/TIE.2008.918488.

Levi, E., Bojoi, R., Profumo, F., Toliyat, H.A., Williamson, S., 2007. Multiphase induction motor drives - a technology status review. IET Electric Power Applications 1, 489–516. doi:10.1049/iet-epa:20060342.

Lim, C.S., Levi, E., Jones, M., Rahim, N.A., Hew, W.P., 2014. FCS-MPC-based current control of a five-phase induction motor and its comparison with PI-PWM control. IEEE Transactions on Industrial Electronics 61, 149–163. doi:10.1109/TIE.2013.2248334.

Lopez, M., Rodriguez, J., Silva, C., Rivera, M., 2015. Predictive torque control of a multidrive system fed by a dual indirect matrix converter. IEEE Transactions on Industrial Electronics 62, 2731–2741. doi:10.1109/TIE.2014.2364986.

Luenberger, D.G., 1971. An introduction to observers. IEEE Transactions on Automatic Control 16, 596–602. doi:10.1109/TAC.1971.1099826.

Martinez, J.L.R., Arashloo, R.S., Salehifar, M., Moreno, J.M., 2015. Predictive current control of outer-rotor five-phase BLDC generators applicable for off-shore wind power plants. Electric Power Systems Research 121, 260–269. doi:10.1016/j.epsr.2014.11.004.

Merabet, A., Ouhrouche, M., Bui, R.T., 2006. Nonlinear predictive control with disturbance observer for induction motor drive, in: 2006 IEEE International Symposium on Industrial Electronics, pp. 86–91.

Riveros, J.A., Barrero, F., Levi, E., Durán, M.J., Toral, S., Jones, M., 2013. Variable-speed five-phase induction motor drive based on predictive torque control. IEEE Transactions on Industrial Electronics 60, 2957–2968. doi:10.1109/TIE.2012.2198034.

Riveros, J.A., Yepes, A., Barrero, F., Doval-Gandoy, J., Bogado, B., Lopez, O., Jones, M., Levi, E., 2012. Parameter identification of multiphase induction machines with distributed windings - Part 2: Time-domain techniques. IEEE Transactions on Energy Conversion 27, 1067–1077. doi:10.1109/TEC.2012.2219862.

Rodriguez, J., Kazmierkowski, M.P., Espinoza, J.R., Zanchetta, P., Abu-Rub, H., Young, H.A., Rojas, C.A., 2013. State of the art of finite control set model predictive control in power electronics. IEEE Transactions on Industrial Informatics 9, 1003–1016. doi:10.1109/TII.2012.2221469.

Verghese, G.C., Sanders, S.R., 1988. Observers for flux estimation in induction machines. IEEE Transactions on Industrial Electronics 35, 85–94. doi:10.1109/41.3067.

Wang, F., Zhang, Z., Davari, A., Rodríguez, J., Kennel, R., 2014. An experimental assessment of finite-state predictive torque control for electrical drives by considering different online-optimization methods. Control Engineering Practice 31, 1–8. doi:10.1016/j.conengprac.2014.06.004.

Xia, C., Wang, M., Song, Z., Liu, T., 2012. Robust model predictive current control of three-phase voltage source PWM rectifier with online disturbance observation. IEEE Transactions on Industrial Informatics 8, 459–471. doi:10.1109/TII.2012.2187912.

Xie, W., Wang, X., Wang, F., Xu, W., Kennel, R.M., Gerling, D., Lorenz, R.D., 2015. Finite-contro-set model predictive torque control with a deadbeat solution for PMSM drives. IEEE Transactions on Industrial Electronics 62, 5402–5410. doi:10.1109/TIE.2015.2410767.

Yepes, A.G., Malvar, J., Vidal, A., Lopez, O., Doval-Gandoy, J., 2015. Current harmonics compensation based on multiresonant control in synchronous frames for symmetrical n -phase machines. IEEE Transactions on Industrial Electronics 62, 2708–2720. doi:10.1109/TIE.2014.2365155.

Yepes, A.G., Riveros, J.A., Doval-Gandoy, J., Barrero, F., Lopez, O., Bogado, B., Jones, M., Levi, E., 2012. Parameter identification of multiphase induction machines with distributed windings - Part 1: Sinusoidal excitation methods. IEEE Transactions on Energy Conversion 27, 1056–1066. doi:10.1109/TEC.2012.2220967.

Zhang, Y., Yang, H., 2014. Model predictive torque control of induction motor drives with optimal duty cycle control. IEEE Transactions on Power Electronics 29, 6593–6603. doi:10.1109/TPEL.2014.2302838.

Chapter 4

Variable Sampling Time as a New Degree of Freedom

Multiphase drives can be considered an emerging technology where most of the applied control methods are defined like an extension of the control techniques normally used in conventional three-phase drives. However, the previous sentence cannot be stated when talking about predictive controllers, whose use in the power electronics' field has been extended at the same time that the multiphase drives' technology emerged. Predictive controllers and multiphase drives have been developed hand in hand and the most common findings when using both together is that the computational cost of the controller is a serious handicap for its implementation, as well as the high generated harmonic content due to the fixed sampling-time nature and the absence of modulation methods in the control algorithm. In the previous chapter, different methods have explored the interest of creating a more precise predictive model of the multiphase machine by including rotor current observers for the estimation of non-measurable parts of the system. The objective is the improvement of the current control performance and, thus, overcome the aforementioned disadvantages. The study has registered a significant reduction in the current harmonics content at the expense of slightly increasing the complexity of the controller.

This chapter introduces a more natural way to face the harmonic problem consisting in the concept of non-uniform sampling time as a new degree of freedom in the model-based predictive technique. The idea deviates from recent studies, which were reviewed in Chapter 2, where a kind of modulation is included in the predictive controller. The basis of the proposed methodology is the optimal selection of both the switching state of the power converter and its time of application between all the possibilities without the necessity of a cost function and with an affordable computational cost. To this end, the lead pursuit concept is applied. The proposal is completely new in essence and firstly proposed to the scientific community by the doctoral student and her supervisors. A five-phase induction machine with symmetrical and distributed windings has been used as a case example to validate the proposal by simulations and experimentation, and draw conclusions.

The next three contributions are the main results of this research. In Contribution 3, a proof of concept study of the model-based variable sampling time controller is presented

and the main differences with respect to conventional fixed-sampling predictive methods are obtained. Simulation and experimental results confirm the effectiveness of the proposal in terms of harmonic reduction and an exhaustive analysis of the computational requirements of the new controller is included. A variation in the proposed controller is introduced in Contribution 4, where the calculation of the application time is refined in a second step when it is necessary. Additionally, a comparison with the most conventional predictive controllers is performed, including low-speed and dynamic operations. The comparative analysis reveals that the variable sampling of the time can improve the control system not only in terms of harmonic content but also in terms of current tracking performance. Finally, in Contribution 5 the Thesis work is summarized and all the proposals are compared since they have the same goals. The lessons learned in this last contribution bring to light the advantages and disadvantages of this research work when facing the drawbacks of predictive controllers.

- **Contribution 3:** M. R. Arahal, C. Martin, F. Barrero, I. Gonzalez-Prieto, and M. J. Duran, "Model-Based Control for Power Converters with Variable Sampling Time: A Case Example using Five-Phase Induction Motor Drives", *IEEE Transactions on Industrial Electronics*, vol. 66, no. 8, pp. 5800-5809, August 2019.

  DOI: 10.1109/TIE.2018.2870390.

  Times cited: 2 (Google Scholar, 8 June 2019).

- **Contribution 4:** M. R. Arahal, C. Martin, F. Barrero, and M. J. Duran, "Assessing Variable Sampling Time Controllers for Five-Phase Induction Motor Drives", *IEEE Transactions on Industrial Electronics*, April 2019, accepted for publication.

  DOI: 10.1109/TIE.2019.2908585.

- **Contribution 5:** C. Martin, M. R. Arahal, F. Barrero, and M. J. Duran, "Model-Based Predictive Current Controllers in Multiphase Drives Dealing with Natural Reduction of Harmonic Distortion", *Energies*, vol. 12, no. 9, 1679, May 2019.

  DOI: 10.3390/en12091679.

IEEE TRANSACTIONS ON INDUSTRIAL ELECTRONICS

Model-Based Control for Power Converters with Variable Sampling Time: A Case Example using Five-Phase Induction Motor Drives

Manuel R. Arahal, Cristina Martin, Federico Barrero, Ignacio Gonzalez-Prieto, and Mario J. Duran

***Abstract*—Discrete-time control of power converters without modulation blocks have been considered in recent times in modern high-performance electromechanical drives, particularly with the appearance of model predictive control in its finite set version. The shortcomings produced by the fixed discretization of time used in this kind of control systems has been analysed, and several methods have been put forward to deal with them. Most of the alternatives increase the complexity of the controller introducing different analytical modulation methods. However, a variable sampling time can be a simpler and more natural solution, at the expense of using a less-known paradigm for implementation. This paper introduces a new control approach based on a model of the system as in predictive controllers but using variable sampling time. It can be applied to modern power converters and drives, including conventional three-phase or advanced multiphase ones. Experimental results are provided to test the ability of the controller using a five-phase induction motor drive as a case example.**

***Index Terms*—Digital control systems, non-uniform sampling, power conversion, predictive control, pursuit algorithms.**

I. Introduction

MOST control systems in electrical applications use a power converter as a mean to interface with the system. In traditional applications the system is driven by a modulation block [1], [2]. However, the elimination of the modulation stage is becoming more frequent in recent years, where the power converter is directly driven by applying the desired control commands [3]. Then, it is a common practice that the controller generates switching state to be held by the power converter during a fixed sampling period. This has a profound impact on harmonic content [4], being quite severe particularly in high power applications where the number of converter commutations per cycle is limited [5].

It is worth pointing out that recent applications of model predictive controllers (MPC), using the finite state or finite control set (FCS) concept [6], fall within this category as they directly drive the converter without the intervention of a pulse width modulation (PWM) block [7]. The removal of the intermediate modulation brings a fast transient response [8], [9]. In addition, the FCS-MPC offers greater flexibility to tackle muti-objective control problems and provides a framework in which multiphase and/or multi-level control systems are more easily designed [10]. However, the high harmonic content is still an important drawback.

Introduction of variable sampling time in the direct digital control (DDC) seems like a promising method to avoid the aforementioned problems, while retaining the benefits of the FCS-MPC. This idea is first introduced in [11], where the sampling period of a FCS-MPC is partitioned into subintervals. The conventional optimization problem is extended to include all possible switching states and all predefined time subintervals. The controller must then choose the best combination of switching state and its time of application (one of the subintervals) that optimizes a cost function. Expectedly, the computational requirements of the controller are greatly increased. Furthermore, the subdivision of the sampling time cannot be made arbitrarily fine because it increases the computing burden. For this reason, the commutation instants are still coarse quantized compared with schemes using modulators such as PWM.

In this paper, a new approach to direct control of power converters using a variable sampling time is proposed and tested. The basic idea introduced in [11] is complemented using the lead-pursuit concept [12] to derive a model-based controller using variable sampling time with fine resolution in the commuting times. Therefore, a new control scheme is obtained that decouples the optimization of the converter state from that of the application time. Both quantities are derived from a model of the system. As a consequence, the application times are not constrained to a fixed sequence of commuting times as in traditional digital control (including FCS-MPC). The feasibility of the proposed controller, named from now on variable sampling time lead-pursuit control (VSTLPC), is tested using a five-phase induction machine (FPIM) driven by a two-level voltage source inverter (VSI). Although the

Manuscript received April 3, 2018; revised July 3, 2018; accepted August 29, 2018. This work was supported in part by the Spanish Ministry of Economy and Competitiveness under Project DPI2016-76144-R, in part by the University of Seville, Spain (V Research Plan, Action II.2).

Manuel R. Arahal is with the System and Automatic Engineering Department, University of Seville, 41092 Seville, Spain (e-mail: arahal@us.es).

Cristina Martin and Federico Barrero are with the Electronic Engineering Department, University of Seville, 41092 Seville, Spain (e-mail: cmartin15@us.es; fbarrero@us.es).

Ignacio Gonzalez-Prieto is with the Electrical and Thermal Engineering Department, University of Huelva, 21819 Huelva, Spain (e-mail: ignacio.gonzalez@die.uhu.es).

Mario J. Duran is with the Electrical Engineering Department, University of Malaga, 29071 Malaga, Spain (e-mail: mjduran@uma.es).

proposal is general and also valid for conventional three-phase drives, a multiphase one has been used as a case example for generality purposes. The FPIM is one of the most promising multiphase machines from the industry perspective, as it is shown in [13]–[15], making it an ideal candidate as case study. Another advantage that appears extending the study to a more general multiphase drive is in relation with their complexity. The larger number of available switching states of the FPIM increases the control requirements as well as its computational cost. By choosing this case study the implementation requirements are set on a demanding scenario.

The paper is organized as follows. Section II summarizes the main ideas in relation with the discrete-time control of power converters, addressing the general DDC algorithm using uniform and variable sampling times. The basis of the VSTLPC is detailed in Section III. The application of the proposed controller to the five-phase system is presented in Section IV together with the description of the experimental system and the analysis of the obtained results. Finally, the conclusions will be presented at the end of the paper.

II. Direct Digital Control of Power Converters

In this section the basic elements of DDC schemes for power converters are reviewed to serve as a framework of the proposed controller. A subdivision is made between controllers based in constant sampling time and those using variable sampling time.

A. Constant Sampling Time DDC

A basic block diagram of DDC of power converters is presented in Fig. 1. It typically contains: i) an analog to digital converter (ADC) that provides the digital acquisition of the electrical and mechanical variables of the system; ii) a computing element that implements the control algorithm and decides the control action u to be applied; iii) the power converter; and iv) the electrical system supplied by the power converter. This control scheme uses a cyclic program in which the functions that define the control algorithm (wait, sample, compute, and actuate) are sequenced within a period T_s referred to as sampling period. The action taken at each discrete time k is a vector $u(k)$ that dictates the state of the converter. Such state is selected by the controller in order to produce in the system a certain behaviour in term of electrical variables (e.g., currents, fluxes, active, and reactive power) and/or mechanical variables (e.g., speed and torque) defined by an external reference signal r. For example, the FCS-MPC technique uses a mathematical model of the system to predict the future evolution of the system variables for each possible control action, and selects the optimal one according to the control objective. The selected state vector is held for the whole sampling period, being the process repeated in the next execution of the control algorithm.

It must be noted that the power converter can only be in a handful of states. Each state produces a certain output of the converter that is constant during the sampling period. The DDC must select the output state that imprints in the system the trajectories for the controlled variables y (e.g., stator currents and flux) closest to the reference values. In practice, this process commands the applied switching sequence according to the given reference and just low-order harmonics components of the system's variables (including the fundamental y_1) are controlled relying in the inherent low-pass filter characteristic of most systems to mitigate higher order harmonics [16].

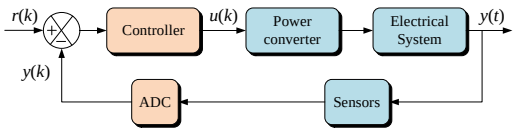

Fig. 1: Basic block diagram of a DDC of power converters.

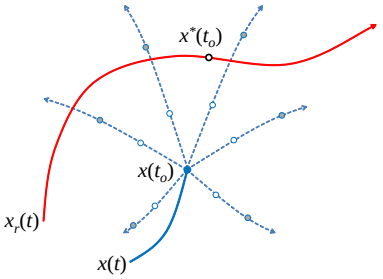

Fig. 2: State-space representation of the alternate evolutions of x after applying different control signals and in different future times.

B. Variable Sampling Time DDC

It was stated in the introduction section that a variable sampling time can mitigate some problems derived from the fixed discretization of the time, e.g., the high harmonic content in the electrical variables. The rationale for using variable sampling time is presented here with the aid of an example.

Suppose that a certain control system uses a power converter in the way previously explained, following the scheme presented in Fig. 1. The actual state of the system (in a state-space representation) is define by x and the reference trajectories r impose at each time a desired state x_r. At any given moment the controller must decide which control action will be used next according to the reference state, since the future evolution of the system depends on the choice made. Consider now the state portrait of Fig. 2, where the state components are plotted against each other. The evolution of the system state $x(t)$ is represented by a solid line, and the actual state at time t_o is $x(t_o)$ (central blue filled circle). The hodograph corresponding to the trajectory of the desired state $x_r(t)$ is shown as a solid line and $x^*(t_o)$ (black unfilled circle) represents the objective state for the actual instant. The dashed lines emerging from $x(t_o)$ are the possible evolution paths obtained by considering the separate application of some control actions (converter configurations). In these paths, two points have been placed consisting on the future state of the

system for two different times of application T_1 and T_2. Thus, the points represent the values $x(t_o+T_1)$ and $x(t_o+T_2)$ with $T_2 > T_1$. These points are marked in the figure as unfilled circles (corresponding to T_1) and grey filled ones (T_2). In this situation, the control algorithm must select the control action and its time of application in order to reach the desired reference. However, it can be seen that in this example the objective $x^*(t_o)$ cannot be exactly achieved due to the scarcity of the considered control actions and time instants.

A way to alleviate this scarcity is to increase the number of possible control actions. But, in a power converter the number of control actions is limited and fixed, and it can only be increased considering more phases or levels, which requires hardware modifications. Notice also that the number of time instants can be, in principle, increased giving a mean to achieve a closer reference tracking. For instance, in the example of Fig. 2 if a value T_i with $T_1 < T_i < T_2$ is allowed then one of the paths lies very close to $x^*(t_o)$. This is the basis of the idea presented in [11], where a finer partition of time is introduced to this end and a complex optimization procedure is carried out over the product of all possible converter configurations times the number of future time instants, which implies a very high computational cost in the multiphase or multi-level applications. In the following section, a new approach of variable sampling time DDC is presented. The new approach uses an exhaustive search over the possible converter configurations, avoiding repetition of this search for different application times.

III. Variable Sampling Time Lead-Pursuit Control

The proposed controller is derived from the lead-pursuit concept used in airplane to airplane fight tactics [12]. It has been applied to autonomous navigation systems and other reference tracking problems. Its basic idea is that hitting a moving target requires some anticipation, since it takes some time for the control action to produce an effect on the system and during such time the target changes its position. This concept is graphically explained in Fig. 3, where the target's position varies with the time following the red line, and at instant t_o it is placed at position $T(t_o)$. The pursuer X must decide the best moving direction. Instead of pointing to the current position of the target, in the lead-pursuit scheme the pursuer takes as objective an advanced position $T(t_o + t_L)$, where t_L is the anticipation time usually called lead time. In airplane fight this might be difficult to estimate, however, in many engineering applications this value is either known (because it results from a preprogrammed reference trajectory) or can be estimated (from past observed values) with enough accuracy.

So, the lead point is considered as a mean to fix a point in the future at which to aim. In the case at hand, the lead allows to determine the objective state as $x^*(t_o) = x_r(t_o+t_L)$, being t_L a parameter of the proposed controller. Thus, the controller must select a converter configuration $S_a \in S$, being $S = \{S_i\}_{i=1,\dots,N}$ the set of all possible configurations, and the time T_a that it must be kept applied to the system. The

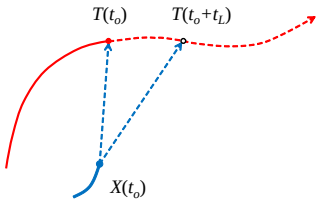

Fig. 3: Representative diagram of the lead-pursuit concept.

control algorithm has two phases. i) S_a is computed using some geometrical considerations drawn from the lead-pursuit concept and from a continuous time model of the system. ii) T_a is computed using a model of the electrical system in order to minimize some error function that depends on the actual state $x(t_o)$ and the desired one $x^*(t_o)$. The controller then uses a receding horizon strategy where S_a is applied during time T_a after which the whole procedure is repeated. The selection of S_a is done maximizing the projection of the future path in the direction of the lead point $x^*(t_o)$. The application time T_a is computed as a minimization of the distance from the end point $x(t_o + T_a)$ to the lead point. Since the end point is a future value, a prediction $\hat{x}(t_o + T_a)$ is used instead. The prediction is obtained using a model of the system, taking $x(t_o)$ as the initial condition and the input signal given by the selected converter configuration S_a. As can be seen, the described method depends on a model of the controlled system and, thus, in their electrical and mechanical parameters. Consequently, it is expected that VSTLPC will be sensible to parameter mismatch in a similar way that FCS-MPC techniques are [17], [18].

The theoretical advantages of VSTLPC over the previously reviewed DDC control schemes, particularly the different FCS-MPC approaches, are:

- The application time is not fixed but obtained from an optimization algorithm, constituting a new degree of freedom in the controller. Also, it will be shown later that this optimization does not need exhaustive exploration, saving computing time in comparison with previous approach [11].
- The resolution of the application time T_a does not interfere with the computational cost of the control algorithm, allowing a fine resolution of commutation times.
- The double prediction used in most FCS-MPC techniques [19] is avoided in the proposed controller, yielding to a potential reduction in the computing time and simplifying the method.
- The sequence of applied converter states does not include preselected configurations such as the application of null voltage vectors used in other approaches [20], [21].

The mathematical derivation of VSTLPC is presented in the followings paragraphs based on the aforementioned ideas. The system is modelled as a set of differential equations that can be accommodated in a space-state representation with the

following transition equation:

$$\frac{dx}{dt} = f(x, S_i) \tag{1}$$

where x is the state vector and S_i the input vector, the switching state of the converter.

The first stage of VSTLPC is the selection of the converter state that imprints in the state variables the closest trajectory to the lead-pursuit direction of $x^*(t_o)$. This is done knowing that the direction of change of x is given by $f(x, S_i)$. Then, the cosine of the angle between $f(x(t_o), S_i)$ and the distance $(x^*(t_o) - x(t_o))$ is maximum for the converter configuration S_a that produces the path with less deviation from the line that joins the actual state to the objective. Using this idea, the switching state S_a is obtained through the definition of the scalar product as follows:

$$S_a = \underset{S_i \in S}{\operatorname{argmax}} \frac{(x^*(t_o) - x(t_o)) \cdot f(x(t_o), S_i)}{\|x^*(t_o) - x(t_o)\| \, \|f(x(t_o), S_i)\|}. \tag{2}$$

This is an optimization problem that can be solved by exhaustive search but it is simpler than procedure in [11], reducing the number of iterations. The state will follow the path given by S_a for as long as this configuration is applied. The application time T_a should then be chosen to minimize the deviation of the end point from the reference trajectory. In mathematical notation

$$T_a = \underset{T}{\operatorname{argmin}} \; \|x^*(t_o) - \hat{x}(t_o + T|t_o)\| \tag{3}$$

where $\hat{x}(t_o + T|t_o)$ is a prediction of the future state at time $t_o + T$ made at time t_o that can be produced using a mathematical model of the system for the selected S_a. The norm $\|.\|$ used in (2) and (3) is the Euclidean 2-norm.

IV. Application to a Real System

The considered system is a symmetrical FPIM with distributed windings equally displaced ($\vartheta = 2\pi/5$), isolated neutral point, and supplied by a five-leg two-level VSI. An schematic representation of the system is shown on the right side of Fig. 4, where the switching state of the VSI is defined by $(S_A, S_B, S_C, S_D, S_E)$. In the next subsections the proposed control scheme is presented, particularizing for the FPIM drive as an illustrative case example and analysing the obtained simulation and experimental results.

A. Definition of VSTLPC for a FPIM

The VSTLPC control algorithm requires the knowledge of the evolution of the system variables (stator currents in this case), and a model of the FPIM drive will be used to this end. According to the vector space decomposition approach, the FPIM can be represented as a set of equations in two orthogonal stationary subspaces, named α–β and x–y as follows:

$$\begin{aligned} \dot{x}(t) &= A\,x(t) + B\,v_s(t) \\ x_s(t) &= C\,x(t) \end{aligned} \tag{4}$$

where the state variables are the α–β and x–y stator and rotor currents $x = (i_{s\alpha}, i_{s\beta}, i_{sx}, i_{sy}, i_{r\alpha}, i_{r\beta})^T$, the input signal is the stator voltage vector applied to the machine $v_s = (v_{s\alpha}, v_{s\beta}, v_{sx}, v_{sy})^T$, and the output signals are the stator currents $x_s = (i_{s\alpha}, i_{s\beta}, i_{sx}, i_{sy})^T$, which constitute the measurable and controlable part of the system state. Coefficients of matrices A and B depend on the rotor speed ω_m and the IM electrical parameters (see [22]). The values of these parameters, which will be used in the simulation and experimental studies, are gathered in Table I.

Stator voltage vector v_s is related to the switching state through the VSI model. In this case, the simplest model has been selected for the sake of speeding up the optimization process in the control algorithm. Then, if the gating signals are arranged in vector $u = (S_A, S_B, S_C, S_D, S_E)^T \in \mathbb{B}^5$ with $\mathbb{B} = \{0, 1\}$, the stator voltages are obtained as

$$v_s = \frac{1}{5} V_{dc}\, M\, C_n\, u \tag{5}$$

being V_{dc} the dc-link voltage, M a coordinate transformation matrix accounting for the spatial distribution of the machine windings, and C_n a connectivity matrix that takes into account how the VSI gating signals are distributed [22]. With this configuration, only 2^5 combinations of switching signals can be constructed. Combining (4) and (5), the evolution of the stator currents can be represented by the following expression:

$$\dot{x}_s(t) = \bar{A}\,x(t) + \bar{B}\,u(t) \tag{6}$$

where two new matrices are introduced: $\bar{A} = C\,A$ and $\bar{B} = \frac{1}{5} V_{dc}\, C\, B\, M\, C_n$.

The proposed control scheme is shown in Fig. 4. It is composed by an outer speed control loop and an inner current control loop. The speed loop independently regulates the stator currents in the d–q reference frame. In our case, the machine is fluxed imposing a constant value of d-current reference i^*_{sd}, while i^*_{sq} constitutes the output of a PI regulator. The input of this PI is the error between the reference rotor speed ω^*_m and the measured one ω_m. These reference values are then rotated into the $\alpha - \beta$ plane using the inverse Park transformation as follows:

$$D^{-1} = \begin{pmatrix} \cos\theta & -\sin\theta \\ \sin\theta & \cos\theta \end{pmatrix} \tag{7}$$

being θ the angle of the rotating reference frame, which is obtained from the measured speed and the estimated slip speed [23]. The resulting α–β reference currents, together with the imposed zero x–y reference currents, are inputs in the proposed VSTLPC controller (see Fig. 4). Following the guidelines presented in section III, these references must be projected a time t_L into the future in order to define the desired state $x^*_s(t_o) = (i^*_{s\alpha}, i^*_{s\beta}, i^*_{sx}, i^*_{sy})|_{t_o+t_L}$. This is done estimating the rotor angle for a future time t_L, $\theta(t_o + t_L)$.

Once the desired references are computed and the measurement of the actual system state is made $x_s(t_o)$, the switching state S_a is selected solving the optimization problem (2) and knowing that x_s varies following the direction of $f(x, u) = \bar{A}\,x + \bar{B}\,u$. Then, the application time T_a is chosen by solving (3). The model of the system, particularized for S_a and discretized using the forward Euler method, is employed

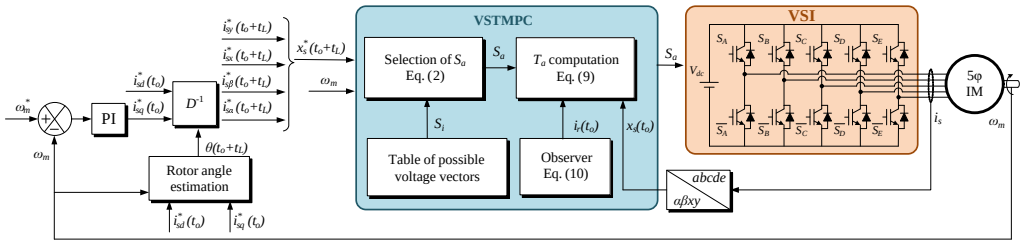

Fig. 4: Schematic representation of the VSTLPC for a FPIM drive.

to predict the future system's output over the selected path as follows:

$$\hat{x}_s(t_o + T|t_o) = x_s(t_o) + Tf(x(t_o), S_a) \tag{8}$$

However, the minimization problem (3) can be analytically solved, saving computing time, using the following expression:

$$T_a = (x_s^*(t_o) - x_s(t_o))^T \frac{f(x(t_o), S_a)}{\|f(x(t_o), S_a)\|^2}. \tag{9}$$

It is important to note that vector x is formed by stator and rotor currents. However, rotor currents are rarely measured in a real system, so they have to be estimated. In this case, this estimation is done using a rotor current observer based on a Luenberger matrix. A full-order version is adopted here since it has been demonstrated in [22] that this configuration produces better rotor current estimations than reduced-order ones, at a negligible increment of the computational cost. The observer produces a current estimation $\hat{x}$ from the system model (4) and a correction term proportional to the estimation error through a gain matrix L, called Luenberger gain matrix as follows:

$$\hat{\dot{x}} = A\,\hat{x} + B\,v - L(C\,\hat{x} - x_s) \tag{10}$$

The design of the observer requires the adequate selection of the eigenvalues of $(A - LC)$, as they determine the convergence towards zero of the observer error. A good strategy, which means that a well-damped dynamic with a fast convergence without endangering stability will be obtained, is to place the observer's eigenvalues in the position defined by the roots of a Butterworth polynomial [22]. In our case, the fourth order polynomial (11) is selected since the system presents two real poles that are maintained in the design of the observer:

$$B_4(s) = T_B^4 s^4 + 2.6131 T_B^3 s^3 + 3.4142 T_B^2 s^2 + 2.6131 T_B s + 1. \tag{11}$$

T_B is a design parameter that defines the speed of the response, with such speed inversely proportional to T_B. Once the desired closed loop observer poles are selected, the coefficients of L are derived using the Kautsky-Nichols algorithm [24].

B. Illustrative Simulation Case

To illustrate the feasibility of our innovative proposal, a representative simulation result is presented in this section. Thus, a simulator has been constructed in the MATLAB environment following the scheme presented in Fig. 4 and using the machine's parameters of Table I.

TABLE I: Electrical and mechanical parameters of the FPIM

Parameter		Value
Stator resistance	R_s (Ω)	19.45
Rotor resistance	R_r (Ω)	6.77
Stator leakage inductance	L_{ls} (mH)	100.7
Rotor leakage inductance	L_{lr} (mH)	38.6
Mutual inductance	L_m (mH)	656.5
Mechanical nominal speed	ω_n (rpm)	1000
Nominal torque	T_n (N·m)	4.7
Nominal current	I_n (A)	2.5
Pole pairs	p	3

Before performing the simulations, it is necessary to tune some parameters of the VSTLPC. The first one is parameter T_B in (11), which is used to design the rotor current observer. It must be noted that matrix A depends on ω_m, so the pole placement problem described in the section before must be solved for different speeds. In other words, observer matrix L must be computed for each rotor speed. Thus, an exhaustive simulation procedure has been performed to select the value of T_B that produces the lowest rotor current observation error (computed as the difference between the estimated rotor currents and the simulated ones). The results obtained for different values of T_B and speeds are shown in Fig. 5, where it can be seen that there is a minimum observation error region for all considered speed values. From these results, and taking into account that the experimental system will produce slightly different values, an optimal T_B equal to 0.001 s has been selected to design the observer for all the speed range.

Although the time of application of the selected switching state (T_a) is an output of the VSTLPC, its value must be limited with minimum and maximum values (T_{min} and T_{max}, respectively) in order to simulate the restrictions that appear in a real system. These restrictions are the microprocessor's capabilities, in term of computational time, and the maximum switching frequency of the power converter. Thus, a minimum value for the application time is selected equal to $T_{min} = 100$ μs in order to take into account both aspects. Regarding T_{max}, it must be chosen avoiding a long sampling period that can deteriorate the system performance. To tune this parameter, again several simulations have been performed for different speed and load torque conditions, and the maximum value

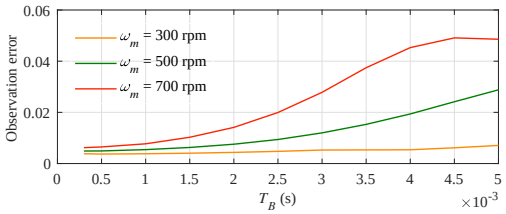

Fig. 5: Dependence of the rotor current observation error on parameter T_B for different rotor speed values.

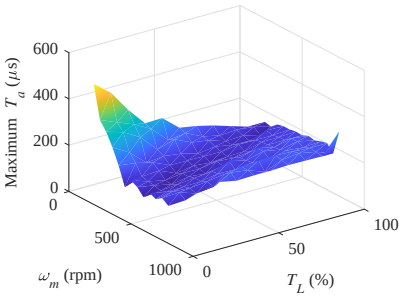

Fig. 6: Maximum application time T_a selected by the VSTLPC for different mechanical speed ω_m and load torque T_L values.

of T_a selected by the VSTLPC has been measured at each case. Fig. 6 displays these values, where the load torque T_L is represented as a percentage of the nominal torque. It can be seen that the maximum applied T_a does not exceed the value of 200 μs in most cases. Thus, it seems reasonable to set a limit of $T_{max} = 3T_{min} = 300$ μs to increase the controller's flexibility without unnecessarily enlarging the sampling time.

Once the controller's parameters have been selected, a simulation test is performed with the following conditions:

- A rotor speed reference of 500 rpm is applied.
- Rated d-current reference is imposed, $i^*_{sd} = 0.57$ A.
- A load torque equal to the 60% of the nominal one is introduced in the system.
- The lead time is set to 100 μs.

The obtained results are summarized in Fig. 7. It can be observed that a smooth tracking performance of the desired stator currents is obtained [Fig. 7(a)]. Note also that the algorithm selects different values for the application time at each sampling period [Fig. 7(b)], and this time never exceeds the imposed minimum and maximum values. The selection process of S_a during a particular sampling instant is depicted in Fig. 7(c), where the evolution of the stator currents are represented in the two orthogonal subspaces α–β and x–y. Red vector defines the desired evolution of the stator currents, while blue vectors represent the current evolution when each possible switching state of the converter is applied. To clarify the representation only the switching states that produce positive values of equation (2) have been plotted, since negative values imply that the stator currents will evolve in the opposite

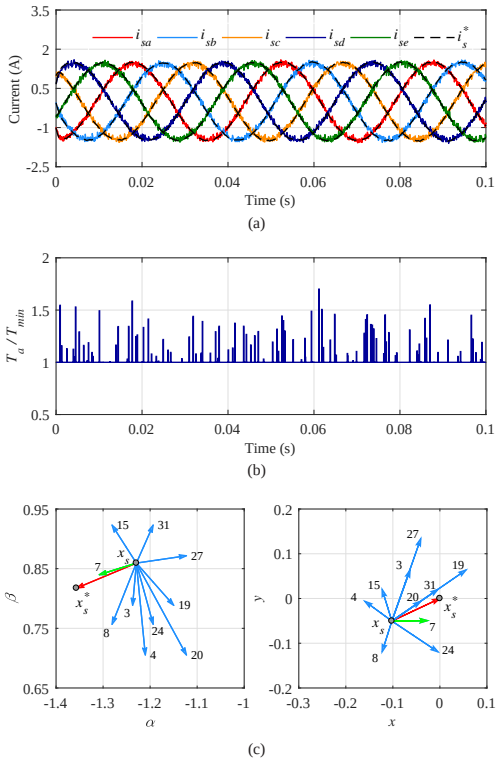

Fig. 7: Simulation results for $\omega^*_m = 500$ rpm when a load of 60% of the nominal torque is applied. (a) Stator phase currents and their references, (b) applied sampling time T_a normalized by its minimum value, and (c) illustration of the optimal S_a value selection process.

direction of the desired one. Finally, green vector stands for the selected S_a, which clearly preforms the closest direction to the reference one when considering both planes. These results state that the control algorithm works as expected.

C. Experimental Results

In any case, there is still a need for doing an experimental analysis of the proposed algorithm to validate its interest. The proposed VSTLPC method has been tested in different steady-state and dynamic situations using a real test rig to corroborate the preliminary analysis. The laboratory experimental setup presented in Fig. 8 has been used for this purpose. It is formed by a 30-slot symmetrical FPIM with distributed windings, whose parameters are the ones presented in Table I. These parameters have been obtained using the experimental methods described in [25] and [26]. The FPIM is supplied by two SKS21F three-phase inverters from Semikron, that are connected to a dc-link voltage of 300

V. The control algorithm is implemented in a TM320F28335 digital signal processor placed on a MSK28335 Technosoft board. An external programmable load torque is generated using an independently controlled dc motor, and the rotor mechanical speed is measured using a GHM510296R/2500 encoder.

First, the steady-state response of the system is studied using the same experimental conditions than in the simulation case (see the list in the section above), including the values of the lead time, the minimum and maximum T_a and T_B. The obtained results are presented in Fig. 9, where Fig. 9(a) and Fig. 9(b) show the phase and α–β–x–y stator currents and their references, Fig. 9(c) presents the measured rotor speed and its reference, and Fig. 9(d) shows the selected T_a at each sampling instant. A good tracking performance of the controlled variables can be observed, with low ripple in the currents. It is important to highlight, despite being reiterative, the variable sampling time of the proposed controller [Fig. 9(d)]. The dynamic response of the system have been also tested by means of a speed reversal test. In this way, a step in the speed reference has been imposed form 500 to -500 rpm at time 0.4 s. In Fig. 10(a), it is seen that the speed is regulated with a fast transient performance, being the rising time about 0.9 s. Stator currents' evolution is the one usually obtained in reversal tests, as it is shown in Fig. 10(b), proving a good performance in terms of current tracking and, again, low ripple.

To extend the previous analysis and quantify the performance of the system under different operating conditions, several steady-state experiments have been carried out for different values of rotor speed ω_m and load T_L. The root mean square error between the phase stator currents and their references RMS_p and the total harmonic distortion of these stator currents THD have been computed, and the results are graphically presented in Fig. 11, being the load torque represented as a percentage of the nominal one. To compare the proposed VSTLPC with predictive techniques, the same tests have been carried out using the conventional FCS-MPC strategy presented in [22]. In general, low values of current tracking error and harmonic content are obtained in all considered operating conditions when the proposed VSTLPC is applied, being these values lower than the ones obtained in the FCS-MPC case and, thus, validating the effectiveness of the proposal. In addition, the tracking error for the proposed controller is almost constant in all the speed range and all applied loads. Only this error is slightly increased with the speed, being this phenomenon enlarged with the increment of the load (Fig. 11 upper plot). On the other hand, the THD values are more influenced by the load, as it can be seen in the lower plot in Fig. 11 where the harmonic content is reduced with T_L. However, the rotor speed does not significantly affect the harmonics. In the FCS-MPC case, the evolution of these performance parameters is similar but with higher values.

It is important to end the analysis of the proposed controller showing its computational cost in comparison with similar control alternatives. Thus, three strategies have been compared in this case: the conventional FCS-MPC with and without rotor current observer recently presented in [22], both using a

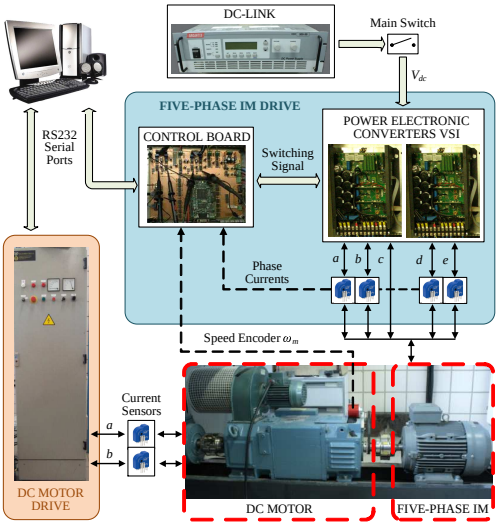

Fig. 8: Experimental test rig.

fixed sampling time in the controller implementation, and the proposed VSTLPC technique. The same full-order Luenberger observer is used in the FCS-MPC and in the VSTLPC in order to do a fair comparison. The effective computational cost τ, which is computed as the time utilized by the microcontroller for the calculations divided by the sampling time $\tau = T_c/T_s$, is used as the comparison ratio at first place in Fig. 12 (left plot). It must be noted that while this ratio is constant in FCS-MPC methods, it is variable for the VSTLPC case because its sampling time (or application time T_a) varies. Then, an average value of T_a has been used in the calculation of τ. In addition, this average application time varies for different operating conditions, increasing its value for higher speeds and higher loads. For this reason, three τ values corresponding with three different operating conditions have been presented in Fig. 12 for the VSTLPC method:

- Case 1: $\omega_m = 300$ rpm and $T_L = 40\%$.
- Case 2: $\omega_m = 700$ rpm and $T_L = 70\%$.
- Case 3: $\omega_m = 700$ rpm and $T_L = 80\%$.

From the obtained results it can be concluded that the proposed VSTLPC technique requires more computational effort for lower speeds and loads, being the effective computational cost higher than using conventional FCS-MPC with and without observer. However, for higher loads and speeds, there is a considerable reduction in the effective computational cost of the VSTLPC that outperforms the benchmark controllers. In terms of absolute computational cost (Fig. 12, right plot), VSTLPC presents a higher computational burden around 55 μs, while the conventional FCS-MPC with and without observer are implemented using the same microprocessor in 36 and 32 μs, respectively.

Finally, it is interesting to mention that a general controller

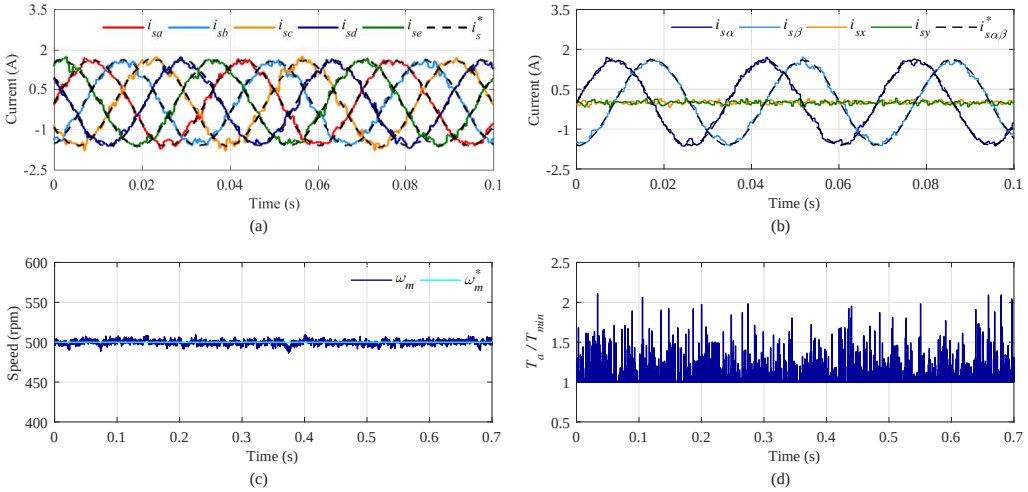

Fig. 9: Experimental results for $\omega_m^* = 500$ rpm with an applied load torque of 60% of the nominal one. (a) Stator phase currents and their references, (b) α–β–x–y stator currents and their references, (c) rotor speed and its reference, and (d) application time T_a normalized using its minimum value.

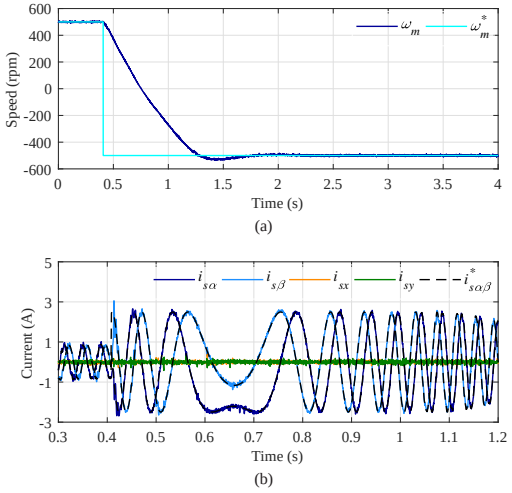

Fig. 10: Dynamic performance of the multiphase drive using the proposed controller. Speed reversal test form 500 to -500 rpm. (a) Rotor speed and its reference, and (b) α–β–x–y stator currents and their references.

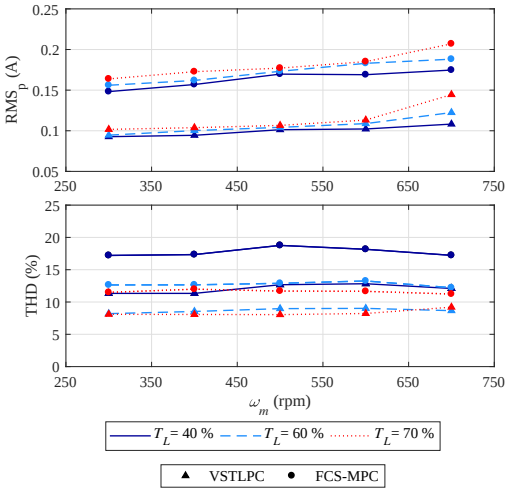

Fig. 11: Experimental RMS_p (upper plot) and THD (lower plot) values when different rotor speeds ω_m and load torques T_L are applied for the proposed controller (VSTLPC) compared with the conventional FCS-MPC method detailed in [22].

has been presented that can be applied to any electrical machine, independently of the number of phases and including conventional three-phase drives. The differences with the case study shown here are the number of switching states of the converter and the model of the system to take into account. The computational cost will obviously increase with the number of phases in the drive.

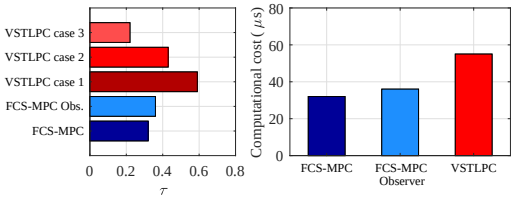

Fig. 12: Effective computational cost τ (left plot) and absolute computatianal cost (right plot) of the proposed controller (VSTLPC) compared with predictive techniques presented in [22] (FCS-MPC with and without observer).

V. Conclusions

One of the most referred problems in the discrete-time control of power converters without modulation blocks, as it is the FCS-MPC, is the high harmonic content that appears in the electric variables of the controlled system. The source of these harmonics comes from the fixed discretization of the time used in this kind of strategies. In this work, a new model-based controller with variable sampling time has been proposed as a simple and natural way to solve the situation. The proposed method uses the lead-pursuit concept to determine the applied optimal control action and, then, a model of the system to find its application time.

A five-phase IM drive has been used as a case example to state the interest and limitations of the proposed control technique. The obtained simulation and experimental results show good tracking performances with low harmonic distortion values in comparison with conventional techniques, which validate the interest of the proposal. In addition, a comparative study of the computational burden of the proposed method has been done to conclude that its computational burden is acceptable, being higher than using conventional FCS-MPC techniques.

References

[1] J. Holtz, "Pulsewidth modulation - A survey," *IEEE Trans. Ind. Electron.*, vol. 39, no. 5, pp. 410–420, Oct. 1992.

[2] G. Calderon-Lopez, A. Villarruel-Parra, P. Kakosimos, S. K. Ki, R. Todd, and A. J. Forsyth, "Comparison of digital PWM control strategies for high-power interleaved dc-dc converters," *IET Power Electron.*, vol. 11, no. 2, pp. 391–398, Feb. 2018.

[3] S. Jin, L. Shi, L. Zhu, W. Cao, T. Dong, and F. Zhang, "Dual two-level converters based on direct power control for an open-winding brushless doubly-fed reluctance generator," *IEEE Trans. Ind. Appl.*, vol. 53, no. 4, pp. 3898–3906, Jul./Aug. 2017.

[4] M. R. Arahal, F. Barrero, M. G. Ortega, and C. Martin, "Harmonic analysis of direct digital control of voltage inverters," *Math. Comput. Simul.*, vol. 130, pp. 155–166, 2016.

[5] B. Wu and M. Narimani, *High-power converters and AC drives*. John Wiley & Sons, 2017.

[6] J. Rodriguez *et al.*, "State of the art of finite control set model predictive control in power electronics," *IEEE Trans. Ind. Inform.*, vol. 9, no. 2, pp. 1003–1016, May. 2013.

[7] P. Karamanakos, K. Pavlou, and S. Manias, "An enumeration-based model predictive control strategy for the cascaded H-bridge multilevel rectifier," *IEEE Trans. Ind. Electron.*, vol. 61, no. 7, pp. 3480–3489, Jul. 2014.

[8] C. S. Lim, N. A. Rahim, W. P. Hew, and E. Levi, "Model predictive control of a two-motor drive with five-leg-inverter supply," *IEEE Trans. Ind. Electron.*, vol. 60, no. 1, pp. 54–65, Jan. 2013.

[9] C. S. Lim, E. Levi, M. Jones, N. A. Rahim, and W. P. Hew, "FCS-MPC-based current control of a five-phase induction motor and its comparison with PI-PWM control," *IEEE Trans. Ind. Electron.*, vol. 61, no. 1, pp. 149–163, Jan. 2014.

[10] F. Barrero, M. R. Arahal, R. Gregor, S. Toral, and M. J. Duran, "A proof of concept study of predictive current control for VSI-driven asymmetrical dual three-phase ac machines," *IEEE Trans. Ind. Electron.*, vol. 56, no. 6, pp. 1937–1954, Jun. 2009.

[11] N. Hoffmann, M. Andresen, F. W. Fuchs, L. Asiminoaei, and P. B. Thøgersen, "Variable sampling time finite control-set model predictive current control for voltage source inverters," in *Proc. IEEE Energy Convers. Congr. Expo. (ECCE)*, pp. 2215–2222, Sep. 2012.

[12] R. Isaacs, *Differential games: a mathematical theory with applications to warfare and pursuit, control and optimization*. Courier Corporation, 1999.

[13] F. Barrero and M. J. Duran, "Recent advances in the design, modeling, and control of multiphase machines - part I," *IEEE Trans. Ind. Electron.*, vol. 63, no. 1, pp. 449–458, Jan. 2016.

[14] M. J. Duran and F. Barrero, "Recent advances in the design, modeling, and control of multiphase machines - part II," *IEEE Trans. Ind. Electron.*, vol. 63, no. 1, pp. 459–468, Jan. 2016.

[15] M. J. Duran, E. Levi, and F. Barrero, *Multiphase Electric Drives: Introduction*. Wiley Encyclopedia of Electrical and Electronics Engineering, 2017.

[16] M. P. Kazmierkowski and L. Malesani, "Current control techniques for three-phase voltage-source PWM converters: a survey," *IEEE Trans. Ind. Electron.*, vol. 45, no. 5, pp. 691–703, Oct. 1998.

[17] C. Martin, M. Bermudez, F. Barrero, M. R. Arahal, X. Kestelyn, and M. J. Duran, "Sensitivity of predictive controllers to parameter variation in five-phase induction motor drives," *Control Eng. Pract.*, vol. 68, pp. 23–31, 2017.

[18] H. A. Young, M. A. Perez, and J. Rodriguez, "Analysis of finite-control-set model predictive current control with model parameter mismatch in a three-phase inverter," *IEEE Trans. Ind. Electron.*, vol. 63, no. 5, pp. 3100–3107, May. 2016.

[19] H. Miranda, P. Cortes, J. I. Yuz, and J. Rodriguez, "Predictive torque control of induction machines based on state-space models," *IEEE Trans. Ind. Electron.*, vol. 56, no. 6, pp. 1916–1924, Jun. 2009.

[20] F. Morel, X. Lin-Shi, J. M. Retif, B. Allard, and C. Buttay, "A comparative study of predictive current control schemes for a permanent-magnet synchronous machine drive," *IEEE Trans. Ind. Electron.*, vol. 56, no. 7, pp. 2715–2728, Jul. 2009.

[21] F. Barrero, M. R. Arahal, R. Gregor, S. Toral, and M. J. Duran, "One-step modulation predictive current control method for the asymmetrical dual three-phase induction machine," *IEEE Trans. Ind. Electron.*, vol. 56, no. 6, pp. 1974–1983, Jun. 2009.

[22] C. Martin, M. R. Arahal, F. Barrero, and M. J. Duran, "Multiphase rotor current observers for current predictive control: A five-phase case study," *Control Eng. Pract.*, vol. 49, pp. 101–111, 2016.

[23] H. Guzman *et al.*, "Comparative study of predictive and resonant controllers in fault-tolerant five-phase induction motor drives," *IEEE Trans. Ind. Electron.*, vol. 63, no. 1, pp. 606–617, Jan. 2016.

[24] J. Kautsky, N. K. Nichols, and P. V. Dooren, "Robust pole assignment in linear state feedback," *Int. J. Control*, vol. 41, no. 5, pp. 1129–1155, 1985.

[25] A. G. Yepes *et al.*, "Parameter identification of multiphase induction machines with distributed windings-Part 1: Sinusoidal excitation methods," *IEEE Trans. Energy Convers.*, vol. 27, no. 4, pp. 1056–1066, Dec. 2012.

[26] J. A. Riveros *et al.*, "Parameter identification of multiphase induction machines with distributed windings-Part 2: Time-domain techniques," *IEEE Trans. Energy Convers.*, vol. 27, no. 4, pp. 1067–1077, Dec. 2012.

Manuel R. Arahal received the M.Sc. and Ph.D. degrees in electrical and electronic engineering from the University of Seville, Seville, Spain, in 1991 and 1996, respectively.

From 1995 to 1998 he was an Assistant Professor and he is currently Full Professor with the Department of Systems Engineering and Automatic Control, University of Seville. His current research interests include industrial applications of model predictive control, artificial intelligence and forecasting techniques.

Cristina Martin was born in Seville, Spain, in 1989. She received the Industrial Engineer degree from the University of Malaga, Malaga, Spain, in 2014.

She has been working toward the Ph.D. degree in electronic engineering in the Department of Electronic Engineering, University of Seville, Seville, Spain, since 2015. Her research interests include modelling and control of multiphase drives, microprocessor and DSP device systems, and electrical vehicles.

Federico Barrero received the M.Sc. and Ph.D. degrees in electrical and electronic engineering from the University of Seville, Seville, Spain, in 1992 and 1998, respectively.

In 1992, he joined the Electronic Engineering Department at the University of Seville, where he is currently Full Professor. His recent interests include the field of control of multiphase AC drives.

Ignacio Gonzalez-Prieto was born in Malaga, Spain, in 1987. He received the Industrial Engineer and M.Sc. degrees in fluid mechanics from the University of Malaga, Malaga, Spain, in 2012 and 2013, respectively, and the Ph.D. degree in electronic engineering from the University of Seville, Seville, Spain, in 2016.

He is currently a Lecturer in the Department of Electrical Engineering, University of Huelva, Spain. His research interests include multiphase machines, wind energy systems, and electrical vehicles.

Mario J. Duran was born in Bilbao, Spain, in 1975. He received the M.Sc. and Ph.D. degrees in electrical engineering from the University of Malaga, Malaga, Spain, in 1999 and 2003, respectively.

He is currently an Associate Professor at the Department of Electrical Engineering, University of Malaga. His research interests include modelling and control of multiphase drives and renewable energies conversion systems.

IEEE TRANSACTIONS ON INDUSTRIAL ELECTRONICS

Assessing Variable Sampling Time Controllers for Five-Phase Induction Motor Drives

Manuel R. Arahal, Cristina Martín, Federico Barrero, and Mario J. Durán

***Abstract*—Finite control set predictive controllers perform a direct digital control of power converters without a modulation stage such as pulse width modulation. Opposed to the inherent positive traits such as high flexibility and enhanced bandwidth, an increase in harmonic content is usually reported. The concept of variable sampling time has been recently introduced as a means to alleviate the harmonic content. The non-uniform sampling approach can be seen as an extra degree of freedom that is conferred to the controller, keeping its model-based feature. This paper goes beyond in the state-of-the-art of variable sampling time controllers, introducing a new scheme for the computation of the sampling time. The resulting variable sampling time controller is experimentally assessed for a two-level five-phase induction motor drive, where steady state and dynamic performance tests confirm the interest of the proposal.**

***Index Terms*—discrete-time control, model-based control, multi-phase drives.**

I. Introduction

THE increasing exigence of high power and high reliability in current industrial applications has recently put the emphasis on the use of multi-phase electrical drives and generators [1]. These electromechanical systems present some advantages over the conventional three-phase ones, such as smaller power per phase that leads to lower current harmonics and torque pulsation. Also, their inherent fault-tolerant capability makes them a suitable option for applications such as ship propulsion and wind energy, where high power/current is required and safety is essential. However, multi-phase systems require sophisticated controllers to provide high performance. In this context Model Predictive Control (MPC) [2], has been applied to multi-phase drives thanks to the availability of powerful microprocessors [3]. Its intuitive formulation provides high flexibility to incorporate multiple control objectives that arise in many applications including multi-phase systems. The Finite Control Set MPC (FCS-MPC) uses a direct digital control of the power converter without a modulation stage such as Pulse Width Modulation (PWM) [4]. Many contributions have been made in the last decade in the predictive control of different systems [5]–[7]. The case of drives is an interesting one, since the dynamics of the machine must be appropriately dealt with by the predictive model [8]–[10]. In particular the multi-phase Induction Machine (IM) case has been studied in detail, where the five-phase IM (FPIM) drive stands as a common test-bench platform in the research community [11], [12].

The elimination of the PWM block in FCS-MPC leads to faster responses compared with more conventional controllers such as Field Oriented Control [11], [13]. However, since only one of the possible switching states of the power converter is applied during every sampling time, the harmonic content can be large compared with modulated schemes [14]. This problem can be particularly severe in high power applications where the number of converter commutations per cycle is limited [15], [16]. A way to get around this problem can be careful selection and tuning of the cost function [11], [17], [18], but it has been recently shown that there are fundamental trade-offs that the FCS-MPC design cannot completely circumvent [19].

The concept of variable sampling time has been recently introduced as a means to alleviate the above cited problems. In this context, the non-uniform sampling approach can be seen as an extra degree of freedom that is conferred to the controller. The idea was introduced in [20] and further developed in [21], where the lead-pursuit concept [22] is used to produce the Variable Sampling Time Lead Pursuit Control (VSTLPC) concept. It was shown in [21] that VSTLPC directly commands the states of the Voltage Source Inverter (VSI) with high resolution in the commuting times and affordable computing requirements. This is done decoupling the selection of the switching state from the calculation of the application time. In this way, the temporal resolution of the application time does not interfere with the computational cost of the control algorithm, allowing timing of commutations on a fine scale unlike the approach in [20] and facilitating for the first time its use in real applications.

The VSTLPC method of [21] uses for the computation of the application time a non-iterative method that depends upon the derivative of the system. In diverse areas (such as continuous systems discretization and numerical integration) the derivative can be approximated differently. For instance, Tustin (bilinear) method for discretization (as well as Euler type II method for numerical integration) use a modified derivative. This idea can be used to refine the computation of the variable sampling time. In this paper, a new scheme for the computation of this variable sampling time is introduced. The new scheme aims at producing more accurate predictions by using a two-step procedure for the computation of the sampling time. In

Manuscript received Month 10, 2018; revised Month 12, 2018; accepted Month 3, 2019.

Manuel R. Arahal is with DISA, Universidad de Sevilla, Seville, E-41092 Spain (phone: +34 954487353; fax: +34 954487343; e-mail: arahal@us.es). Cristina Martín and Federico Barrero are with DINEL, Universidad de Sevilla, Seville, E-41092 Spain (e-mail: cmartin15@us.es, fbarrero@us.es). Mario J. Durán is with DIE, Universidad de Málaga, Malaga, E-41092 Spain (e-mail: mjduran@uma.es).

this way the lead time considered in VSTLPC is refined when necessary. It is interesting to mention that the lead pursuit approach is not only new but also quite general, since it can be applied to different systems not just electromechanical drives. Other researchers can incorporate this principle to their particular application outperforming previous published methods thanks to the new degree of freedom provided by the VST.

In addition of the novelty of the method, comparison testing is done against two FCS-MPC techniques. The paper presents a rigorous assessment by means of simulations and experimental tests that include steady state and transient regimes. To this end two discretizations of the IM dynamics are considered for the FCS-MPC methods. In what follows, the proposed VSTLPC controller is presented for the case of stator current control of a FPIM drive. In Section III, the FCS-MPC techniques used in the comparisons are revisited. The assessment of the VSTLPC technique is done in Sections IV and V. Finally, the conclusions are summarized in the last section.

II. Variable Sampling Time Lead Pursuit Control with Iterated Computation of the Application Time

The scheme of the new controller is shown in Fig. 1. The control algorithm has two steps: in the first one the measurements of i_s, ω_r are made and the VSI state for the next period (S_a) is selected using the lead pursuit idea. In the second step, the application time T_a is computed using an iterated procedure.

A continuous-time state-space representation is used in the stationary subspaces α–β and x–y, defined as

$$\dot{x}(t) = f(x(t), S(t)) \tag{1}$$

where the stator and rotor currents are included as components of the state $x = (i_{s\alpha}, i_{s\beta}, i_{sx}, i_{sy}, i_{r\alpha}, i_{r\beta})^T$. The control signal is the vector of VSI switches position $S = (S_1, S_2, S_3, S_4, S_5)^T \in \mathbb{B}^5$ with $\mathbb{B} = \{0, 1\}$. Function f depends on the VSI connections, the IM electrical parameters, and also on the instantaneous value of rotor speed ω_r.

At time t_o the controller aims at an advanced reference $x^*(t_o + t_L)$, where t_L is the lead time. This reference comes from the outer speed controller (see Fig. 1) and it is advanced using a future value of the rotational angle in the inverse of the Park transformation, $\theta(t_o + t_L)$. Thus, at the first step of VSTLPC, the switching vector that enables the closest approximation to the advanced reference is selected by means of

$$S_a = \underset{S_i}{\operatorname{argmax}} \frac{(x^*(t_o + t_L) - x(t_o)) \cdot f(x(t_o), S_i)}{\|x^*(t_o + t_L) - x(t_o)\| \cdot \|f(x(t_o), S_i)\|} \tag{2}$$

At the second step, the application time is computed and refined. In the first step, a minimization of the deviation from the advanced reference $r = x^*(t_o + t_L)$ is performed. The solution is obtained as

$$T_a = (r - x(t_o))^T \frac{f(x(t_o), S_a)}{\|f(x(t_o), S_a)\|^2}. \tag{3}$$

A second step is then performed as a way of refinement. The rationale is that, if $\|T_a - L\| > \epsilon$ then the intended target is reached at a time that differs from the lead time L in a quantity that is deemed significant (i.e greater than ϵ). Then the advanced reference is recomputed as $x^*(t_o + T_a)$ and the refined application time is obtained using expression (3) again with the newly advanced reference. In this way, the application time is corrected from the previous technique presented in [21] that is useful for cases where the needed T_a is not close enough to the lead time. Note that this circumstance can take place for a variety of reasons. For instance a perturbation can take the state away from its intended value, the algorithm will try to correct the deviation using a appropriate voltage vector for a significant amount of time. During that time the reference value can move significantly, prompting for a re-evaluation of the target r and application time.

Rotor currents are difficult and expensive to be measured. In this work a full state estimation x^e is used for predictive purposes. A matricial form is usually employed to derive the observer

$$\dot{x}(t) = A(\omega_r(t))x(t) + BS(t) \tag{4}$$
$$x^m(t) = Cx(t) \tag{5}$$

where matrices x^m is the measurement vector and matrices A, B and C are easily obtained from the IM model and VSI connections. The full-order observer model can be defined as $\dot{x}^e = A_o x^e + B_o S - LC_o(x^e - x)$, where A_o, B_o, C_o are the state space representation used by the observer, and L is the observer gain. The observer design requires the adequate selection of the eigenvalues of $A - LC$. A pole placement technique is used to determine matrix L, which dictates the convergence of the observer error. As a designing criteria fast convergence and well-damped dynamics are sought. In this case a fourth order polynomial $B_4(s) = T_B^4 s^4 + 2.613 T_B^3 s^3 + 3.414 T_B^2 s^2 + 2.613 T_B s + 1$ is selected with $T_B = 10^{-3}$(s) producing a time constant of about 200 (μs).

III. FCS-MPC Techniques

Fig. 2 shows the diagram of the FCS-MPC technique for a FPIM drive, where the VSI switching state S_{opt} is computed minimizing a cost function J that penalizes deviations of stator current from its reference i_s^*. Two kinds of models are usually considered: models with Euler discretization and models with a discretization derived from the Cayley-Hamilton (CH) theorem [23]. The Euler-discretized model is derived from (4) considering the state space vector split into a measurable part $x^m = (i_{s\alpha}, i_{s\beta}, i_{sx}, i_{sy})^T$ and an unmeasurable part $x^u = (i_{r\alpha}, i_{r\beta})^T$. Matrices A and B are accordingly divided, producing

$$\dot{x}^m(t) = A_{11}x^m(t) + A_{12}x^u(t) + B_1 S(t) \tag{6}$$
$$\dot{x}^u(t) = A_{21}x^m(t) + A_{22}x^u(t) + B_2 S(t). \tag{7}$$

Euler discretization leads to

$$x^{mp}(k+1) = (I + A_{11}T_s)\, x^m(k) + B_1 T_s S(k) + \hat{G}(k) \tag{8}$$

where I is the identity matrix, T_s is the sampling time and $\hat{G}(k)$ is an estimation of the contribution of $x^u(k)$ to $x^m(k+$

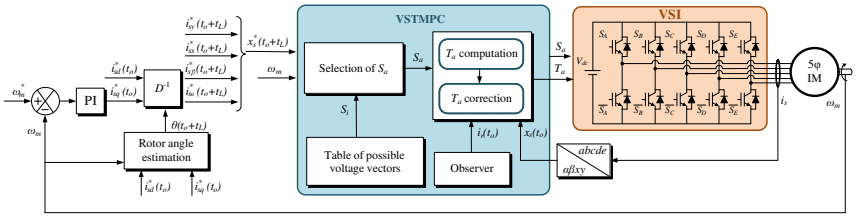

Fig. 1. Block diagram of the new variable sampling time lead pursuit control scheme, applied to a five-phase IM drive.

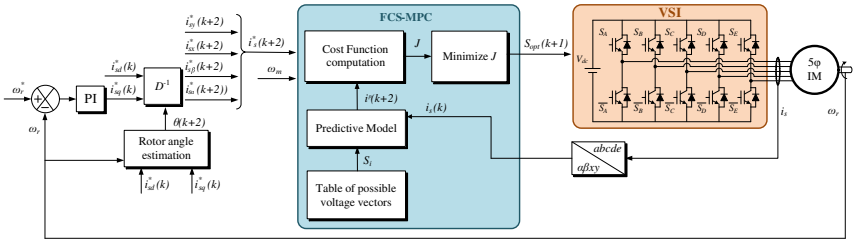

Fig. 2. Diagram of FCS-MPC technique applied to a five-phase IM drive.

1). The estimation is usually obtained by holding its previous value $\hat{G}(k-1)$ that can be computed at time k as $\hat{G}(k-1) = x^m(k) - Qx^m(k-1) - RS(k-1)$, with $Q = (I + A_{11}T_s)$ and $R = B_1T_s$. This discretization has been widely used due to its simplicity. The discretization of [23] produces a model in the form

$$x^p(k+1) = A_d x(k) + B_d S(k) \tag{9}$$

where $A_d = e^{AT_s}$ and $B_d = A^{-1}(A_d - I)B$ are matrices that must be computed at each sampling time. In order to simplify the implementation of the equations, some off-line calculations can be done. Thus, matrix A is divided into a constant part and a variable one that depends on the rotor speed, so $A = A_c + A_w$ and consequently $A_d = e^{A_c T_s} \cdot e^{A_w T_s}$. The elements of the first exponential are computed off-line. The elements of $e^{A_w T_s}$ are computed at every sampling period using the Cayley-Hamilton theorem, resulting in an analytical expression that can be easily realized by a DSP program (for more details see [23]).

In both cases (Euler and CH discretization), the calculation time used by FCS-MPC is significant compared with the sampling time T_s due to the optimization phase. This leads to an important delay between the stator current measurements and the application of the selected switching vector [4]. To overcome this, it is usual to compute a two-step prediction $x^p(k+2)$ that is considered in the cost function

$$J(k+2) = \|e^p_{\alpha\beta}(k+2)\|^2 + \lambda_{xy}\|e^p_{xy}(k+2)\|^2 \tag{10}$$

where $e^p(k+2)$ is the two-step ahead predicted error $e^p(k+2) = i^*_s(k+2) - i^p_s(k+2)$, $i^p_s(k+2)$ is the two-step ahead prediction for stator currents, and λ_{xy} is a tuning parameter that allows to place more emphasis on the torque/flux production plane α–β or the copper losses related plane x–y [11]. The optimal VSI state to be applied at $k+1$ is then derived by exhaustive search over all possible VSI configurations.

IV. Simulation Results

In this section the proposed VSTLPC with the new calculation of the sampling time is tested in a variety of situations. For this purpose, a MATLAB simulator for the VSTLPC technique presented in Fig. 1 is constructed, where the parameters of the FPIM are the ones presented in Table II. In all simulations, the value of T_a is capped to the interval $[T_a^{min}, T_a^{max}]$,where $T_a^{min} = 50$ (μs) and $T_a^{max} = 150$ (μs). The lead time is set to $t_L = 90$ (μs), a constant reference value of $i^*_d = 0.57$ (A) is set in order to produce the rated flux, and a DC-link voltage of 300 (V) is imposed.

The following comparisons make use of the proposed VSTLPC with improved application time calculation and the FCS-MPC with Euler discretization (MPC-EU) that constitutes the traditional predictive approach. Also, the FCS-MPC with a discretization based on the Cayley-Hamilton theorem (MPC-CH) is used. Please note that, the Euler discretization is still used in many applications due (arguably) to its simplicity. Thus, the results for this technique must be taken as a baseline for comparison. The discretization of MPC-CH offers more precise predictions at the cost of a more complex predictive model that takes some extra computations. It is worth remarking that other discretizations such as Tustin could in principle be used. However, experimental results show that the performance and computational burden of these discretizations lie in between the MPC-EU and MPC-CH cases.

A preliminary assessment of the controller is done imposing a reference speed of 500 (rpm) and a load torque equal to the 40% of the nominal torque. Under these conditions,

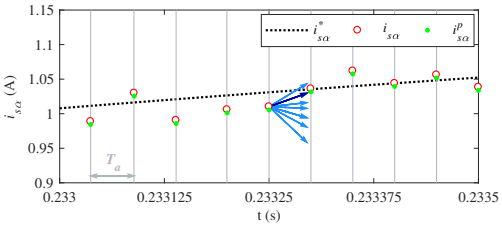

Fig. 3. Simulation test at 500 (rpm) speed and 40% of load illustrating the operation of the new VSTLPC. The trajectories of measured stator α-current ($i_{s\alpha}$), its reference ($i^*_{s\alpha}$) and prediction ($i^p_{s\alpha}$) are shown. The S_a selection process is illustrated for a single instance with blue vectors, the selected one is shown in a darker tone. It is worth noting the different values for the application time T_a, producing varying widths between marks. Vertical lines have been added to remark this effect.

TABLE I
PERCENTAGE OF IMPROVEMENT OF THE PROPOSED VSTLPC OVER MPC-EU AND MPC-CH TECHNIQUES IN THE (A) RMSE_p AND (B) THD VALUES. EACH COLUMN REPRESENTS AN OPERATING REGIME IN THE FORM (ω_m (RPM), T_L (%)).

(A)	100, 40	400, 60	700, 70
VSTLPC vs. MPC-EU	17.5 %	31.3 %	44.8 %
VSTLPC vs. MPC-CH	10.5 %	12.4 %	22.3 %
(B)	100, 40	400, 60	700, 70
VSTLPC vs. MPC-EU	11.3 %	7.6 %	4.9 %
VSTLPC vs. MPC-CH	9.4 %	7.1 %	4.4 %

the evolution of the simulated stator α-current together with its reference is depicted in Fig. 3. The sampling periods are marked with vertical grey lines to remark the variable-sampling nature of the controller. The VSTLPC operation is illustrated at $t = 0.23325$ (s) by showing the predictions for each possible voltage vector that produces an advance towards the reference. The S_a selection process is represented with blue vectors that describe the direction of change of $i_{s\alpha}$ for the VSI states that produce a positive value of (2). This restriction is made to simplify the representation. The predictions use the derivative and the calculated T_a value. The selected S_a is represented by the dark blue vector.

The simulation results discussion is complemented with a comparative analysis of the proposal against existing FCS-MPC techniques. The comparison is done first under steady-state situation. In order to provide a fair comparison, the sampling time of the FCS-MPC methods is fixed to 50 (μs) which implies that the FCS-MPC techniques will apply the optimization process with the lowest sampling time of the VSTLPC techniques. The weighting factor for the cost function in the FCS-MPC controllers is set to 0.5, which is a commonly found value [11]. Also, a Gaussian measurement noise has been introduced in the measured stator currents to simulate a more realistic scenario. Equal simulation conditions than before are applied for the VSTLPC, but the variable sampling time is in the range from 50 (μs) to 150 (μs).

Fig. 4 summarizes the comparison done on the basis of the mean square tracking error of the phase currents (RMSE_p) and

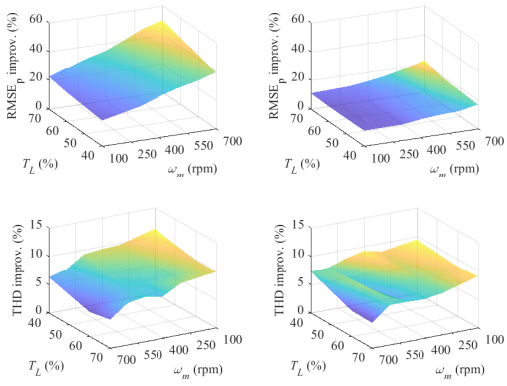

(VSTLPC vs. MPC-EU) (VSTLPC vs. MPC-CH)

Fig. 4. Percentage of improvement of the proposed VSTLPC over MPC-EU (left side) and over MPC-CH (right side) techniques in the RMSE_p (top) and THD values (bottom).

the Total Harmonic Distortion in the phase currents (THD). Table I presents the percentage of improvement obtained with the proposed VSTLPC over the other techniques for both figures of merit in three different operating points, where the operating conditions for the simulations are defined in each column by a rotor speed ω_m (rpm) and load torque T_L (percentage of the nominal torque). It can be observed that the proposed VSTLPC outperforms the current tracking performance of conventional FCS-MPC techniques with lower harmonic content and lower tracking error. The difference is higher when the VSTLPC is compared with the MPC-EU, since the CH discretization produces more precise predictions than the most conventional Euler technique. Note also that the improvement depends on the operating point, being the best cases from the VSTLPC perspective those operating points with the highest speed and load. These results will be contrasted by experimentation in the next section.

V. EXPERIMENTAL RESULTS

In this section, the experimental assessment of the proposed VSTLPC technique is obtained, comparing the dynamic and steady-state performances of VSTLPC versus FCS-MPC techniques. A wide range for the speed and torque operation is considered in steady state including the low speed regime. The dynamic assessment is based on speed and torque step tests and speed reversal tests.

To this end, the test-rig presented in Fig. 5 is employed. It consists of a 30-slot symmetrical FPIM with distributed windings, for which the electrical parameters of the equivalent model (see Table II) were obtained using conventional AC time-domain and stand-still tests. The IM is supplied by two conventional three-phase two-level inverters from Semikron (SKS22F modules) with one unused open phase. They are supplied by an external DC-link voltage of 300 (V). The controller uses a MSK28335 Technosoft board that includes

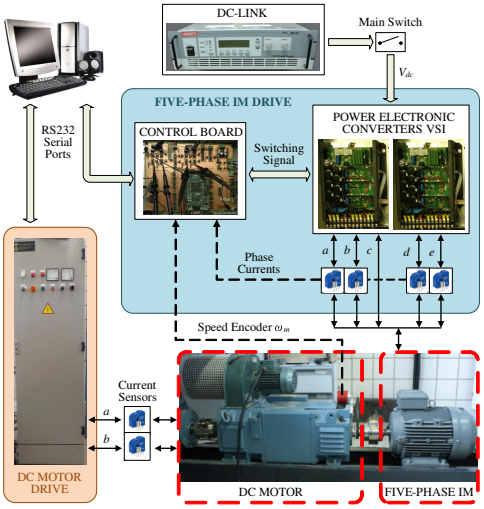

Fig. 5. Experimental test-rig.

TABLE II
ELECTRICAL AND MECHANICAL PARAMETERS OF THE FPIM

Parameter		Value
Stator resistance	R_s (Ω)	19.45
Rotor resistance	R_r (Ω)	6.77
Stator leakage inductance	L_{ls} (mH)	100.7
Rotor leakage inductance	L_{lr} (mH)	38.6
Mutual inductance	L_m (mH)	656.5
Mechanical nominal speed	ω_n (rpm)	1000
Nominal torque	T_n (N·m)	4.7
Nominal current	I_n (A)	2.5
Pole pairs	P	3

a TMS320F28335 DSP where the VSTLPC and FCS-MPC algorithms run.

The rotor mechanical speed is measured using a GHM510296R/2500 digital encoder. Finally, an independently controlled DC machine is used to impose a load torque in the shaft of the IM machine. The experimental test bench corresponds to the real system previously reproduced in simulations using MATLAB.

The proposed VSTLPC will be compared with the FCS-MPC techniques with two discretization methods, MPC-EU and MPC-CH. As in the simulation cases, the weighting factor λ_{xy} is set to 0.5 but, in this case, the sampling time in FCS-MPC controllers is set to 100 (μs) which is enough for the time-consuming Cayley-Hamilton model to be iterated. Accordingly, the minimum application time in the VSTLPC is fixed to $T_a^{min} = 100$ (μs). In this way the proposed VSTLPC does not have the obvious advantage of issuing more control actions per cycle than its competitors (see [14] for a more elaborate version of this argument).

Other parameters of the VSTLPC are the maximum application time $T_a^{max} = 300$ (μs) and the lead time $t_L = 150$ (μs).

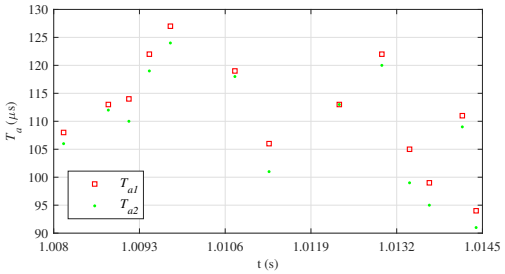

Fig. 6. Experimental values of T_a with refinement (T_{a2}) and without refinement (T_{a1}).

Please note that for FCS-MPC algorithms everything runs at 100 (μs), and for VSTLPC everything is synchronised with the selected variable sampling time that lies in the $[T_a^{min}, T_a^{max}]$ interval.

The experimental conditions are defined by the mechanical reference speed and by the external torque load provided by the DC machine. These variables are indicated for each test as they cover a wide operating range. A constant d-current is set to 0.57 (A) in order to obtain rated flux production.

A. Steady-State Performance

The steady-state performance analysis is first done comparing with the existing variable sampling time controller proposed in [21]. Fig. 6 shows how the proposal refines the obtained application time. The comparison is obtained testing the multiphase drive at a particular operating point (500 rpm speed and 60% load). Note that the proposal refines up to 10 % the obtained sampling time and this figure increases if the allowed T_a^{min} is reduced.

The comparison with FCS-MPC techniques is done on the basis of the same figures of merit as in the simulation section, defined for a time-window comprising several fundamental periods. Table III collects the obtained experimental results for different rotor speeds ω_m (rpm) and load torques T_L (%). The three sections of this table presents, (a) the RMSE_p, (b) the THD and (c) the number of commutations per cycle (NCPC).

It can be seen that, compared with the FCS-MPC techniques, the VSTLPC scheme provides better current tracking with less distortion and a similar number of commutations. Undoubtedly this variation in the definition of the VSTLPC method improves the controller's performance (see the improvement of figures of merits in relation with the current tracking and harmonic generation) in comparison with FCS-MPC competitors. These results agree with the simulations previously presented in Table I and Fig. 4, corroborating the effectiveness of the proposal compared with FCS-MPC methods.

Fig. 7 shows the obtained experimental values in a steady-state test performed at low speed $\omega_m = 100$ (rpm) with a load torque around 40% of the nominal one, in order to show the evolution with the time of the system's variables for

TABLE III
EXPERIMENTAL COMPARISON OF VSTLPC WITH MPC-EU AND MPC-CH IN TERMS OF (A) $RMSE_p$ (A), (B) THD (%) AND (C) NCPC.

(a)	100,40	100,70	400,40	400,70	700,40	700,70
MPC-EU	0.150	0.160	0.157	0.173	0.175	0.207
MPC-CH	0.111	0.117	0.110	0.109	0.118	0.167
VSTLPC	0.085	0.079	0.094	0.104	0.108	0.145
(b)	100,40	100,70	400,40	400,70	700,40	700,70
MPC-EU	18.58	11.92	17.34	11.99	17.23	11.24
MPC-CH	13.26	08.73	12.28	08.18	12.38	09.20
VSTLPC	09.91	05.57	11.33	08.07	12.10	09.16
(c)	100,40	100,70	400,40	400,70	700,40	700,70
MPC-EU	926	679	251	196	107	76
MPC-CH	812	618	229	182	94	67
VSTLPC	1058	786	261	203	107	79

each controller. Since the PI-based speed regulator has been identically tuned for all controllers, the speed performance is quite similar in the three cases (see top plots in Fig. 7).

Besides that, it is apparent that the proposed controller produces a better α tracking with lower x content, which results in lower harmonic spectrum (see middle and bottom plots in Fig. 7). It is interesting to remark that the x-current content for the VSTLPC is the lowest, producing lower copper losses and, consequently, higher efficiency of the system. Recall that the λ_{xy} ratio used for FCS-MPC is 0.5 and by increasing λ_{xy} the x-current content of FCS-MPC would diminish at the price of higher RMS tracking error as shown in [17], [19]. The speed ripple is quite the same for both approaches so lower harmonic content means better dc-link utilization (less losses).

B. Dynamic Performance

The performance of the proposed controller has been analyzed in three different transient conditions, forcing different speed and torque steps. A speed step test is performed first, yielding the results shown in Fig. 8, where the speed reference goes from 0 to 500 (rpm) at 60% of the nominal torque. It can be seen that the transient performance of the rotor speed and d–q currents are similar for all cases. However, it is interesting to check that d–q currents have a small offset for FCS-MPC controllers that is not present in the proposed VSTLPC.

The torque step test of Fig. 9 shows the adequacy of the proposed controller for speed regulation in the presence of changing external load. Again, similar transient performances are obtained for all considered controllers, both in the speed and the currents, and small offsets can be seen for FCS-MPC controllers, this time principally for q-currents tracking.

Finally, Fig. 10 shows the obtained experimental values for a speed reversal test where the reference of the mechanical speed goes from $+500$ to -500 (rpm). It can be seen that the rising time is about the same for all controllers with slightly less overshoot for the VSTLPC method. It is remarkable that, the x-current content for the proposed controller is the lowest of the group, as well as the ripple in the α-current, being these results in accordance with those obtained in steady state and proving the interest and benefits of the proposed control method.

VI. CONCLUSIONS

The use of predictive controllers in power converters and drives has grown up in recent times due to the flexibility they offer in the design of the control objective. However, these controllers avoid the use of modulation techniques, producing higher harmonic contents than classical controllers do.

Predictive controllers with variable sampling time based on the lead pursuit concept, recently introduced in the scientific literature, offer a natural way to alleviate the problem. A new variable sampling time scheme with improved application time computation has been introduced. The new scheme has been tested in simulation and by means of experimental tests.

A five-phase induction motor drive has been used as a case example to provide a comparison with predictive controllers, including the computationally intensive Cayley-Hamilton based version. Both steady-state and dynamic tests have been performed in a laboratory setup, including low speed regime. The comparisons show that the proposed variable sampling time technique offers better results, even though the predictive controllers fully exploit their capabilities, while the proposed technique was not similarly optimized.

REFERENCES

[1] M. J. Duran, E. Levi, and F. Barrero, *Multiphase Electric Drives: Introduction*, 1st ed. NY, USA: Wiley Encyclopedia of Electrical and Electronics Engineering, 2017.

[2] E. F. Camacho and C. Bordons, *Model predictive control*, 2nd ed. London, UK: Springer, 2013.

[3] S. Kouro, M. A. Perez, J. Rodriguez, A. M. Llor, and H. A. Young, "Model predictive control: MPC's role in the evolution of power electronics," *IEEE Industrial Electronics Magazine*, vol. 9, DOI 10.1109/MIE.2015.2478920, no. 4, pp. 8–21, Dec. 2015.

[4] D. Holmes and D. Martin, "Implementation of a direct digital predictive current controller for single and three phase voltage source inverters," in *IEEE Industry Applications Conference.*, vol. 2, pp. 906–913. IEEE, Oct. 1996.

[5] M. Narimani, B. Wu, V. Yaramasu, Z. Cheng, and N. R. Zargari, "Finite control-set model predictive control (FCS-MPC) of nested neutral point-clamped (NNPC) converter," *IEEE Transactions on Power Electronics*, vol. 30, no. 12, pp. 7262–7269, Dec. 2015.

[6] S. Odhano, P. Zanchetta, M. Tang, and C. A. Silva, "MPC using modulated optimal voltage vector for voltage source inverter with LC output filter," in *IEEE Energy Conversion Congress and Exposition*, pp. 6865–6871. IEEE, Sep. 2018.

[7] M. Vali, V. Petrovic, S. Boersma, J.-W. van Wingerden, L. Y. Pao, and M. Kuhn, "Adjoint-based model predictive control for optimal energy extraction in waked wind farms," *Control Engineering Practice*, vol. 84, DOI 10.1016/j.conengprac.2018.11005, pp. 48 – 62, Mar. 2019.

[8] G. Cimini, D. Bernardini, A. Bemporad, and S. Levijoki, "Online model predictive torque control for permanent magnet synchronous motors," in *IEEE International Conference on Industrial Technology*, pp. 2308–2313. IEEE, Mar. 2015.

[9] S. S. Yeoh, T. Yang, L. Tarisciotti, C. I. Hill, S. Bozhko, and P. Zanchetta, "Permanent-magnet machine-based starter–generator system with modulated model predictive control," *IEEE transactions on transportation electrification*, vol. 3, no. 4, pp. 878–890, Dec. 2017.

[10] J. Zou, W. Xu, J. Zhu, and Y. Liu, "Low-complexity finite control set model predictive control with current limit for linear induction machines," *IEEE Transactions on Industrial Electronics*, vol. 65, DOI 10.1109/TIE.2018.2807369, no. 12, pp. 9243–9254, Dec. 2018.

[11] C. S. Lim, E. Levi, M. Jones, N. A. Rahim, and W. P. Hew, "FCS-MPC-based current control of a five-phase induction motor and its comparison with PI-PWM control," *IEEE Trans. Ind. Electron.*, vol. 61, DOI 10.1109/TIE.2013.2248334, no. 1, pp. 149–163, Jan. 2014.

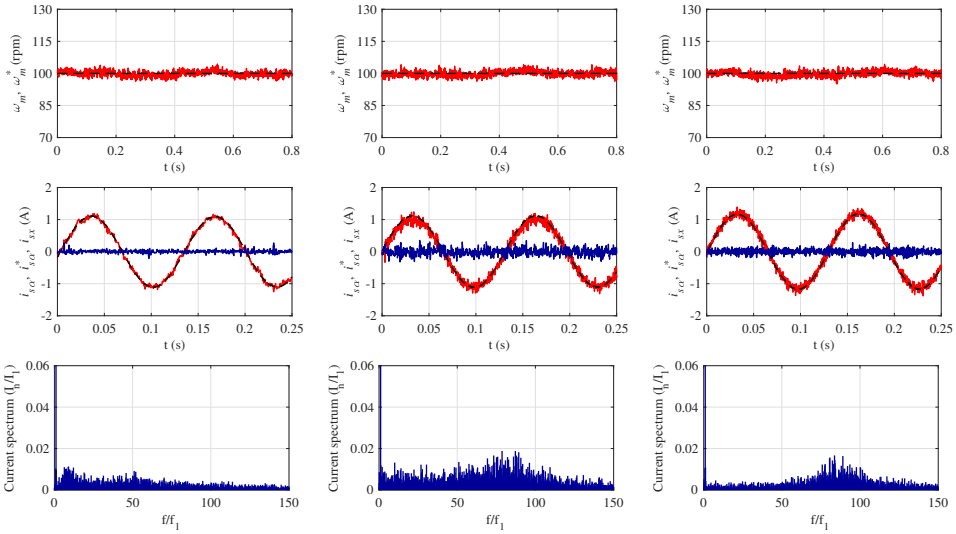

Fig. 7. Steady-state test for low speed $\omega_m = 100$ (rpm) with a load torque of 40% of the nominal one for VSTLPC (left), MPC-EU (center) and MPC-CH (right), presenting (top) rotor speed and its reference, (middle) stator α and x currents and their references, and (bottom) spectrum of the a-current. References are in dashed black lines while the measured variables are in solid coloured lines.

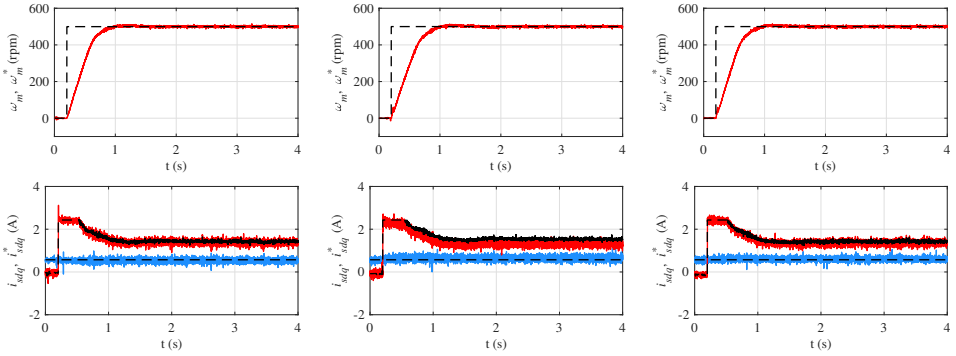

Fig. 8. Speed step test from 0 to 500 (rpm) at 60% of the nominal torque for VSTLPC (left), MPC-EU (center) and MPC-CH (right), presenting (top) rotor speed with its reference, (bottom) d–q currents with their references. References are in dashed black lines while the measured variables are in solid coloured lines.

[12] M. J. Duran and F. Barrero, "Recent advances in the design, modeling, and control of multiphase machines - part II," *IEEE Trans. Ind. Electron.*, vol. 63, DOI 10.1109/TIE.2015.2448211, no. 1, pp. 459–468, Jan. 2016.

[13] H. A. Young, M. A. Perez, J. Rodriguez, and H. Abu-Rub, "Assessing finite-control-set model predictive control: A comparison with a linear current controller in two-level voltage source inverters," *IEEE Industrial Electronics Magazine*, vol. 8, DOI 10.1109/MIE.2013.2294870, no. 1, pp. 44–52, Mar. 2014.

[14] M. R. Arahal, F. Barrero, M. G. Ortega, and C. Martin, "Harmonic analysis of direct digital control of voltage inverters," *Math. Comput. Simulat.*, vol. 130, DOI 10.1016/j.matcom.2016.02001, pp. 155–166, Dec. 2016.

[15] B. Wu and M. Narimani, *High-power converters and AC drives*, 2nd ed. USA: Wiley-IEEE Press, 2017.

[16] S. S. Lee and Y. E. Heng, "Current controller of three-phase VSI using FCS-MPC with optimal active and zero vector selection for balanced loss distribution and switching loss reduction," *International Transactions on Electrical Energy Systems*, vol. 27, no. 2, pp. 1–16, Jul. 2017.

[17] M. R. Arahal, A. Kowal, F. Barrero, and M. Castilla, "Cost function optimization for multi-phase induction machines predictive control," *Revista Iberoamericana de Automática e Informática industrial*, vol. 16, DOI 10.4995/riai.2018.9771, no. 1, pp. 48 – 55, Jan. 2019.

[18] A. G. Bartsch, G. H. Negri, M. S. Cavalca, J. de Oliveira, and A. Nied, "Cost function tuning methodology for FCS-MPC applied to PMSM drives," in *Power Electronics Conference (COBEP), 2017 Brazilian*, DOI 10.1109/COBEP.2017.8257320, pp. 1–6. IEEE, Nov. 2017.

[19] M. R. Arahal, F. Barrero, M. J. Duran, M. G. Ortega, and C. Martin, "Trade-offs analysis in predictive current control of multi-phase induction machines," *Control Engineering Practice*, vol. 81, DOI 10.1016/j.conengprac.2018.09012, pp. 105 – 113, Dec. 2018.

[20] N. Hoffmann, M. Andresen, F. W. Fuchs, L. Asiminoaei, and P. B. Thøgersen, "Variable sampling time finite control-set model

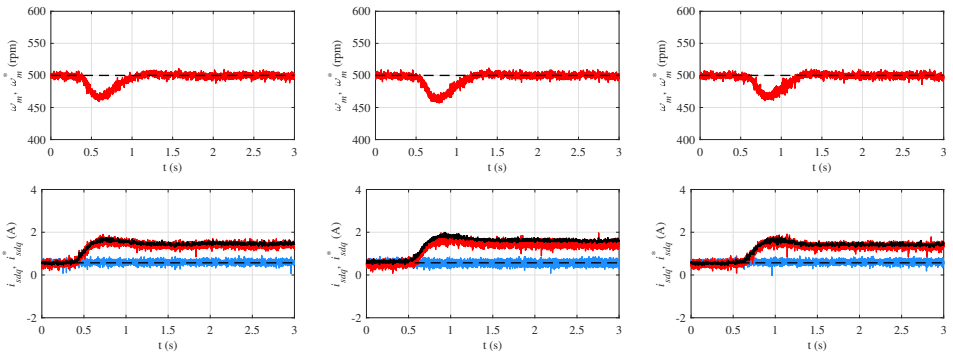

Fig. 9. Torque step test from 0 to 60% of the nominal torque at 500 (rpm) for VSTLPC (left), MPC-EU (center) and MPC-CH (right), presenting (top) rotor speed with its reference, (bottom) d–q currents with their references. References are in dashed black lines while the measured variables are in solid coloured lines.

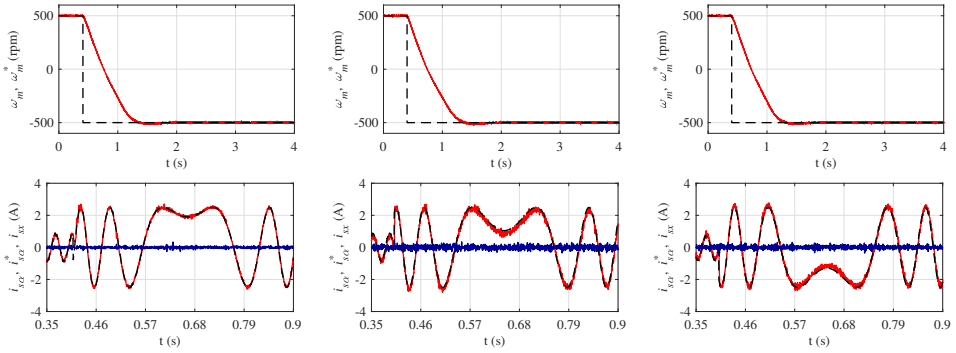

Fig. 10. Speed reversal test from $+500$ to -500 (rpm) for VSTLPC (left), MPC-EU (center) and MPC-CH (right), presenting (top) rotor speed with its reference, (bottom) α and x currents with their references. References are in dashed black lines while the measured variables are in solid coloured lines.

predictive current control for voltage source inverters," in *2012 IEEE Energy Conversion Congress and Exposition (ECCE)*, DOI 10.1109/ECCE.2012.6342440, pp. 2215–2222, Sep. 2012.

[21] M. R. Arahal, C. Martin, F. Barrero, I. Gonzalez-Prieto, and M. J. Duran, "Model-based control for power converters with variable sampling time: A case example using five-phase induction motor drives," *IEEE Transactions on Industrial Electronics*, DOI 10.1109/TIE.2018.2870390, 2018.

[22] R. Isaacs, *Differential games: a mathematical theory with applications to warfare and pursuit, control and optimization*, 1st ed. NY, USA: Dover Publications, 1999.

[23] H. Miranda, P. Cortes, J. I. Yuz, and J. Rodriguez, "Predictive torque control of induction machines based on state-space models," *IEEE Trans. Ind. Electron.*, vol. 56, DOI 10.1109/TIE.2009.2014904, no. 6, pp. 1916–1924, Jun. 2009.

Manuel R. Arahal was born in Dos Hermanas, Seville, Spain 1966. He received the Industrial Engineering master degree in 1991 and the Ph.D. in 1996 both at the Universidad de Sevilla, Spain.

He is currently a full professor at the Ingeniería de Sistemas y Automática department of the University of Seville.

Prof. Arahal has authored more than 50 published papers in scientific journals and has received the Best Paper Awards from the IEEE Transactions on Industrial Electronics for 2009 and from the IET Electric Power Applications for 2010-2011.

Cristina Martín was born in Seville, Spain, in 1989. She received the Industrial Engineer degree from the Universidad de Málaga, Malaga, Spain, in 2014.

She is pursuing the Ph.D. in electronic engineering in the Department of Electronic Engineering at the Universidad de Sevilla, Seville, Spain.

Ms. Martín research interests include modelling and control of multiphase drives, microprocessor and DSP device systems, and electrical vehicles.

Federico Barrero received the M.Sc. and Ph.D. in Electrical and Electronic Engineering from the University of Seville, Spain, in 1992 and 1998, respectively.

He joined the Electronic Engineering Department at the University of Seville in 1992, where he is currently Full Professor.

Prof. Barrero has more than 100 published papers in scientific journals and received the Best Paper Awards from the IEEE Transactions on Industrial Electronics for 2009 and from the IET Electric Power Applications for 2010-2011.

Mario J. Durán was born in Bilbao (Spain) in 1975. He received the M.Sc. and Ph.D. degrees in Electrical Engineering from the University of Málaga Spain, in 1999 and 2003, respectively.

He is currently a Full Professor with the Department of Electrical Engineering at the University of Málaga. His research interests include modeling and control of multiphase drives and renewable energies conversion systems

energies

MDPI

Article

Model-Based Predictive Current Controllers in Multiphase Drives Dealing with Natural Reduction of Harmonic Distortion

Cristina Martin [1], Federico Barrero [1,*], Manuel R. Arahal [2] and Mario J. Duran [3]

[1] Electronic Engineering Department, University of Seville, 41092 Seville, Spain; fbarrero@us.es
[2] System and Automatic Engineering Department, University of Seville, 41092 Seville, Spain; arahal@us.es
[3] Electrical Engineering Department, University of Malaga, 29071 Malaga, Spain; mjduran@uma.es
* Correspondence: fbarrero@us.es; Tel.: +34-954-48-13-04

Received: 14 March 2019; Accepted: 29 April 2019; Published: 3 May 2019

Abstract: An important drawback in the application of model-based predictive controllers for multiphase systems is the relatively high harmonic content. Harmonics arise due to the fixed sampling-time nature and the absence of modulation methods in the control technique. Recent research works have proposed different procedures to overcome this disadvantage at the expense of increasing the complexity of the controller and, in most cases, the computational requirements. There are, however, natural ways to face this harmonic generation that have been barely explored in the scientific literature. These alternatives include the use of variable sampling times or the application of the observer theory, whose utility has been stated without excessively increasing the computational cost of the controller. This paper presents the basis of both methodologies, analyzing their interest as natural alternatives to mitigate the generation of harmonic components in modern electrical drives when using predictive controllers. A five-phase induction machine is used as a case example to experimentally validate the study and draw conclusions.

Keywords: predictive current control; harmonic distortion; multiphase drives; observer; variable sampling

1. Introduction

The increasing interest for multiphase drives in real applications [1,2], added to the complexity of designing appropriate controllers for these multivariable systems, have put the emphasis on model predictive control methods (MPC) and particularly on the finite control set MPC (FCS-MPC) [3]. The FCS-MPC is a kind of fast direct control method that commands the power converter without using pulse width modulation (PWM) blocks, providing excellent transient performance and lower switching frequency than PWM blocks with conventional proportional-integral controllers (PI-PWM), under comparable conditions [4,5]. This issue has been extensively investigated in [6], where FCS-MPC and PI-PWM current controllers are compared, concluding that the FCS-MPC provides a faster transient evolution at the expense of a lower steady-state performance, something that is, in general, inevitable in multiphase drives due to the existence of nonflux/torque producing current components. Additionally, the simple and multi-objective formulation of the FCS-MPC algorithm makes it an excellent option in multiphase drives, being that five-phase induction machine (IM) is one of the most investigated configurations [7].

However, an important drawback appears in the FCS-MPC implementation, which is the high current/voltage harmonic content. This problem has been recently examined in [8], concluding that the fixed-time discretization nature of the control method, along with the fact that only one of the possible power converter states is applied during each sampling interval, favour the appearance of not

only high magnitude harmonics but also inter-harmonics and electrical noise. Some recent solutions based on the selective harmonic elimination concept can reduce harmonics of the integer multiples of the fundamental frequency [9,10], but they do not cancel inter-harmonics and electrical noise.

A careful design of the cost function, which represents the control objectives of the FCS-MPC, can also help in the reduction of the harmonic content [11]. For example, a precise tuning of the weighting factors that weight each control objective can be decisive [4,6,12], as well as the limitation of the commutation frequency in the converter by the restriction of the available changes in the switches of the converter's legs [13]. However, these techniques generally increase the controller complexity and the computational requirements, another important handicap in the application of FCS-MPC methods to multiphase drives. Furthermore, they can lead to suboptimal solutions when not all the possible control actions are taken into account. In addition, there exists an interdependence between the harmonic content and other control aspects, such as the switching frequency or the operating point, which can be seen as fundamental trade-offs that the cost function design cannot completely bypass [14].

A quite different alternative for the harmonic mitigation consists in adding a modulation stage in the FCS-MPC algorithm [15] or applying more than one switching state of the power converter during the same sampling time [16], which is in essence a kind of modulation. However, these techniques produce higher switching frequencies than conventional FCS-MPC methods when identical sampling time is imposed, and could increase the high computational cost of the predictive controller.

The use of simpler natural solutions can alleviate the harmonic problem that the previously cited techniques suffer. One of them is the newly proposed variable sampling time lead pursuit controller (VSTLPC) [17], which introduces the concept of non-uniform sampling time as a new degree of freedom in the model-based predictive technique. In this way, both the switching state of the power converter and its time of application are optimally selected between all the possibilities without the necessity of a cost function and with an affordable computational cost. A different alternative consists of the improvement of the predictive model, since the selected control action depends on it. In this context, the observer theory has been recently incorporated in the FCS-MPC for the estimation of non-measurable parts of the system model, leading to significant improvement of the system performance. Rotor current observers based on the Luenberger theory and Kalman filters are usually applied in the FCS-MPC current control of multiphase IM replacing the traditional backtracking procedures [18,19]. This work focuses on the study of VSTLPC and rotor-current observers as natural ways to reduce the harmonic distortion and electrical noise in predictive controllers. The basis of compared techniques will be reviewed in Sections 2 and 3, where a five-phase IM drive is used as a well-known case example of multiphase drives. Experimental results to corroborate the utility of these techniques are presented in Section 4, while the obtained conclusions are summarized in the last section.

2. Rotor Estimation in FCS-MPC Techniques: The Observer Approach

Considering a five-phase IM drive supplied by a two-level five-phase voltage source inverter (VSI) as the controlled system under study, the general scheme of the applied FCS-MPC current control is illustrated in Figure 1a. The main goal is to find the switching state (S_{opt}) that forces the stator currents (i_s) to follow the references (i_s^*). To this end, a prediction of the future stator currents (i_s^p) is computed using an electrical model of the IM drive (predictive model) and the measured i_s and rotor speed (ω_r). The prediction and references are then compared inside a predefined cost function (J) to find the switching state that minimizes their difference. The algorithm is iterated and repeated using a constant sampling period.

In this process, the predictive model plays an important role and the best agreement with the real system will improve the predictions and, consequently, the performance of the regulated system. The five-phase IM can be represented, using the well-known vector space decomposition approach, by a set of equations expressed in the two orthogonal α–β and x–y subspaces as follows:

$$\begin{aligned} \dot{x}(t) &= f(x(t), S(t)) \\ x_s(t) &= C\,x(t), \end{aligned} \tag{1}$$

where the state variables are the stator and rotor currents $x = (i_{s\alpha}, i_{s\beta}, i_{sx}, i_{sy}, i_{r\alpha}, i_{r\beta})$, the control signal is the switching state of the VSI that is arranged in vector $S = (S_A, S_B, S_C, S_D, S_E) \in \mathbb{B}^5$ with $\mathbb{B} = \{0, 1\}$, the output signals are the stator currents $x_s = (i_{s\alpha}, i_{s\beta}, i_{sx}, i_{sy})$, and function f depends on the IM parameters, the spatial distribution of the windings, the VSI connections and the instant value of the rotor speed. Further details of the multiphase IM drive modeling can be encountered in [20], and in [18] for the particular five-phase case. The discretization of these non-linear equations provides the predictive model (2), normally using the forward Euler method or a more complicated technique based on the Cayley–Hamilton theorem, which improves the tracking and prediction performance [21].

$$\begin{aligned} x^p(k+1) &= x(k) + T_s f(x(k), S(k)) \\ x_s^p(k+1) &= C\,x^p(k+1). \end{aligned} \tag{2}$$

In any case, a second-step prediction $x^p(k+2)$ is usually applied to compensate the delay that introduces the computation of the control algorithm [4]. Then, the cost function, usually defined as in (3) from the squared error between the predictions and reference currents $\hat{e} = i_s^*(k+2) - i_s^p(k+2)$, is computed for all the available switching vectors of the VSI to obtain the next control action to be applied.

$$J = \|\hat{e}_{\alpha\beta}\|^2 + \lambda_{xy}\|\hat{e}_{xy}\|^2. \tag{3}$$

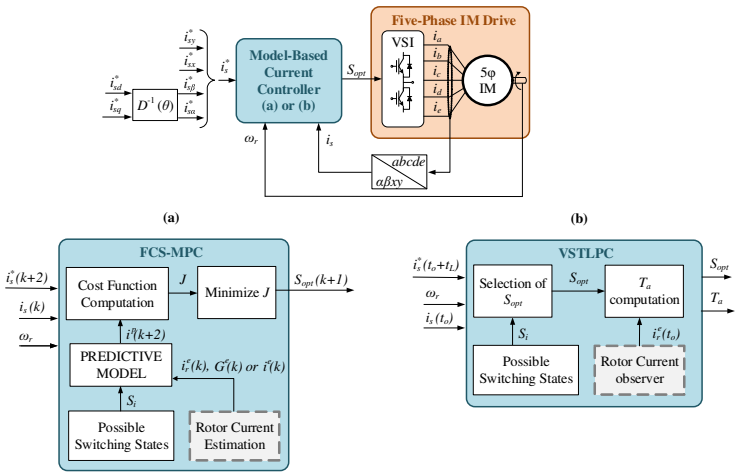

Figure 1. Simplified scheme of the five-phase induction machine (IM) drive current controller using (**a**) finite control set (FCS)-predictice control methods (MPC) and (**b**) variable sampling time lead pursuit controller (VSTLPC) techniques.

This cost function includes a weighting factor λ_{xy} to put more or less emphasis in the x–y control plane, which is related to the copper losses in our case since sinusoidal winding distribution is assumed in the IM. The tuning of this parameter is not a simple issue [11], but a value of 0.5 is usually accepted because it provides a good trade-off between both planes [6]. Stator current references in the d–q

rotating reference frame are imposed and then rotated using the inverse of the Park transformation D^{-1} and the rotational angle θ [6], obtaining α–β current references. Furthermore, x–y references are set to zero to minimize the stator copper losses.

While stator currents are measured, rotor ones are commonly estimated using a simple backtracking procedure that consists in lumping into term G all non-measurable quantities and other uncertainties of the system. This term is recalculated every sampling period using the system model and past values of the measured variables. Thus, the predictive model can be rewritten as:

$$x_s^p(k+1) = x_s(k) + T_s f_s(x_s(k), S(k)) + G^e(k), \tag{4}$$

being f_s the part of the function f in (2) related only to the stator currents, and superscript e stands for estimated values. Using this method, the rotor estimation error will be compensated at each sampling period, being this effect accentuated by smaller sampling periods. However, even a small amount of electrical noise has an important effect in the prediction error, which can even lead to a wrong selection of the switching vector and produce a high disturbance in the tracking performance. Another commonly used backtracking procedure is the one applied in [6], where an open-loop observer based on the system model is used to obtain estimated values of the rotor variables as follows:

$$x_r^e(k) = x_r^e(k-1) + T_s f_r(x(k-1), S(k-1)). \tag{5}$$

Rotor currents are updated every k instant using the previous values of the measured variables and the applied switching state. Notice that function f_r is the part of function f in (2) that provides the rotor current values. Although a more precise rotor current estimation can be obtained with this approximation, the previous problems still remain and the noise can degrade the control performance.

An alternative to aforementioned techniques goes through the use of closed-loop observers, where the rotor current estimation is done using Kalman filters or Luenberger-based observers. Among them, the full-order version of the Luenberger observer has shown the best rotor estimation result at the expense of a slight increment in the computational cost [18]. In this Luenberguer-based approach, estimation of both stator and rotor currents x^e is computed using the system model (1) plus a correction term weighted by the Luenberger matrix L:

$$\dot{x}^e(t) = f(x^e(t), S(t)) - L(C\,x^e(t) - x_s(t)). \tag{6}$$

The design of the observer consists in a pole placement problem in which matrix L is obtained as a result. A good practice consists of placing the observer's eigenvalues in the position defined by the roots of a Butterworth filter polynomial, permitting a fast convergence towards zero of the estimation error, as well as a well-dumped dynamic without compromising the stability. Although the design of the observer requires the solution of this problem, it can be done off-line and simple expressions of L can be obtained for all the operating speed range that, in turn, does not excessively increase the computational cost of the controller. Also, the Luenberger observer has demonstrated to be more robust under model uncertainties than previous backtracking procedures, showing better rotor current estimations and, consequently, improving the performance of the controlled system.

3. Variable Sampling Time in Predictive Controllers

An alternative model-based predictive current controller named VSTLPC is detailed in [17], where the sampling time is a new degree of freedom that is calculated by the control algorithm at each iteration. The schematic representation of the VSTLPC current control applied to a five-phase IM is detailed in Figure 1b. Similarly to FCS-MPC, the optimal switching state (S_{opt}) of the power converter is selected in order to produce the desired stator current response defined by the reference (i_s^*). However, the application time of the converter state is not fixed and equal to the sampling time, but it is also decided by the controller.

The control algorithm starts with the selection of S_{opt} based on the measurement of the stator currents (i_s) and rotor speed (ω_r) and using the lead-pursuit concept: hitting a moving target requires some anticipation, since it takes some time for the control action to produce an effect on the system and during such time the target changes its position. In this way, the controller points to an advanced stator current reference $i_s^*(t_o + t_L)$, where t_o is the present time instant and t_L is the anticipation time or lead time. Then, the switching vector that produces the closest trajectory of stator currents to the reference is selected. The ideal trajectory would be the one formed by measured currents and advanced references, which is defined by $(x_s^*(t_o + t_L) - x_s(t_o))$ in our case. Following that $f_s(x, S)$ is a vector that determines how stator currents evolve, the cosine of the angle between vectors $f_s(x(t_o), S)$ and $(x_s^*(t_o + t_L) - x_s(t_o))$ is the maximum for the switching state that minimizes the deviation from the objective. Consequently, the optimal switching vector S_{opt} is selected through the definition of the scalar product:

$$S_{opt} = \underset{S_i}{\operatorname{argmax}} \frac{(x_s^*(t_o + t_L) - x_s(t_o)) \cdot f_s(x(t_o), S_i)}{\|x_s^*(t_o + t_L) - x_s(t_o)\| \, \|f_s(x(t_o), S_i)\|}. \tag{7}$$

The above expression is an optimization problem that takes into account all possible switching states. It is necessary to remember that vector $x(t_o)$ in function f_s is formed by measured stator currents and the estimated rotor ones. Note that rotor currents are obtained in [17] using the Luenberger observer detailed in the previous section.

The application time T_a of the selected voltage vector is obtained minimizing the deviation between the stator references and predicted currents:

$$T_a = \underset{T}{\operatorname{argmin}} \left\| x_s^*(t_o + t_L) - x_s^p(t_o + T) \right\|, \tag{8}$$

where $x_s^p(t_o + T)$ is obtained using the system equations (2) for the selected S_{opt}. This minimization problem is finally solved using:

$$T_a = (x_s^*(t_o + t_L) - x_s(t_o))^T \frac{f_s(x(t_o), S_{opt})}{\|f_s(x(t_o), S_{opt})\|^2}. \tag{9}$$

After that, a receding horizon process is applied where the selected vector is released during the obtained application time and the control algorithm is repeated. Comparing with FCS-MPC techniques, the VSTLPC method permits a fine resolution of commuting times thanks to the non-uniform sampling, which can mitigate the generated harmonic distortion. This hypothesis will be analyzed in the next section, where a comparative analysis of the generated harmonic distortion using FCS-MPC and VSTLPC techniques is done.

4. Harmonic Distortion Using FCS-MPC and VSTLPC Techniques: Comparative Analysis

A current control performance analysis of the revised controllers is done using the experimental test bench shown in Figure 2. The main component is a 30-slot symmetrical five-phase IM with distributed windings, whose electrical parameters are gathered in Table 1. These have been obtained through the experimental tests described in [22,23]. Two three-phase two-level inverters from Semikron (SKS22F modules) supply the IM, and an external DC-link voltage of 300 V is connected to them. The multiphase system is controlled using a MSK28335 Technosoft board that includes a TMS320F28335 digital signal processor (DSP). The rotor mechanical speed (ω_m) is measured using a GHM510296R/2500 digital encoder. Finally, an independently controlled DC machine is used to impose an external variable load torque in the shaft of the IM.

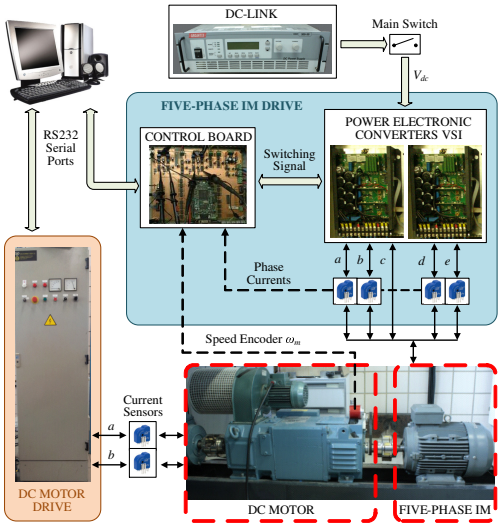

Figure 2. Experimental test rig.

Table 1. Estimated parameters of the IM.

Parameter		Value
Stator resistance	R_s (Ω)	19.45
Rotor resistance	R_r (Ω)	6.77
Stator leakage inductance	L_{ls} (mH)	100.7
Rotor leakage inductance	L_{lr} (mH)	38.6
Mutual inductance	L_m (mH)	656.5
Mechanical nominal speed	ω_n (rpm)	1000
Nominal torque	T_n (N·m)	4.7
Nominal current	I_n (A)	2.5
Pole pairs	P	3

The controllers used in the comparison are the FCS-MPC technique with the conventional backtracking procedure (MPC-C1) and the open-loop observer (MPC-C2), the FCS-MPC method with a closed-loop rotor current observer (MPC-OB), and the VSTLPC. Equal cost functions are applied in MPC-C1, MPC-C2 and MPC-OB with a weighting factor of 0.5, for the reasons presented in Section 2. The Luenberger rotor current observer is designed using a fourth order Butterworth filter (10), since the system presents two real poles that are maintained in the design of the observer:

$$B_4(s) = T_B^4 s^4 + 2.61 T_B^3 s^3 + 3.41 T_B^2 s^2 + 2.61 T_B s + 1. \tag{10}$$

A value of $T_B = 0.001$ s has been optimally selected by simulations in order to produce the lowest observation error in all speed range. Regarding the sampling time, it is imposed as $T_s = 100$ µs for the three FCS-MPC techniques with fixed discretization. For the case of the VSTLPC method, the sampling time is limited by a minimum value of $T_{min} = 100$ µs to make a fair comparison with the other controllers, and a maximum value of $T_{max} = 300$ µs to avoid larger sampling periods that could deteriorate the control performance [17]. The lead time is set to $t_L = 100$ µs.

First, several steady-state tests have been carried out for each controller and the performance analysis is done on the basis of the mean square tracking error of the phase currents (RMSe_p), the total

harmonic distortion in the phase currents (THD_p), and the number of commutations per cycle (NCPC) in the VSI legs. In all tests, the d-current reference is fixed to 0.57 A to produce the rated flux and the system is closed-loop speed controlled using an outer PI regulator that provides the q-current reference. In this way, it is possible to drive the machine to a constant rotor speed in the range of 50 rpm to 700 rpm. In addition, a variable load torque between the 40% to the 70% of the nominal torque is imposed. The obtained results are plotted in Figure 3. In each column, the VSTLPC technique is compared with one of the other controllers in terms of the three aforementioned figures of merits. In such a way, the interest of including the non-fixed sampling against the FCS-MPC methods is revealed.

Regarding the current tracking performance and the harmonic content, lower values of $RMSe_p$ and THD_p are observed in the VSTLPC technique in all considered operating conditions when it is compared with the MPC-C1 and MPC-C2 methods, being the difference bigger in the first comparison. However, the opposite occurs when the VSTLPC and MPC-OB techniques are compared. In this case, the $RMSe_p$ and the THD_p values are lower for the MPC-OB, indicating that the inclusion of the rotor current observer in the FCS-MPC is enough to produce a significant improvement in the current control performance with respect to the conventional techniques. It must be noticed that the backtracking procedure based on the open-loop rotor current observer (MPC-C2) provides better results than the most conventional rotor estimation approach (MPC-C1), demonstrating a higher robustness to external disturbances as it was stated in Section 2. In terms of the number of commutations per cycle, the VSTLPC produces the highest values, being this effect accentuated by the decrease of the speed, while the MPC-OB presents the lowest values in most cases.

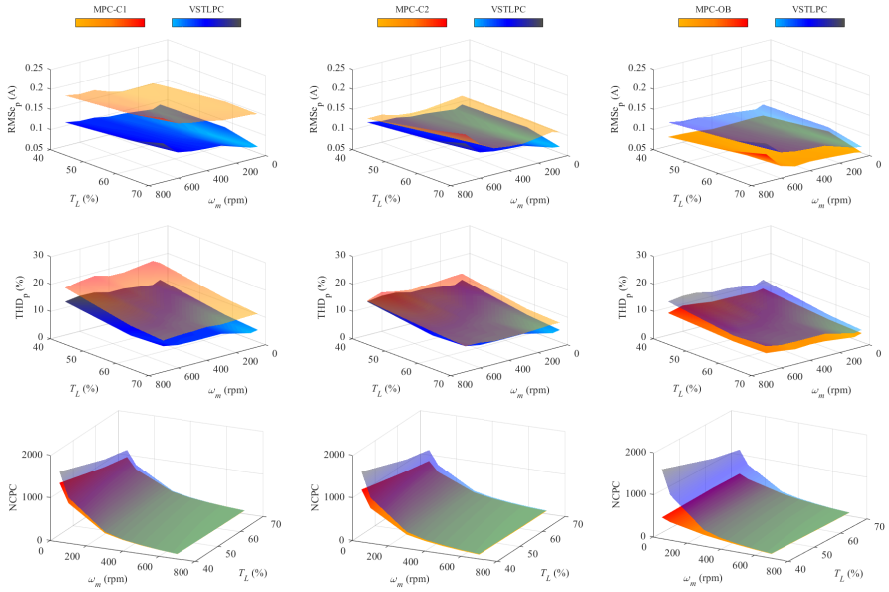

(**a**) VSTLPC vs. MPC-C1 (**b**) VSTLPC vs. MPC-C2 (**c**) VSTLPC vs. MPC-OB

Figure 3. Experimental root mean square error of phase currents ($RMSe_p$), total harmonic distortion (THD) and number of commutations per cycle (NCPC) values for each controller under different operating conditions.

It is interesting to mention that, in general, the evolution with the speed and the torque of all performance parameters is similar for all considered control techniques, regardless of the different values between them.

To complete the previous analysis, Figures 4 and 5 show the current control performance of all considered controllers for two of the analyzed operating conditions: 100 rpm and 60% of the nominal torque (Figure 4), and 600 rpm and 70% of the nominal torque (Figure 5). For the first experiment, the circular α–β and x–y current trajectories and their references appear in the upper plots, while in the second test the evolution with the time of the α and x currents are shown. In both tests, the spectrum of the $a-$phase current is plotted and zoomed in the lower plots. These spectrums show harmonics and inter-harmonics that have been measured following the guidelines of the ICE standard [24], but after adapting the normative to the case under study. Thus, 9 and 10 cycles of the current signal have been used for the spectrum calculation in the 100 rpm and 600 rpm cases, respectively, in order to guarantee a good resolution.

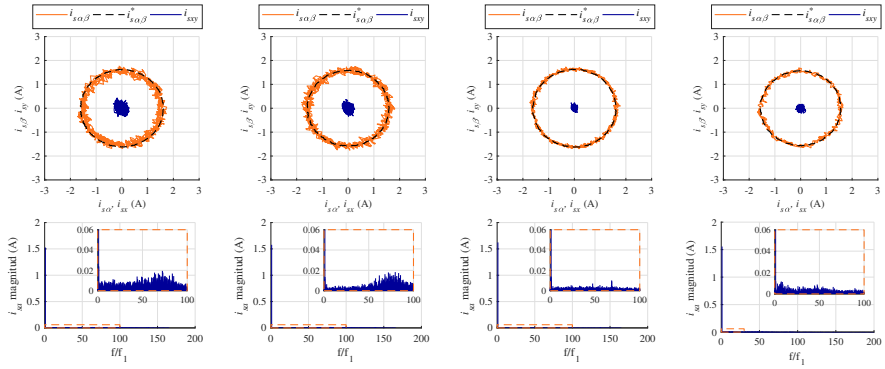

(**a**) MPC-C1 (**b**) MPC-C2 (**c**) MPC-OB (**d**) VSTLPC

Figure 4. Experimental steady-state test for 100 rpm and a load torque of 60% of the nominal one. Upper plots present the α–β and x–y current trajectories, and the lower plots present the a-current spectrum.

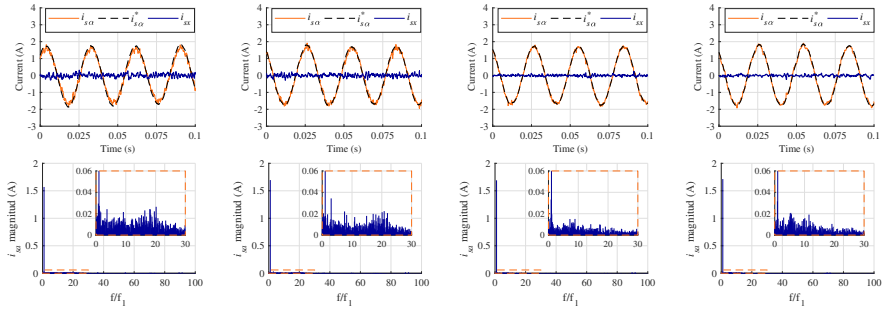

(**a**) MPC-C1 (**b**) MPC-C2 (**c**) MPC-OB (**d**) VSTLPC

Figure 5. Experimental steady-state test for 600 rpm and a load torque of 70% of the nominal one. Upper plots present the α and x current trajectories, and the lower plots present the a-current spectrum.

It can be seen that the worst current tracking performance is obtained with the MPC-C1 technique, which presents a small offset in the tracking of the α–β currents. This offset is a characteristic of most predictive controllers [3] but it is significantly reduced by the application of the closed-loop observer and the variable sampling. The harmonic and noise content is also reduced with the new controllers (MPC-OB and VSTLPC), as evidenced by the lower ripple in the α–β–x–y currents and the reduced magnitude in the current spectrum in comparison with conventional FCS-MPC techniques (MPC-C1 and MPC-C2). This, in turn, leads to a more efficient flux and torque production with lower copper losses. Focusing on the current spectrum, it is interesting to see that the MPC-C1 technique presents a more continuous spectrum with high magnitude of harmonics in a large frequency domain, while the MPC-C2 method shows significant harmonic distortion principally at high frequencies (this effect is more accentuated at lower speeds and loads). Conversely, the MPC-OB and VSTLPC approaches effectively reduce the harmonic magnitude in all the frequency domain. Although the VSTLPC presents some peaks of distortion at low frequencies for specific operating points, the total harmonic distortion is still lower than in conventional FCS-MPC methods (Figure 3).

Three dynamic tests have also been done in order to validate the current control performance during the transient. The first one consists in a speed reversal test from -500 to 500 rpm imposing a load torque equal to the 60% of the nominal one. The second test is a speed step from 0 to 500 rpm imposing a load torque of the 60% too. Finally, the third test is a torque step from 0% to 60% of the nominal torque at 500 rpm. Since all controllers present similar speed response in each test, only the speed evolution for the case of the VSTLPC method is presented in Figure 6 for simplicity reasons. Diversely, the d–q currents evolution with time for each controller is presented in Figures 7–9 for the speed reversal, the speed step and the torque step experiments, respectively. Regarding the transient performance, it can be stated that it is quite similar for all controllers. This fact demonstrates that the inclusion of the closed-loop rotor current observer and the variable sampling time does not deteriorate the fast transient performance that characterizes the predictive controller. Furthermore, superior current tracking and lower harmonic distortion are provided by the MPC-OB and VSTLPC techniques, as it was expected by the previous steady-state results. This is evidenced by the $d-q$ currents performance in Figures 7–9, where the current ripple and the previously cited offset are higher when using the conventional MPC-C1 and MPC-C2 methods even during the transient. Consequently, the harmonic content is also higher in that cases comparing to the recently proposed current control approaches.

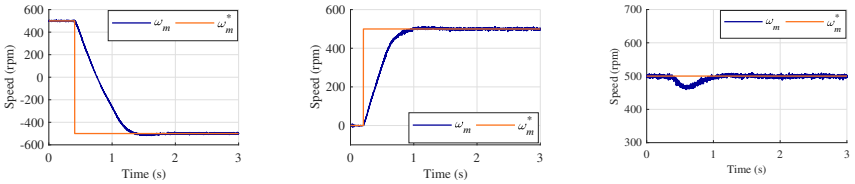

Figure 6. Rotor speed dynamic for the VSTLPC: (**a**) reversal test from -500 to 500 rpm, (**b**) speed step test from 0 to 500 rpm, both tests with a load torque of 60%, and (**c**) torque step test from 0% to 60% of the nominal torque at 500 rpm.

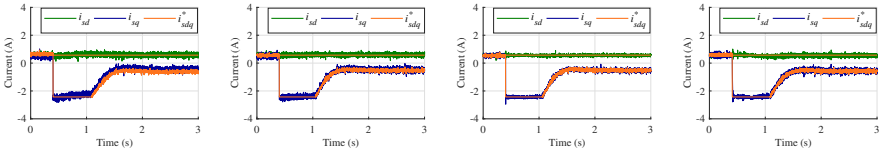

(**a**) MPC-C1 (**b**) MPC-C2 (**c**) MPC-OB (**d**) VSTLPC

Figure 7. Evolution of d–q currents and their references for each controller in a reversal test from −500 to 500 rpm with a load torque of the 60%.

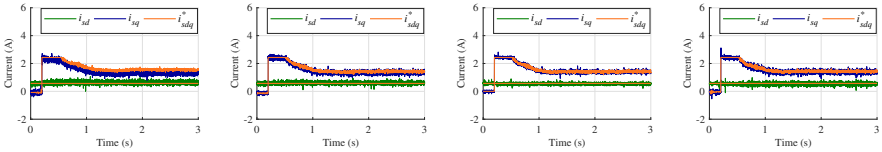

(**a**) MPC-C1 (**b**) MPC-C2 (**c**) MPC-OB (**d**) VSTLPC

Figure 8. Evolution of d–q currents and their references for each controller in a speed step test from 0 to 500 rpm with a load torque of the 60%.

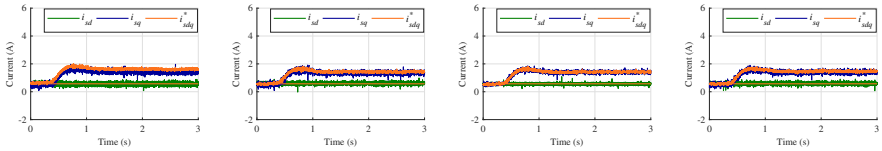

(**a**) MPC-C1 (**b**) MPC-C2 (**c**) MPC-OB (**d**) VSTLPC

Figure 9. Evolution of d–q currents and their references for each controller in a torque step test from 0% to 60% of the nominal torque at 500 rpm.

To conclude the comparative assessment, the computational cost of analyzed controllers was studied. The conventional MPC-C1 and MPC-C2 approaches require, in the DSP-based experimental system, a computational cost around 32 µs and 34 µs, respectively. On the other hand, the MPC-OB and the VSTLPC techniques require 36 µs and 55 µs, respectively. This increment is completely affordable taking into account that the minimum sampling time is 100 µs. It must be noticed that the computational burden of the VSTLPC strongly depends on the operating point, as it was stated in [17], being the previously indicated computational cost a mean value.

To summarize, the VSTLPC and MPC-OB techniques outperform the conventional FCS-MPC methods in terms of harmonic content and tracking performance, but the closed-loop observer provides the best results in all the operating range. Regarding the NCPC, the VSTLPC provides the highest values while the lowest values are produced, in the most cases, by the MPC-OB. Note that the obtained benefits do not excessively increase the computational cost of the controller and do not compromise the fast transient response of the regulated system.

5. Conclusions

Model-based current predictive controllers applied to multiphase machines directly commands the power converter providing faster transient performance and lower switching frequencies than conventional PI-PWM methods. However, they suffer from high harmonic content in the electric variables, principally due to the inaccuracy of the prediction model and the fixed time discretization. In this work, a state of the art analysis of the situation has been done, where different predictive control

techniques are compared, natural ways to reduce the obtained harmonic distortion are presented, and experiments are carried out using a five-phase IM drive as a case study to conclude the benefits and drawbacks of the analyzed control methods.

Author Contributions: conceptualization, F.B. and M.R.A.; methodology, C.M. and M.R.A; software, C.M.; validation, C.M.; formal analysis, C.M.; investigation, C.M.; resources, F.B.; data curation, C.M.; writing—original draft preparation, C.M. and F.B.; writing—review and editing, C.M., F.B., M.R.A. and M.J.D.; visualization, F.B.; supervision, F.B. and M.R.A.; project administration, C.M. and F.B.; funding acquisition, F.B.

Funding: this research received no external funding.

Acknowledgments: the authors would like to thank the University of Seville for its support under the V Research Plan, Action II.2.

Conflicts of Interest: the authors declare no conflict of interest.

References

1. Duran, M.J.; Levi, E.; Barrero, F. Multiphase Electric Drives: Introduction. In *Wiley Encyclopedia of Electrical and Electronics Engineering*; John Wiley & Sons, Inc.: Hoboken, NJ, USA, 2017; pp. 1–26.
2. Bojoi, R.; Rubino, S.; Tenconi, A.; Vaschetto, S. Multiphase electrical machines and drives: A viable solution for energy generation and transportation electrification. In Proceedings of the 2016 International Conference and Exposition on Electrical and Power Engineering (EPE), Iasi, Romania, 20–22 October 2016; pp. 632–639.
3. Kouro, S.; Perez, M.A.; Rodriguez, J.; Llor, A.M.; Young, H.A. Model Predictive Control: MPC's Role in the Evolution of Power Electronics. *IEEE Ind. Electron. Mag.* **2015**, *9*, 8–21.
4. Arahal, M.; Barrero, F.; Toral, S.; Duran, M.; Gregor, R. Multi-phase current control using finite-state model-predictive control. *Control Eng. Pract.* **2009**, *17*, 579–587.
5. Young, H.A.; Perez, M.A.; Rodriguez, J.; Abu-Rub, H. Assessing Finite-Control-Set Model Predictive Control: A Comparison with a Linear Current Controller in Two-Level Voltage Source Inverters. *IEEE Ind. Electron. Mag.* **2014**, *8*, 44–52.
6. Lim, C.S.; Levi, E.; Jones, M.; Rahim, N.A.; Hew, W.P. FCS-MPC-Based Current Control of a Five-Phase Induction Motor and its Comparison with PI-PWM Control. *IEEE Trans. Ind. Electron.* **2014**, *61*, 149–163.
7. Tenconi, A.; Rubino, S.; Bojoi, R. Model Predictive Control for Multiphase Motor Drives—A Technology Status Review. In Proceedings of the 2018 International Power Electronics Conference, IPEC-Niigata 2018-ECCE Asia, Niigata, Japan, 20–24 May 2018; pp. 732–739.
8. Arahal, M.R.; Barrero, F.; Ortega, M.G.; Martin, C. Harmonic analysis of direct digital control of voltage inverters. *Math. Comput. Simulat.* **2016**, *130*, 155–166.
9. Aggrawal, H.; Leon, J.I.; Franquelo, L.G.; Kouro, S.; Garg, P.; Rodriguez, J. Model predictive control based selective harmonic mitigation technique for multilevel cascaded H-bridge converters. In Proceedings of the IECON 2011-37th Annual Conference of the IEEE Industrial Electronics Society, Melbourne, Australia, 7–10 November 2011; pp. 4427–4432.
10. Aguilera, R.P.; Acuña, P.; Lezana, P.; Konstantinou, G.; Wu, B.; Bernet, S.; Agelidis, V.G. Selective Harmonic Elimination Model Predictive Control for Multilevel Power Converters. *IEEE Trans. Power Electron.* **2017**, *32*, 2416–2426.
11. Arahal, M.R.; Kowal, A.; Barrero, F.; del Mar Castilla, M. Cost Function Optimization for Multi-phase Induction Machines Predictive Control. *RIAI* **2018**, *16*, 1–8.
12. Mamdouh, M.; Abido, M.A.; Hamouz, Z. Weighting Factor Selection Techniques for Predictive Torque Control of Induction Motor Drives: A Comparison Study. *Arab. J. Sci. Eng.* **2018**, *43*, 433–445.
13. Duran, M.J.; Prieto, J.; Barrero, F.; Toral, S. Predictive Current Control of Dual Three-Phase Drives Using Restrained Search Techniques. *IEEE Trans. Ind. Electron.* **2011**, *58*, 3253–3263.
14. Arahal, M.R.; Barrero, F.; Duran, M.J.; Ortega, M.G.; Martin, C. Trade-offs analysis in predictive current control of multi-phase induction machines. *Control Eng. Pract.* **2018**, *81*, 105–113.
15. Gonzalez, O.; Ayala, M.; Rodas, J.; Gregor, R.; Rivas, G.; Doval-Gandoy, J. Variable-Speed Control of a Six-Phase Induction Machine using Predictive-Fixed Switching Frequency Current Control Techniques. In Proceedings of the 2018 9th IEEE International Symposium on Power Electronics for Distributed Generation Systems (PEDG), Charlotte, NC, USA, 25–28 June 2018; pp. 1–6.

16. Barrero, F.; Arahal, M.R.; Gregor, R.; Toral, S.; Duran, M.J. One-Step Modulation Predictive Current Control Method for the Asymmetrical Dual Three-Phase Induction Machine. *IEEE Trans. Ind. Electron.* **2009**, *56*, 1974–1983.
17. Arahal, M.R.; Martin, C.; Barrero, F.; Gonzalez-Prieto, I.; Duran, M.J. Model-Based Control for Power Converters with Variable Sampling Time: A Case Example Using Five-Phase Induction Motor Drives. *IEEE Trans. Ind. Electron.* **2019**, *66*, 5800–5809.
18. Martin, C.; Arahal, M.R.; Barrero, F.; Duran, M.J. Multiphase rotor current observers for current predictive control: A five-phase case study. *Control Eng. Pract.* **2016**, *49*, 101–111.
19. Rodas, J.; Martin, C.; Arahal, M.R.; Barrero, F.; Gregor, R. Influence of Covariance-Based ALS Methods in the Performance of Predictive Controllers With Rotor Current Estimation. *IEEE Trans. Ind. Electron.* **2017**, *64*, 2602–2607.
20. Levi, E. *The Industrial Electronics Handbook: Power Electronics and Motor Drives*, 2nd ed.; CRC Press: Boca Raton, FL, USA, 2011.
21. Miranda, H.; Cortes, P.; Yuz, J.I.; Rodriguez, J. Predictive Torque Control of Induction Machines Based on State-Space Models. *IEEE Trans. Ind. Electron.* **2009**, *56*, 1916–1924.
22. Yepes, A.G.; Riveros, J.A.; Doval-Gandoy, J.; Barrero, F.; Lopez, O.; Bogado, B.; Jones, M.; Levi, E. Parameter Identification of Multiphase Induction Machines with Distributed Windings-Part 1: Sinusoidal Excitation Methods. *IEEE Trans. Energy Convers.* **2012**, *27*, 1056–1066.
23. Riveros, J.A.; Yepes, A.G.; Barrero, F.; Doval-Gandoy, J.; Bogado, B.; Lopez, O.; Jones, M.; Levi, E. Parameter Identification of Multiphase Induction Machines with Distributed Windings-Part 2: Time-Domain Techniques. *IEEE Trans. Energy Convers.* **2012**, *27*, 1067–1077.
24. *General Guide on Harmonics and Interharmonics Measurements for Power Supply Systems and Equipment Connected Thereto*; ICE Std. 61000-4-7; IECEE, Geneva, Switzerland, 2002.

Chapter 5

Conclusions and Future Works

5.1 Conclusions

The general objective of this Thesis work has been the development of new model-based predictive current control techniques for multiphase drives with the aim to overcome the most critical problems that conventional predictive controllers present in their applications to this kind of systems, putting the focus on the reduction of the high harmonic content in the stator currents. Two different types of predictive stator current controllers have been implemented based on the FCS-MPC technique. Experimental validations have been conducted using a five-phase induction machine with distributed windings as a case study, although the methods can be extended to multiphase machines with a higher number of phases or with different constructive technologies adjusting the machine model equations. Consequently, the obtained conclusions encourage the use of predictive controllers in multiphase drives as a powerful alternative to most conventional controllers like FOC or DTC methods.

In the first place, the observer theory has been extended to the rotor current estimation in a FCS-MPC current controller, instead of using the common sample and hold method employed by most of the MPC practitioners. The Luenberger observer has been selected with the innovative inclusion of a Butterworth filter structure in order to solve the complex pole placement problem that characterizes this type of observer. Simulation and experimental results have demonstrated that it is possible to enhance the predictions using this rotor observer and, in turn, outperform the current control performance in comparison with conventional FCS-MPC techniques, principally in terms of harmonic content and switching frequency. It can be concluded, consequently, that the incorporation of observers in predictive control strategies leads to a natural reduction of the harmonic content, permitting the generation of torque with lower ripple and higher efficiency thanks to the reduction of the copper and VSI losses. Furthermore, two observer designs have been tested, a reduced-order observer and a full-order one, being the latter the best solution in reducing the current ripple, especially in the x–y plane, with similar computational cost.

Although the observer theory in conjunction with the FCS-MPC technique provides a significant improvement of the current performance, it can be more reasonable to tackle

the harmonic content problem from its origin. Recent studies have shown that the absence of modulation stage in the FCS-MPC technique together with the fixed discretization of the control algorithm promote the apparition of high magnitude harmonics and inter-harmonics in the currents, as well as electrical noise. Consequently, a more spread current spectrum is obtained in comparison with modulation-based control methods. In this work, a novel model-based variable sampling time current controller has been developed in order to give freedom to the VSI commuting times, but retaining the advantages of the FCS-MPC technique. The interest of the proposal, based on the lead-pursuit concept, has been stated by simulation and experimentation along with its advantages and disadvantages in comparison with FCS-MPC methods with and without rotor current observer. In particular, the harmonic content is effectively improved in both α–β and x–y planes, as well as the current tracking performance, in comparison with conventional FCS-MPC techniques. However, this is not the case when it is compared with the FCS-MPC approach with a rotor observer.

A study of the computational burden of the proposed methods has been also carried out. Although both the incorporation of a rotor current observer and the implementation of the variable sampling time lead-pursuit control require additional calculations compared with conventional FCS-MPC methods, the increase in the computational cost is acceptable and still permits their implementation in modern available microprocessors. However, we assume that more research work must be done in the development and implementation of variable sampling time lead pursuit controllers to finally become a clear competitor to FCS-MPC methods.

5.2 Summary of the research work

It is worth mentioning that, apart from the journal publications presented as contributions in Chapters 3 and 4, an important number of papers published in indexed journals, contributions in conferences of recognized prestige, as well as a book chapter have been derived from the work performed during the Doctoral Thesis period. Hereunder, all the publications are chronologically listed:

- M. R. Arahal, F. Barrero, M. J. Duran, and **C. Martin**, "Harmonic Distribution in Finite State Model Predictive Control", *International Review of Electrical Engineering*, vol. 10, no. 2, pp. 172-179, March 2015.
- H. Guzman, M. Bermudez, **C. Martin**, F. Barrero, M. J. Duran, *Application of DSP in Power Conversion Systems - A Practical Approach for Multiphase Drives*, InTech, October 2015.
- **C. Martin**, M. R. Arahal, F. Barrero, M. J. Duran, and S. Toral, "Rotor current observer in finite-state model predictive control of five-phase IM", in *41st Annual Conference of the IEEE Industrial Electronics Society (IECON)*, Yokohama, Japan, November 2015, pp. 701-706.
- **C. Martin**, M. R. Arahal, F. Barrero, and M. J. Duran, "Multiphase rotor current observers for current predictive control: A five-phase case study", *Control Engineering Practice*, vol. 49, pp. 101-111, April 2016.

- M. J. Duran, F. Barrero, I. Gonzalez-Prieto, H. Guzman, A. Pozo, M. Bermudez, and **C. Martin**, "A scientific approach in wind energy courses for electrical engineers", in *Technologies Applied to Electronics Teaching (TAEE)*, Seville, Spain, June 2016, pp. 1-6.

- **C. Martin**, M. R. Arahal, F. Barrero, and M. J. Duran, "Five-Phase Induction Motor Rotor Current Observer for Finite Control Set Model Predictive Control of Stator Current", *IEEE Transactions on Industrial Electronics*, vol. 63, no. 7, pp. 4527-4538, July 2016.

- J. Rodas, F. Barrero, M. R. Arahal, **C. Martin**, and R. Gregor, "Online Estimation of Rotor Variables in Predictive Current Controllers: A Case Study Using Five-Phase Induction Machines", *IEEE Transactions on Industrial Electronics*, vol. 63, no. 9, pp. 5348-5356, September 2016.

- **C. Martin**, M. Bermudez, F. Barrero, and H. Guzman, "Application of Modern Microprocessor in Power Conversion Systems: A Practical Approach for Multiphase Drives", in *12th International Scientific Conference on Electrical, Computer, Electronics and Engineering*, Dubai, United Arab Emirates, September 2016.

- M. R. Arahal, F. Barrero, M. G. Ortega, and **C. Martin**, "Harmonic analysis of direct digital control of voltage inverters", *Mathematics and Computers in Simulation*, vol. 130, pp. 155-166, December 2016.

- J. Rodas, **C. Martin**, M. R. Arahal, F. Barrero, and R. Gregor, "Influence of Covariance-Based ALS Methods in the Performance of Predictive Controllers With Rotor Current Estimation", *IEEE Transactions on Industrial Electronics*, vol. 64, no. 4, pp. 2602-2607, April 2017.

- N. Rios-Garcia, M. J. Duran, I. Gonzalez-Prieto, **C. Martin**, and F. Barrero, "An Open-phase Fault Detection Method for Six-phase Induction Motor Drives", in *International Conference on Renewable Energies and Power Quality (ICREPQ'17)*, Tenerife, Spain, April 2017, pp. 473-478.

- **C. Martin**, M. Bermudez, F. Barrero, M. R. Arahal, X. Kestelyn, and M. J. Duran, "Sensitivity of predictive controllers to parameter variation in five-phase induction motor drives", *Control Engineering Practice*, vol. 68, pp. 23-31, November 2017.

- I. Gonzalez-Prieto, M. J. Duran, J. J. Aciego, **C. Martin**, and F. Barrero, "Model Predictive Control of Six-Phase Induction Motor Drives Using Virtual Voltage Vectors", *IEEE Transactions on Industrial Electronics*, vol. 65, no. 1, pp. 27-37, January 2018.

- **C. Martin**, M. R. Arahal, F. Barrero, M. J. Duran, and I. Gonzalez-Prieto, "Variable sampling time model predictive control of multiphase induction machines", in *IEEE 15th International Workshop on Advanced Motion Control (AMC)*, Tokyo, Japan, March 2018, pp. 287-292.

- I. Gonzalez-Prieto, M. J. Duran, N. Rios-Garcia, F. Barrero, and **C. Martin**, "Open-Switch Fault Detection in Five-Phase Induction Motor Drives Using Model Predictive Control", *IEEE Transactions on Industrial Electronics*, vol. 65, no. 4, pp. 3045-3055, April 2018.
- M. R. Arahal, **C. Martin**, F. Barrero, I. Gonzalez-Prieto, and M. J. Duran, "Model-Based Control for Power Converters with Variable Sampling Time: A Case Example using Five-Phase Induction Motor Drives", *IEEE Transactions on Industrial Electronics*, vol. 66, no. 8, pp. 5800-5809, August 2019.
- M. R. Arahal, F. Barrero, M. J. Duran, M. G. Ortega, and **C. Martin**, "Trade-offs analysis in predictive current control of multi-phase induction machines", *Control Engineering Practice*, vol. 81, pp. 105-113, December 2018.
- M. R. Arahal, **C. Martin**, A. Kowal, M. Castilla, and F. Barrero, "Cost function optimization for predictive control of a five-phase IM drive", *Optimal Control Applications and Methods*, pp. 1-10, March 2019.
- M. Bermudez, **C. Martin**, F. Barrero, and X. Kestelyn, "Predictive controllers considering electrical constraints: a case example for five-phase induction machines", *IET Electric Power Applications*, March 2019. Accepted for publication.
- M. R. Arahal, **C. Martin**, F. Barrero, and M. J. Duran, "Assessing Variable Sampling Time Controllers for Five-Phase Induction Motor Drives", *IEEE Transactions on Industrial Electronics*, April 2019. Accepted for publication.
- **C. Martin**, F. Barrero, M. R. Arahal, and M. J. Duran, "Model-Based Predictive Current Controllers in Multiphase Drives Dealing with Natural Reduction of Harmonic Distortion", *Energies*, vol. 12, no. 9, 1679, May 2019.
- I. Gonzalez-Prieto, M. J. Duran, M. Bermudez, F. Barrero, and **C. Martin**, "Assessment of Virtual-Voltage-based Model Predictive Controllers in Six-phase Drives under Open-Phase Faults", *IEEE Journal of Emerging and Selected Topics in Power Electronics*, May 2019. Accepted for publication.

Additionally, a summary of these achievements is presented in Table 5.1, where the journal publications have been divided depending on the journal rank provided by InCited Journal Citation Reports (Web of Science). In this table, it is also remarked the participation in two research projects supported by the Spanish Government (DPI2013-44278-R and DPI2016-76144-R) that have partially funded this work, and two international stays with a total duration of six months at European Universities that further remark the internationalization of the PhD student research. The first stay took place at l'École Nationale Supérieure d'Arts et Métiers of Lille (France) under the supervision of Prof. Xavier Kestelyn, and the second one at the Liverpool John Moores University (United Kingdom) under the supervision of Prof. Emil Levi.

5.3 Future works

Electric mobility is becoming a mass market reality in industry, where current propulsion systems are almost exclusively based on three-phase electric motors of either synchronous

Table 5.1 Summary of additional achievements during this Doctoral Thesis.

Achievement	Number
Journal publications	16
• In Q1 journals	8
• In Q2 journals	6
• In Q3 journals	2
Conference papers	5
Book chapters	1
Participation in R&D projects	2
3-month international stays	2

or induction type. This trend is expected to continue in future, where numerous emerging variants of electric machines hold good prospects for mobility applications. This is the case of multiphase electric drives, which have stated their interest in electric propulsion and generation systems. However, the multiphase drive's field is not mature yet, and many control aspects of such a complex multivariable system must be analyzed to reach a state of industrial maturity. In this context, the work presented in this Doctoral Thesis can be seen as a basic research that must be complemented with additional studies in order to move into a real industrial application and, thus, extend the interest of multiphase machines to the research community.

Regarding the innovative variable sampling time lead-pursuit current controller, more research and new developments are expected, since it constitutes a promising alternative to FCS-MPC methods but has just been introduced and firstly tested in this Thesis work. In particular, alternative implementations of the lead-pursuit algorithm can be investigated with the aim of reducing the computational cost and the switching frequency, and further improving the control performance in terms of harmonic content.

On the other hand, the presented work has been focused in the particular case of a five-phase induction machine with symmetrical and distributed windings supplied by a two-level five-phase VSI. The extension of the proposed methods to different multiphase topologies is another future research line in order to better fit with industry application. In this regard, machines with higher number of phases or fed by modular multilevel converters can be an interesting alternative in high-power applications. Furthermore, the concentrated windings arrangement provides the possibility of torque enhancement by the injection of higher order current harmonics. Minor modifications in the current controllers proposed in this Thesis will be required for the cited configurations, principally related to changes in the system's model.

The integration of the proposed current controllers with appropriate speed and torque control methods is also necessary, yielding a multiphase drive for variable-speed applications. Although this aspect has been considered in some of the Thesis' contributions, further analysis must be done in order to find the most adequate control strategy for the particular application. In this regard, conventional FOC and DTC methods are well-established competitors in the scientific literature. The application of sensorless techniques

for the speed and torque control of multiphase drives is also an emerging research field where the observer theory has application.

The exploration of the fault-tolerant capability of multiphase drives has been in the spotlight of the research community in the last years. On this subject, MPC techniques have been recently investigated as a way to obtain a flexible and high-performance post-fault control of the multiphase drives in applications where, for safety or economical reasons, keeping the system operation is crucial. Consequently, it is expected that the extension of the proposed controllers to the post-fault operation can be easily done following the same guidelines than the ones applied in conventional MPC techniques.

Bibliography

[1] Amsterdam Roundtables Foundation and McKinsey & Company. (2014) Electric vehicles in europe: gearing up for a new phase? [Online]. Available: https://www.mckinsey.com/featured-insights/europe/electric-vehicles-in-europe-gearing-up-for-a-new-phase

[2] M. J. Duran, E. Levi, and F. Barrero, *Multiphase Electric Drives: Introduction*. Wiley Encyclopedia of Electrical and Electronics Engineering, 2017.

[3] E. E. Warg and H. Härer, "Preliminary investigation of an inventor-fed 5-phase induction motor," *Proceedings of the Institution of Electrical Engineers*, vol. 116, no. 6, pp. 980–984, June 1969.

[4] T. M. Jahns, "Improved reliability in solid-state AC drives by means of multiple independent phase drive units," *IEEE Transactions on Industry Applications*, vol. IA-16, no. 3, pp. 321–331, May 1980.

[5] H. A. Toliyat, T. A. Lipo, and J. C. White, "Analysis of a concentrated winding induction machine for adjustable speed drive applications. I. Motor analysis," *IEEE Transactions on Energy Conversion*, vol. 6, no. 4, pp. 679–683, Dec. 1991.

[6] E. Levi, R. Bojoi, F. Profumo, H. A. Toliyat, and S. Williamson, "Multiphase induction motor drives – a technology status review," *IET Electric Power Applications*, vol. 1, no. 4, pp. 489–516, July 2007.

[7] E. Levi, "Multiphase electric machines for variable-speed applications," *IEEE Transactions on Industrial Electronics*, vol. 55, no. 5, pp. 1893–1909, May 2008.

[8] R. Bojoi, S. Rubino, A. Tenconi, and S. Vaschetto, "Multiphase electrical machines and drives: a viable solution for energy generation and transportation electrification," in *2016 International Conference and Exposition on Electrical and Power Engineering (EPE)*, Oct. 2016, pp. 632–639.

[9] W. Cao, B. C. Mecrow, G. J. Atkinson, J. W. Bennett, and D. J. Atkinson, "Overview of electric motor technologies used for more electric aircraft (MEA)," *IEEE Transactions on Industrial Electronics*, vol. 59, no. 9, pp. 3523–3531, Sep. 2012.

[10] E. Jung, H. Yoo, S. Sul, H. Choi, and Y. Choi, "A nine-phase permanent-magnet motor drive system for an ultrahigh-speed elevator," *IEEE Transactions on Industry Applications*, vol. 48, no. 3, pp. 987–995, May 2012.

[11] F. Barrero and M. J. Duran, "Recent advances in the design, modeling, and control of multiphase machines – Part I," *IEEE Transactions on Industrial Electronics*, vol. 63, no. 1, pp. 449–458, Jan. 2016.

[12] M. J. Duran and F. Barrero, "Recent advances in the design, modeling, and control of multiphase machines – Part II," *IEEE Transactions on Industrial Electronics*, vol. 63, no. 1, pp. 459–468, Jan. 2016.

[13] E. Levi, "Advances in converter control and innovative exploitation of additional degrees of freedom for multiphase machines," *IEEE Transactions on Industrial Electronics*, vol. 63, no. 1, pp. 433–448, Jan 2016.

[14] R. H. Nelson and P. C. Krause, "Induction machine analysis for arbitrary displacement between multiple winding sets," *IEEE Transactions on Power Apparatus and Systems*, vol. PAS-93, no. 3, pp. 841–848, May 1974.

[15] E. Levi, N. Bodo, O. Dordevic, and M. Jones, "Recent advances in power electronic converter control for multiphase drive systems," in *2013 IEEE Workshop on Electrical Machines Design, Control and Diagnosis (WEMDCD)*, March 2013, pp. 158–167.

[16] N. Bodo, M. Jones, and E. Levi, "A space vector PWM with common-mode voltage elimination for open-end winding five-phase drives with a single DC supply," *IEEE Transactions on Industrial Electronics*, vol. 61, no. 5, pp. 2197–2207, May 2014.

[17] M. I. Daoud, A. A. Elserougi, A. M. Massoud, R. Bojoi, A. S. Abdel-Khalik, and S. Ahmed, "Zero-/low-speed operation of multiphase drive systems with modular multilevel converters," *IEEE Access*, vol. 7, pp. 14 353–14 365, Jan. 2019.

[18] D. C. White and H. H. Woodson, *Electromechanical Energy Conversion*. John Willey and Sons, New York, 1959.

[19] C. L. Fortescue, "Method of symmetrical co-ordinates applied to the solution of polyphase networks," *Transactions of the American Institute of Electrical Engineers*, vol. XXXVII, no. 2, pp. 1027–1140, July 1918.

[20] E. Clarke, *Circuit Analysis of A-C Power, vols. 1 and 2*. John Willey and Sons, New York, 1941 (vol. 1) and 1950 (vol. 2).

[21] Y. Zhao and T. A. Lipo, "Space vector PWM control of dual three-phase induction machine using vector space decomposition," *IEEE Transactions on Industry Applications*, vol. 31, no. 5, pp. 1100–1109, Sep. 1995.

[22] I. Zoric, M. Jones, and E. Levi, "Vector space decomposition algorithm for asymmetrical multiphase machines," in *2017 International Symposium on Power Electronics (Ee)*, Oct. 2017, pp. 1–6.

[23] H. A. Toliyat, T. A. Lipo, and J. C. White, "Analysis of a concentrated winding induction machine for adjustable speed drive applications. II. Motor design and performance," *IEEE Transactions on Energy Conversion*, vol. 6, no. 4, pp. 684–692, Dec. 1991.

[24] L. A. Pereira, C. C. Scharlau, L. F. A. Pereira, and J. F. Haffner, "General model of a five-phase induction machine allowing for harmonics in the air gap field," *IEEE Transactions on Energy Conversion*, vol. 21, no. 4, pp. 891–899, Dec. 2006.

[25] E. Levi, *The Industrial Electronics Handbook: Power Electronics and Motor Drives*, 2nd ed. Boca Raton, FL: CRC Press, 2011.

[26] R. Bojoi, "Analysis, design and implementation of a dual three-phase vector controlled induction motor drive," Master's thesis, Politecnico di Torino, 2002.

[27] A. G. Yepes, J. A. Riveros, J. Doval-Gandoy, F. Barrero, O. Lopez, B. Bogado, M. Jones, and E. Levi, "Parameter identification of multiphase induction machines with distributed windings – Part 1: Sinusoidal excitation methods," *IEEE Transactions on Energy Conversion*, vol. 27, no. 4, pp. 1056–1066, Dec. 2012.

[28] J. A. Riveros, A. G. Yepes, F. Barrero, J. Doval-Gandoy, B. Bogado, O. Lopez, M. Jones, and E. Levi, "Parameter identification of multiphase induction machines with distributed windings – Part 2: Time-domain techniques," *IEEE Transactions on Energy Conversion*, vol. 27, no. 4, pp. 1067–1077, Dec. 2012.

[29] A. M. Trzynadlowsk, *Control of Induction Motors*. Elsevier, 2000.

[30] H. S. Che, M. J. Duran, E. Levi, M. Jones, W. Hew, and N. A. Rahim, "Postfault operation of an asymmetrical six-phase induction machine with single and two isolated neutral points," *IEEE Transactions on Power Electronics*, vol. 29, no. 10, pp. 5406–5416, Oct. 2014.

[31] G. Pellegrino, R. I. Bojoi, and P. Guglielmi, "Unified direct-flux vector control for AC motor drives," *IEEE Transactions on Industry Applications*, vol. 47, no. 5, pp. 2093–2102, Sep. 2011.

[32] L. Zheng, J. E. Fletcher, B. W. Williams, and X. He, "A novel direct torque control scheme for a sensorless five-phase induction motor drive," *IEEE Transactions on Industrial Electronics*, vol. 58, no. 2, pp. 503–513, Feb. 2011.

[33] L. Gao, J. E. Fletcher, and L. Zheng, "Low-speed control improvements for a two-level five-phase inverter-fed induction machine using classic direct torque control," *IEEE Transactions on Industrial Electronics*, vol. 58, no. 7, pp. 2744–2754, July 2011.

[34] M. J. Duran, J. Prieto, F. Barrero, J. A. Riveros, and H. Guzman, "Space-vector PWM with reduced common-mode voltage for five-phase induction motor drives," *IEEE Transactions on Industrial Electronics*, vol. 60, no. 10, pp. 4159–4168, Oct. 2013.

[35] K. Hasse, "Zur dynamik drehzahlgeregelter antriebe mit stromrichtergespeisten asynchron-kurzschlußläufermaschinen (On dynamic of the speed controlled static AC drive with squirrel-cage induction machine)," Ph.D. dissertation, Technical University Darmstadt, Darmstadt, West Germany, 1969.

[36] F. Blaschke, "The principle of field orientation as applied to the new transvector closed-loop system for rotating-field machines," *Siemens Review*, vol. 34, no. 3, pp. 217–220, 1972.

[37] G. K. Singh, K. Nam, and S. K. Lim, "A simple indirect field-oriented control scheme for multiphase induction machine," *IEEE Transactions on Industrial Electronics*, vol. 52, no. 4, pp. 1177–1184, Aug. 2005.

[38] H. S. Che, E. Levi, M. Jones, W. Hew, and N. A. Rahim, "Current control methods for an asymmetrical six-phase induction motor drive," *IEEE Transactions on Power Electronics*, vol. 29, no. 1, pp. 407–417, Jan. 2014.

[39] K. Iffouzar, S. Taraft, H. Aouzellag, K. Ghedamsi, and D. Aouzellag, "DRFOC of polyphase induction motor based on fuzzy logic controller speed," in *2015 4th International Conference on Electrical Engineering (ICEE)*, Dec. 2015, pp. 1–7.

[40] N. Oikonomou, "Control of medium-voltage drives at very low switching frequency," Ph.D. dissertation, Elektrotechnik, Informationstechnik und Medientechnik der Bergischen Universität Wuppertal, 2008.

[41] J. Prieto, "Continuous and discontinuous modulation techniques for multiphase drives: analysis and contributions," Ph.D. dissertation, Universidad de Sevilla, Spain, 2016.

[42] W. N. W. A. Munim, M. J. Duran, H. S. Che, M. Bermudez, I. Gonzalez-Prieto, and N. A. Rahim, "A unified analysis of the fault tolerance capability in six-phase induction motor drives," *IEEE Transactions on Power Electronics*, vol. 32, no. 10, pp. 7824–7836, Oct. 2017.

[43] I. Gonzalez-Prieto, M. J. Duran, and F. J. Barrero, "Fault-tolerant control of six-phase induction motor drives with variable current injection," *IEEE Transactions on Power Electronics*, vol. 32, no. 10, pp. 7894–7903, Oct. 2017.

[44] L. Zheng, J. E. Fletcher, B. W. Williams, and X. He, "Dual-plane vector control of a five-phase induction machine for an improved flux pattern," *IEEE Transactions on Industrial Electronics*, vol. 55, no. 5, pp. 1996–2005, May 2008.

[45] A. S. Abdel-Khalik, M. I. Masoud, and B. W. Williams, "Improved flux pattern with third harmonic injection for multiphase induction machines," *IEEE Transactions on Power Electronics*, vol. 27, no. 3, pp. 1563–1578, March 2012.

[46] M. Mengoni, L. Zarri, A. Tani, L. Parsa, G. Serra, and D. Casadei, "High-torque-density control of multiphase induction motor drives operating over a wide speed range," *IEEE Transactions on Industrial Electronics*, vol. 62, no. 2, pp. 814–825, Feb. 2015.

[47] L. Parsa, H. A. Toliyat, and A. Goodarzi, "Five-phase interior permanent-magnet motors with low torque pulsation," *IEEE Transactions on Industry Applications*, vol. 43, no. 1, pp. 40–46, Jan. 2007.

[48] K. Wang, Z. Q. Zhu, and G. Ombach, "Torque improvement of five-phase surface-mounted permanent magnet machine using third-order harmonic," *IEEE Transactions on Energy Conversion*, vol. 29, no. 3, pp. 735–747, Sep. 2014.

[49] I. Takahashi and T. Noguchi, "A new quick-response and high-efficiency control strategy of an induction motor," *IEEE Transactions on Industry Applications*, vol. IA-22, pp. 820–827, Sep. 1986.

[50] M. Depenbrock, "Direct self-control (DSC) of inverter-fed induction machine," *IEEE Transactions on Power Electronics*, vol. 3, no. 4, pp. 420–429, Oct. 1988.

[51] G. S. Buja and M. P. Kazmierkowski, "Direct torque control of PWM inverter-fed AC motors – a survey," *IEEE Transactions on Industrial Electronics*, vol. 51, no. 4, pp. 744–757, Aug. 2004.

[52] ABB Group. (2015) Direct torque control (DTC), a motor control technique for all seasons. [Online]. Available: https://library.e.abb.com/public/0e07ab6a2de30809c1257e2d0042db5e/ABB_WhitePaper_DTC_A4_20150414.pdf

[53] D. Casadei, F. Profumo, G. Serra, and A. Tani, "FOC and DTC: two viable schemes for induction motors torque control," *IEEE Transactions on Power Electronics*, vol. 17, no. 5, pp. 779–787, Sep. 2002.

[54] K. Hatua and V. T. Ranganathan, "Direct torque control schemes for split-phase induction machine," *IEEE Transactions on Industry Applications*, vol. 41, no. 5, pp. 1243–1254, Sep. 2005.

[55] F. Yu, X. Zhang, M. Qiao, and C. Du, "The direct torque control of multiphase permanent magnet synchronous motor based on low harmonic space vector PWM," in *2008 IEEE International Conference on Industrial Technology*, April 2008, pp. 1–5.

[56] Z. Zhang, R. Tang, B. Bai, and D. Xie, "Novel direct torque control based on space vector modulation with adaptive stator flux observer for induction motors," *IEEE Transactions on Magnetics*, vol. 46, no. 8, pp. 3133–3136, Aug. 2010.

[57] Y. Gao and L. Parsa, "Modified direct torque control of five-phase permanent magnet synchronous motor drives," in *APEC 07 – Twenty-Second Annual IEEE Applied Power Electronics Conference and Exposition*, Feb. 2007, pp. 1428–1433.

[58] L. Parsa and H. A. Toliyat, "Sensorless direct torque control of five-phase interior permanent-magnet motor drives," *IEEE Transactions on Industry Applications*, vol. 43, no. 4, pp. 952–959, July 2007.

[59] A. Taheri, A. Rahmati, and S. Kaboli, "Comparison of efficiency for different switching tables in six-phase induction motor DTC drive," *Journal of Power Electronics*, vol. 12, no. 1, pp. 128–135, Jan. 2012.

[60] M. Bermudez, "Novel control techniques in multiphase drives: Direct control methods (DTC and MPC) under limit situations," Ph.D. dissertation, École Nationale Supérieure d'Arts et Métiers, France, and Universidad de Sevilla, Spain, 2018.

[61] R. Karampuri, J. Prieto, F. Barrero, and S. Jain, "Extension of the DTC technique to multiphase induction motor drives using any odd number of phases," in *2014 IEEE Vehicle Power and Propulsion Conference (VPPC)*, Oct. 2014, pp. 1–6.

[62] M. Bermudez, I. Gonzalez-Prieto, F. Barrero, H. Guzman, X. Kestelyn, and M. J. Duran, "An experimental assessment of open-phase fault-tolerant virtual-vector-based direct torque control in five-phase induction motor drives," *IEEE Transactions on Power Electronics*, vol. 33, no. 3, pp. 2774–2784, March 2018.

[63] T. Geyer, *Model Predictive Control of High Power Converters and Industrial Drives*. Wiley, 2017.

[64] C. E. Garcia, D. M. Prett, and M. Morari, "Model predictive control: Theory and practice – a survey," *Automatica*, vol. 25, no. 3, pp. 335–348, May 1989.

[65] S. Kouro, M. A. Perez, J. Rodriguez, A. M. Llor, and H. A. Young, "Model predictive control: MPC's role in the evolution of power electronics," *IEEE Industrial Electronics Magazine*, vol. 9, no. 4, pp. 8–21, Dec. 2015.

[66] P. Cortes, M. P. Kazmierkowski, R. M. Kennel, D. E. Quevedo, and J. Rodriguez, "Predictive control in power electronics and drives," *IEEE Transactions on Industrial Electronics*, vol. 55, no. 12, pp. 4312–4324, Dec. 2008.

[67] J. Rodriguez and P. Cortes, *Predictive Control of Power Converters and Electrical Drives*. Wiley-IEEE Press, 2012.

[68] S. Vazquez, J. Rodriguez, M. Rivera, L. G. Franquelo, and M. Norambuena, "Model predictive control for power converters and drives: Advances and trends," *IEEE Transactions on Industrial Electronics*, vol. 64, no. 2, pp. 935–947, Feb. 2017.

[69] J. Rodriguez, M. P. Kazmierkowski, J. R. Espinoza, P. Zanchetta, H. Abu-Rub, H. A. Young, and C. A. Rojas, "State of the art of finite control set model predictive control in power electronics," *IEEE Transactions on Industrial Informatics*, vol. 9, no. 2, pp. 1003–1016, May 2013.

[70] F. Barrero, M. R. Arahal, R. Gregor, S. Toral, and M. J. Duran, "A proof of concept study of predictive current control for VSI-driven asymmetrical dual three-phase ac machines," *IEEE Transactions on Industrial Electronics*, vol. 56, no. 6, pp. 1937–1954, June 2009.

[71] M. Arahal, F. Barrero, S. Toral, M. Duran, and R. Gregor, "Multi-phase current control using finite-state model-predictive control," *Control Engineering Practice*, vol. 17, no. 5, pp. 579–587, May 2009.

[72] J. Zou, W. Xu, J. Zhu, and Y. Liu, "Low-complexity finite control set model predictive control with current limit for linear induction machines," *IEEE Transactions on Industrial Electronics*, vol. 65, no. 12, pp. 9243–9254, Dec. 2018.

[73] C. S. Lim, E. Levi, M. Jones, N. A. Rahim, and W. P. Hew, "FCS-MPC-based current control of a five-phase induction motor and its comparison with PI-PWM control," *IEEE Transactions on Industrial Electronics*, vol. 61, no. 1, pp. 149–163, Jan. 2014.

[74] C. Lim, E. Levi, M. Jones, N. A. Rahim, and W. Hew, "A comparative study of synchronous current control schemes based on FCS-MPC and PI-PWM for a two-motor three-phase drive," *IEEE Transactions on Industrial Electronics*, vol. 61, no. 8, pp. 3867–3878, Aug. 2014.

[75] H. Miranda, P. Cortes, J. I. Yuz, and J. Rodriguez, "Predictive torque control of induction machines based on state-space models," *IEEE Transactions on Industrial Electronics*, vol. 56, no. 6, pp. 1916–1924, June 2009.

[76] R. Kennel, J. Rodriguez, J. Espinoza, and M. Trincado, "High performance speed control methods for electrical machines: An assessment," in *2010 IEEE International Conference on Industrial Technology*, March 2010, pp. 1793–1799.

[77] W. Xie, X. Wang, F. Wang, W. Xu, R. M. Kennel, D. Gerling, and R. D. Lorenz, "Finite-control-set model predictive torque control with a deadbeat solution for PMSM drives," *IEEE Transactions on Industrial Electronics*, vol. 62, no. 9, pp. 5402–5410, Sep. 2015.

[78] M. Mamdouh, M. A. Abido, and Z. Hamouz, "Weighting factor selection techniques for predictive torque control of induction motor drives: A comparison study," *Arabian Journal for Science and Engineering*, vol. 43, no. 2, pp. 433–445, Feb. 2018.

[79] J. A. Riveros, F. Barrero, E. Levi, M. J. Duran, S. Toral, and M. Jones, "Variable-speed five-phase induction motor drive based on predictive torque control," *IEEE Transactions on Industrial Electronics*, vol. 60, no. 8, pp. 2957–2968, Aug. 2013.

[80] E. J. Fuentes, C. A. Silva, and J. I. Yuz, "Predictive speed control of a two-mass system driven by a permanent magnet synchronous motor," *IEEE Transactions on Industrial Electronics*, vol. 59, no. 7, pp. 2840–2848, July 2012.

[81] C. Garcia, J. Rodriguez, C. Silva, C. Rojas, P. Zanchetta, and H. Abu-Rub, "Full predictive cascaded speed and current control of an induction machine," *IEEE Transactions on Energy Conversion*, vol. 31, no. 3, pp. 1059–1067, Sep. 2016.

[82] J. Rodriguez, R. M. Kennel, J. R. Espinoza, M. Trincado, C. A. Silva, and C. A. Rojas, "High-performance control strategies for electrical drives: An experimental assessment," *IEEE Transactions on Industrial Electronics*, vol. 59, no. 2, pp. 812–820, Feb. 2012.

[83] M. J. Duran, J. A. Riveros, F. Barrero, H. Guzman, and J. Prieto, "Reduction of common-mode voltage in five-phase induction motor drives using predictive control techniques," *IEEE Transactions on Industry Applications*, vol. 48, no. 6, pp. 2059–2067, Nov. 2012.

[84] P. Cortes, J. Rodriguez, C. Silva, and A. Flores, "Delay compensation in model predictive current control of a three-phase inverter," *IEEE Transactions on Industrial Electronics*, vol. 59, no. 2, pp. 1323–1325, Feb. 2012.

[85] S. Kouro, P. Cortes, R. Vargas, U. Ammann, and J. Rodriguez, "Model predictive control – a simple and powerful method to control power converters," *IEEE Transactions on Industrial Electronics*, vol. 56, no. 6, pp. 1826–1838, June 2009.

[86] M. R. Arahal, C. Martin, A. Kowal, M. del Mar Castilla, and F. Barrero, "Cost function optimization for multi-phase induction machines predictive control," *Optimal Control Applications and Methods*, pp. 1 – 10, March 2019.

[87] R. P. Aguilera, P. Acuña, P. Lezana, G. Konstantinou, B. Wu, S. Bernet, and V. G. Agelidis, "Selective harmonic elimination model predictive control for multilevel power converters," *IEEE Transactions on Power Electronics*, vol. 32, no. 3, pp. 2416–2426, March 2017.

[88] Q. Yuan, J. Qian, H. Wu, W. Yin, and Q. Jiang, "Stator current harmonic elimination control for the high-power synchronous motors with online implementation," *IET Power Electronics*, vol. 12, no. 4, pp. 801–809, Jan. 2019.

[89] M. Azab and M. A. Awadallah, "Selective harmonic elimination in VSI-fed induction motor drives using swarm and genetic optimisation," *International Journal of Power Electronics*, vol. 5, no. 1, pp. 56–74, May 2013.

[90] F. Wang, S. A. Davari, Z. Chen, Z. Zhang, D. A. Khaburi, J. Rodriguez, and R. Kennel, "Finite control set model predictive torque control of induction machine with a robust adaptive observer," *IEEE Transactions on Industrial Electronics*, vol. 64, no. 4, pp. 2631–2641, April 2017.

[91] P. Cortes, S. Kouro, B. La Rocca, R. Vargas, J. Rodriguez, J. I. Leon, S. Vazquez, and L. G. Franquelo, "Guidelines for weighting factors design in model predictive control of power converters and drives," in *2009 IEEE International Conference on Industrial Technology*, Feb. 2009, pp. 1–7.

[92] S. A. Davari, D. A. Khaburi, and R. Kennel, "An improved FCS–MPC algorithm for an induction motor with an imposed optimized weighting factor," *IEEE Transactions on Power Electronics*, vol. 27, no. 3, pp. 1540–1551, March 2012.

[93] M. R. Arahal, F. Barrero, M. J. Duran, M. G. Ortega, and C. Martin, "Trade-offs analysis in predictive current control of multi-phase induction machines," *Control Engineering Practice*, vol. 81, pp. 105–113, Dec. 2018.

[94] C. Martin, M. Bermudez, F. Barrero, M. R. Arahal, X. Kestelyn, and M. J. Duran, "Sensitivity of predictive controllers to parameter variation in five-phase induction motor drives," *Control Engineering Practice*, vol. 68, pp. 23 – 31, Nov. 2017.

[95] C. A. Rojas, J. I. Yuz, C. A. Silva, and J. Rodriguez, "Comments on 'predictive torque control of induction machines based on state-space models'," *IEEE Transactions on Industrial Electronics*, vol. 61, no. 3, pp. 1635–1638, March 2014.

[96] S. Chai, L. Wang, and E. Rogers, "Model predictive control of a permanent magnet synchronous motor with experimental validation," *Control Engineering Practice*, vol. 21, no. 11, pp. 1584–1593, Nov. 2013.

[97] F. Morel, X. Lin-Shi, J. M. Retif, B. Allard, and C. Buttay, "A comparative study of predictive current control schemes for a permanent-magnet synchronous machine drive," *IEEE Transactions on Industrial Electronics*, vol. 56, no. 7, pp. 2715–2728, July 2009.

[98] X. Zhang, B. Hou, and Y. Mei, "Deadbeat predictive current control of permanent-magnet synchronous motors with stator current and disturbance observer," *IEEE Transactions on Power Electronics*, vol. 32, no. 5, pp. 3818–3834, May 2017.

[99] M. Siami, D. A. Khaburi, A. Abbaszadeh, and J. Rodriguez, "Robustness improvement of predictive current control using prediction error correction for permanent-magnet synchronous machines," *IEEE Transactions on Industrial Electronics*, vol. 63, no. 6, pp. 3458–3466, June 2016.

[100] S. Kwak, U. C. Moon, and J. C. Park, "Predictive-control-based direct power control with an adaptive parameter identification technique for improved AFE performance," *IEEE Transactions on Power Electronics*, vol. 29, no. 11, pp. 6178–6187, Nov. 2014.

[101] H. A. Young, M. A. Perez, and J. Rodriguez, "Analysis of finite-control-set model predictive current control with model parameter mismatch in a three-phase inverter," *IEEE Transactions on Industrial Electronics*, vol. 63, no. 5, pp. 3100–3107, May 2016.

[102] B. Bogado, F. Barrero, M. R. Arahal, S. Toral, and E. Levi, "Sensitivity to electrical parameter variations of predictive current control in multiphase drives," in *IECON 2013 - 39th Annual Conference of the IEEE Industrial Electronics Society*, Nov. 2013, pp. 5215–5220.

[103] J. Sawma, F. Khatounian, E. Monmasson, L. Idkhajine, and R. Ghosn, "Analysis of the impact of online identification on model predictive current control applied to permanent magnet synchronous motors," *IET Electric Power Applications*, vol. 11, no. 5, pp. 864–873, May 2017.

[104] C. Xia, M. Wang, Z. Song, and T. Liu, "Robust model predictive current control of three-phase voltage source PWM rectifier with online disturbance observation," *IEEE Transactions on Industrial Informatics*, vol. 8, no. 3, pp. 459–471, Aug. 2012.

[105] Z. Chen, J. Qiu, and M. Jin, "Adaptive finite-control-set model predictive current control for IPMSM drives with inductance variation," *IET Electric Power Applications*, vol. 11, no. 5, pp. 874–884, May 2017.

[106] H. Yang, Y. Zhang, J. Liang, B. Xia, P. D. Walker, and N. Zhang, "Deadbeat control based on a multipurpose disturbance observer for permanent magnet synchronous motors," *IET Electric Power Applications*, vol. 12, no. 5, pp. 708–716, April 2018.

[107] S. A. Davari, D. A. Khaburi, F. Wang, and R. M. Kennel, "Using full order and reduced order observers for robust sensorless predictive torque control of induction motors," *IEEE Transactions on Power Electronics*, vol. 27, no. 7, pp. 3424–3433, July 2012.

[108] M. J. Duran, J. Prieto, F. Barrero, and S. Toral, "Predictive current control of dual three-phase drives using restrained search techniques," *IEEE Transactions on Industrial Electronics*, vol. 58, no. 8, pp. 3253–3263, Aug. 2011.

[109] Y. Luo and C. Liu, "A simplified model predictive control for a dual three-phase PMSM with reduced harmonic currents," *IEEE Transactions on Industrial Electronics*, vol. 65, no. 11, pp. 9079–9089, Nov. 2018.

[110] T. Geyer and D. E. Quevedo, "Multistep finite control set model predictive control for power electronics," *IEEE Transactions on Power Electronics*, vol. 29, no. 12, pp. 6836–6846, Dec. 2014.

[111] P. Karamanakos, T. Geyer, N. Oikonomou, F. D. Kieferndorf, and S. Manias, "Direct model predictive control: A review of strategies that achieve long prediction intervals for power electronics," *IEEE Industrial Electronics Magazine*, vol. 8, no. 1, pp. 32–43, March 2014.

[112] M. R. Arahal, F. Barrero, M. J. Duran, and C. Martin, "Harmonic distribution in finite state model predictive control," *International Review of Electrical Engineering*, vol. 10, no. 2, pp. 172–179, April 2015.

[113] F. Barrero, M. R. Arahal, R. Gregor, S. Toral, and M. J. Duran, "One-step modulation predictive current control method for the asymmetrical dual three-phase induction machine," *IEEE Transactions on Industrial Electronics*, vol. 56, no. 6, pp. 1974–1983, June 2009.

[114] R. Gregor, F. Barrero, S. Toral, M. R. Arahal, J. Prieto, and M. J. Duran, "Enhanced predictive current control method for the asymmetrical dual-three phase induction machine," in *2009 IEEE International Electric Machines and Drives Conference*, May 2009, pp. 265–272.

[115] O. Gonzalez, M. Ayala, J. Rodas, R. Gregor, G. Rivas, and J. Doval-Gandoy, "Variable-speed control of a six-phase induction machine using predictive-fixed switching frequency current control techniques," in *2018 9th IEEE International Symposium on Power Electronics for Distributed Generation Systems (PEDG)*, June 2018, pp. 1–6.

[116] I. Gonzalez-Prieto, M. J. Duran, J. J. Aciego, C. Martin, and F. Barrero, "Model predictive control of six-phase induction motor drives using virtual voltage vectors," *IEEE Transactions on Industrial Electronics*, vol. 65, no. 1, pp. 27–37, Jan. 2018.

[117] C. Xue, W. Song, and X. Feng, "Finite control-set model predictive current control of five-phase permanent-magnet synchronous machine based on virtual voltage vectors," *IET Electric Power Applications*, vol. 11, no. 5, pp. 836–846, May 2017.

[118] N. Hoffmann, M. Andresen, F. W. Fuchs, L. Asiminoaei, and P. B. Thøgersen, "Variable sampling time finite control-set model predictive current control for voltage source inverters," in *2012 IEEE Energy Conversion Congress and Exposition (ECCE)*, Sep. 2012, pp. 2215–2222.